The regulation and function of Hyaluronan in renal proximal tubule epithelial cells

Wisam Dhafer Rashid Selbi (M.B.Ch.B)

Thesis presented for the degree of Philosophiae Doctor

October, 2005

Institute of Nephrology,
Cardiff University College of Medicine,
Heath Park,
Cardiff CF14 4XN
United Kingdom

Declaration

This work has not previously been accepted in substance for any degree and is not being concurrently submitted in candidature for any degree.

Signed ______________ (Candidate)

Date 14/4/2006

Statement 1

This thesis is the result of my own investigation, except where otherwise stated. Other sources are acknowledged by footnotes giving explicit references. A bibliography is appended.

Signed ______________ (Candidate)

Date 14/4/2006

Statement 2

I hereby give consent for my thesis, if accepted, to be available for photocopying and for inter-library loan, and for the title and summary to be made available to outside organisations.

Signed ______________ (Candidate)

Date 14/4/2006

Dedication

In the name of God, the most merciful, the most passionate

This work is humbly dedicated to all my family:

My father (Che'che'wai)
&
My mother (Ha'ha'wai)
&
My Mayyasa

& in memory of
Sajjad.

Acknowledgements

I am grateful to all the people who helped my during my research years for without their help and support I would not have reached this stage.

My supervisor and mentor Prof Aled Phillips for his patience, support and guidance throughout the project and for his optimism despite all the hurdles. Prof John Williams, Prof Nicholas Topley, Dr Robert Steadman and Dr T. Bowen for their support and valuable advice.

I would like to thank the people at the Institute of Nephrology (past and present) for their help and time in teaching me and for providing a peaceful environment to work in. Dr John Martin, Dr Donald Fraser, Dr Ya-chung Tian (aka Eric), Dr Takafumi Ito, Dr Xiao Zhang (aka Tony), Dr Gareth Thomas, Dr Ruth Mackenzie, Dr Robert Jenkins, Dr Jamie Monslow, Dr Rachael Evans, Dr Rachael McLaughlin, Cheryl Ward, Tarnjit Khera and Daryn Michael.

I am eternally gratefully to my family who patiently tolerated me in spite of everything. My father for his financial and moral support. My mother for her prayers. My Mayyasa for her love and passion. I thank you for your patience, trust and faith.

From "*He who teaches me a letter, I shall owe him a lifetime*", I thank you all one more time. I am eternally grateful to you.

Summary

Hyaluronan (HA), a high molecular weight glycoaminoglycan, is widely distributed throughout the human body. It is implicated in a variety of biological processes ranging from cellular proliferation and wound healing to tumour invasion and organ fibrosis. In the kidney, HA is weakly expressed in the cortical region; however, its expression is greatly altered during the process of renal inflammation and fibrosis. Renal proximal tubule cells produce HA *via* the action of two hyaluronan synthase (HAS) isoforms: HAS2 and HAS3. The aim of this work was to investigate the regulation and function of HA in the proximal tubule cell which is the most common cell type in the renal cortex.

This work has demonstrated that:

i. HK-2 cells, a proximal tubule cell line, produce two distinct extracellular HA structures, namely: peri-cellular HA coats and HA cables. HA cables can mediate monocyte binding and prevent access to potential inflammatory receptors as ICAM-1.

ii. BMP-7, a known renal protective cytokine, has a role in HA regulation in the proximal tubule cells. BMP-7 increased the formation of HA cables. This increase in HA cables resulted in increased monocyte binding which was CD44-dependent. This novel anti-inflammatory mechanism of BMP-7 is partially due to its alteration of the dynamics of HA metabolism (synthesis and degradation). IL-1β, a known pro-inflammatory cytokine, did not stimulate HA cable formation although it stimulated HA synthesis.

iii. Hyaluronan synthase 2 (HAS2) over-expression resulted in increased HA production by HK-2 cells. This resulted in the formation of big peri-cellular HA coats and increased intracellular HA. HA cable formation, however, was reduced. Functionally, the peri-cellular coats were shown to be important in cell migration and inhibition of HA coat formation resulted in reduction of the enhanced cell migration. The reduction in HA cables was associated with a reduction in monocyte binding.

iv. Hyaluronan synthase 3 (HAS3) over-expression also resulted in increased HA production. Although HAS3 is known to be the constitutive HAS isoform in HK-2 cells (unlike the inducible HAS2), over-expression of HAS3 resulted in increased HA cable formation in addition to increased peri-cellular HA coats. Functionally, HAS3 over-expression resulted in enhanced cell migration and increased monocyte binding.

v. HA binding proteins (Hyaladherins) differentially affected extracellular HA structures. Inter-alpha-trypsin inhibitor (IαI) is important in the formation of HA coats as well as HA cables. Tumour necrosis factor-stimulated gene-6 (TSG-6) is seen to be crucial to the formation of HA coats but not HA cables, while the role of versican in either structures is not fully determined yet although it is thought to be more crucial to the formation of HA cables.

Publications & presentations to learned societies

Publications:

Wisam Selbi, Carol de la Motte, Vincent Hascall, Anthony Day, Timothy Bowen and Aled Phillips: Characterisation of hyaluronan cable structure and function in renal proximal tubular epithelial cells. *Manuscript in preparation.*

Wisam Selbi, Anthony J. Day, Marilyn S. Rugg, Csaba Fülöp, Carol A. de la Motte, Timothy Bowen, Vincent C. Hascall and Aled Phillips: Over-expression of hyaluronan synthase 2 alters hyaluronan distribution and function in proximal tubular epithelial cells. *Journal of American Society of Nephrology*, in press.

Wisam Selbi, Carol de la Motte, Vincent Hascall and Aled Phillips: BMP-7 modulates Hyaluronan-mediated Proximal Tubule-Monocyte interaction. *Journal of American Society of Nephrology*, 2004 May; 15:1199-1211.

Presentations:

Wisam Selbi, Carol de la Motte, Vincent Hascall and Aled Phillips: Hyaluronan Synthase 2-derived pericellular Hyaluronan: Effects on Renal Proximal Tubule cells. October, 2004; *33rd American Society of Nephrology (ASN) meeting*, St. Louis, USA; Poster.

Wisam Selbi, Carol de la Motte, Vincent Hascall and Aled Phillips: Hyaluronan coats and cable-like structures: Effects on Renal Proximal Tubule Cells. June, 2004; *Welsh Association of Renal Physicians and Surgeons annual meeting*, Carden Park, North Wales, UK; Oral.

Wisam Selbi, Carol de la Motte, Vincent Hascall and Aled Phillips: BMP-7 modulates Hyaluronan-mediated Proximal Tubule-Monocyte interaction. November, 2003; *32nd American Society of Nephrology (ASN) meeting*, San Diego, USA; Poster.

Abbreviations

b-HABP	Biotinylated-hyaluronan binding protein
BMP-7	Bone morphogenic protein-7
CA	Cell-associated fraction
CD44	Cluster of differentiation 44
cDNA	Complementary DNA
CM	Conditioned medium fraction
CS	Chondroitin sulphate
Da	Dalton
D-MEM	Dulbecco's-modified Eagle's medium
DN	Diabetic nephropathy
dNTP	Deoxynucleotide triphosphate
dpm	Disintegration per minute
DTT	Dithiothreitol
ECM	Extracellular matrix
ER	Endoplasmic reticulum
ERK	Extracellular signal-related kinase
ESRD	End-stage renal disease
FACS	Fluorescence activated cell sorting
FCS	Foetal calf serum
FITC	Fluorescein Isothiocyanate
GN	Glomerulonephritis
HA	Hyaluronan
HAS	Hyaluronan synthase
HC	Heavy chain
HK-2	Human kidney cells-2
HYAL	Hyaluronidase
IαI	Inter-alpha-trypsin inhibitor
ICAM-1	Intercellular adhesion molecule-1
IL-1	Interleukin-1
IU	International unit
kDa	Kilodalton
MAPK	Mitogen activated protein kinase

MCP	Monocytes chemotactic protein
mRNA	Messenger RNA
MW	Molecular weight
NO	Nitrous oxide
ORF	Open reading frame
PαI	Pre-alpha inhibitor
PAGE	Polyacrylamide gel electrophoresis
PBS	Phosphate-buffered saline
PCR	Polymerase chain reaction
PDGF	Platelet-derived growth factor
PG	Proteoglycans
PMN	Polymorph neutrophils
RE	Restriction enzyme
RT	Room temperature
RT-PCR	Reverse transcription-PCR
RHAMM	Receptor of hyaluronan-mediated motility
rpm	Revolutions per minute
SD	Standard deviation
SDS	Sodium dodecyl sulphate
TGF-β1	Transforming growth factor-beta1
TE	Trypsin-accessible cell-surface extract
TNF-α	Tumour necrosis factor-alpha
TSG-6	Tumour necrosis factor-stimulated gene-6
VCAM-1	Vascular adhesion molecule-1
WB	Western blotting

Table of contents

Chapter I

General introduction

1.1 The kidney: Functional anatomy and basic physiology

Adult human kidneys are 11-14 cm (about 3 vertebral bodies) in length, and are located retroperitoneally on either side of the aorta and inferior vena cava in the upper dorsal region of the abdominal cavity. The right kidney is usually a few centimetres lower because the liver lies above it. Both kidneys rise and descend several centimetres with respiration. Each kidney contains approximately 1 million nephrons (functional units; figure 1.1) and weighs approximately 15 g. There is a rich blood supply, 20-25% of cardiac output, although there is considerable physiological variation in this. Intralobular branches of the renal artery give rise to the glomerular afferent arterioles.

Renal functions can be broadly classified into four categories: (*i*). Maintenance of homeostasis via regulation of extracellular fluid volume and composition, and acid-base balance. (*ii*). Hormonogenesis: as the production of renin which is important in regulating renal blood pressure, and erythropoietin which increases the number of circulating erythrocytes. (*iii*). Vitamin D3 activation; A function performed by the proximal tubule cells, and (*iv*). Gluconeogenesis: This is acquired by the kidney only in unusual circumstances such as prolonged starvation and confers the ability to synthesize and secrete glucose produced from non-carbohydrate sources (such as amino acids) (reviewed in [1]).

The functional unit in the kidney is the "nephron". Each nephron is composed of one glomerulus, a proximal convoluted tubule, a loop of Henle, a distal convoluted tubule and a collecting duct. The structure of the nephron is illustrated in figure 1.1B.

The basement membrane around the glomerular capillaries and the cells lying on either side of it form the filtration barrier. This allows free passage of water and small solutes; cells and large molecules are retained in the glomerular capillaries. Variations in the calibre of the afferent and efferent arterioles control the filtration pressure at the glomerular basement membrane (GBM). This is normally tightly regulated in order to maintain a constant glomerular filtration rate (GFR) despite varying systemic blood pressure and renal perfusion pressure. In response to a reduction in perfusion pressure, constriction of the efferent arteriole restores filtration pressure. This response of the efferent arteriole is dependent on angiotensin II production. After leaving the glomerulus, the efferent arteriole goes on to supply the distal nephron and medulla [1].

The glomerulus contains three main cell types: endothelial, epithelial and mesangial cells. The GBM is produced by fusion of the basement membranes of the endothelial and epithelial cells. Both of these cells are specialised in structure and function. The glomerular endothelial cells contain pores (fenestrae) which allow access of circulating molecules to the underlying GBM. On the other side of the GBM, glomerular epithelial cells (podocytes) put out multiple long foot processes which interdigitate with those of adjacent epithelial cells. These are non-dividing cells whose integrity is critical to the structure and function of the glomerulus. The death of the podocytes may lead to adhesion of the underlying GBM to Bowman's capsule, followed by the formation of a focal glomerular scar. The normal filtration barrier requires integrity of the junctions between the epithelial cells and the epithelial slit diaphragm apparatus as well as the GBM itself. The filtration barrier at the glomerulus is normally absolute to proteins the size of albumin (67 kDa) or larger, with those of 20 kDa or less able to filter freely. Between these sizes there is a gradient of clearance, the behaviour of individual molecules being influenced by their shape and charge. Anionic proteins are relatively less freely filtered than cationic proteins. Little lipid is filtered. Mesangial cells lie in the central region of the glomerulus. They have similarities to vascular smooth muscle cells (e.g. contractility), but also some macrophage-like properties. In health, bone marrow-derived macrophages are occasionally found in glomeruli and in the interstitium. Tubular cells (discussed below) are polarised, with a brush border (proximal tubule), lying on their own basement membrane at their base (figure 1.1C and D). Interstitial cells between tubules can be classified into two main types. Fibroblast-like cells in the cortex are capable of producing erythropoietin in response to hypoxia in addition to its production of the ECM components while lipid-laden interstitial cells are believed to be important in prostaglandin production and are mostly found in the inner medulla [1].

1.2 Renal proximal tubule cells (PTCs)

1.2.1 Histology

The renal proximal tubule extends from the glomerulus to the thin limb of the loop of Henle. Its average length is 15 mm and its diameter approximates 60-70 μm. PTCs are the most abundant cell type in the cortex. Cells of the proximal tubule are continuous with parietal epithelial cells of the glomerulus (podocytes) while the tubular lumen is continuous with the urinary space. *In vivo*, the proximal tubule is lined by a single layer of polarized columnar epithelial cells with characteristic features such as (figure 1.1C and D): *(i)* The presence of tight junctions between cells. *(ii)* Extensive lateral inter-digitations making it difficult to see the outlines of individual cells between adjacent cells. *(iii)* Irregularly-spaced nuclei. *(iv)* Clear vesicles in the apical pole beneath the brush border reflecting extensive apical endosomal system and *(v)* Large numbers of mitochondria, which provide the energy source for fluid and electrolyte reabsorption. The apical aspect of the PTCs has a special feature of brush borders, which result in a 40-fold increase in the surface area of the cells [1].

1.2.2 Function in health and disease

The polarized structure of PTCs is important to maintain their unique function in electrolyte, acid-base and solute balance. PTCs also contribute to tubular basement membrane formation as they can secrete collagen type IV and laminin.

PTCs are antigen-presenting cells and contribute to the body's ability to distinguish its own cells from foreign bodies. PTCs express several key immune surface molecules known to assist in the presentation of antigens and to coordinate the T-cell response to infection. Examples of these molecules are human leukocyte alleles (HLA) class II antigens and adhesion molecules (mainly inter-cellular adhesion molecule-1; ICAM-1) (reviewed in [2]). Through a series of soluble and cell-based cytokines and cytokine receptors as well as other molecules the blood cell-derived immune system and the PTCs communicate and interact with each other. It is interesting that PTCs are derived from the same embryonic compartment as bone marrow cells, which give rise to the body's blood and immune system. Moreover, circulating bone marrow stem cells are capable of engrafting into the kidney and of differentiating into renal tubular cells in animal models of acute renal failure [3].

PTCs also have the capacity to acquire a myofibroblastic phenotype during renal injury. Transforming growth factor-β1 (TGF-β1) is thought to play an important role in the regulation of epithelial-mesenchymal transdifferentiation (EMT). Addition of TGF-β1 resulted in *de novo* expression of fibroblasts-specific protein-1 (Fsp-1) in cultured rat PTCs with the acquisition of fibroblastic markers (such as vimentin and α-smooth muscle actin) and loss of epithelial markers (such as cytokeratin) [4].

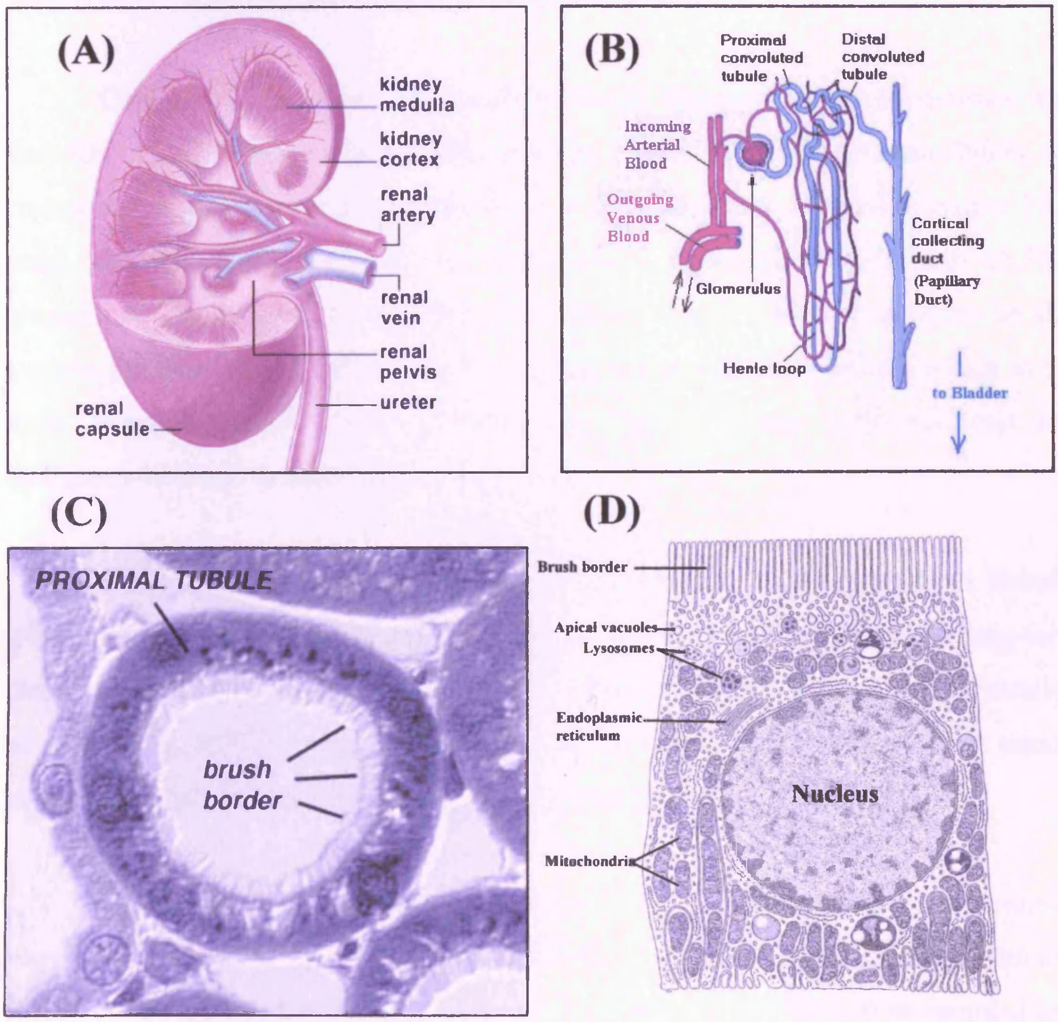

Figure 1.1: The kidney, the nephron and the proximal tubule.

(A) The kidney and its main macroscopic structures. **(B)** Structure of the nephron. **(C)** Cross-section of the proximal tubule shown by electron microscopy. **(D)** A schematic diagram of one proximal tubule cell with its main organelles. Adapted from: http://www.members.tripod.com/vzajic/nephron.

1.3 Chronic Renal Failure and End-Stage Renal Disease

Definition, causes and consequences

Chronic renal failure (CRF) is a progressive irreversible loss in renal function which classically develops over a period of years. Initially, it is manifested only as a biochemical abnormality. Eventually, loss of the excretory, metabolic and endocrine functions of the kidney leads to the development of the clinical symptoms and signs of renal failure, which are referred to as uraemia. End-stage renal disease (ESRD; with glomerular filtration rate [GFR] < 5 ml/min) is the final stage of CRF which is incompatible with life without renal replacement therapy.

CRF may be caused by any condition which destroys the normal structure and function of the kidney. In about 75% of cases (UK renal registry report 2004), the causes are established as: congenital diseases (e.g. polycystic kidney disease 6.1%), renal vascular diseases (7.7%; e.g. renal artery stenosis), hypertension (5.1%), glomerular disease (9.4%; with IgA nephropathy being the most common in this group), pyelonephritis (7.6%), systemic diseases (e.g. diabetes mellitus which is the most common specific cause [17.9%] and systemic lupus erythematosus) and malignancies (such as myeloma).

The social and economic consequences of CRF are considerable. In Britain, about 104 new patients per million of the adult population are accepted for long-term dialysis treatment each year. In spite of the availability of dialysis and transplantation as treatments, ESRD reduces the life quality and span dramatically with an annual mortality in dialysis patients ranging between 10-20% [5].

The incidence of CRF is increasing and currently in Britain the prevalence of stages 3-5 CRF (with GFR<60 ml/min/1.73m^2) in the general population is estimated as 5.1% (UK renal registry report 2004). The progression of CRF can be retarded and currently aggressive treatment of hypertension and blockade of angiotensin II by angiotensin converting enzyme (ACE) inhibitors or angiotensin II receptor antagonists in patients with proteinuria are the preferred guidelines. The search for other treatment modalities is greatly needed but it requires more understanding of the pathogenesis of CRF.

1.4 Tubulointerstitial fibrosis

Fibrosis is defined as expansion of stromal elements at the expense of highly differentiated parenchymal cells within the tissue. In renal disease, the expansion of stromal elements disrupts the kidney architecture and impairs fluid and solute exchange. The pathological changes associated with CRF and ESRD are progressive expansion of the tubulointerstitial space and subsequent fibrosis. The expansion of the interstitial volume is the result of proliferation of fibroblasts within the interstitium, infiltration of monocytes and the excessive production of matrix within the interstitium by all these cells and by the tubule epithelial cells.

1.4.1 Association with renal function

Previous structural-functional studies have shown that pathological changes in the tubulointerstitium are more related to deterioration of renal function than other histological markers (like glomerular changes) in the kidney [6, 7]. This correlation are reported in different renal diseases including diabetic nephropathy [8-10], chronic sclerosing interstitial nephritis, mesangioproliferative GN, membranoproliferative GN [11, 12] and renal amyloidosis [13]. Furthermore, in experimental models of renal disease, treatments that improved renal function appeared to reduce interstitial fibrosis. For example, prednisolone administration leads to a reduction in the interstitial infiltrate and increment in GFR but had no effect on glomerular sclerosis in experimental focal glomerular sclerosis [14] while the response in diabetic nephropathy to angiotensin II antagonist treatment is reflected by resolution of tubulointerstitial fibrosis and not of glomerulosclerosis [15].

1.4.2 Pathogenesis of tubulointerstitial fibrosis

Recent studies have focused on the molecular basis of interstitial fibrosis due to the strong correlation between the degree of interstitial fibrosis and loss of renal function. While glomerulosclerosis often occurs in parallel and may share some pathogenetic features, there are likely to be events that are unique to each region of the kidney as well. Few growth factors and vasoactive molecules initiate responses that culminate in fibrosis while many other factors trigger events that contribute indirectly to fibrosis. Observations from *in vivo* and *in vitro* experiments in this field point to the fact that it is unlikely that any single molecule acting in isolation will be able to trigger the full spectrum of fibrotic events. The fibrogenic cascade has been arbitrarily divided into 4 sequential phases [16]: Cellular activation and injury phase, the fibrogenic signalling phase, the fibrogenic phase and finally, the destructive phase.

1. Cellular activation & injury phase: subdivided into:

A. Tubular cell activation

In response to various injurious stimuli, tubular cells begin to produce molecules that propagate renal injury, facilitate interstitial inflammation and/or directly contribute to fibrosis (figure 1.2). PTCs are capable of producing various cytokines including: TGF-β1 [17], ET-1 [18], TNF-α [19], PDGF-B and IL-6 [20], MCP-1 [21] and IL-8 [22]. In addition, PTCs express receptors for a number of these molecules [19, 23-26]. The tubular cells may be exposed to bioactive molecules that originate in the plasma or inflamed glomeruli and appear in the glomerular ultra-filtrate (apical activation) [27]. In some diseases such as diabetes, PTCs may be exposed to conditions of elevated glucose either apically as a result of glycosuria, or basally as a result of elevated interstitial tissue concentrations of glucose. Regarding diabetes, *in vitro* studies have shown that high glucose conditions applied apically or basolaterally produced the same incremental effect on fibronectin secretion that was detected in the basolateral compartment only [28] while TGF-β1 production is only triggered by basolateral exposure to glucose. In addition, high glucose conditions induced type IV collagen secretion and reduced net gelatinolytic activity [29]. Tubular activation may also be modulated in response to other events that occur during the course of chronic renal disease including increased filtration of other urinary proteins (chemoattractants, complement proteins and cytokines), increased ammoniogenesis, ischaemia, lipiduria, tubular hypermetabolism and tubulointerstitial crystal deposition [30].

B. Inflammatory cell infiltration

Regardless of aetiology, progressive renal disease is characterized histologically by an interstitial infiltrate of mononuclear cells. Circulating leukocytes migrate from blood vessels into tissues under both normal and pathological conditions. In inflammation, their capture and subsequent migration is a multi-step process involving rolling, activation and firm adhesion to the endothelial cells followed by transmigration into the underlying tissue. This process is characterized by the sequential activation of adhesion molecules and their ligands on both leukocytes and endothelial cells following a co-ordinated response to inflammatory mediators [31, 32].

Leukocyte adhesion molecules such as selectins, leukocyte integrins and members of the immunoglobulin super family (ICAMs and VCAMs play a vital role in the process of leukocyte recruitment (discussed below). Each of these adhesion molecules has its own mode of action that facilitates the co-ordinated sequence of events which results in the presentation of leukocytes to the inflammatory site. In chronic renal disease, the tubules have been noted to express *de novo* or to up-regulate their expression of several leukocyte adhesion molecules as ICAM-1, VCAM-1 and osteopontin that may facilitate mononuclear cell recruitment [33-36].

As a source of several profibrotic molecules, monocytes and macrophages in particular are thought to directly contribute to the fibrogenic process [37]. Although most of these cells have migrated from the circulation through the peritubular capillary endothelium into the interstitial space, some may originate from *in situ* proliferation of resident interstitial macrophages and in anti-GBM GN, local macrophage proliferation represents the major mechanism of macrophage accumulation during the progression of the disease [38]. Chemotactic cytokines (chemokines) such as MCP-1 are believed to play an important role in monocyte recruitment. PTCs increase MCP-1 production when stimulated with pathophysiologically relevant concentrations of albumin through NF-κB activation [39]. MCP-1 production has been reported *in vivo* in both human disease [40] and in animal models of chronic renal disease [35, 41, 42]. Other potent monocyte chemoattractants that have been implicated in the pathogenesis of tubulointerstitial disease include: 1. Complement proteins (such as C3a and C5a) which are activated by tubular cells via the alternative complement pathway [43] and may also be produced (C3 mainly) by PTCs when they are stimulated with serum proteins [44]. 2. Macrophage-stimulating protein (MSP): a member of the plasminogen-related growth factors which is produced in the kidney solely by the tubular cells and leads to the induction of growth, migration, invasion and IL-6 synthesis in mesangial cells [45] in addition to its known macrophage-stimulating effects [46, 47]. 3. Albumin binding neutral lipid [48]. 4. Oxidized low-density lipoproteins [49].

C. Appearance of interstitial myofibroblasts and the activation of interstitial fibroblasts

This event is also considered as a prerequisite for renal fibrosis. Studies of human renal biopsies indicate that the presence of interstitial myofibroblasts correlates with the risk of progressive renal disease [50-52]. Myofibroblasts are characterized by their expression of α-smooth muscle actin and ED-A fibronectin [53], which are not expressed by normal fibroblasts. In addition to their unique phenotype, myofibroblasts are considerably more profibrotic than resident interstitial fibroblasts although their origin is a subject of controversy. Theories include differentiation and/or proliferation of resident fibroblasts [54], migration of perivascular cells and/or transdifferentiation and migration of tubular cells [55]. The transformation of the phenotype, function and number of tubular interstitial cells sets the stage for subsequent events. At this early phase, renal damage may be repaired and kidney function restored to normal levels. However, if renal injury persists passed this point, changes in tubular cells and ongoing interstitial inflammation will result in destructive renal scarring [16].

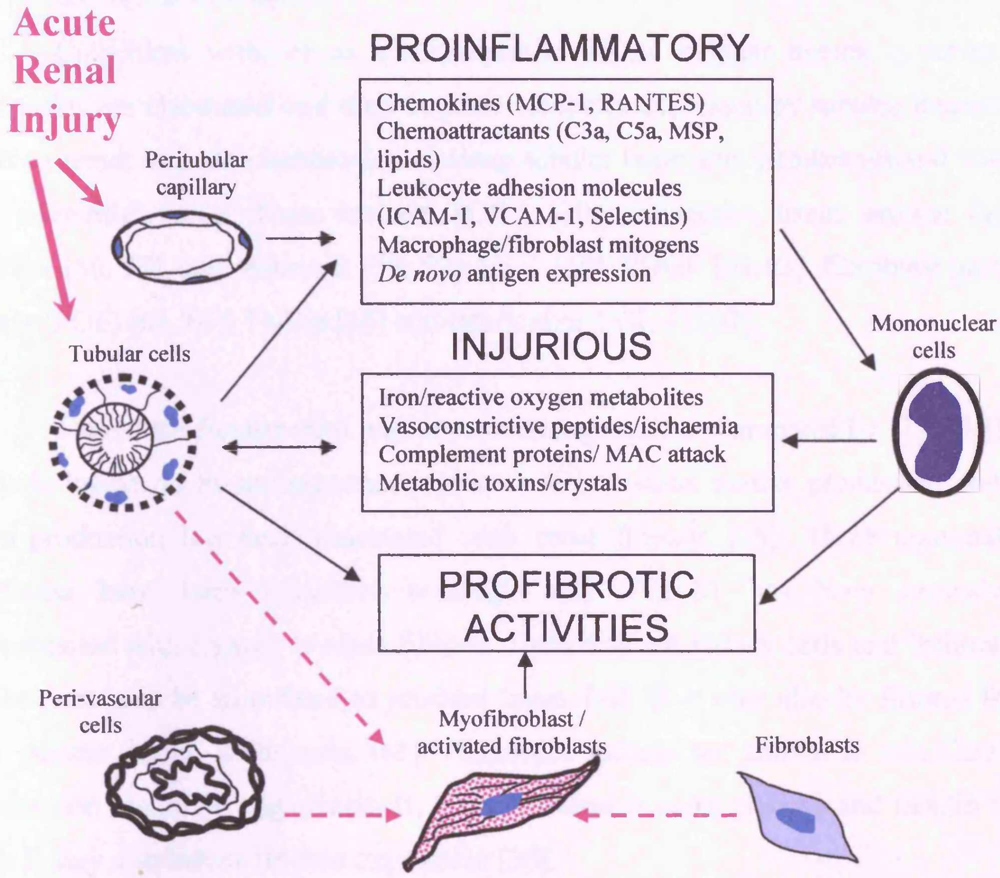

Figure 1.2: Cellular activation and injury phase.

The initial renal insult may have tubular effects that lead to the production and release of proinflammatory and injurious molecules, triggering interstitial inflammation and ongoing tubulointerstitial damage. Activation of peritubular capillary endothelial cells may facilitate the recruitment of interstitial mononuclear cells. Left unchecked, these cellular changes lead to the activation of interstitial fibroblasts and the appearance of interstitial myofibroblasts. Modified from Eddy *et al.* [16].

2. Fibrogenic signalling phase

Coincident with, or as a consequence of the cellular events, a series of molecules are elaborated and their cognate receptors expressed by tubular interstitial cells to result in matrix accumulation along tubular basement membranes and within the interstitial space. These include TGF-β [30], connective tissue growth factor (CTGF)[56, 57], angiotensin II [58, 59], ET-1 [60], PDGF [61-63], fibroblast growth factor (FGF) [64, 65], TNF-α [66] and interleukin-1 (IL-1) [67].

One of the fundamental pathways to fibrogenesis is dominated by TGF-β [16]. This is known to be an important regulator of interstitial matrix production and its over-production has been associated with renal fibrosis [16]. Three mammalian isoforms have been identified although only TGF-β1 has been extensively investigated with regards to renal fibrosis. Both resident kidney cells and infiltrating leukocytes may be stimulated to produce latent TGF-β. It may also be filtered from the plasma during proteinuria [68]. Numerous factors are known to stimulate its production including angiotensin II, ET-1, ischaemia, high glucose and insulin [69-72]. It may also induce its own expression [30].

Activation of TGF-β triggers several events that promote fibrosis. This includes the transcription of matrix-encoding genes, inhibitors of matrix degrading enzymes, inhibition of matrix binding integrin receptors, transformation of fibroblasts into myofibroblasts, transdifferentiation of tubular epithelial cells into myofibroblasts and chemotaxis of fibroblasts and monocytes [30]. Up-regulated expression of TGF-β is a feature of all human and experimental models of renal fibrosis. For example, transgenic mice over-expressing TGF-β develop glomerular and interstitial fibrosis [73, 74]. In addition, treatment of rats with replication-defective adenoviral vectors that express the soluble TGF-β type II receptor attenuates interstitial collagen accumulation in models of proteinuria and ureteral obstruction [75].

Antifibrotic factors

While the kidney is producing cytokines and growth factors that promote fibrosis, it is possible that other factors may be released to counteract these effects. Examples of these antifibrotic factors include: interferon gamma (IF-γ), hepatocyte growth factor (HGF), insulin-like growth factor-1 (IGF-1) and BMP-7 [16]. IFN-γ significantly decreases interstitial collagen accumulation when infused directly into the kidney [66]. HGF treatment of nephritic mice has been reported to inhibit tubulointerstitial fibrosis via a significant reduction in renal production of PDGF and TGF-β and interstitial myofibroblast formation [76]. TGF-β is also known to inhibit HGF formation, illustrating reciprocal interactions between these pro- and antifibrotic growth factors [68]. However, the discovery that HGF-over-expressing mice develop cystic renal disease and glomeruloscelrosis [77] illustrates the need for further studies to clarify the role of HGF in renal fibrosis. IGF-1 has been shown to significantly reduce interstitial collagen accumulation in neonatal rats with obstructive uropathy [78] while in a different setting, IGF-1 may promote fibrotic effects [79]. The anti-fibrotic effects of BMP-7 will be discussed in detail below.

3. Fibrogenic phase

The synthesis, secretion and activation of one or more of the fibrogenic molecules by tubulointerstitial cells results in the activation of a new group of genes that lead to the accumulation of ECM proteins within the interstitial space. Generally, 2 processes can lead to excessive accumulation of matrix proteins which causes progressive renal scarring: a. increased synthesis and b. decreased degradation [16].

Excessive ECM production

Evidence for increased matrix protein synthesis includes increased matrix gene mRNA levels in the kidney, noting that transcription is the rate-limiting step of protein expression for most matrix molecules, and the *de novo* appearance of proteins that are not normally present in the renal interstitium [16]. The interstitial scar consists of several molecules and the unique functional role of each constituent remains unclear. These include normal interstitial matrix proteins (collagens I, III, V, VII, XV and fibronectin) and matrix proteins that are usually restricted to tubular basement membranes (collagen IV and laminin) (reviewed in [30]). Limited *in situ* hybridization studies indicate that interstitial myofibroblasts are the primary source of these proteins although tubular cells and other interstitial cells may contribute as well [80]. Novel proteins include splice variants of fibronectin and novel chains of laminin and type IV collagen that are produced by damaged kidneys. In addition to providing structural support, these matrix proteins also interact with cellular receptors especially of the integrin family. As a consequence, the nature of the interstitial matrix may significantly influence the behaviour of the neighbouring cells. Fibronectin also has chemotactic properties that may perpetuate interstitial inflammation [16].

The interstitial scar can be viewed as a dynamic scaffold that changes as the renal disease progresses. Initially, the scaffold is relatively unstable and susceptible to degradation. With time, cross-linking bridges add stability and confer relative resistance to proteases. This maturing process is poorly understood but may involve enzymatic modification by glycosylation, oxidation or transglutamination [81]. Changes in matrix composition such as the ratio of collagen I to collagen III may also contribute to the stabilizing process.

Another class of molecules that plays an essential role in the composition of the interstitium are secreted proteoglycans, whose core protein is covalently bound to high molecular weight glycosaminoglycans such as chondroitin and heparin sulphate. Proteoglycans may act as a potential reservoir for growth factors such as bFGF and TGF-β. These sequestered growth factors are generally inactive but represent a reserve that could be readily mobilized. Decorin and biglycan are small proteoglycans that have the ability to bind and inhibit TGF-β. They too may accumulate in the kidney during progressive scarring [82-84].

Impaired matrix remodelling and decreased ECM degradation

Matrix remodelling is the result of multiple concurrent processes that vary according to the initiating stimulus. The processes during renal fibrosis not only involve changes that stabilize the scaffold, but events that may also break down and degrade some of the proteins [16]. A key step during the initiation of renal fibrosis is the production of protease inhibitors. At exactly the same time that matrix synthesis is accelerated, the enzymatic machinery that regulates this process by degradative remodelling is inactivated. The potential power of this process should not be underestimated considering that early renal fibrotic lesions can be completely reversed, presumably by matrix-degrading protease activity, if the primary process is halted. As examples, reversible tubulointerstitial fibrosis has been demonstrated in rats with acute nephrotic syndrome [85] and in humans with diabetic nephropathy [86]. It is possible that some types of progressive renal disease are caused by impairment of renal collagenolytic activity alone with little or no change in the rate of collagen synthesis. This has been demonstrated in rats that develop renal fibrosis after ligation of a renal vein or ureter [87]. Several matrix-degrading proteases are synthesized by normal kidney cells and are thought to help maintain normal renal architecture. The most prominent proteases are members of the matrix metalloproteinase (MMP) family although the serine proteinases (plasmin and cathepsin G) and the lysosomal cysteine proteases (cathepsin B, H and L) may also be active in the kidney [16]. Based on their perceived specificity for matrix proteins, MMPs have been sub-divided into four groups: collagenases, gelatinases, stromelysins and matrilysins. However, the high degree of overlap among MMP substrate specificities and the notion that MMPs can cleave a growing list of substrates that are not part of the ECM [88, 89] render this nomenclature imprecise. In addition to their matrix-degrading activity, MMPs are reported to have a wide range of cellular effects such as stimulating activation and proliferation (Table 1.1).

The major contributory role of tubular epithelial cells to MMP production has been emphasized by the study of Zaoui *et al.* [90] in which sequential assessment of MMP-2 and -9 in cortical, glomerular, tubular and urinary extracts showed increasing release of gelatinases (MMP-2 and -9) along the nephron segments in fructose-fed rats (a Diabetes Mellitus type II model) compared to control rats. In addition, areas of glomeruloscelrosis and tubular atrophy were concurrently stained with anti-MMP-9 antibody along with α-smooth muscle actin (a marker of myofibroblastic differentiation).

Table 1.1: Biological activities generated by MMP-mediated cleavage.
Modified from Visse *et al.* [91].

Biological Effect	Responsible MMPs	Substrate Cleaved
Keratinocyte migration and re-epithelialization	MMP-1	Type I collagen
Osteoclast activation	MMP-13	Type I collagen
Neurite outgrowth	MMP-2	Chondroitin sulphate proteoglycan
Adipocyte differentiation	MMP-7	Fibronectin
Cell migration	MMP-1,- 2, -3 MT1-MMP	Fibronectin CD44
Mammary epithelial cell apoptosis	MMP-3	Basement membrane
Epithelial-mesenchymal conversion (mammary epithelial cells)	MMP-3	E-cadherin
Mesenchymal cell differentiation with inflammatory phenotype	MMP-2	Not identified
Generation of angiostatin-like fragment	MMP-3, -7, -9 & -12	Plasminogen
Generation of endostatin-like fragment	MMPs	Type XVIII collagen
Enhanced collagen affinity	MMP-2, -3, -7, -9, -13 (but not MMP-1)	BM-40 (SPARC/osteonectin)
Kidney tubulogenesis	MT1-MMP	Type I collagen
Increased bioavailability of IGF1 and cell proliferation	MMP-1, -2, -3 MMPs MMP-11	IGFBP-3 IGFBP-5 IGFBP-1
Activation of VEGF	MMPs	CTGF
Epithelial cell migration	MMP-2, MT1-MMP	Laminin 5γ2 chain
Apoptosis (amnion epithelial cells)	Collagenase	Type I collagen
Pro-inflammatory	MMP-1, -3, -9	Processing IL-1ß from the precursor
Tumor cell resistance	MMP-9	ICAM-1
Anti-inflammatory	MMP-1, -2, -9 MMP-1, -2, -3, -13, -14	IL-1β degradation MCP-3
Increased bioavailability of TGF-β	MMP-2, -3, -7	Decorin
Disrupted cell aggregation and increased cell invasion	MMP-3, MMP-7	E-cadherin
Reduced cell adhesion and spreading	MT1-MMP, MT2-MMP, MT3-MMP	Cell surface tissue transglutaminase
Fas receptor–mediated apoptosis	MMP-7	Fas ligand
Reduced IL-2 response	MMP-9	IL-2Rα

4. The destructive phase

As matrix proteins continue to accumulate within and expand the interstitial space, they begin to have destructive effects on kidney structures and subsequently function [16]. The increasing interstitial matrix isolates tubules from their oxygen supply (post-glomerular peritubular capillaries) in addition to its destructive effect on the capillaries themselves. Therefore, two main histological features are noted here: loss of renal tubules and loss of peritubular capillaries [92]. While the tubules atrophy, sometimes the glomeruli remain unaffected or slightly affected. Glomeruli that lack their distal nephron segment (i.e. atubular) are non-functional [93]. The hypoxic impulse is thought to have an important role in this phase as tubular cells exposed to hypoxic conditions in vitro show decreased MMP activity and increased synthesis of collagen [94].

Although it is evident now that the process of renal fibrosis is very complicated with many players at the cellular and molecular level, new studies have begun to identify possible targets for therapeutic interventions with a view of slowing, preventing and in some cases even reversing renal scar formation.

1.5 Bone Morphogenic Protein-7 (BMP-7)

1.5.1 Bone Morphogenic Proteins

Over the past 20 years, members of one subgroup of the transforming growth factor-β subfamily, named generically bone morphogenic proteins (BMPs), have been recognized as critical in controlling organogenesis (reviewed in [95]). Comprising an ever-growing number of identified homologs, the BMPs represent almost one third of the TGF-β subfamily, with more than 30 members already described. Individually, the members of this subfamily of secreted molecules are termed either BMPs, osteogenic proteins (OPs), cartilage-derived morphogenic proteins (CDMPs), or growth and differentiation factors (GDFs). They have been classified into several subgroups according to their structural similarities (table 1.2). The molecular cloning of many BMP-encoding genes and their identification as TGF-β relatives enhanced the interest in these molecules and allowed expression and functional studies to be performed. Unexpectedly, given the nature of the assay that led to the identification of these proteins, it became rapidly evident that their patterns of expression, as well as their physiological functions, were not restricted to skeleton development. Other functions of BMPs include cell proliferation and differentiation, apoptosis, morphogenesis, patterning of various organs, including the kidney and the skeleton and general organogenesis.

1.5.2 BMP-7: nature and expression

BMP-7 (also called osteogenic protein-1; OP-1) is a homodimeric member of the BMP subfamily whose broad expression has been extensively studied [96, 97]. As other members of the family, BMP-7 is synthesized as large precursor proteins that undergo proteolytic processing at RXXR sites to yield mature active dimers of disulfide-linked monomers [98]. The three-dimensional structure of the protein was reported in 1996 by Griffith *et al.* [99].

BMP-7 starts to be expressed during early gastrulation, localizing in the ectoderm at the periphery of the embryo. At 8.5 and 9.5 days post-coitum (dpc), BMP-7 is strongly expressed in the surface ectoderm and the notochord, in the neuroepithelium extending toward the prospective forebrain, and in the developing gut [96]. BMP-7 is also expressed in the atrial and ventricular chambers of the heart. This expression in the heart continues throughout development. During eye development, BMP-7 expression is detected in the surface ectoderm, the lens placode, and the optic vesicle [96]. In the developing skeleton, BMP-7 is expressed in the developing limb, in the mesenchymal cells localized between the developing digits, and in the chondrogenic zones. In many cells of the developing kidney, BMP-7 plays a critical role. At 9.5 dpc, BMP-7 transcripts are detected in the Wolffian ducts, which give rise to the ureteric buds. At 12.5 dpc, BMP-7 is expressed, predominantly, in the ureteric bud epithelium but weaker expression is also detected in the surrounding condensed mesenchymal cells. Later on, its transcripts are present in the same structures but also in the peritubular aggregates and the podocytes of the glomeruli [100, 101]. BMP-7 can also promote nephrogenesis by isolated metanephric mesenchyme [102], and act as a survival factor for the nephrogenic mesenchyme by preventing apoptosis and expanding the progenitor cell population in conjunction with basic fibroblast growth factor (bFGF) [103]. Also worth noting is that BMP-7 is the only member of the BMPs for which expression is not overlapped in the metanephric mesenchyme, suggesting the possibility of a unique role for BMP-7 in metanephric development.

Consistent with their wide pattern of expression, mutations in BMP-encoding genes can affect many organogenetic processes. Some of these mutations cause early embryonic lethality precluding, for now, the analysis of the role of these proteins during skeleton development. The deletion of the gene encoding BMP-7 causes a perinatal lethality in mice caused by uraemia. In the absence of BMP-7 there is a failure of kidney morphogenesis, the deficient mice exhibiting small dysgenic kidneys that have less than 3 glomeruli per histological section compared with approximately 100 in normal mice. This defect was tracked down to an epithelial-mesenchymal interaction occurring between 12.0 and 12.5 dpc and leading to cell death of the metanephric mesenchymal cells [100, 101]. A series of molecular analyses suggest that BMP-7 is one of the earliest glomerular inducers.

In the adult animal, BMP-7 expression subsides in other organs but remains high in the kidney. BMP-7 RNA expression in the normal kidney is largely confined to the medullary tubules (tentatively identified as collecting tubules), peripheral glomerular cells (presumptive podocytes) and renal artery adventitial cells [104, 105]. The study by Gould *et al.* confirmed the previous reports and showed that BMP-7 expression is detectable in mouse collecting duct, thick ascending limb, distal convoluted tubule and podocytes within glomeruli with no expression in the proximal tubule cells [106]. Nevertheless, PTCs expressed mRNA for known BMP receptors including: ActR-I, BMPR-IA, ActR-II, ActR-IIB and BMPR-II [106]. However, the physiological functions of BMP-7 in the adult kidney, unlike the pathophysiological effects, remain unclear.

Table 1.2: Bone morphogenic protein superfamily.
Modified from von Bubnoff *et al.*[95].

BMP	Major tissue of expression	Other names	Mammalian cDNA sequenced
BMP-2	Cartilage, bone	BMP-2a	Bovine, human, mouse, rat, reindeer
BMP-3	Cartilage, bone, ovary	Osteogenin	Bovine, human, rat
BMP-3b	Muscle, bone, brain, lung	GDF-10	Human, rat, mouse, reindeer
BMP-4	Cartilage, bone, prostate	BMP-2b	Human, mouse, reindeer
BMP-5	Bone		Bovine, human
BMP-6	Cartilage	Vgr-1	Bovine, human, mouse, rat
BMP-7	Bone, kidney	OP-1	Bovine, human, mouse, rat
BMP-8a,b	Testis, placenta	OP-2, OP-3	Human, mouse
BMP-9	Liver	GDF-2	Human
BMP-10	Bone, heart		Human, mouse
BMP-11	Neurogenesis		Human, mouse
BMP-12	Cartilage	GDF-7, CDMB-3	Human, mouse
BMP-13	Cartilage	GDF-6, CDMB-2	Human, mouse, bovine
BMP-14	Cartilage	GDF-5, CDMB-1	Bovine, mouse, human
BMP-15	Oocytes	GDF-9	Human, mouse

1.5.3 BMP-7 in renal diseases

It is known now that during renal injury, BMP-7 expression in the kidney is decreased as well as BMP-7 serum levels [107]. Recent studies have shown that BMP-7 prevents kidney damage *in vivo* in numerous animal models of disease. In models of renal ischaemia, administration of BMP-7 reduces severity of renal injury and suppresses inflammation by down-regulation of intercellular adhesion molecules [104]. Interstitial inflammation and fibrogenesis associated with unilateral ureteral obstruction (UUO) are also prevented *in vivo* by administration of BMP-7 [108]. This is consistent with *in vivo* studies demonstrating counteraction of TGF-β1-induced epithelial-to-mesenchymal transition and reversal of chronic renal injury in the nephrotoxic serum nephritis model by BMP-7 [109]. In the streptozocin model of diabetic nephropathy, BMP-7 therapy markedly ameliorated glomerular pathology, decreased tubulointerstitial volume and reduced proteinuria [110].

In vitro studies shed some further light on the mechanistic basis of the mode of action of BMP-7. In mesangial cells, BMP-7 reduces TGF-β1-induced ECM effects [111]. Specific membrane-bound, high affinity BMP-7 receptors have also been characterised on adult rat kidney tubular cells [112]. BMP-7 also antagonises TNFα-stimulated increases in expression of pro-inflammatory cytokines and chemokines in PTCs [106]. This is of particular significance as it is clear that progression of renal disease best correlates with the degree of interstitial fibrosis [10, 113-115]. Recent *in vitro* studies suggest that BMP-7 counteracts TGF-β1 mediated changes in PTC phenotype, favouring retention of an epithelial cell phenotype, and inhibiting the epithelial-to-mesenchymal transition [109]. This resulted from a direct Smad-dependent counteraction of the TGF-β1 signalling pathway by BMP-7, which reversed chronic renal injury. Interestingly although these data suggest that BMP-7 may modify PTC response to TGF-β1, at least *in vitro*, BMP-7 does not directly affect expression of TGF-β1 [116].

1.6 Leukocyte adhesion molecules

The infiltration of leukocytes to sites of injury is a highly complex but well-orchestrated event. When injury occurs, a number of relatively small proteins (like cytokines, chemokines and products of infectious agents) are released from the site of damage. These in turn up-regulate a variety of carbohydrate-rich protein molecules, on the endothelial cell surfaces of the blood vessels in the area, that are capable of slowing down, selecting and firmly capturing leukocytes [117]. The class of leukocytes captured initially depends on the array of adhesion molecules on the endothelium. The major steps of adhesion, described primarily for neutrophils, have included a primary event, during which leukocytes are engaged by the vessel wall and then retarded by a repeated transient interaction, followed by release. This results in a stuttered traversing of the length of the vessel known as "rolling", which is followed by a secondary firm adhesion of the rolling cells and subsequent transmigration [31, 32]. Primary adhesion is attributed in many systems to the interaction between the lectin domain of members of the selectin family and their carbohydrate ligands on endothelial cells, whereas secondary adhesion is due to heterodimeric β2 integrins interacting with their endothelial cell ligands (members of the immunoglobulin superfamily) (reviewed in [118]).

1.6.1 The immunoglobulin superfamily (IgSF)

Since the concept of the immunoglobulin superfamily was proposed in 1982 [119], it has been expanded to embrace over 70 members, including both single- and multi-gene representatives. The IgSF represent a group of structurally heterogeneous proteins that contain at least one extracellular Ig domain and all cells of the body express members of this IgSF.

ICAM-1 (CD54) is a transmembrane glycoprotein of 505 amino acids with a molecular weight ranging between 80-114 kDa depending on cell type (due to differences in the degree of glycosylation). ICAM-1 expression can be detected in a number of cell types, including monocytes and endothelial cells. Its expression, however, is widely inducible in many cells including B and T lymphocytes, thymocytes, dendritic cells, endothelial cells, fibroblasts, keratinocytes, chondrocytes and epithelial cells [120]. In the kidney, unstimulated PTCs show little ICAM-1 expression which is inducible by TNF-α or IF-γ [121]. Ligands for ICAM-1 are: LFA-1 (CD18/CD11a) [122], which is highly expressed by monocytes [123], Mac-1 (CD18/CD11b) [124] and CD43 [125].

VCAM-1 (CD106) is another member of the IgSF consisting of 720 amino acids with a molecular weight of about 25 kDa. It is mainly a cytokine-induced (IL-1, TNF-α) molecule that is found in endothelial cells [126], mesenchymal cells [127, 128]. Normally, PTCs don't express VCAM-1 but expression is up-regulated when PTCs are stimulated with TNF-α or IF-γ [121]. The preferred ligand for VCAM-1 is VLA-4 ($\alpha4\beta1$ integrin) [129] although it can bind to other integrins such as $\alpha4\beta7$ [130].

Although the IgSF contains many members, only ICAM-1 and VCAM-1 are known to mediate leukocyte adhesion to non-endothelial cells such as fibroblasts and epithelial cells [131]. Therefore, they are the most likely members of the IgSF to participate in leukocyte accumulation in extravascular tissue.

1.6.2 The integrin family

The integrins are a family of heterodimeric membrane glycoproteins expressed on diverse cell types which function as the major receptors for ECM and as cell-cell adhesion molecules. All integrins consist of two-covalently associated subunits, α and β. As adhesion molecules, the integrins play an important role in numerous biological processes such as platelet aggregation, inflammation, immune function, wound healing, tumour metastasis and tissue migration during embryogenesis [132]. The main "leukocyte-borne" integrins are: LFA-1, Mac-1, VLA-4 and $\alpha4\beta7$.

Lymphocyte-function associate molecule-1 (LFA-1 or CD11a/CD18) is $\alpha L\beta2$ integrin that is restricted to the haematopoietic tissue. LFA-1 is mainly constitutively expressed on most leukocyte populations, being especially abundant on lymphocytes and monocytes, but it is also up-regulated in activated T-cells [133]. LFA-1 has a key role in mediating leukocyte adhesion to endothelium during inflammatory responses through binding to ICAM-1. It is also involved in most immune phenomena involving T lymphocytes such as adhesion of cytotoxic T cells to their target cells, mixed lymphocyte reactions, antigen-specific and ConA-induced T cell proliferation, and T cell-dependent antibody response (reviewed in [134]). More recently *in vitro* experiments showed that interaction between monocytic LFA-1 and PTCs ICAM-1 results in activation of PTCs and increased generation of TGF-$\beta1$ [135].

Leukocyte adhesion receptor Mo1 (Mac-1 or CD11b/CD18) is another $\beta2$ integrin ($\alpha M\beta2$) that requires activation to engage in its reaction to ICAM-1. It is present on blood monocytes, macrophages and granulocytes. Mac-1 mediates PMN and monocyte adherence to endothelium and subsequently PMN extravasation to sites of inflammation [136, 137]. Mac-1 also binds complement fragment iC3b, which stimulates chemotaxis, phagocytosis and apoptosis by the leukocytes [138]. Additionally, fibrinogen, microbial products and denatured proteins may bind to this αM-type integrin [138].

1.6.3 The selectin family

Despite the diminutive size of the family (three members) and the fact that protein sequences were obtained in 1989, there is already an extensive literature on the selectins. The reason behind this productivity is the strong evidence that E-, P- and L-selectins are involved in the inflammatory response and therefore represent novel therapeutic targets. All the selectins are structurally similar and recognise the same carbohydrate moieties sialyl Lewis^x and sialyl Lewis^a and other sulphate-modified forms and their interactions are Ca^{+2}-dependent [132]. L- and P-selectins (but not E-selectin) are also reported to bind versican through its CS chains [139]. E-selectin (also termed CD62E and endothelial leukocyte adhesion molecule-1; ELAM-1) is expressed mainly on the endothelium. P-selectin (CD62P) is expressed on platelets, endothelial cells and megakaryocytes, while L-selectin (leukocyte adhesion molecule-1; LAM-1) is expressed exclusively on haematopoietic cells like neutrophils and leukocytes [140, 141]. In terms of functionality, all the selectins are involved in mediating PMN, lymphocyte and monocyte "rolling" on the endothelial cells at inflammatory sites [132], which is considered a key early step in the cascade of events required for leukocyte egress from the blood vessel. It is worth noting here that not all primary "rolling" interactions are mediated by the selectin adhesion molecules, in clonal lymphoid B and T cells as well as activated normal lymphocytes this interaction is primarily mediated by CD44/HA interaction [142].

1.7 Hyaluronan (HA)

1.7.1 History and nature

HA (*synonymous* hyaluronic acid, hyaluronate; from Greek *hyaloid* [vitreous] and uronic acid) was discovered in the vitreous humour and characterized as a polysaccharide by Meyer & Palmer in 1934 [143]. Its exact chemical structure was elucidated 20 years after its discovery [144]. Since its discovery, HA has been detected in all vertebrate organs and fluids studied with the highest concentrations found in loose connective tissues. For a long time HA was regarded as an inert filling material between the cells and hence attracted little attention. About forty years after its discovery, HA was used as therapeutic agent to treat the joints of track horses [145] and in the 1980s, HA became an established aid in ophthalmic surgery [146, 147]. Nowadays, HA has many different clinical applications which will be discussed below.

HA belongs to the glycoaminoglycan (GAG) family (formerly known as acid mucopolysaccharides) and is made of a repeated sequence of D-glucuronic acid and D-N-acetylglucosamine residues that are linked together via alternating β-1,4 and β-1,3 glycosidic bonds [144]. This disaccharide structure (figure 1.3) is then repeated to form a hyaluronan molecule or HA chain.

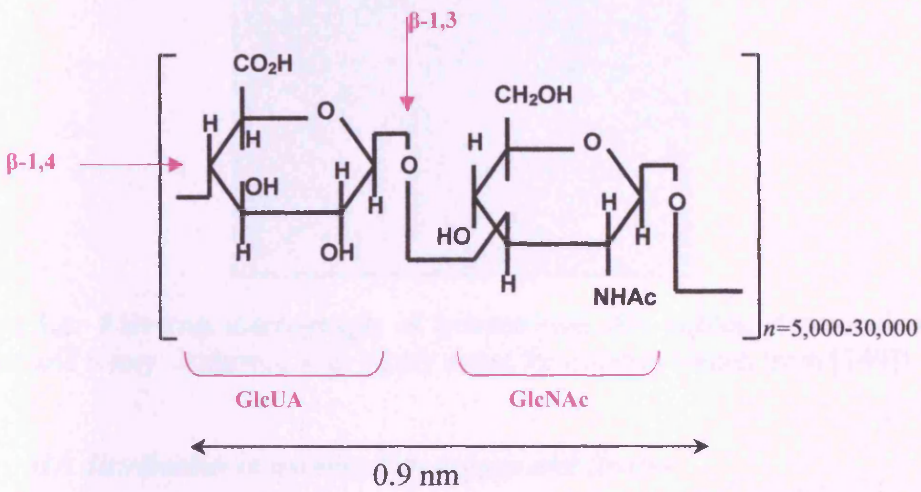

Figure 1.3: Chemical structure of HA: The repeating disaccharide unit is made of D-glucuronic acid (GlcUA) and D-N-acetylglucosamine (GlcNAc) linked via alternating β-1,4 and β-1,3 glycosidic bonds.

HA differs from other GAGs in many aspects. All GAGs, apart from HA, contain sulphate groups and their polysaccharide chains are relatively short (<50 kDa, commonly between 15-20 kDa), while the number of repeat disaccharides in a completed HA chain can approach 30,000 units in some tissues. It can, therefore, have a molecular mass of up to 10 x 10^6 Da and an extended length of more than 15 μm if straightened (figure 1.4) (reviewed in [148]). In addition, HA, unlike other GAGs, is not associated with a core protein and it is considered as the sole GAG that's produced by both mammalian cells and bacteria. In free solution under physiological conditions of pH and strength, HA forms a stiffened and expanded random coil due to hydrogen bonding of adjacent sugar units and mutual repulsion between carboxyl groups. In dilute solution it occupies a very large solvent domain but as the concentration increases, individual molecules entangle and form a continuous network. Its conformation can also be modified by interaction with numerous specific binding proteins (discussed later).

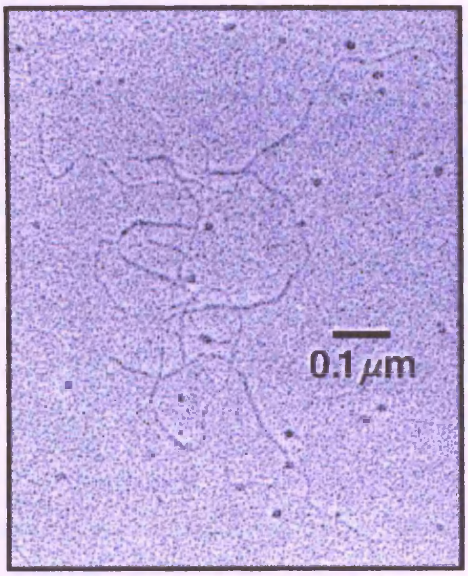

Figure 1.4: Electron micrograph of intertwined HA cables: deposited on a flat surface and rotary shadowed with heavy metal for contrast (taken from [149]).

1.7.2 HA distribution in mammalian organs and tissues

A painstaking analysis of the body of the rat by Reed *et al.* [150] should be broadly applicable to other mammals. About 56% of total HA was recovered from skin and ~27% from the skeleton and joints. The remaining HA was from muscles and internal viscera. Comparative studies in other mammals showed that the highest HA concentration is found in typical connective tissues such as umbilical cord, synovial fluid, skin and vitreous body [151, 152]. Notable amounts are also present in the kidney, lung and brain but very little in the liver. The lowest concentration is found in blood serum [153]. Regarding HA distribution in normal kidney, most of the HA is concentrated in the renal papillae with minimal amount in the cortex [154].

1.7.3 HA biosynthesis

Before conclusive reports from 2 laboratories confirmed that HA synthesis occurred at the inner surface of the plasma membrane [155, 156], HA was thought to be synthesised in the Golgi apparatus (like most GAGs) as based on electron microscopic autoradiography of cells labelled with ^{3}H-glucosamine [157]. However, metabolic labelling with ^{3}H-glucosamine is not a reliable marker for HA, since it will be incorporated into many other GAGs. Other reports raised more doubts about the direct involvement of the Golgi apparatus in HA synthesis: HA synthesis was not inhibited by monensin, which interferes with secretion in trans-Golgi vesicles [158]. HA synthesis did not require a protein primer [159] or lipid intermediates [160] and it was not inhibited by cycloheximide [161], xylosides [162] or tunicamycin [163]. Adding to the controversy, Goldberg *et al.* hypothesised that synthesis at the plasma membrane represents an "alternative" synthetic pathway as their findings showed that the ionophore monensin inhibits extracellular accumulation of HA in rat fibrosarcoma cells but not in human articular chondrocytes or rat chondrosarcoma cells [164]. This is due, as speculated by Philipson *et al.* [155], to the interruption of transport of the HA synthase to the cell surface.

HA is synthesized in the plasma membrane by a membrane-bound protein (termed HA synthase or HAS; figure 1.5) whose genetic code was determined in bacteria, mouse and human before the end of the last century. Four cDNAs have been identified and cloned in humans, and are numbered in the order they were discovered; HAS1 [165], HAS2 [166] and HAS3 (two isoforms) [167]. The chromosomal locations for the human HAS genes have also been elucidated, with HAS1 at 19q13.3-13.4, HAS2 at 8q24.12 and HAS3 at 16q22.1 [167]. The HAS enzyme adds sugar units from nucleotide precursors to the chain on the cytoplasmic aspect of the membrane and translocates the growing chain to the pericellular space and unlike the synthesis of other GAGs, HA synthesis occurs at the reducing end of the chain [168]. It is worth noting here that to date more than 20 HA synthases have been recognized in a variety of organisms, all these but one (isolated from *Pasteurella multocida*) comprise a family of proteins with shared structural and mechanistic features (reviewed by Weigel *et al.* [169]).

Although it is widely accepted that HA synthesis occurs at the plasma membrane as mentioned above, recent reports suggest intracellular HA synthesis. Majors *et al.* suggested that a "dormant" HAS isoform is present on/close to the endoplasmic reticulum (ER) and is activated when the ER is stressed [170]. Also, work from the Cleveland group showed that HAS2 is closely situated to the nucleus of colonic smooth muscle cells that were stimulated with viral-mimic RNA (De La Motte, CA and Hascall, VC – personal communication).

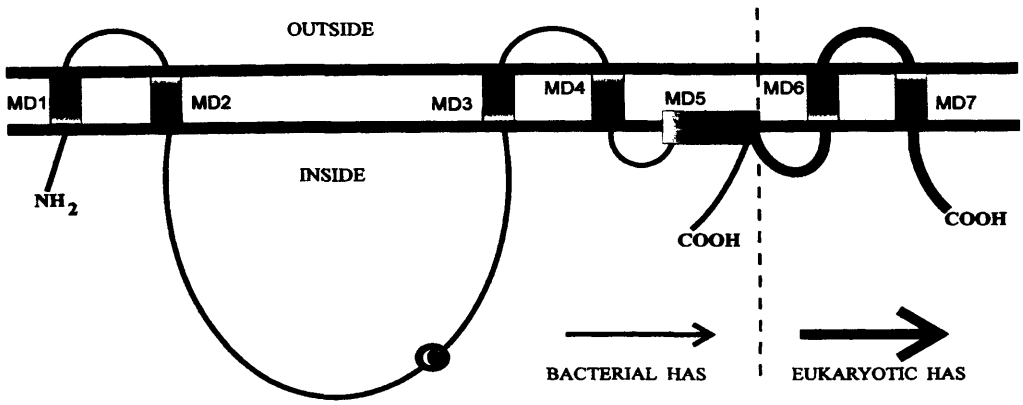

Figure 1.5: Proposed membrane topology for the HAS family: Very similar hydropathy plots and primary structure (28-71% identity) among all the HAS isozymes suggest that they are similarly organized within the membrane. The scheme depicts the N and C termini and the large central domain, between MD2 (Membrane Domain) and MD3, inside the cell (where HA synthesis occur). The larger eukaryotic HASs (thick line with 7 MDs) have additional amino acids in all regions compared with the bacterial HASs (thin line with 5 MDs), except for the highly conserved carboxyl 178 residues of the central domain and MD1-MD5. The conserved Cys is indicated by the circled C. MD5 can be modelled as an amphipathic helix, which would orient the C terminus of all HAS members inside the cell (adapted from Weigel *et al.* [171]).

1.7.4 Mechanism of HA synthesis by the HAS proteins

Virtually all known enzymes catalyse a reaction that uses one or two (or more rarely, three) substrates to produce one or two products. The HAS enzymes are an exception to this rule. HA synthase has two different enzymatic activities within the same enzyme [172]. The HA product after each sugar addition becomes a substrate for the next sugar addition. The overall reaction for the synthesis of one HA disaccharide unit is shown in the formula below:

$$\text{UDP-GlcA} + \text{UDP-GlcNAc} + (\text{HA})_n \longrightarrow (\text{HA})_{n+1} + 2\,\text{UDP}$$

One HA disaccharide unit is added to the HA chain using the substrates uridine diphosphate glucuronic acid (UDP-GlcA) and uridine diphosphate N-acetylglucosamine (UDP-GlcNAc). Although the synthase is only adding one HA disaccharide unit, it must exhibit six different functions to achieve this process. It requires two specific binding sites for the UDP-GlcA and UDP-GlcNAc sugar precursors and two different glycosyltransferase activities for the addition of the substrates to the HA chain by β-1,3 and β-1,4 linkages. It also requires a binding site that anchors the growing HA polymer to the enzyme and a ratchet-like transfer reaction that moves the growing polymer one sugar at a time [168, 172]. This later activity is likely coincident with the stepwise advance of the polymer through the membrane as HA was shown to be synthesised at the inner surface of plasma membrane [156]. All these activities are present in a relatively small protein ranging from 419 (*Streptococcal pyogenes* HAS) to 558 (*Xenopus laevis* HAS) amino acids. In addition, all the available evidence supports the suggestion that only *Streptococcal pyogenes* HAS protein is required for HA biosynthesis in bacteria or *in vitro* although reports indicate that the larger eukaryotic HAS family members are part of multicomponent complexes [173]. Since the eukaryotic HAS proteins are ~40% larger than that of *Streptococcal pyogenes*, their additional protein domains could be involved in more elaborate functions such as intracellular trafficking and localization, regulation of enzyme activity and mediating interactions with other cellular components.

1.7.5 Enzymatic properties of the three human HAS isoforms

Although the 3 HAS isoforms are expressed in mammalian cells, all catalyse the same biosynthetic reaction. Each isoform when individually expressed in mammalian cells, with no intrinsic ability to synthesize HA, leads to *de novo* biosynthesis of HA [174], thus each HAS protein appears to be independently active. However, the respective HAS transfectants differ in their ability to form HA matrix when HAS isoforms are individually expressed at similar levels as HAS1-transfectants formed significantly smaller coats than HAS2- or HAS3-transfectants [174].

Because the biological and physiological roles of HA are related to its size, it is important to determine the molecular sizes synthesised by different HAS isoforms. HAS1 and HAS3 transfectants secreted HA with an estimated molecular weight of 2×10^5 to 2×10^6 Da while HAS2 secreted HA of more than 2×10^6 [174]. These findings suggest that the size distribution of the products may be partly determined by the intrinsic enzymatic properties of HAS proteins. In agreement with this theory, the recombinant protein of each HAS isoform synthesized HA of different size *in vitro* [174]. However, HA synthesized by recombinant HAS3 was significantly smaller in molecular weight than that secreted from the transfectants. It is therefore more likely that the intracellular environment and additional mechanisms involving accessory molecules affect the molecular size distribution of HA.

1.7.6 Transcriptional and post-transcriptional regulation of HAS

The metabolism of HA is a dynamic process in vertebrates and the biosynthesis is both spatially and temporally controlled. The presence of three HAS isoforms with different enzymatic properties raises the question of whether or not the expression is also regulated in a different fashion. Several lines of evidence show that increased transcription of HAS, induced by different growth factors and cytokines, is responsible for the increase in HA production, and that transcriptional regulation is unique to each gene and is stimulus-specific [175-183]. For example, Kennedy *et al.* have shown that while both IL-1β and TNF-α stimulated HA synthesis in adult fibroblasts, IL-1β stimulation led to an increase in HAS1 mRNA with no effect on either HAS2 or HAS3 while TNF-α increased HAS3 mRNA with slight effect on HAS1 and no effect on HAS2 [177].

A variety of potential binding sites for transcription factors have been found in the promoter region of the mouse HAS1 gene including: CCAAT box, AP-2, GATA and GAGA [184]. Recent work from our laboratory has shown the absence of the common TATA box, while CCAAT and Sp-1 binding sites were detected in the promoter region of human HAS2 gene (Monslow J *et al.* – unpublished observation).

Physical stimuli also affect HA regulation, Yung *et al.* demonstrated that mechanical injury to a mesothelial monolayer induces HAS2 mRNA and suppresses HAS3 mRNA but with a net increase in total secreted HA [185]. Others have reported that HAS3 mRNA (but not HAS2) was up-regulated in chick chondrocytes after applying mechanical strain [186]. Recklies *et al.* [187] demonstrated that changes in the transcriptional level of HAS genes did not always correlate with changes in the secretion of HA after the exposure of synovial cells to growth factors and the response to these growth factors was cell-type specific. This suggests that the synthesis can also be regulated post-transcriptionally.

Regarding HA regulation in PTCs, neither TGF-β1 nor PDGF had an effect on HA generation while IL-1β or high glucose stimulated HA synthesis via NK-κB activation [175]. Notably here, the increase in HA generation was concomitant with up-regulation of HAS2 mRNA with no effect on HAS3 mRNA and inhibition of either gene transcription or protein synthesis abolished HA synthesis in response to IL-1β or high glucose. Increased HA generation was also noted in mechanically wounded PTC monolayers but the mechanism of this increment was not elucidated in that study [188]. Thus, the regulation of HA synthesis by HAS proteins appear to be a multifaceted process involving enzymatic properties and both transcriptional and post-transcriptional regulation.

1.7.7 Manipulation of the HAS genes: lessons from knockouts and over-expressions

The presence of multiple HAS proteins implies that each isoform has a different biological significance. Genetic manipulation of HAS may provide clues as to the respective roles of the isoforms in the broad range of physiological functions performed by HA. The study by Camenisch *et al.* [189] demonstrated that HA was virtually absent in HAS2$^{-/-}$ E9.5 mouse embryos. Lack of HA (in these mice) led to defective HA-mediated epithelial-to-mesenchymal transformation (EMT) and finally to severe cardiac malformations and embryonic fatality. Interestingly, the HAS2 knockout embryos closely resembled that of heart defect (*hdf*) mice lacking the HA-binding protein versican (discussed below), showing that a composite matrix requiring HA and versican is essential for forming cardiac jelly to support cushion morphogenesis and subsequent cardiac development. However, heterozygous mice for HAS2 were fertile and exhibited no obvious abnormalities. Moreover, HAS1 or HAS3 knockout mice were viable and fertile (Itano, Kimata, Spicer and McDonald, unpublished data).

Increased synthesis of HA is often related to tumour malignancy. Genetic manipulation of HAS genes in cancer cells allows one to investigate the role of HA in tumour formation and progression. Over-expression of HAS2 enhanced anchorage-independent growth and tumourigenicity of human fibrosarcoma [190]. Similarly, over-expression of HAS3 promoted the growth of a prostate cancer cell line along with increased angiogenesis [191]. While HAS1 over-expression restored the metastatic ability of mouse mammary carcinoma cells that were defective in HA synthesis [192]. Taken together, these findings suggest that HAS isoforms differ in their involvement in tumour progression. While the HA synthesized by HAS2 or HAS3 may play roles in cancer growth, HAS1-derived HA may participate in conferring tumour metastasis. However, some reports conflict with the above. For example, HAS2 transfection of glioma cells caused a reduction in tumour growth rate [193] and anti-sense inhibition of HAS2 or HAS3 significantly diminished adhesion of prostate cancer cells to bone marrow endothelial cells [194] suggesting that HAS2 and HAS3 are also involved in cancer metastasis. These conflicting results could be attributable to the characteristics and expression levels of HAS isoforms and the differences in cell types used for transfection.

1.7.8 HA turnover and degradation

Before discovering that lymphatic vessels carry a considerable amount of HA from the tissues to the blood [195], it was thought that all HA turnover occurred within the tissue. However, in densely structured tissues such as bone and cartilage, it is probable that HA turnover occurs by metabolic degradation *in situ* concurrently with that of collagen and other proteoglycans since there is no lymphatic drainage. In skin and joints, about 20-30% of HA turnover occurs by local metabolism and the rest is removed by the lymphatic pathways. Metabolic studies have shown that the half-life of a HA molecule in different tissue varies greatly [196-198]. The half-life of the polymer in skin and joints is about 12 h; in the anterior chamber of the eye it is 1-1.5 h although in the vitreous body it is about 70 days. On reaching the blood stream, about 85-90% is eliminated in the liver by receptor-facilitated uptake and catabolism in the hepatic sinusoidal endothelial cells. The kidneys extract about 10% but excrete only 1-2% in urine. The normal fractional turnover of plasma HA in humans is about 15-35% per minute, which explains the low plasma levels in the face of high lymphatic input (reviewed in [199]). This means that approximately one-third (~5 g) of total HA in the human body is metabolically removed and replaced during an average day. This rapid turnover was unexpected as HA has been regarded as a structural component in connective tissue and structural components are usually quite stable. However, the rapid turnover facilitates the use of HA in physiological regulatory mechanisms.

HA can be degraded via the action of oxygen free radicals, peroxynitrites and ultraviolet (UV) irradiation or by the hyaluronidase (HYAL) family of enzymes [200, 201]. Hyaluronidase activity was first identified as a "spreading factor" in extracts from mammalian testes. The term "hyaluronidase" was introduced by Karl Meyer in 1940 to denote the enzymes that degrade hyaluronan. In humans, six HYAL genes have been identified. They occur in clusters of three at two chromosomal locations. HYAL1, HYAL2 and HYAL3 make up the cluster on chromosome 3p21.3 and share about 40% similarity. HYAL4, HYALP1 and SPAM1 (Sperm adhesion molecule 1) make up the second cluster on chromosome 7q31.3. These genes code respectively for HYAL1-4 and PH-20. With the possible exception of HYAL4 and PHYAL1 (a pseudogene), all the HYALs degrade HA [202, 203].

The degradation of HA occurs in a stepwise fashion with quantum decreases in polymer size. From the cluster on chromosome 3, HYAL1 and HYAL2 constitute the major hyaluronidases of somatic tissues. HYAL2 cleaves high molecular weight HA to a limited product of approximately 20 kDa (about 50 disaccharide units) and is bound to the plasma membrane by a glycophosphatidylinositol (GPI)-anchor [204] (although a portion of HYAL2 also occurs in a soluble form). Beside its function in HA digestion, HYAL2 has been reported to have a role in oncogenesis by acting as a cell surface receptor for some retroviruses [204]. On the other hand, evidence of tumour suppressor function of HYAL2 is also available as HYAL2 can accelerate apoptosis [205] and suppress tumour growth in mice [206].

HYAL1 appears to be lysosomal, cleaving the 20 kDa chains (produced by HYAL2 action) into small HA disaccharides (reviewed in [207] & [208]) which are further degraded by the action of 2 enzymes on the non-reducing end: a beta-glucuronidase and a beta-N-acetyl glucosaminidase to yield glucuronic acid and N-acetylglucosamine [209]. HYAL1 is also the only plasma hyaluronidase [210] with no known tissue origin and the only urine hyaluronidase [211]. Although it is considered as a lysosomal enzyme, it has a pH optimum of 3.8, well below the pH 4.5 inside the lysosomes.

Very little is known about HYAL3. Transcripts have been found in the brain and liver, but the protein product remains uncharacterised [212]. Expression occurs in chondrocytes [213], and increases when fibroblasts undergo chondrocyte differentiation [214]. There may be coordinate expression of HYAL2 and 3 as they are both up-regulated by inflammatory cytokines such as TNFα, whereas HYAL1 is not [213].

PH-20 is expressed in testes. It facilitates the penetration of sperm through the cumulus mass that surrounds the ovum and has a role in fertilisation [215]. At first thought to be sperm-specific, it is now known to be expressed in the epididymis [216], female genital tract [217], breast [218] and foetal tissues [202].

1.7.9 HA signalling pathway

HA signalling can be mediated via several HA receptors. Generally, epithelial cells express mainly CD44 [219], although RHAMM is also reported to be expressed in epithelial cell such as bronchial epithelial cells [220]. The biochemical mechanisms by which HA-CD44 interactions are transduced into intracellular signals that bring about cellular effects are the subject of many investigations. The binding of CD44 isoforms to HA affects cell adhesion to ECM components and is implicated in the processes of aggregation, proliferation, migration and angiogenesis [221-224]. It is clear, that in some cell types, the multivalent interaction of polymeric HA with CD44 causes clustering of CD44 in the plasma membrane and that this event is associated with phosphorylation of CD44, interactions with the cytoskeleton and changes in cell behaviour [225, 226]. It has been shown that activation of various components of intracellular signalling pathways including Rac1 [222, 227], phosphoinositide 3'-kinase [228], erbB-2 [229], c-Src kinase [230] and NF-κB [231, 232] and that rearrangement of cytoskeletal elements, e.g. ankyrin [233] and ezrin [234] result from interaction of HA with CD44 in different cell types.

Hyaluronan is also involved in the regulation of MMP expression although its effect is variable. HA-CD44 interaction down-regulated MMP-9 mRNA expression in osteoclast-like cells [235] and reduced cell migration. On the other hand, increased MMP-9 expression in chondrocytes was shown upon degrading HA [236], an effect that was suppressed by anti-CD44 Ab and unseen upon adding high molecular weight HA to these cells. More recently, HA-oligosaccharides have been reported to induce MMP-9 and MMP-13 but this induction is neither CD44- nor RHAMM-dependent [237].

The binding of exogenous HA to cell surface RHAMM plays a key role in activating signal cascades, probably as a co-receptor for integral membrane proteins. Although the role(s) of intracellular RHAMM protein forms are not yet known, their ability to associate with kinases [238, 239], calmodulin [240, 241] and the cytoskeleton [240, 242] predicts that they play key roles in cytoskeletal assembly. Cell surface RHAMM has been shown to activate signalling pathways including Src [238], extracellular signal-regulated kinase (Erk) [243], and Ras [244, 245]. This is reviewed in greater detail in [246].

CD44 and RHAMM can perform separate functions in regulating cell signalling. For instance, CD44, but not cell surface RHAMM, can mediate adhesion of endothelial cells to HA and regulate proliferation [247]. In contrast, cell surface RHAMM, but not CD44, is required for migration of B lymphocytes and endothelial cells [247, 248]. In addition, cell surface RHAMM but not CD44 appears to be essential for activation of protein tyrosine kinase cascades by endothelial cells in response to HA [243]. On the other hand, HA-CD44 but not RHAMM interactions have been implicated in the cellular uptake of HA, which in turn affects growth regulation and tissue integrity [249, 250]. Deletion of either CD44 or RHAMM does not result in embryonic lethality and, therefore, either these two proteins share some functions and/or other cellular hyaladherins are able to compensate for the loss of CD44 or RHAMM [246].

There is growing evidence for the presence of intracellular HA. It was first found to be intracellular when it was isolated from rat brain nuclei in 1976 [251] but this report did not receive widespread attention. More recently, intracellular HA has been detected in the cytoplasm of vascular smooth muscle cells during late prophase/early prometaphase of mitosis and in key subcellular compartments such as the nucleus and lamellae during cell locomotion and following serum stimulation [252, 253]. In addition, the identification of intracellular HA binding proteins

(IHABPs), including RHAMM, P32, CDC37 and IHABP4 lends further support to the intracellular presence of HA [254-256].

Intracellular HA can be derived from either the extracellular environment by internalisation [252] or synthesised from an as yet unidentified intracellular source [257]. There is evidence that intracellular HA is seen during mitotic events after viral infection [258] and following the onset of ER stress [170].

1.7.10 Hyaluronan in the kidney

In the normal kidney, HA is expressed mainly in the interstitium of the renal papilla (figure 1.6) and alteration in papillary interstitial HA has been implicated in regulating renal water handling by affecting physicochemical characteristics of the papillary interstitial matrix and influencing the interstitial hydrostatic pressure [154]. The lipid-laden interstitial cells are thought to be the major source of hyaluronan synthesis in the inner medulla and therefore they function to regulate hydration as the amount of medullary hyaluronan correlates with the hydration state [259].

More recently, alterations in HA synthesis within the glomerulus of the kidney have been implicated in the pathogenesis of renal diseases such as diabetic nephropathy [260, 261]. In animal experiments, Mahadevan *et al.* demonstrated increased HA production in the glomeruli of diabetic rats [260]. *In vitro* studies from this group also demonstrated that HA production in response to a raised glucose environment can contribute to mesangial hypercellularity [261].

Although HA is not a major constituent of the normal renal corticointerstitium, it is known to be expressed around proximal tubular cells after renal injury caused by diverse diseases [262-265]. Interaction of CD44 with HA participates in the tubulointerstitial inflammatory response in the murine model of tubulointerstitial nephritis [262]. The function of CD44-HA interactions has been implied in the regenerating proximal tubule, participating in the process of recovery after ischaemic injury [263]. Increased HA in acutely rejected human kidney grafts was also identified [266]. Furthermore, the previous study has demonstrated the correlation of CD44 and HA expression in the glomeruli and interstitium with proteinuria.

Clinically, interstitial CD44 and HA expression have also been found to be correlated with changes in creatinine clearance rate. Increased deposition of interstitial HA has been shown to correlate with both proteinuria and renal function in progressive renal disease [267].

Previous work from our laboratory has examined the regulation of HA synthesis by renal PTC *in vitro* under conditions that mimic the diabetic state or inflammatory conditions [175]. These studies have demonstrated that exposure of PTC to elevated D-glucose concentrations or IL-1β leads to NF-κB-dependent transcriptional activation of the HA synthase HAS2 and stimulation of HA synthesis. Previous work has also characterized PTC expression of the HA-receptor CD44 and demonstrated that stimuli inducing HA synthesis by PTC also regulate PTC-HA interactions, with increased binding and internalization resulting from post-translational modification of CD44 by O-glycosylation [219]. *In vitro*, HA oligosaccharides induce PTC chemokines and leukocyte adhesion molecule expression [268, 269]. These findings suggest a role for HA in the pathogenesis of renal interstitial inflammation.

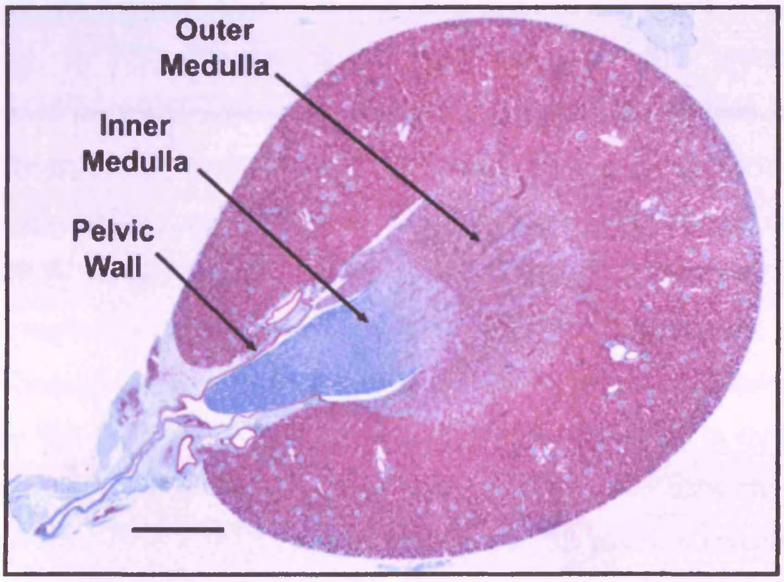

Figure 1.6: HA in the kidney: Alcian blue staining of normal rat kidney revealing distribution of hyaluronan in inner medulla. Bar = 2 mm (taken from Knepper *et al.* [270]).

1.7.11 Extracellular HA structures: coats and cables

Several cell types exhibit highly hydrated, HA-dependent pericellular matrices or 'coats'. They are usually 5-10 μm in thickness and can be destroyed by hyaluronidase treatment [271-273]. These pericellular matrices provide the essential environment for certain biological processes like proliferation and migration [253]. During tissue formation or remodelling, such matrices provide a hydrated, fluid environment in which assembly of other matrix components and presentation of growth and differentiation factors can readily occur without interference from the highly structured fibrous matrix usually found in fully differentiated tissues. Embryonic mesenchymal cells, including the precursors of muscle and cartilage, embryonic glial cells, neural crest cells and even some embryonic epithelial cells exhibit prominent pericellular matrices. In some cases, such as cartilage, the pericellular coat is a unique structural component that protects cells and contributes to the characteristic properties of the differentiated tissue (reviewed in [274]). The HA pericellular structures are also reported to have some hyaladherins in them: aggrecan [275], versican [276], PTX3 [277], TSG-6 [278] and IαI [279], and are thought to be anchored directly to the cell via the CD44 receptor [280].

Much less work has been done regarding HA cable-like structures because of their novelty. In 1999, De La Motte *et al.* reported, while investigating the mechanisms of increased leukocyte adhesion in inflammatory bowel disease, that monocytes bound preferentially via their CD44 receptor and not via their β_2-integrins [281] to virally-infected smooth muscle cells that express high levels of VCAM-1. Further work by the same group showed that the increase of leukocyte binding was due to their interaction with HA cable-like structures [258], and that IαI has a crucial role in the formation of these structures. These HA cables also stain positive for other hyaladherins like versican although this is not thought to be crucial in cable formation (De La Motte, CA – personal communication). Majors *et al.* have shown that the formation of HA cables is linked to the induction of ER stress in colonic and aortic smooth muscle cells [170], while Wang *et al.* have linked the cable formation in mesangial cells to high glucose exposure [282]. All the reports above have shown leukocytes binding to HA cables and speculated that these cable structures are involved in certain pathological conditions, namely inflammatory bowel disease and diabetes mellitus. The cellular origin(s) of these cables remains elusive. Theories include a dormant HAS isoform that is present on the ER and is activated once the cell is stressed to produce these unique structures [170]. Also, it is thought that HA cables, unlike HA coats, are attached to their cells of origin via their synthesising enzymes i.e. HAS and are not attached to CD44 receptors.

1.8 Hyaluronan-binding proteins: The Hyaladherins

The many and differing biological roles of HA are thought to be due not only to its intrinsic properties but to the proteins bound to it. These are called the hyaladherins [283]. The figure from Day and Prestwich [283] gives a schematic representation of the structure of the currently known hyaladherins (figure 1.7). The link module superfamily includes proteins that bind HA through one or more common consensus binding sites known as the link module (thus named after it was first described in a link protein). Of direct relevance to this work are: CD44, TSG-6 and versican (of the link module superfamily) and IαI which does not contain the link module.

Also shown in figure 1.7, are other proteins that bind HA via alternative mechanisms. Of note is RHAMM, the second major cell surface receptor for HA which also does not contain the link module.

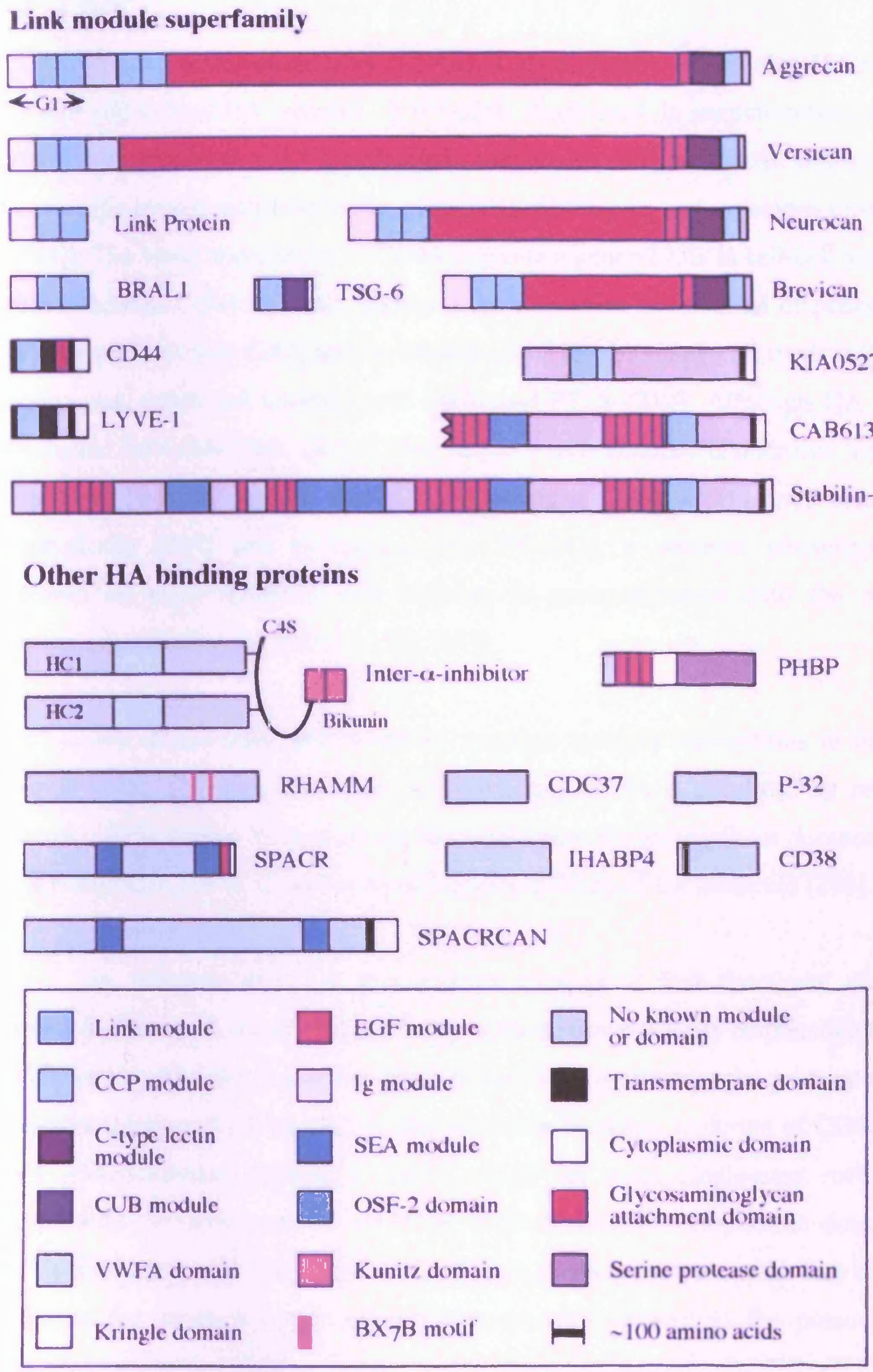

Figure 1.7: The modular organisation of the hyaladherins.
Taken from Day and Prestwich [283].

1.8.1 CD44

Cluster of differentiation-44 (CD44), a glycoprotein termed also H-CAM, is the major cell surface HA receptor. It is widely distributed. In haematopoietic tissue, CD44 is expressed on B and T lymphocytes, monocytes and neutrophils. Other CD44-positive cells include epithelial cells, glial cells, fibroblasts and myocytes (reviewed in [284]). The broad distribution of CD44 suggests a general role in cell-cell and cell-matrix adhesion. CD44 has been shown to be important in retention of pericellular matrix by chondrocytes [280] and in catabolism of HA by many cell types including chondrocytes, epidermal keratinocytes [285] and PTCs [219]. Although HA is the main ligand for CD44 [286, 287], CD44 variants with attached chondroitin sulphate are able to bind fibronectin, laminin and collagen [288]. CD44 may also bind homotypically [289] and to osteopontin [290-292], a secreted phosphoprotein expressed on many epithelial cell surfaces in communication with the outside environment including the nephron [293, 294].

CD44, unlike other HA receptors, requires multiple interactions to hold its substrate [295]. The data show that CD44 binding to HA is regulated by receptor clustering [295], degree of sulphate moiety addition to the extracellular domain [296] and glycosylation [297], as well as by alternative splicing of the molecule [298].

The structure of CD44 glycoprotein consists of four functional domains (figure 1.8). The distal extracellular domain is the region primarily responsible for the binding of HA. The membrane-proximal extracellular domain is the primary site of alternative splicing of CD44 mRNA that produces the many isoforms of CD44. The CD44 transmembrane domain is fairly typical of most single-pass membrane glycoproteins. In most isoforms of CD44, a 70-amino-acid cytoplasmic domain or "tail" is also expressed. This cytoplasmic domain exhibits protein motifs that indicate a capacity for interaction with cytoskeleton proteins as well as the potential for intracellular signalling [298].

In addition to its major function as an anchoring protein for HA-rich pericellular matrices, CD44 contributes to HA internalization (leading to HA degradation) [298] and is also linked to inflammation, cancer metastasis and invasion (reviewed in [299]). For example, CD44/HA interactions have been reported to be important in the pathology of arthritis [300], atherosclerosis [301], lung [250] and skin inflammation [302]. While in the haematopoietic cells, ligation of CD44 with cross-linking antibodies activates peripheral blood T cells, causing increased IL-2 levels [303, 304]. Likewise, monocytes treated similarly release higher levels of the pro-inflammatory cytokines IL-1 and TNF-α [304, 305]. Macrophage CD44/HA interaction has been shown to up-regulate IL-12 as well as the chemokines RANTES, macrophage inflammatory protein-1α (MIP-1α) and MIP-1β [306]. In addition to signalling the production of soluble mediators, DeGrendele *et al.* have shown that activation of T cell-associated CD44 is required for leukocyte extravasation into inflammatory sites [307], and Brooke *et al.* have shown that CD44 is critical to the secondary leukocyte recruitment observed during inflammation of the central nervous system and in experimental encephalomyelitis [308]. CD44 is reported to mediate leukocyte motility on HA-coated plates [309], although other HA receptors (like RHAMM) are present on PMN leukocytes. Also, CD44 on the surface of leukocytes has been shown to enhance their functions including cell killing and phagocytosis [310, 311].

In the normal kidney, CD44 expression is weak with few CD44-positive interstitial and urothelial cells [312]. However, CD44 expression is reported to be increased in several pathological conditions like lupus nephritis [312] and acute ischaemic injury [263]. It is thought that *de novo* CD44expression after renal injury is vital in the process of re-epithelialization which is mediated via cellular proliferation and migration across portions of denuded proximal tubule basement membrane [263]. Primary PTCs express at least 5 CD44 variants [219], with the most prominent variant expressed being CD44s (s for standard; also called CD44H since it is the most predominant variant in haematopoietic cells). CD44 expressed by the PTCs binds and internalizes HA although its mRNA expression is not altered by stimuli that increases HA generation in these cells [219].

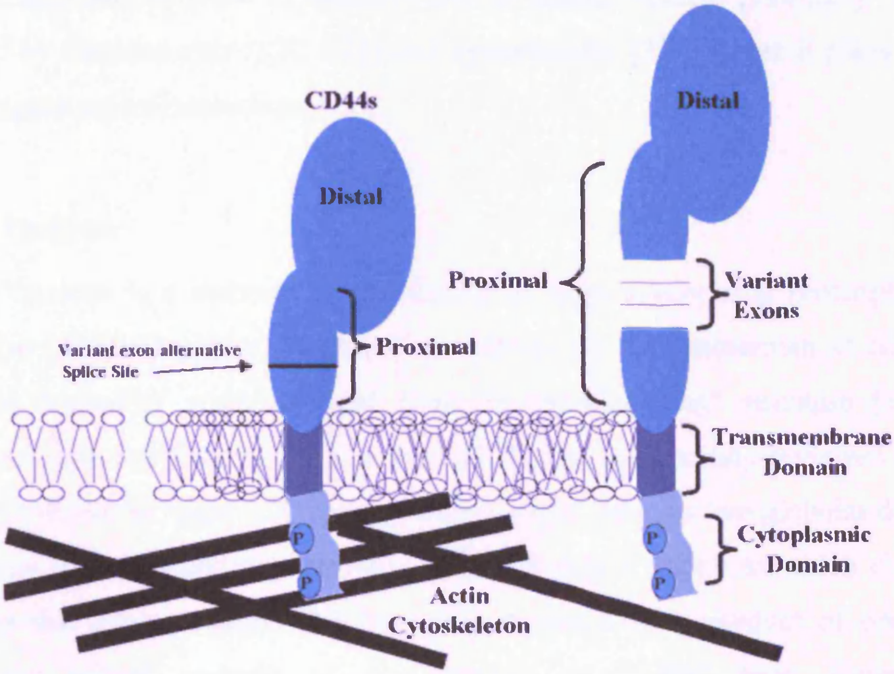

Figure 1.8: Protein Domains of CD44.

The four principal protein domains of CD44 are diagrammed including (1) the distal extracellular domain (link protein-homologous domain), (2) the membrane proximal extracellular domain, (3) the transmembrane domain, and (4) the intracellular cytoplasmic domain. Also shown is an isoform of CD44 containing protein extensions within the membrane proximal extracellular domain (3 exons shown in yellow). These protein extensions are absent in CD44s, the most common isoform of CD44. Adapted from [298].

1.8.2 TSG-6

Originally, TSG-6, (also called TNF-induced protein-6; Tnfip-6) was reported as a gene of unknown function, which was regulated in mesenchymal cells by TNF-α [313]. The secreted protein product of this gene (~35 kDa) is now known to contain a consensus binding site for HA, known as the link module as shown in figure 1.7. The tertiary structure of its binding site has been elucidated [314]. TSG-6 is known to form a stable, covalent complex with the HC of IαI [315], and several cooperative functions have been ascribed to the complex as mentioned earlier [315].

Under normal conditions, TSG-6 serves a role in reproductive physiology in the process of ovulation [315], and cervical ripening [316]. Under pathological conditions, TSG-6, probably through a mechanism involving its link module, is a potent inhibitor of PMN migration [317], which is an important inflammatory event. Up-regulated TSG-6 is also associated with the inflammatory process of rheumatoid arthritis and osteoarthritis in humans and in animal models [318-321]. TSG-6 is secreted by chondrocytes [322, 323] and synoviocytes [324] where it plays a part in down-regulating inflammation.

1.8.3 Versican

Versican is a member of the family of large aggregating proteoglycans, or hyalectins [325]. The term "versican" was proposed by Zimmerman *et al.* from its potential "versatile" reactivity and from its "proteoglycan" structure [326]. The macromolecule was first reported in 1983 [327] and was recently reviewed by Wight [325]. As shown in figure 1.7, versican core protein contains two globular domains at the amino (G1) and carboxyl termini (G3) and a mid region to which chondroitin sulphate side chains attach. The protein is a single gene product of one of four alternately spliced variants of the versican or CSPG2 gene. Expressed by mesenchymal cells, it can be present at molecular weights greater than 10^6 Da [325, 327] depending on the number and size of the chondroitin sulphate side chains. The G1 domain contains two copies of the specialized HA-binding link protein molecule. The carboxy terminus G3 domain contains two EGF-like repeats, and a lectin-like domain that can bind to other matrix proteins such as fibulin 1 [328]. Due to the molecule's complexity, this protein is capable of binding many ligands simultaneously, a feature that makes it important to matrix organisation.

Reports have shown the versican can be an important component of matrix during the normal processes of proliferation and cell migration [276]. Mitogens that induce smooth muscle cell proliferation, such as PDGF and TGF-β, induce versican [276]. Certain cancers are also associated with increased levels of versican [329]. Versican can play a role in embryonic development, where site-specific expression of this proteoglycan seems to direct cell migration in the development of the neural crest and heart [325].

Versican, through its multiple binding moieties, may be important in cross-linking HA to other matrix structures, and may participate in leukocyte adhesion. Recently, L-selectin, a leukocyte receptor important to inflammatory extravasation [132](discussed later), has been shown to be a counter-ligand for versican [139, 330, 331]. Association of versican, mostly in conjunction with HA, is observed in pathological conditions as atherosclerosis [332], lung oedema [333], asthma [334], lipid-induced renal damage [335], and skin aging [336]. Based on the known properties of versican and its involvement with other inflammatory conditions, exploring the function of versican may provide insights into changes in renal disease.

1.8.4 Inter alpha trypsin inhibitor

The IαI family is a group of serum protease inhibitors that binds to proteases with a weaker affinity than other, more abundant serum inhibitors. This family includes four plasma proteins, designated according to their behaviour in non-denaturing electrophoresis at pH values greater than 8 (figure 1.9): free bikunin, pre-α-inhibitor (PαI), inter-α-like inhibitor (IαLI) and IαI. Each of the last three proteins exists as distinct assembly of one bikunin chain covalently linked with one or more unique HCs designated HC1, HC2 and HC3. The covalent inter-chain link in the molecules is quite unusual as it is made up of a chondroitin 4-sulphate glycan bond that has been termed a protein-glycosaminoglycan-protein (PGP) cross-link [337].

The three chains and the bikunin chain are encoded by four genes on three different chromosomes [338]. The bikunin component, which carries a 7 kDa chondroitin sulphate chain, is responsible for the protease activity of these family members (reviewed in [339]). A unique feature of these protease inhibitors is their ability to inhibit both soluble and cell-receptor bound plasmin activity [340]. Despite low intrinsic plasmin inhibitory activity, the interaction of bikunin with TSG-6 potentiates the plasmin inhibitory activity [324].

IαI-family proteins are synthesised mainly in hepatocytes. The HCs, but not bikunin, are also synthesised in the brain [341]. Iida *et al.* have demonstrated increased expression of bikunin mRNA transcripts in whole kidney tissue in response to ethylene glycol-induced hyperoxaluria [342] and previous work in the Institute has demonstrated that PTCs produce PαI (1 bikunin chain + 1 HC3) [343].

IαI-related proteins are important in the formation of HA-based matrices of certain cells, including those of fibroblasts and mesothelial cells [344, 345], and of the cumulus cells during expansion of the cumulus oophorus in the pre-ovulatory follicle [346-348]. IαI is so crucial to the reproductive process that bikunin-null mice are infertile [279] because of failure of the cumulus oophorus to expand.

When IαI in serum encounters HA within extravascular tissue, as may also occur with vascular leakage during an inflammatory response, HCs can be covalently transferred from chondroitin sulphate chains to HA by transesterification and therefore may contribute to the structure of the resulting matrix. IαI HCs proteins, also termed SHAP (serum-derived HA-associated proteins), have been identified in rheumatoid arthritis in humans [349]. In addition, changes in IαI-component tissue distribution have been linked to pathological conditions as diverse such as kidney stones [350], malignancies [351, 352], and inflammation [353].

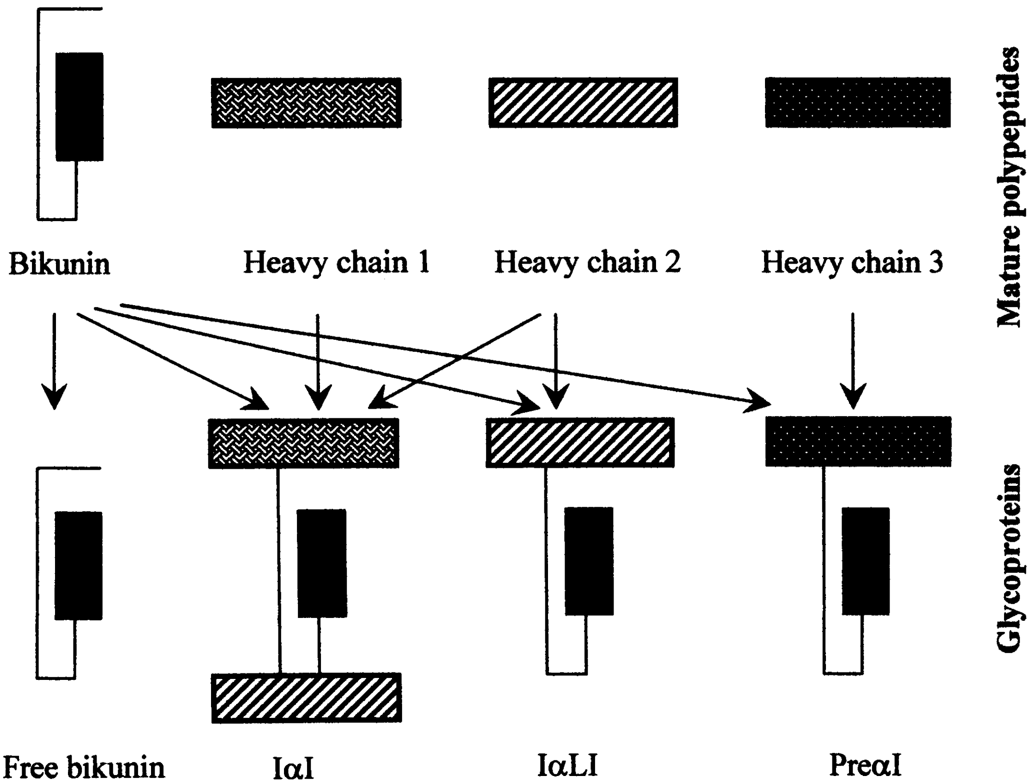

Figure 1.9: Current view of the structure of the IαI family proteins (taken from [343]).

1.9 Project aims

This thesis examines the regulation and function of HA in PTC. The specific aims were:

1. To assess the capability of PTCs to produce HA cables, and to assess the functionality of such structures if they are produced by these cells.
2. To examine the effect of BMP-7 on HA regulation and whether it influences HA cable formation and, to contrast the effect of BMP-7 of HA regulation with a known HA synthesis stimulant (IL-1β).
3. To examine the role of different hyaladherins in the formation of HA cables.
4. To examine the structural and functional consequences of HAS2- and HAS3-driven HA synthesis by using an over-expression system. This was done by: (*i*) Analysing the alterations in HA synthesis and extracellular structures (HA quality and quantity), and by (*ii*) Investigating the changes in two specific functions in the transfected cells, namely monocytes binding and cell migration.

Chapter II
Methods

2.1 Tissue culture

2.1.1 Selection of a proximal tubule cell line

In addition to the lack of human PTCs source and their relatively short *in vitro* life span, the need of repeated isolation and confirmation of preparation uniformity are major limiting factors for not using primary cells in experiments.

The HK-2 cell line was selected because it is been shown to retain the functional characteristics of fully differentiated proximal tubule cells. The HK-2 cell line has been derived by transduction of human proximal tubule cells with Human Papilloma Virus 16 E6/E7 genes. Features of the HK-2 cells identical to human proximal tubular cells include: *a.* Sodium-dependent and phlorizin-sensitive sugar transport. *b.* Adenylate cyclase responsiveness to parathyroid hormone. *c.* positive for: alkaline phosphatase, gamma glutamyltranspeptidase, leucine aminopeptidase, acid phosphatase, cytokeratin, $\alpha3\beta1$ integrin and fibronectin. *d.* negative for: Factor VIII-related antigen, 6.19 antigen and CALLA endopeptidase which are markers of distal tubular cells.

To date, extensive comparison of HK-2 cells with primary proximal tubule cells has not yielded any differences in innate behaviour (like migration and proliferation) nor in response to certain cytokines (as IL-1β and TGF-β1) [175, 188, 354, 355].

2.1.2 HK-2 cell culture conditions

HK-2 cells (American Type Culture Collection, Manassas, VA, USA) were cultured in a 1:1 mixture of Dublecco's modified Eagle's medium (D-MEM) and Ham's F12 medium (Invitrogen, Paisley, UK) supplemented with 10% bovine calf serum (Biological Industries Ltd, Cumbernauld, UK), 20mM Hepes buffer (Invitrogen), 2mM L-glutamine (Invitrogen), 5μg/ml bovine Insulin (Sigma-Aldrich, Poole, UK), 5μg/ml human Apo-transferrin (Sigma-Aldrich), 5ng/ml Sodium Selenite (Sigma-Aldrich) and 0.4μg/ml Hydrocortisone (Sigma-Aldrich). Cells were kept in a humidified incubator (Cell House 170, Heto Holten, Derby, UK) at 37^{o} C in an atmosphere of 5% CO_2. Fresh growth medium was added to the cells every 3-4 days until confluence. Confluent cells were either used in experiments, or passaged at a ratio of 1:3 to 1:5. Cells were made quiescent by removing serum 48 h prior to the start of the experiment. All experiments (except where indicated) were done in serum-free conditions.

2.1.3 Sub-culturing HK-2 cells

Confluent cells were subcultured by treatment with Trypsin/EDTA (GIBCO/BRL Life Technologies) diluted 1:1 with PBS (GIBCO/BRL Life Technologies). After 5-10 minutes, and with gentle agitation, cells were detached from the flask. The resulting cell suspension was treated with an equal volume of FCS to neutralize the protease activity. The cells were collected by centrifugation at 1500 rpm for 7 min. Cells were re-suspended in fully supplemented medium and seeded into fresh tissue culture flasks (Falcon, Becton Dickinson, Oxford, UK).

2.1.4 Selection of a monocytic cell line

Difficulties in achieving similar monocyte conditions, in addition to the relatively low yield of monocytic cells after isolation from peripheral blood samples necessitated the usage of an immortalised monocytic cell line. U937 monocytic cells were originally derived from the pleural fluid of a patient with diffuse histiocytic lymphoma [356].

Morphologically the cells are monoblastic and the histochemical profile, non-specific esterases (like ANAE, NASDAE) and β-glucuronidase reveal a monocytic lineage [356, 357]. Acid and alkaline phosphatases, which are markers of PBMN, are weakly detected in U937 cells. U937 cells release lysozyme into the culture medium, a monocyte-specific characteristic [358]. The surface of these cells bears few Fc, C3 and chemotactic peptide receptors when compared to normal monocytes [356]. U937 cells express receptors for both insulin and histamine [359]. Only small numbers of U937 are phagocytic and they do not have the capacity for micro-organism and tumour cell killing. [360, 361].

Advantages of using U937 monocytes include: *a.* Rapid growth with population doubling time between 20-48 h (allowing the production of large number of cells quickly). *b.* Easily labelled with ^{51}Cr (helps for quantification procedure). *c.* No tendency to attach to tissue culture plastic (important for adhesion studies). *d.* As peripheral blood monocytes, U937 cells express both CD44 and CD11a/CD18 integrin by which U937 can interact with HA or ICAM-1 respectively [362].

2.1.5 U937 cell culture conditions

U937 cells were purchased from American Type Culture Collection. The cells were grown in suspension culture in RPMI-1640 medium (Invitrogen) containing 2 mM glutamine, 10% FCS and 100 U/ml penicillin (Invitrogen). The cells were subcultured 3 times/week and 24 h before doing experiments. Cells were subcultured at a ratio of 1:5 – 1:7 with fresh supplemented medium.

2.1.6 Separation of human monocytes

Few experiments with human peripheral blood monocytes were done to confirm the observations obtained from experiments done with the U937 cells. More comparative experiments were done in the department and have shown similar results between freshly-separated monocytes and U937 cells [135, 363].

Total mononuclear cells were separated from heparinized peripheral blood (100 units/ml, taken from healthy donors) by centrifugation on Ficoll-Hypaque density gradients (Amersham Biosciences)[364]. The isolated peripheral blood mononuclear leukocytes (PBML) were resuspended in RPMI-1640 medium supplemented with 5% FCS in a Teflon beaker to prevent attachment during labelling. Isolated cells were used on the same day and viability was always more than 90% as assessed by trypan dye exclusion.

2.2 Assessment of cell count and viability

2.2.1 Cell counting using a haemocytometer

Cells (HK-2 or monocytes) for counting were well re-suspended in culture medium. Trypan blue dye was added to a sample of the cell suspension (final concentration=0.2% w/v) incubated for 5 min at room temperature before pipetting a small volume into both chambers of a haemocytometer (Weber Scientific Ltd, Teddington, UK). The chambers were left to be filled by capillary action. Trypan blue dye is a vital stain recommended for use in estimating the proportion of viable cells in a population [365]. Chemically, trypan blue is an acid that contains 2 chromophores. The reactivity of this dye is based on the fact that chromophore is negatively charged and does not react with the cell unless the membrane is damaged thus viable cells do not take up the dye while non-viable cells do.

Cells were counted in 10 big squares (5 from each chamber of the haemocytometer) and if the cell numbers were not between 50-200/square then a re-count with a different dilution was made. For accurate counting, cells touching square borders (top or right borders) were counted while cells in touch with bottom or left borders were not counted. A separate count was done for viable and non-viable cells.

The formula used to calculate cell number is:

Cells/ml = (Mean cell count/square) x (dilution factor) x 10^4

The formula used to calculate cell viability is:

Cell viability (%) = (total viable / total viable and non-viable) x 100

2.2.2 Alamar blue assay

Alamar blue assay is designed to measure quantitatively the proliferation of human cells [366]. The assay incorporates an oxidation-reduction indicator (REDOX) that both fluoresces and changes colour in response to chemical reduction of the growth medium resulting from cell growth. The REDOX indicator is demonstrated to be minimally toxic to living cells thus it is suitable for repeated use to establish a growth curve and to assess the cytotoxic effect of some compounds and cytokines. Data may be collected using either fluorescence-based or absorbance-based instrumentation. In all experiments, fluorescence was monitored at 544nm excitation wavelength and 590nm emission wavelength using a Fluostar Optima Meter (BMG Labtechnologies Ltd, Aylesbury, UK).

A linear relationship between cell number and alamar blue fluorescence was established in HK-2 cells (figure 2.1). HK-2 cells were harvested by trypsinization (as described in HK-2 subculture) and resuspended in serum-free medium. Cells were counted using a haemocytometer and a range of different cell numbers were plated into a 24-well plate (Falcon). The culture medium volume was standardized in all wells and alamar blue reagent was added to make up 10% of the final volume. The plate was incubated for 60 min at 37°C. 100 µl aliquots of medium were transferred into a black 96-well plate (Thermo Labsystems, MA, USA) and fluorescence was measured.

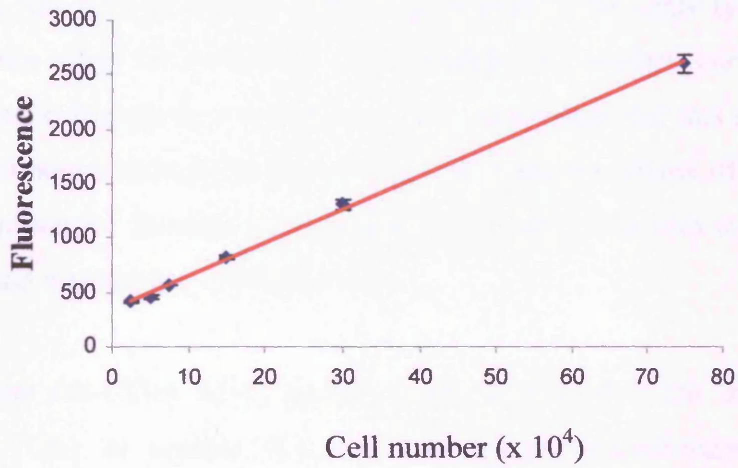

Figure 2.1: Linear relationship between HK-2 cell number and alamar blue fluorescence: Values represent averages of 3 wells (± SD), regression line calculated using Microsoft Excel (R^2=0.998).

2.3 Leukocytes adhesion assay

This assay was done as described by DiCorleto *et el* [362]. HK-2 cells were plated into a 24-well plate (Falcon) and grown until confluence before removing serum for 48 h after which HK-2 cells were either stimulated with either IL-1β (R&D Systems, MN, USA), BMP7 (Creative BioMolecules Inc., MA, USA) or medium only for further 24 h (before addition of labelled monocytes) or, in the case of transfected cells, allowed to interact with monocytes. U937 cells (up to 70 x 10^6 cells/ml) were collected by centrifugation and then labelled for 90 min at 37°C with 100 µCi ^{51}Cr as sodium chromate (Amersham Biosciences) in 1 ml culture medium. Monocytes were then washed with culture medium (x3) and collected by centrifugation. An aliquot of monocytes were incubated with trypan blue dye before counting in a haemocytometer and accordingly U937 monocytes were resuspended at 10^6 viable cells/0.5ml in RPMI-1640 culture medium.

Just before the binding phase, HK-2 cells' media were removed and cells were washed with serum-free medium (x1). 10^6 monocytes were added to each well of HK-2 cells. This number of monocytes represents a ratio of about 10:1 between U937 cells and HK-2 cells and was selected to ensure complete coverage of the HK-2 monolayer by the monocytes. The binding phase of the assay was done at 37°C for 1 h. The wells were then washed with cold RPMI-1640 medium (x3) before lysing with 1% triton X-100 (for 10 min at room temperature). The cells lysates were then transferred into tubes for radiolabel quantification. A standard curve of monocyte number against radioactivity was done for each experiment and was used to calculate the number of bound monocytes (figure 2.2). Spontaneous release of chromium from monocytes in control incubations (without HK-2 cells) was also measured in each experiment and was always less than 10%.

In case anti-CD44 Ab (5 μg/ml; mouse monoclonal; The Binding Site Ltd, Birmingham, UK) or soluble ICAM-1 (200 ng/ml; recombinant human; R&D Systems) were added to the monocytes, and incubated at 37°C for 60 min before the binding phase.

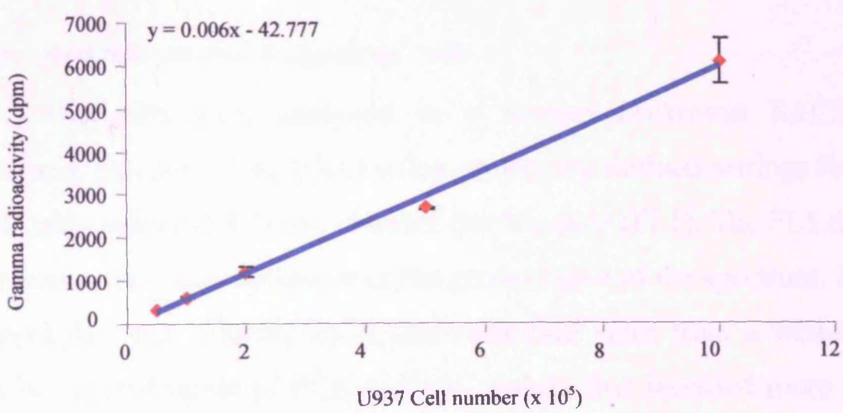

Figure 2.2: Linear relationship between U937 cell number and incorporated radioactivity: Values represent averages of 3 wells (± SD).

2.4 Fluorescence Activated Cell Sorter (FACS) Analysis

2.4.1 Preparation and staining for cells

HK-2 cells were grown in 6-well plate (Falcon) and growth arrested for 48 h before FACS analysis. HK-2 cells were trypsinized as done for routine HK-2 subculturing and resuspended in PBS, spun again and resuspended in 0.5 ml FACS buffer (PBS containing: 10 mM EDTA pH 7.35, 15 mM Sodium Azide and 1% w/v Bovine Serum Albumin). 100 μl aliquots of the cell suspension were transferred into a round-bottom 96-well plate (Falcon). Anti-CD44 Ab (Rat monoclonal; Calbiochem Corporation, Nottingham, UK) was added to the wells so that the final concentration of the Ab would be 1/500 of the stock concentration. The cells were incubated with the Ab for 30 min at 4°C before spinning the plate at 3000 x g for 4 min at 4°C, cells were resuspended in FACS buffer. Two more washes were done using FACS buffer. FITC-conjugated rabbit anti-rat Ab (1/50 final concentration; DakoCytomation, Denmark) was added to the cells and left at 4°C for 30 min in the dark. Further three washes with FACS buffer were done before resuspending the cells in 250 μl FACS buffer and transferring into 6ml tubes (Falcon) for analysis. Each FACS analysis was done with 2 controls: First control was HK-2 cells processed with no antibodies (to detect autofluorescence) while the second control was HK-2 cells incubated with FITC-conjugate anti-rat Ab only (to detect fluorescence due to non-specific binding).

2.4.2 Acquisition and analysis of cells

The cells were analysed in a Becton Dickinson FACScaliber (Becton Dickinson, San Jose, CA, USA) using previously defined settings for forward scatter (FCS), side scatter (SSC) and channel fluorescence (FL1). The FL1 detector measures fluorescence readings optimally in the green region of the spectrum. 10,000 cells were acquired for each sample. HK-2 cells analysed were from a well-defined group of cells in the mid-range of FCS and SSC values that included more than 50% of the cells counted.

2.5 RNA extraction and analysis

2.5.1 Cell lysis and RNA extraction

Total RNA was extracted from HK-2 cells with 0.5 ml of Trireagent (Sigma-Aldrich) per well of a 6-well plate. The lysate was incubated for 10 min at room temperature to allow RNA-protein dissociation. Chloroform (0.2 ml; Sigma-Aldrich) was added (to induce phase separation of RNA, DNA and proteins) and incubated on ice for 5 min before spinning at 16000 x g for 20 min at 4°C. The top aqueous layer (containing the RNA) was collected and 0.5 ml of Isopropanol (Sigma-Aldrich) was added and incubated overnight at -70°C to induce RNA precipitation. Next day, the sample was spun for 20 min at 16000 x g at 4°C to pellet the RNA, the supernatant was removed and discarded. Two washes were performed with 1 ml 70% ethanol and repeat spinning at 16000 x g 4°C for 20 min. After the final wash, the supernatant was removed and the pellet was air-dried for 0.5-1 hour in a fume hood before being dissolved in 20 μl sterile water.

2.5.2 Measurement of RNA quality and quantity

RNA was routinely quantified by measuring the absorbance at 260 nm (A_{260}) in Beckman DU64 single beam spectrophotometer (Beckman Instruments, High Wycombe, UK) using RNase-free quartz cuvettes. To ensure significance, only samples with readings between 0.15 and 1.0 were further processed. To achieve absorbance readings at this range, 2μl of samples were diluted into 100 μl sterile water and transferred into the cuvette for absorbance measurement. 1 unit of absorbance at 260nm corresponds to 40μg of RNA per ml (A_{260}=1 → 40μg/ml). The ratio of the readings at 260nm and 280nm (A_{260}/A_{280}) was used as an index of RNA purity with respect to other contaminants that absorb UV such as protein. Only samples with ratios of 1.5–2.1 were further processed.

In parallel, RNA integrity was confirmed by electrophoresis of 2 μl of samples in a 1% agarose gel containing ethidium bromide (0.2 μg/ml). Typically, the 28S ribosomal RNA (5.0 Kb) bands would be present with intensity approximately twice that of the 18S rRNA (1.9kb) band (figure 2.3). Equal intensities of the two bands generally indicate that some degradation has occurred since the 28S rRNA is more labile than the 18S rRNA.

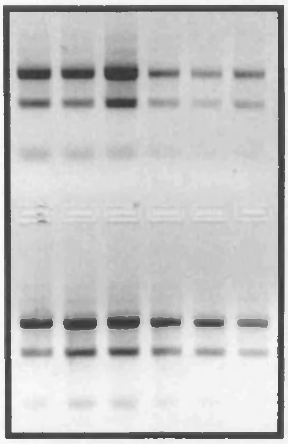

Figure 2.3: Intact RNA on 1% Agarose gel: Extracted from HK-2 cells in 6-well plate.

2.5.3 Reverse Transcription-Polymerase Chain Reaction

Random hexameric (hexadeoxyribonucleotides) primers were used to initiate cDNA synthesis from internal sites within the mRNA molecule. This method can be used to prime cDNA synthesis from mRNA molecules which do not possess a poly$(A)^+$ tail. The reaction mixture contained:

1 μl purified RNA (1 μg/μl) + 2 μl random hexamers (100 μM; Pharmacia Biosystems, Milton Keynes, UK) + 5 μl dNTPs (2.5 mM; Invitrogen) + 2 μl 10x PCR buffer (Applied Biosystems, Beaconsfield, UK) + 10 μl Dithiothreitol (100 mM, Invitrogen).

The 1st phase of the transcription reaction was done using a GeneAmp PCR system 9700 Thermocycler (Applied Biosystems). The reaction was incubated for 4 min at 95°C followed by cooling to 4°C for 5 min, then 1 μl Superscript Reverse Transcriptase (200 U/μl; Invitrogen) and 1 μl RNAsin (40 U/μl; Promega) was added for each reaction. For the second phase of the transcription reaction (using the same Thermocycler), the samples were annealed at 62°C for 10 min followed by cDNA synthesis at 42°C for 60 min, and finally denaturation at 95°C for 5 min. The single stranded complementary DNA (cDNA) was stored at 20°C until PCR was done.

PCR was done in a total volume of 50 μl/reaction. The primers used were all 18-30 nucleotides in length and their GC content were between 40-60% (table 2.1). The reaction mixture contained:

2 μl cDNA + 1.25 μl Forward Primer (20 mM) + 1.25 μl Reverse Primer (20 mM) + 4 μl dNTPs (2.5 mM; Invitrogen) + 5 μl PCR 10x buffer + 0.25 μl Taq Polymerase (10 U/ml; Amplitaq Gold, Applied Biosystems) + 36.25 μl H_2O

PCR amplification was done using a GeneAmp PCR system 9700 Thermocycler. PCR was done over a range of cycle numbers (28-40) to ensure that the amplification was in the linear range of the curve and to obtain the best discrimination of alterations in gene expression. Test reactions for all the genes investigated were determined previously in our department (except for ICAM-1, for which a series of test PCRs were done before establishing the best cycle number; figure 2.4). The PCR protocol was as follows: 1st cycle: 72°C for 10 min, 94°C for 3 min, 55°C for 1 min, 72°C for 1 min. 2nd – cycle before last: 94°C for 40 seconds, 55°C for 1 min, 72°C for 1 min. The final cycle was 94°C for 1 min and 60°C for 10 min. Negative controls were included in all PCR experiments. A negative PCR (-PCR) control consisted of a PCR reaction containing water instead of cDNA while a negative RT (-RT) control contained water instead of RNA.

2.5.4 Detection of PCR products

One tenth of the amplified cDNA (5 μl) was mixed with 5 μl loading buffer (H_2O containing 15% Ficoll Type 400 (Sigma), 0.25% Orange G (Sigma)) and separated by electrophoresis using a 3% agarose gel (Invitrogen) made up in TEA buffer (40 mM Tris, 40 mM Acetic Acid, 10 mM EDTA) with Ethidium bromide (0.2 μg/ml). 123 base pair ladder (Invitrogen) was used to confirm that the PCR products were of the expected size. The gel was run at 90V until the loading buffer reached the edge of the gel. PCR products were visualised under ultraviolet light, digital images were captured and analysed using Chemidoc System (BioRad, Hemel Hempstead, UK). In all the experiments included in this work, none of the negative controls showed any detectable bands.

Primer	Sequence	Product Size	Cycle Number
β-Actin	F=5'-CCTTCCTGGGCATGGAGTCCT-3' R=5'-GGAGCAATGATCTTGATCTT-3'	204 bp	28
HAS2	F=5'-GCAGGCGGAAGAAGGGACAAC-3' R=5'-TCAGGCGGATGCACAGTAAGGA-3'	313 bp	36
HAS3 v1	F=5'-AGTGCAGCTTCGGGGATGA-3' R=5'-TGATGGTAGCAATGGCAAAGAT-3'	453 bp	36
HYAL1	F=5'-CAGGCGTGAGCTGGATGGAGA-3' R=5'-GTATGTGCAACACCGTGTGGC-3'	400 bp	36
HYAL2	F=5'-GAGTTCGCAGCACAGCAGTTC-3' R=5'-CACCCCAGAGGATGACACCAG-3'	446 bp	32
HYAL3	F=5'-GATCTGGGAGGTTCCTGTCC-3' R=5'-TGTCCACCAGGTCGTCATGG-3'	150 bp	36
TSG-6	F=5'-GGTGTGTACCACAGAGAAGCA-3' R=5'-GGGTTGTAGCAATAGGCATCC-3'	284 bp	40
HC3	F=5'-AGTACCCCGAGAACGCTATCCTG-3' R=5'-TGGCCCTCTCATCCTCGTTGTCC-3'	411 bp	36
Bikunin	F=5'CGTTGGCGGAAAGGTGTCTGTG-3' R=5'-ACCCCCTGATCCTTCCTCTTCT-3'	399 bp	36
ICAM-1	F=5'AAAGTCATCCTGCCCCGGGG-3' R=5'-AGGGCAGTTTGAATAGCA-3'	189 bp	32

Table 2.1: PCR Primers (Invitrogen): F: Forward primer; R: Reverse primer.

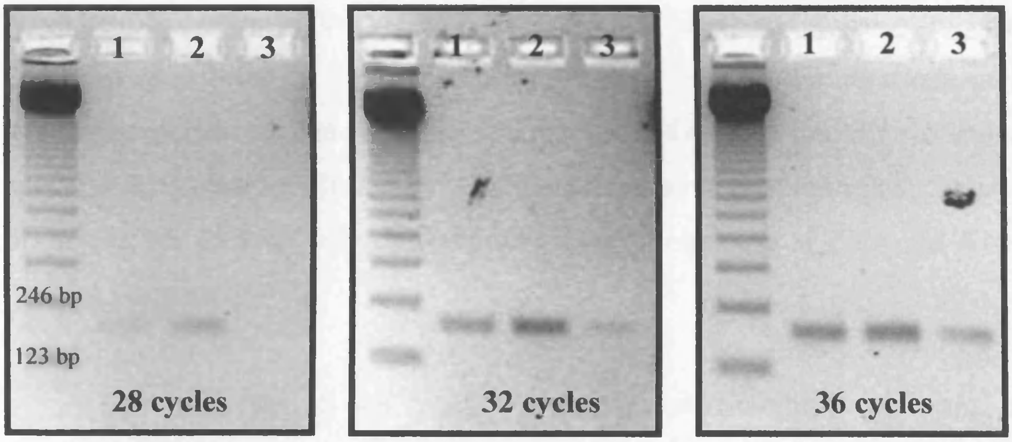

Figure 2.4: 3% Agarose gel electrophoresis showing ICAM-1 PCR products: HK-2 cells were serum-starved for 48 h then stimulated with serum-free medium as control (lane 1), 1 ng/ml IL-1β (lane 2) or 400 ng/ml BMP-7 (lane 3) for 6 h. RNA was extracted followed by RT PCR as described above. Products from 32 cycles PCR show the most discriminating differences.

2.6 DNA cloning and transfection of HK-2 cells

2.6.1 History and mechanism of transfection

"Transfection" is defined as the process of introducing nucleic acid into cells by non-viral methods. The process is distinct from "infection" which is a viral method of nucleic acid introduction into cells. Transfection is generally used to study gene function or; less commonly; it can be used for therapeutic purposes. Transfection is achieved using either chemical reagents (DEAE-dextran or calcium phosphate co-precipitation or Lipofection using artificial liposomes) or physical methods (as direct microinjection, electroporation or biolistic particle delivery).

Vaheri and Pagano [367] were the first to use DEAE-dextran for transfer of nucleic acids into cultured mammalian cells in 1965. In 1972, Graham and van der Eb [368] published their systematic examination of calcium phosphate co-precipitation. Both studies paved the way for future experiments necessitating DNA transfer into eukaryotic cells. By 1980, artificial liposomes were being used to deliver DNA into cells [369]. The next advancement in liposomal vehicles was the development of synthetic cationic lipids by Felgner and colleagues [370]. Liposome-mediated delivery offers advantages such as relatively high efficiency of gene transfer, ability to transfect certain cell types that are intransigent to calcium phosphate or DEAE-dextran, successful delivery of DNA of all sizes from oligonucleotides to yeast artificial chromosomes [370-374], delivery of RNA [375] and delivery of protein [376]. Cells transfected by liposome techniques can be used for transient and for longer term experiments that rely upon integration of the DNA into the chromosome or episomal maintenance. Unlike the DEAE-dextran or calcium phosphat, liposome-mediated nucleic acid delivery can be used for *in vivo* transfer of DNA and RNA to animals and humans [377].

A lipid with overall net positive charge at physiological pH is the most common synthetic lipid component of liposomes developed for gene delivery. FuGENE 6 Transfection Reagent (Roche Diagnostics Ltd, Lewes, UK) is an advanced non-liposomal lipid formulation that transfects a wide variety of eukaryotic cells with high efficiency and minimal cytotoxicity. It is effective for the transfection of DNA (very large plasmids [10 kb], oligonucleotides, or nucleotides) into eukaryotic cell types, including primary cultures and "hard-to-transfect" cell lines. It has been in use in our department and proved to be efficient in transfecting epithelial cells [355]. The amount of positive charge contributed by the cationic lipid component of the transfection reagent exceed the amount of negative charge contributed by the phosphate in the DNA backbone, resulting in tliposomes containing plasmid cDNA with a net neutral or positive charge on the vesicles. By the process of endocytosis or fusion with the plasma membrane via the lipid moieties of the liposome, these liposome complexes enter into the cells. Following endocytosis, the complexes appear in the endosomes, and later in the nucleus. It is still unclear how the nucleic acids are released from the endosomes and traverse the nuclear membrane before integration with the genomic DNA. The neutral lipid L-dioleoyl phosphatidyl ethanolamine (DOPE), often mixed with the cationic transfection lipid, is considered a "Fusogenic" lipid [378] and it is thought that its role may be to release these complexes from the endosomes, as well as to facilitate fusion of the outer cell membrane with the liposome/nucleic acid complexes.

2.6.2 *Plasmid preparation*

2.6.2.1 pcDNA4/TO expression vector

pcDNA4/TO is a 5.1 kb expression vector (Invitrogen; figure 2.5). The vector contains 2 important elements:

A. Hybrid promoter: consisting of the human cytomegalovirus immediate-early (CMV) promoter and tetracycline operator 2 ($TetO_2$) sites for high-level tetracycline-regulated expression in a wide range of mammalian cells.

B. Zeocin resistance gene: for the selection of stable cell lines [379].

Although the presence of $TetO_2$ sites within the CMV promoter allow tetracycline-regulated expression of the gene of interest [380], cells that are transfected only with pcDNA4/TO (and not co-transfected with pcDNA6/TR vector that expresses the Tet repressor) will show a constitutive over-expression of the gene of interest.

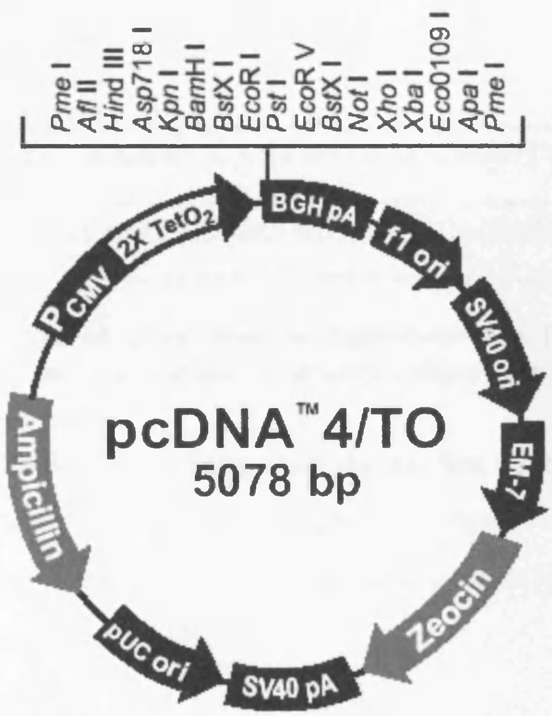

Figure 2.5: Diagrammatic representation of pcDNA/TO vector: Showing key components of the vector, including the multiple cloning site (bases 967-1077).

2.6.2.2 HAS2-pcDNA4/TO preparation

HAS2 ORF (sequence can be retrieved from the National Centre for Biotechnology Information (NCBI) database at http://www.ncbi.nlm.nih.gov; accession number NM_005328 [166]) was provided kindly by Dr Bowen (Institute of Nephrology, Cardiff University College of Medicine). A modified PCR was used to reproduce the original HAS2 ORF using a combination of polymerases to increase the fidelity of the PCR product [381]. The combination included *Taq* polymerase (Promega) and *Pfu* polymerase (Promega) in a 9:1 ratio. The highest cloning efficiency is generally achieved with DNA cleaved by 2 different restriction enzymes that produce non-complementary overhangs. Ligating templates prepared in this manner is referred to as "directional cloning" because the insert DNA can be ligated into the vector in only one orientation. This will reduce the background level of non-recombinants because re-ligation of the vector to itself would be greatly hindered. The primers designed to reproduce the HAS2 ORF included sites for 2 different restriction enzymes (*Pst I & Not I*; table 2.2) to ensure cloning in the sense orientation of HAS2 ORF into the pcDNA4/TO vector.

Pst I Forward Primer	5'-CC***CTGCA G***ACCATGGATTGTGAGAGGTTTCTATGTATC-3'
Not I Reverse Primer	5'-CC***GC GGCCGC***TCATACATCAAGCACCATGTCATATTG-3'

Table 2.2: Sequences of the primers used to reproduce the HAS2 ORF: RE recognition sites are in bold italics and space in between indicate the site of action.

PCR was done for 20-30 cycles (figure 2.6), the reaction mixture contained: 0.45 µl *Taq* polymerase + 0.05 µl *Pfu* polymerase (Invitrogen) + 5 µl *Pfu* buffer (10X) + 1 µl Forward primer (10 pmol/µl) + 1 µl Reverse primer (10 pmol/µl) + 1 µl HAS2 ORF + 4 µl dNTPs + 37.5 µl H_2O

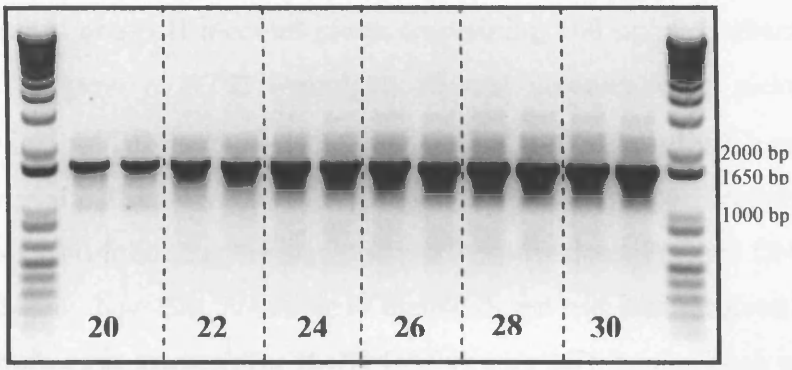

Figure 2.6: 1% Agarose gel electrophoresis showing HAS2 ORF: DNA was amplified using the polymerase combination, numbers indicate number of PCR cycles. Samples from 20 cycles reaction were used for subsequent cloning reactions.

After the amplification reaction, HAS2 ORF (using sample from 20 cycles PCR) was subjected to RE digestion using *Pst I* and *Not I* to cleave any over-hanged bases. The sample was then run on a 1.5% agarose gel (to prevent gel damage during extraction) followed by extraction (using 1 ml pipette tip with filter) and purification of the HAS2 ORF using the Qiaquick PCR purification kit (Qiagen) following the manufacturer's protocol.

HAS2 ORF was inserted into the vector using a standard ligation reaction (using Promega *Ligase* enzyme). Experiments showed that the best ligation resulted when the vector/insert molar ratio was 1:3. The ligation reaction was done at 16°C overnight and contained:

12 µl HAS2 ORF + 4 µl pcDNA4/TO + 2 µl ligase buffer (Promega) + 1 µl ligase (Promega) + 1 µl H_2O

2.6.2.3 Bacterial transformation, plasmid isolation and purification

Following the ligation reaction, reproduction of the cloned vector was done by bacterial transformation (JM109 competent *E. coli*; Promega). 10 µl of the ligation reaction was incubated with 40 µl of freshly thawed *E. coli* for 15 min on ice. To facilitate cDNA entry into the bacteria, a heat shock (42°C for 45 seconds) was applied followed by 5 min incubation on ice before incubation with 150 µl of SOC medium (Invitrogen) for 90 min at 37°C in an orbital shaker; 200 rpm (to allow recovery from heat shock and to express the newly introduced DNA). Afterwards, bacteria were streaked onto LB medium plates (containing 100 μg/ml Carbenicillin; Sigma) and left to grow at 37°C overnight. Several colonies were picked for screening, grown in 5 ml LB medium with Carbenicillin (100 μg/ml) for 8 h at 37°C. 1.5 ml of the bacterial culture was used for plasmid extraction and purification using MiniPrep kit (QIAGEN) following the manufacturer's instructions. Purified DNA was subjected to RE double-digestion. A sample of the RE digest was then resolved by 1% agarose gel electrophoresis to check for HAS2 ORF (figure 2.7). 1 ml of each positive sample (with HAS2 ORF inserted into pcDNA4/TO) was re-cultured in 100 ml LB medium (with 100 μg/ml Carbenicillin) at 37°C overnight (to increase the yield of transformed bacteria). Plasmid extraction and purification was done using MaxiPrep kit (Qiagen). Plasmid DNA concentration was measured using a Beckman DU 64 single beam spectrophotometer using the following formula:

cDNA concentration (μg/ml) = Absorbance at 260 nm (A_{260}) x 50

The A_{260}/A_{280} ratio is used as an indicator of DNA purity. Purified plasmid DNA ratio values were always higher than 1.8 and considered suitable for mammalian cell transfection.

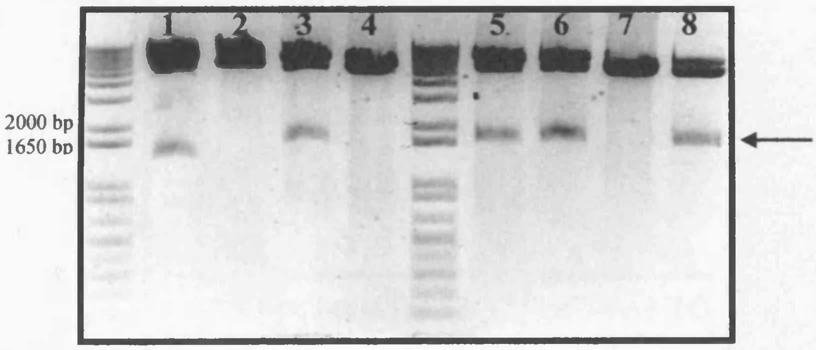

Figure 2.7: 1% Agarose gel electrophoresis of RE digests: Transformed *E.coli* were picked from LB plates, plasmid DNA wan then extracted and subjected to *Pst I* and *Not I* digestion. Clones 2, 4 and 7 had empty vector (re-circularised pcDNA4/TO) while clones 3, 5, 6 and 8 had an insert of approximately 1700 bp (arrow).

2.6.2.4 HAS3-pcDNA4/TO preparation

HAS3 ORF (sequence can be retrieved from the National Centre for Biotechnology Information (NCBI) database at http://www.ncbi.nlm.nih.gov; accession number NM_005329 [167]) was provided kindly by Dr Bowen (Institute of Nephrology, Cardiff University College of Medicine). The HAS3 ORF was already cloned into pCI-neo mammalian expression vector (Promega). The pCI-neo vector is ideal for transient expression or stable expression by selecting transfected cells with the antibiotic G418 (an aminoglycoside). However, repeated experiments showed that HK-2 cells are resistant to the G418 antibiotic at doses even higher than that recommended by the vector manufacturer. Hence, all attempts to establish HAS3/pcI-neo stable-transfected cell lines have failed. Because of this, the decision was made to cut the HAS3 ORF from the pCI-neo vector and clone it into the pcDNA4/TO expression vector.

HAS3 ORF was excised using 2 different RE enzymes (*Xho I* and *Xba I*; at 37°C overnight). pcDNA4/TO was digested by *Xho I* and *Xba I* (at 37°C overnight). Those RE were selected because they cut once only through pcDNA4/TO and so HAS3 ORF obtained by *Xho I* and *Xba I* digestion can be cloned directly into pcDNA4/TO that was also digested by these enzymes. The digestion reactions were resolved by agarose gel electrophoresis (figure 2.8). The HAS3 ORF was extracted (using 1 ml pipette tip with filter) from the gel and purified using the Qiaquick PCR purification kit (Qiagen).

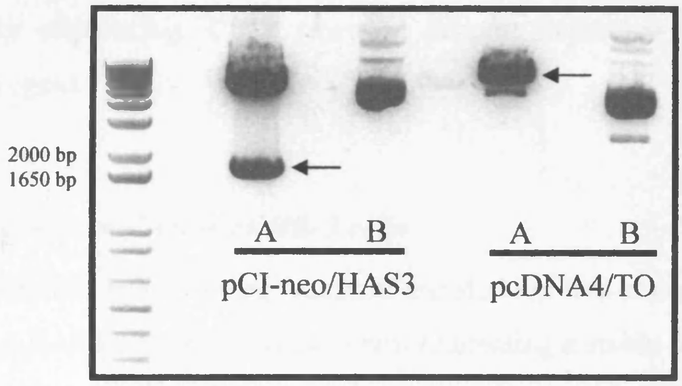

Figure 2.8: 1.5% Agarose gel electrophoresis showing products of RE digestions: In (A), samples were digested with *Xho I* and *Xba I* while (B) shows undigested vectors (used to confirm the action of RE). Arrows indicate the samples that were extracted and ligated.

Before the ligation, both HAS3 ORF and pcDNA4/TO were treated with shrimp alkaline phosphatase (SAP; Promega) at 37°C for 30 min (to remove the phosphate groups from 5'- termini to prevent re-circularisation of vector). SAP was then deactivated by heating to 65°C for 30 min before proceeding to cloning. HAS3 ORF was cloned into pcDNA4/TO using a standard ligation reaction (using Promega

Ligase enzyme) as described above. Following the ligation, reproduction of the cloned vector was done by bacterial transformation as described above. RE digestion to check for the presence of HAS3 ORF in the pcDNA4/TO vector was done using *Xho I* and *Xba I* enzymes (figure 2.9).

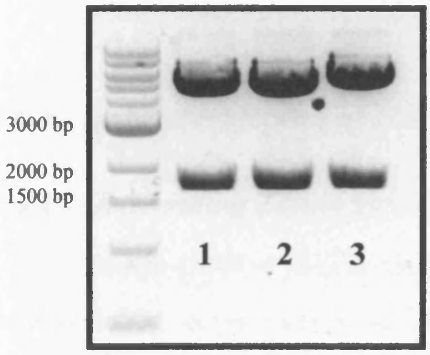

Figure 2.9: 1% Agarose gel electrophoresis showing products of RE digestion: all samples were digested with *Xho I* and *Xba I*. (1 and 2) represent product of HAS3-pcDNA4/TO ligation while (3) represents the original HAS3-pCI-neo. The inserts match in size as predicted while the vectors differ.

2.6.2.5 cDNA sequencing reaction

The identity of the cloned PCR products in the positive samples and the fidelity of the amplification were confirmed by sequencing. Samples were submitted to the Sequencing Service (University of Dundee, Dundee, UK). 2 standard primers were used for sequencing: CMV (forward primer; Invitrogen) and BGH (reverse primer; Invitrogen).

2.6.3 Transient transfection of HK-2 cells

The rationale behind doing transient transfection was to confirm the activity of our HAS2 and HAS3 expression vectors before creating a stable cell line. The activity would be positive if there is: *a*. An increment in specific HAS isoform mRNA transcription (to be detected by RT PCR). *b*. An increment in HA synthesis (to be detected by HA ELISA and gel chromatography) and *c*. bigger exclusion zones when particle exclusion assay is utilised.

All experiments were done using 50-80% confluent HK-2 cells (as recommended by the manufacturer), seeded into 6-well plates and serum starved for 48 h (because serum is a known HA-producing stimulus). Transfection mixtures were prepared in advance to reduce any bias in transfection conditions. The transfection mixtures were made by incubating the plasmid cDNA with FuGENE 6 in a ratio of 1:3 in serum-free medium (final volume = 100 μl) at room temperature for 15 min. HK-2 cell medium was replaced with fresh serum-free medium prior to the addition of the transfection mixture (for each well: 1 μg cDNA + 3 μl FuGENE6). The plates were then incubated at 37°C until the end of the experiment.

2.6.4 Stable transfection of HK-2 cells

2.6.4.1 Determining Zeocin sensitivity

Zeocin (MW=1535Da; Invitrogen) is a formulation of phleomycin D1, a basic water-soluble, copper-chelated glycopeptide isolated from *stertomyces vertivillus*. This copper-chelated form is inactive. When the antibiotic enters the cell, the copper cation is reduced from Cu^{+2} to Cu^{+1} and removed by sulfhydryl compounds in the cell. Upon removal of the copper, Zeocin is activated and will bind DNA and cleave it, causing cell death. The Zeocin resistance protein binds stoichiometrically to Zeocin and inhibits its DNA strand cleavage activity. Expression of this protein in cells confers Zeocin resistance. Mammalian cells exhibit a wide range of susceptibility to Zeocin with effective concentrations ranging from 50 μg/ml to 1000 μg/ml.

To determine Zeocin sensitivity in HK-2 cells, a "kill-curve" was done. HK-2 cells were seeded in a 24-well plate to achieve 25-50% confluence. 24 h later, alamar blue measurement was done followed by addition of supplemented medium with varying concentrations of Zeocin (0, 50, 100, 200, 400, 600, 800, 1000 μg/ml) to each well. The medium was replenished every 4 days after alamar blue measurement. The Zeocin concentration selected (400 μg/ml) killed more than 99% of the cells after 8 days (figure 2.10).

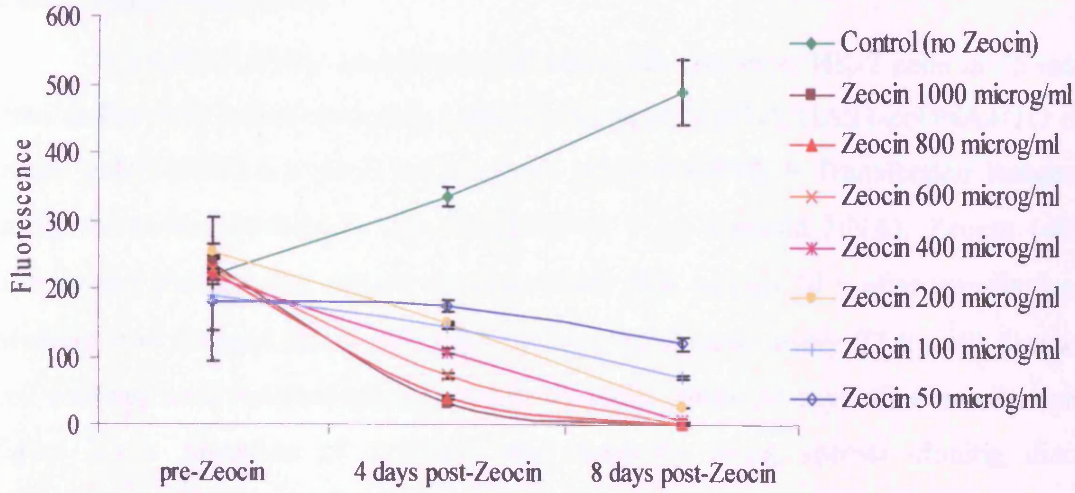

Figure 2.10: Zeocin "kill-curve" in HK-2 cells: Data represents the average of 3 wells ± SD.

Cells dying due to zeocin toxicity exhibited the following morphological features (figure 2.11): *a.* Vast increase in size. *b.* Abnormal cell shape with the appearance of long appendages. *c.* Presence of large empty vesicles in the cytoplasm (breakdown of the endoplasmic reticulum and Golgi apparatus or scaffolding proteins). *d.* Breakdown of plasma and nuclear membrane (appearance of many holes in these membranes).

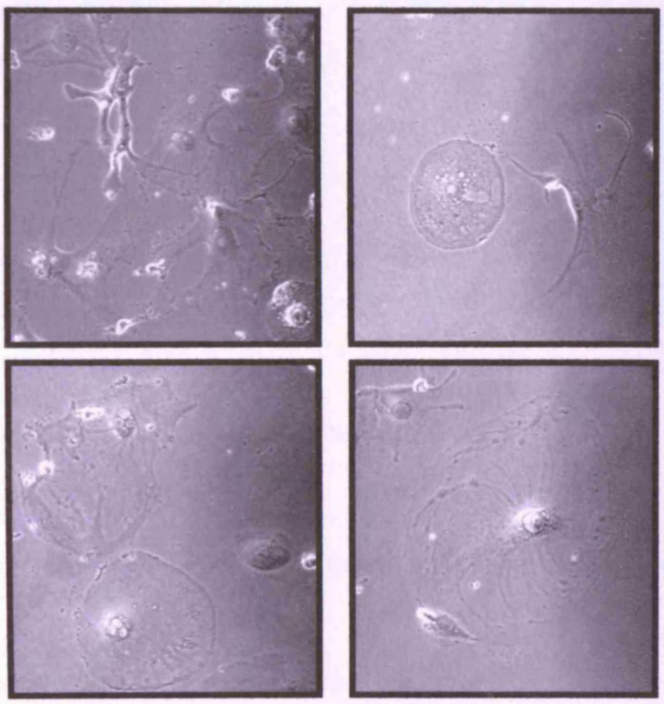

Figure 2.11: Effect of Zeocin on untransfected HK-2 cells: Zeocin (400µg/ml) was added to HK-2 cells 24 h after transfection. Medium (with Zeocin) was replaced every 3 days. Pictures were taken at day 5 post-transfection using light microscopy (magnification x 100). Cells display typical Zeocin toxicity features.

2.6.4.2 Stable transfection

To establish stable transfected cell lines, sub-confluent HK-2 cells in 35 mm Petri dishes were transfected with either HAS2-pcDNA4/TO, HAS3-pcDNA4/TO or empty pcDNA4/TO (as mock transfection) using FuGENE 6 Transfection Reagent under serum-free conditions (3μl FuGENE 6, 1 μg plasmid DNA). Zeocin (400 μg/ml) was added to the culture medium (with 10% serum) 24 h after transfection. Medium was changed afterwards with (200 μg/ml Zeocin) every 72 h until distinct cell colonies were macroscopically visible (usually within 21 days after transfection; figure 2.12). Selection of colonies was done by using special cloning discs (Scienceware, Bel-Art products, NJ, USA) impregnated with trypsin/EDTA. Discs were left on HK-2 colonies for no longer than 5 min and then transferred into new 35 mm dishes (containing 200 μg/ml Zeocin). Cells were left to grow until cells were more than 50% confluent. Cells were then subcultured into 75cm^2 culture flasks from which cells were either frozen or processed for further experimentation. Transfected cell lines were maintained in 200 μg/ml Zeocin (to prevent growth of cells that have lost their plasmids) except during experimental time.

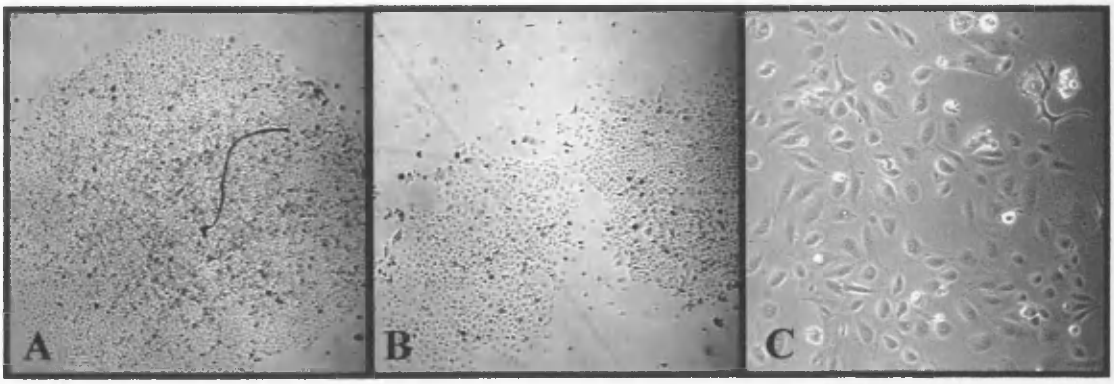

Figure 2.12: Transfected HK-2 clones: Light microscopy photographs of growing clones; cells shown in the pictures are HAS2-transfected HK-2 cells (**A** and **B** magnification x 250; **C** magnification x 100).

2.7 Hyaluronan measurement and molecular weight analysis

2.7.1 Determination of HA concentration

Hyaluronan concentration in conditioned medium was measured by enzyme-linked binding protein assay (HA quantitative test kit from Coregenix Inc., Colorado, USA). The assay uses a naturally occurring Hyaluronan binding protein (HABP) to specifically capture HA and an enzyme-conjugated (Horseradish Peroxidase, HRP) version of the HABP to detect and measure the HA captured from the sample. The intensity of the colour after the final step is measured in a spectrophotometer at 450 nm. HA levels in experimental and control samples are determined against a reference curve prepared from the reagent blank (0 ng/ml) and the HA reference solutions provided with the kit (50, 100, 200, 500, 800 ng/ml). The assay has no cross-reactivity to other glycosaminoglycans. To ensure that equal cell numbers were studied in these experiments, alamar blue readings were taken for all the samples and there was no significant difference between them. All the measurements were done using the same amount of medium; therefore, the HA results are expressed as an absolute concentration of HA.

All the HA ELISA experiments were corrected for cell number estimated by the alamar blue assay. Culture media were removed and stored at -70°C and replaced with fresh medium containing 10% alamar blue reagent. After 60 min incubation at 37°C, 100 µl of culture medium was transferred into a 96-well plate and fluorescence was measured. There were no significant differences in cell number between experimental groups in any of the HA ELISA data presented.

2.7.2 Analysis of ^{3}H-radiolabelled Hyaluronan

In vitro ^{3}H-labelling of HA was performed as previously described [185]. Growth-arrested confluent HK-2 cells were stimulated with fresh medium with or without specific cytokines in the presence of 20 µCi/ml ^{3}H-glucosamine (Amersham Biosciences) for a specific time (indicated for each experiment).

Supernatant samples were collected and treated with an equal volume of 200 µg/ml pronase (Sigma-Aldrich) in 2X pronase buffer (100 mM Tris-HCL pH 8.0, 0.1% Na Azide) for 24 h at 37°C to analyse HA released into the culture medium (Conditioned Medium fraction; CM). The remaining cell monolayer was incubated with 10 µg/ml trypsin (Sigma-Aldrich) in PBS for 10 min at room temperature to remove pericellular, protein-bound ^{3}H-hyaluronan (Trypsin extract fraction; TE) prior to the addition of an equal volume of 200 µg/ml pronase in 2X pronase buffer for 24 h at 37°C. Following trypsinisation, 100 μg/ml pronase in 1X pronase buffer was added to the cell pellet for 24 h at 37°C to solubilise the remaining cells-associated ^{3}H-hyaluroanan (Cell associated fraction; CA).

Each of the fractions was subsequently gravitationally passed over DEAE ion-exchange columns (Amersham Biosciences) equilibrated with 8 M urea buffer (8 M urea in 20 mM Bis Tris buffer, pH 6 containing 0.2% Triton-X100). The columns were washed using 8 M urea buffer until the radioactivity returned to background level (to remove low molecular weight peptides and unincorporated radiolabel). HA was then eluted with 0.3 M NaCl urea buffer until the radioactivity returned to background. The remaining Glycosaminoglycans were eluted with 8 ml of 4 M Guanidine HCl buffer (containing 50 mM Sodium Acetate, 0.5% Triton X-100, 0.05% (w/v) Sodium Azide; pH 6).

Equal volumes (2 for each sample) of eluted HA were incubated with 3 volumes of 1.3% wt/vol potassium acetate in 95% ethanol in the presence of 50 μg/ml of each of HA, heparin (Sigma-Aldrich) and chondroitin sulphate (Sigma-Aldrich) as co-precipitants at 4°C overnight. The precipitated HA was collected by spinning at 1500 rpm for 10 min and washed twice with 95% ethanol before leaving the precipitate to dry at room temperature for 30 min.

For each sample, two HA precipitates were prepared with one directly re-suspended with 500 μl 4M Guanidine HCl buffer and the other incubated with 1 IU *Streptococcal hyaluronidase* (ICN Biomedicals, Basingstoke, UK) in 200 μl Hyaluronidase buffer (20 mM Sodium Acetate containing 0.05% Sodium Azide, 0.15 M NaCl) at 37°C for 24 h prior to addition of 300 μl 4 M Guanidine HCl buffer.

Each sample was run through a dissociating Sephacryl S-500 (Amersham Biosciences) column (1.5m x 0.6cm) and collected using a fraction collector (Pharmacia Biotech, NJ, USA; pump speed=2.4 ml/hour, 0.6 ml/fraction) prior to quantification of radioactivity using a β counter. For β counting, an equal volume of 70% ethanol was added to each tube in addition to 4ml of scintillation liquid (InstaGel Plus; PerkinElmer Life and Analytical Science, MA, USA). The column was calibrated with: (*a*) ^{3}H-glucosamine hydrochloride, M_r 215 Da; (*b*) ^{35}S-chondroitin sulphate GAG, M_r 25 x 10^3 Da; (*c*) ^{35}S-decorin, M_r 10 x 10^4 Da; (*d*) ^{35}S-versican, M_r 1.3 x 10^6 Da [382].

Since *Streptococcal* hyaluronidase will not degrade other GAG, the value of the hyaluronidase-treated portion subtracted from the non-hyaluronidase-treated portion was taken as hyaluronan-associated radioactivity (multiplied by -1 for correction).

2.8 Western blotting

2.8.1 Gel preparation

Gradient gels (5-20%) were used for IαI western blotting. The gels components were shown in the below table:

	Stacking	5%	10%	20%
H_2O	6.1 ml	5.68 ml	4 ml	
1.5 M Tris(pH 8)	-	2.5 ml	2.5 ml	2.5 ml
0.5 M Tris(pH 6.8)	2.5 ml	-	-	-
10% SDS	100 µl	100 µl	100 µl	100 µl
30% Bis-acrylamide	1.3 ml	1.67 ml	3.34 ml	5.01 ml
10% APS	50 µl	50 µl	50 µl	50 µl
Temed	10 µl	5 µl	5 µl	5 µl

2.8.2 Sample preparation and electrophoresis

Confluent HK-2 cells were growth arrested for 48 h after which cells were washed once with PBS and lysed by the addition of SDS sample buffer (2% SDS, 10% v/v glycerol, 60 mM Tris and 5% v/v mercaptoethanol) [383]. This was designated as "total" extract. For the IαI WB, a duplicate monolayer of HK-2 cells was digested with *Streptococcal* hyaluronidase (2 IU for 1 h at 37°C) to release matrix molecules bound to HA. Following the enzymatic digestion, the hyaluronidase digest and the remaining cells were collected and incubated with SDS sample buffer and referred to as "matrix" and "cell" extracts respectively. Samples were stored at -20°C until analysis. When the gels were ready, samples were thawed on ice and then heated to 100°C for 5-10 min before cooling on ice. Equal volumes were loaded into the gels. 10 µl of dye-conjugated protein standards (See Blue Plus Two; Invitrogen) were loaded in an adjacent well. Gels were electrophoresed in a discontinuous vertical minigel apparatus (Beckton Dickinson) using 1X "running" buffer (10X buffer: Tris HCl 30 g (pH 8.3), Glycine 144 g, SDS 10 g, made up with water to 1 litre) at 150V for 60 min.

2.8.3 Transblotting

After finishing electrophoresis, the gel was removed from the casting membrane and placed on a nitrocellulose membrane (Amersham Pharmacia) immersed in "transfer" buffer (1.44% w/v Glycine, 0.3% w/v Tris, 20% v/v methanol). Both membrane and gel were sandwiched in an inner layer of filter paper and an outer layer plastic wool before electroblotting at 100 V for 90 min in chilled transfer buffer. The appearance of protein standard bands indicated successful transfer.

2.8.4 Blocking, primary and secondary antibodies

Membrane blocking was done using 5% w/v non-fat milk in PBS-Tween for 60 min at 37°C, followed by three washes lasting 5 min each on a shaker. Primary antibodies used were: *a.* anti-IαI Ab (Rabbit polyclonal, dilution 1:1000; DakoCytomation). *b.* anti-active ERK Ab (Rabbit polyclonal, dilution 1:1000; Promega) which recognises the dually phosphorylated active form of MAPK (p44/ERK1 and p42/ERK2). *c.* anti-total ERK Ab (Rabbit polyclonal, dilution 1:5000; Promega). All the primary antibodies were diluted in 5% w/v non-fat milk in PBS-Tween (10 ml/membrane) and the membranes were incubated at 4°C overnight. Incubation was followed by three washes, 5 min each on a shaker. Appropriate HRP-conjugated secondary antibodies (Sigma) were diluted in 5% w/v non-fat milk in PBS-Tween and the membranes were incubated for 1 h at room temperature.

2.8.5 Detection

The membrane was developed using the ECL enhanced chemiluminescence system (Amersham Biosciences). The membrane was dabbed dry on filter paper, 1 ml of each of reagents A and B were mixed, applied to the membrane and incubated for 2 min. Excess reagents were removed afterwards with filter paper, the membrane was wrapped in cling film and exposed immediately to chemiluminescence photographic film (Amersham Biosciences). Exposure times varied between 1-10 min.

2.8.6 Membrane stripping and reprobing

After detecting active MAPK as described above, the membrane was stripped of antibodies by incubating in "stripping" buffer (100 mM 2-mercaptoethanol, 2% w/v SDS, 62.5 mM Tris-HCl (pH 6.7)) for 30 min at 50°C followed by two washes, 10 min each in PBS-Tween. The membrane was then blocked and probed (for total MAPK) as described above.

2.9 Immunocytochemistry

All immunocytochemistry experiments were done using 8-well multi-chamber slides (Invitrogen) and analysed by confocal laser scanning microscopy (TCS-40; Leica Microsystems, Cambridge, UK). HK-2 cells were seeded and grown to different degrees of confluency (indicated for each experiment) with supplemented medium containing 10% FCS. Afterwards, cells were either fixed or stimulated with different stimuli under serum-free conditions and then fixed. One PBS wash was routinely done prior to fixation.

Two fixation methods were used depending on antibodies' manual instructions: *a*. Paraformaldehyde (3%) was used as a cross-linking fixative; the mechanism of fixation involves formation of covalent bonds between adjacent amine-containing groups through a Schiff acid-base reaction. These bonds form both inter- and intra-molecularly. Paraformaldehyde was added to the cells and incubated for 15 min at room temperature. Cells were subsequently permeabilised using 0.2% Triton in PBS for 5 min at room temperature after which cells were washed once with PBS. *b*. Methanol (100% ice-cold) was used to simultaneously denaturate and precipitate samples. Although quantitative comparisons of different fixation protocols have shown that cultured cells fixed with cold methanol shrink by as much as 50% [384], methanol-fixed samples preserve their antibody binding sites as epitopes are not covalently modified as they might be with paraformaldehyde fixation. Also, using methanol fixation circumvented the necessity for detergent treatment as methanol permeabilises cell membranes.

After fixation, cells were incubated with 10% FCS in PBS (30-60 min at RT) to block non-specific binding. This step was followed by primary antibody incubation diluted according to the manufacturer's instruction (table 2.3) at 4°C overnight. Cells were then washed with PBS (x3) and incubated with appropriate secondary antibody (Table 2.3) for 60 min at room temperature. Cells were then subjected to another PBS wash (x3). Slides were finally mounted with Vectashield mounting medium (Vector Laboratories, Burlingame, CA, USA) with or without DAPI.

Primary Antibody	**Concentration or dilution**	**Source/Type**	**Company**
b-HABP	5 μg/ml	Bovine	Seikagaku
anti-CD68	5 μg/ml	Mouse monoclonal	PharMingen
anti-CD44	10 μg/ml	Rat monoclonal	Calbiochem
anti-Versican	1 in 500	Mouse monoclonal (clone 2B1)	Seikagaku
anti-IαI	1 in 200	Rabbit polyclonal	DakoCytomation
anti-TSG6	5 μg/ml	Rat monoclonal (clone Q75)	Kind gift from Prof. AJ Day [385]
anti-KDEL	5 μg/ml	Mouse monoclonal	Stressgen
anti-E-cadherin	5 μg/ml	Rabbit polyclonal	Santa Cruz Biotechnology
anti-cytokeratin	1 in 50	Mouse monoclonal	DakoCytomation
anti-ZO1	1 in 100	Rabbit polyclonal	Zymed Labs.
Secondary Antibody			
Fluorescein Avidin-D	20 μg/ml	-	Vector Labs.
anti-rabbit Alexa Fluor 568	10 μg/ml	Goat	Molecular Probes
anti-rabbit FITC	1 in 40	Swine polyclonal	DakoCytomation
anti-mouse Alexa Fluor 568	10 μg/ml	Rabbit	Molecular Probes
anti-mouse FITC	1 in 40	Rabbit	DakoCytomation
anti-rat H-L	1 in 40	Rabbit	BioMeda corp.

Table 2.3: Primary and secondary antibodies used in immunocytochemistry.

2. 10 Cell migration studies

2.10.1 Scratch wound experiments

Cell migration was examined as previously described [354, 386]. Confluent HK-2 cells were grown to confluence in a 24-well plate (Falcon) and then serum starved for 48 h. Two intersecting, perpendicular wounds were generated using a sterile 1 ml pipette tip. The cells were then washed with PBS once before incubation with serum-free medium with or with out cytokines. Migration of HK-2 cells into the denuded area was monitored using Axiovert 100M inverted microscope fitted with a digital camera (ORCA-1394; Hamamatsu Photonics K.K. Hamamatsu, Japan) and images of the denuded area were captured as a digitalised sequence (figure 2.13). The rate of motility of cells was calculated as the number of cells entering the central denuded area during standard periods of time. Cell number was expressed as cells per mm^2 of original denuded area per time point. A positive control was included in all experiments and it was composed of standard culture medium with 0.1% FCS.

2.10.2 5-BrdU immunostaining

HK-2 cell proliferation in the wounding experiments was studied by 5-bromo-2'-deoxyuridine (5-BrdU; Sigma-Aldrich) labelling before proceeding to immunocytochemistry as described previously [188, 386]. 5-BrdU is incorporated into the DNA of cells entering the S-phase of the cell cycle, thus it can be used as an indicator of cellular proliferation. HK-2 cells were wounded as described above and incubated with medium containing 5-BrdU (0.01 mM). At certain time points, cells were fixed in ice-cold acetone/methanol (1:1) for 90 sec. Cells were washed with Tris-buffered saline (TBS; pH 7.6) once and then incubated with 95% (v/v) formaldehyde in Trisodium citrate (0.15 M) for 45 min at 70°C to denature double-stranded DNA. Cells were incubated in 50% FCS for 30-60 min at room temperature to block non-specific binding. Monoclonal anti-BrdU antibody (mouse; Sigma-Aldrich, 1:1000) was added and incubated for 30 min at room temperature followed by washing with TBS (x3) before addition of anti-mouse alkaline phosphatase-conjugated antibody (DakoCytomation) for 30 min at room temperature. Finally, BrdU was detected by staining with FAST RED (Sigma-Aldrich). Digital pictures were taken using Kodak DC290 digital camera and Leitz DIAVERT microscope.

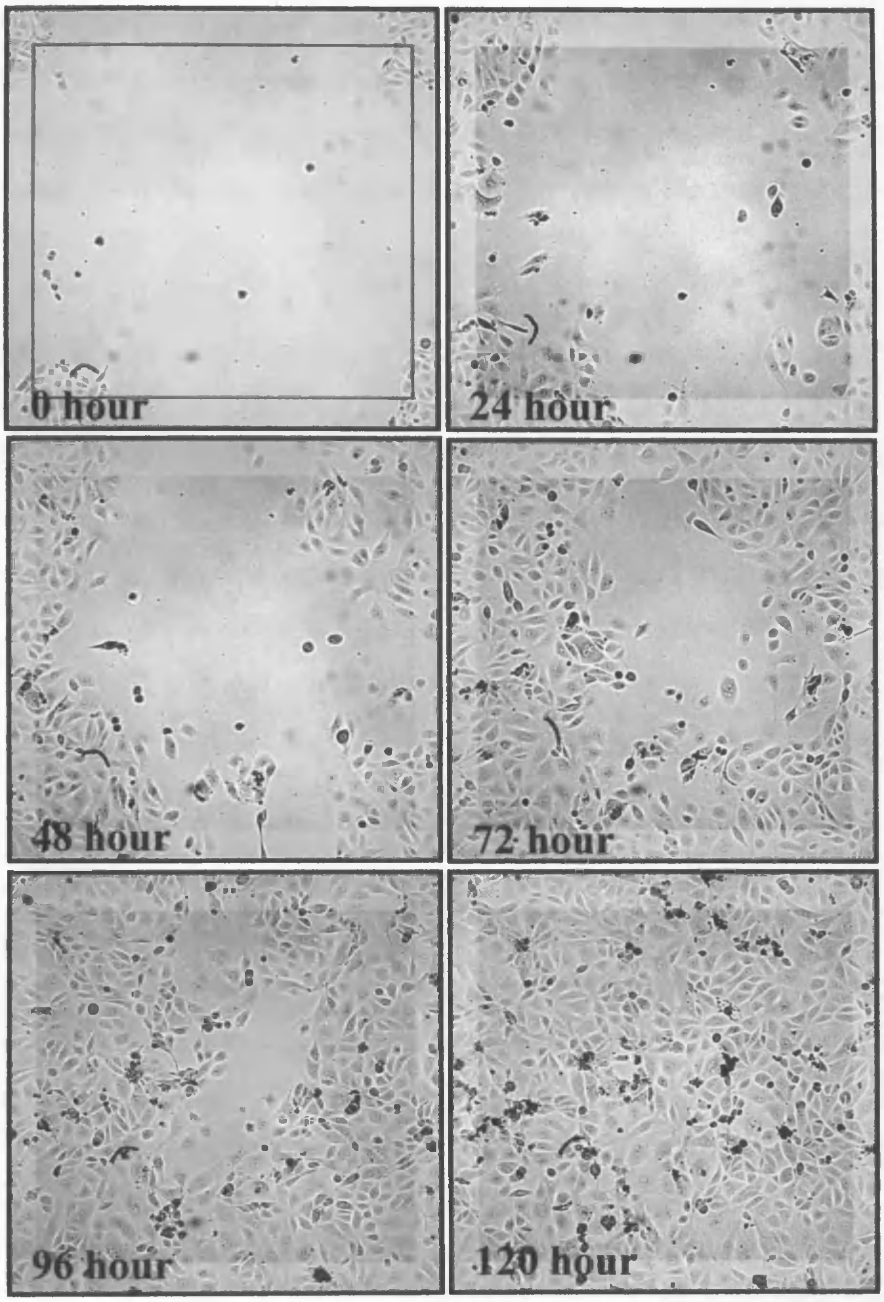

Figure 2.13: Wound closure in unstimulated HK-2 cells: Sequential phase-contrast photos of the wounded area were taken at the 0 h and every 24 h thereafter. The black square in 0 h represents the denuded area in which migrating cells were counted (highlighted areas in the other time points).

2.11 Particle exclusion assay

HA dependent pericellular matrices were visualised by the particle exclusion assay in which formalised horse erythrocytes (TCS Biosciences Ltd, Claydon, UK) were excluded from the cell membrane due to the size of the coat and the negative charge of HA.

Sub-confluent of cells cultured in 35 mm dishes were washed with PBS (x2). Formalised horse erythrocytes were washed in PBS and centrifuged at 1000 x g for 7 min at 4°C. This was repeated twice to remove any traces of sodium azide. The pellet was resuspended in serum-free medium at about 10^8 cells per ml. 500 µl of the erythrocytes suspension was added to each 35 mm dish and swirled gently to distribute the suspension evenly. The dished were incubated at 37°C for 15 min to allow the erythrocytes to settle around the cell layer. Photographs were taken using Axiovert 100M inverted microscope fitted with a digital camera (ORCA-1394; Hamamatsu Photonics).

2.12 Statistical analysis

Comparison of groups of data was done by student's t-test, using the "two sample assuming unequal variances" within Microsoft excel (2003 edition). Two-sided tests with a hypothesised mean difference of zero and alpha level of 0.05 were performed. Implicit in this analysis is the assumption that the data populations were normally distributed, although this was not formally tested.

Chapter III
Extracellular HA structures: HA cables and the role of BMP-7 and IL-1β in its regulation

3.1 Introduction

To date, most work investigating the functional consequences of HA has been done by either adding exogenous HA or by defining stimuli that increase HA generation. Much less has been done to define the way in which cells (and PTCs in particular) package HA and what this means in terms of cell function and HA regulation. The work in this chapter aims to shed light on this, less understood, side of HA.

As mentioned in chapter one, extracellular HA is present in 2 main forms: soluble and pericellular (structural). The pericellular form is further subdivided into coats and cable-like structures. De La Motte *et el.* have clearly demonstrated that HA in a novel cable-like form mediated the adhesion of resting monocytes to colonic smooth muscle cells and that the expression of these cable-like structures was influenced by viral infection [258]. As predicted from their large size, these HA cables needed more time to form (17 h post-viral infection) compared to the HA coats (4 hours-post viral infection). Inflammatory cell infiltrates, and particularly monocyte/macrophage infiltrates, have been implicated in the pathogenesis of a wide diversity of renal diseases [387-389]. Understanding the mechanism by which HA mediates inflammatory cell recruitment and its regulation, therefore, has important relevance to kidney disease. The adhesion assay used here was originally developed by DiCorleto and De La Motte for investigating endothelial cell expression of adhesion molecules [362]. The assay exploits the fact that U937 monocytic cells carry the ligands for most of the recognized leukocyte adhesion molecules [64].

BMP-7 is an important potential therapeutic agent for renal diseases. Its relationship with HA regulation is shown in other systems but not in the kidney. For example, in normal human articular chondrocytes, BMP-7 promoted the assembly of ECM through the up-regulation of HAS2 and CD44 mRNA [179]. How BMP-7 achieves its anti-fibrotic effect is still elusive in spite of the extensive research in this area. Further, influence of BMP-7 on HA regulation by PTCs is not known yet.

The role of endoplasmic reticulum (ER) stress in the formation of HA cables was recently reported [170] in colonic smooth muscle cells [170]. The ER is a dynamic membranous organelle with diverse functions including: 1. Protein synthesis, modification, folding and subunit assembly. 2. Steroid synthesis. 3. Lipid synthesis. 4. Glycogen production. 5. Sequestration of Calcium. 6. Maintenance of Calcium homeostasis. Many infectious agents, environmental toxins and adverse metabolic conditions interfere with ER function and homeostasis and induce ER stress [390-393]. Cells elicit an ER stress response/unfolded protein response in an attempt to restore homeostasis by eliminating the discrepancy between ER capacity and demand [390-393]. How the ECM is affected by ER stress is not known yet. Majors *et el.* have reported that induction of ER stress was associated with increased monocytes binding that was mediated via HA cables [170]. Further, the increase in HA cables was not associated with *de novo* protein synthesis but rather with more HAS activity. Finally, IL-1β has been linked with ER stress as it causes excessive nitric oxide (NO) production via NF-κB activation [394-396]. Since IL-1β stimulate HA production in HK-2 cells [175], the association of ER stress and HA cables was examined in this chapter.

Specifically, the aims in this chapter were to:

1. Establish the capability of HK-2 cells to produce HA cable-like structures.
2. Assess the potential of these cables in mediating monocyte binding and elucidate the mechanism of such interactions.
3. Determine whether the anti-fibrotic factor BMP-7 affect the formation of HA cables.
4. Determine whether a known HAS-inducer (IL-1β) can induce cable formation.
5. Investigate whether IL-1β/BMP-7 influence ER stress and its relation with HA cables.

3.2 Results

3.2.1 Visualisation of Hyaluronan: extracellular cable-like structures are produced by HK-2 cells

Confocal imaging of HK-2 cells was used to examine the organisation of HA on the cell surface. HA was identified with a biotinylated preparation of the Hyaluronan-binding protein and detected with fluorescent Avidin-D. Photomicrographs of fixed growth-arrested HK-2 cells demonstrated a thin, diffusely-arranged layer of HA over the cell surface (HA coats). In addition, HA was identified in cable-like structures that spanned several cell lengths (figure 3.1). These cables appear to be composed of coalescing bundles of thinner HA strands originating from neighbouring cells. HK-2 expression of HA cables was variable, although they were present in both sub-confluent and confluent cells (figure 3.1A and D). The number and the size of these cables appear to relate directly to cell number as more and bigger cables were noted in confluent monolayers compared to sub-confluent cultures.

Confirmation of the nature of the HA content of the cable structures was sought by treatment of confluent monolayers of HK-2 cells with bovine testicular hyaluronidase prior to addition of b-HABP. Following limited hyaluronidase digestion, we were unable to identify any of the cable-like structures in either confluent or sub-confluent cells (figure 3.1B and E). Specificity of testicular hyaluronidase in removing HA based structures was confirmed in parallel experiments in which confluent monolayers of unstimulated cells were treated with 1U *Streptomyces* hyaluronidase (ICN Biochemicals, Ohio USA) prior to visualisation of HA (figure 3.1C) as *Streptomyces* hyaluronidase is considered more specific than bovine testicular.

High power confocal images also suggested an association between HA cables and the cell nuclei (figure 3.2). Using fluorescent microscopy, HA cables appear to traverse cells (figure 3.2B), and by visualisation of cell nuclei by staining with DAPI, HA cables could be seen in intimate contact with the nuclear area (figure 2C).

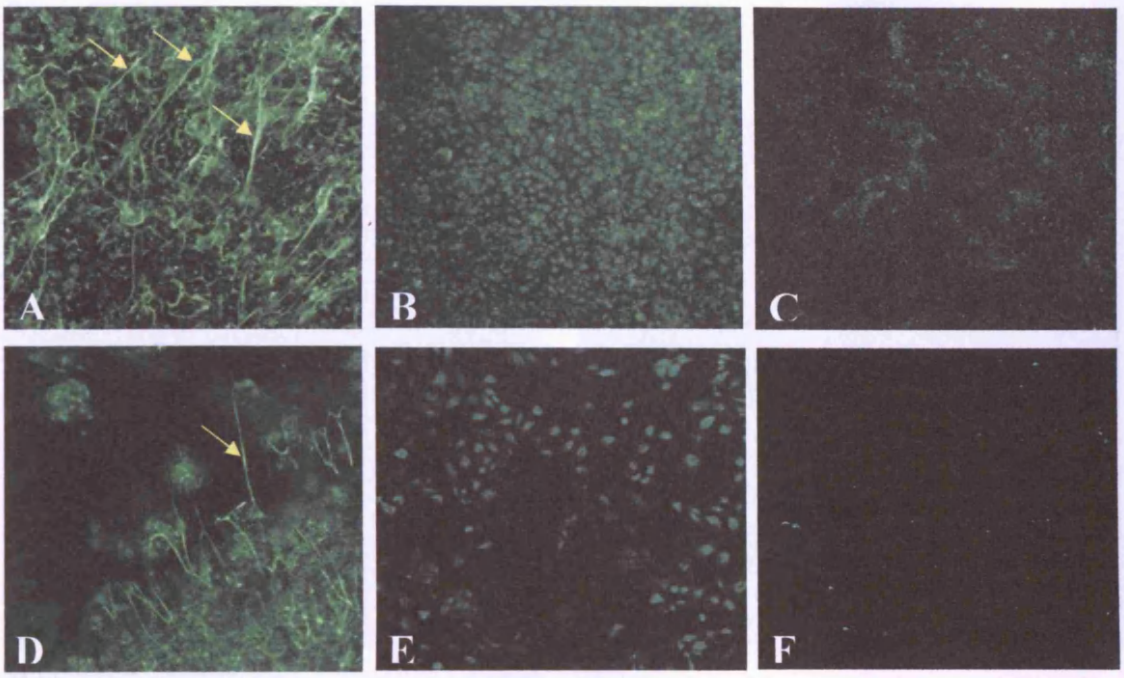

Figure 3.1: Expression of HA on HK-2 cells.

Confluent (**A, B** and **C**) and sub-confluent (**D** and **E**) monolayers of HK-2 cells were serum deprived for 48 h prior to fixation with methanol and detection of HA by addition of biotinylated HABP. HA cables (arrows) were present in both confluent and sub-confluent HK-2 cultures.

To confirm the nature of HA staining, in parallel experiments, cells were treated with bovine testicular hyaluronidase (200 μg/ml) at 37°C for 5 min, prior to fixation and addition of biotinylated HABP (**B** and **E**).

Specificity of testicular hyaluronidase was confirmed by removal of cell surface HA using 1U of *Streptomyces* hyaluronidase (at 37°C for 60 min) prior to visualisation of HA (**C**).

In (**F**), only FITC-labelled streptavidin was added and it shows minimal non-specific binding to confluent monolayers of HK-2 cells. Sections were imaged by confocal microscopy.

A-F magnification x 100.

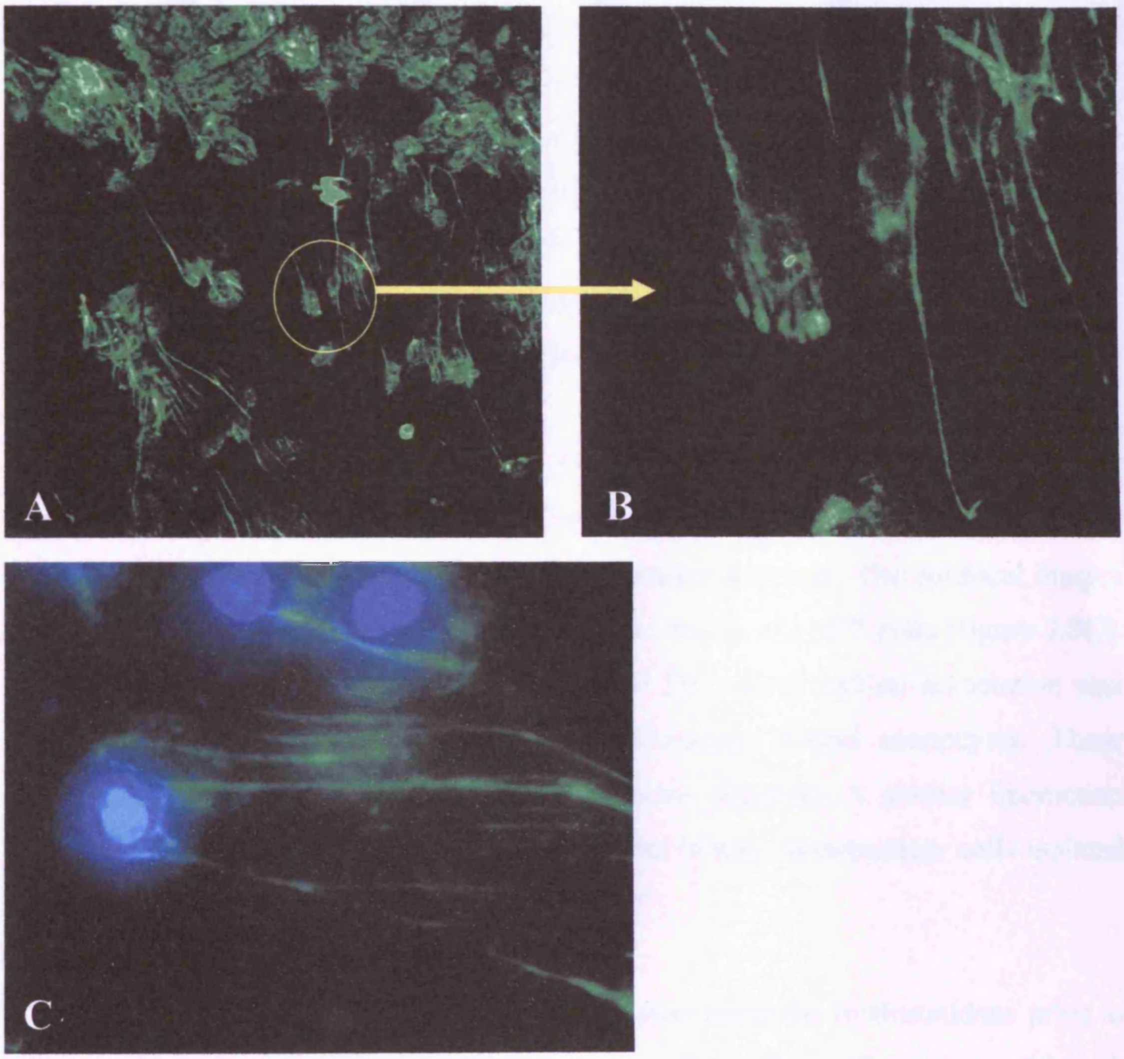

Figure 3.2: HA cables are closely associated with HK-2 cells nuclei.

HK-2 cells were fixed and stained for HA as described in chapter two. Pictures were taken using confocal microscopy in **A** (magnification x 100) and **B** (magnification x 400), and fluorescence microscopy in **C** (magnification x 400) where cell nuclei were visualised with DAPI staining.

3.2.2 Monocytes bind to extracellular HA cables

To study the functionality of HA cables, monocytes binding was assessed in order to know whether these extracellular HA structures provide a site of attachment or not. Observations made by light microscopy revealed that unstimulated HK-2 cells bind U937 cells abundantly. Cell localisation was determined by DAPI staining of nuclei. Adherent U937 cells appeared as either cells bound individually, or cells bound in chains (figure 3.3A). These observations, however, can't confirm whether HA is involved in the adhesion process or not.

The relationship between bound U937 cells and HA cable structures was examined by confocal microscopy. U937 cells added to monolayers of unstimulated HK-2 cells were detected with anti-CD68 monoclonal antibody. The confocal images showed co-localisation of the HA cables and the chains of U937 cells (figure 3.3C). Monocytes were also present in areas devoid of HA cables and no association was seen between pericellular HA coats and individually bound monocytes. These findings suggested the involvement of a different receptor. A similar interaction between monocytes and HA cables was seen with human mononuclear cells isolated from peripheral blood and HA cables (figure 3.3F).

Treatment of HK-2 monolayers with bovine testicular hyaluronidase prior to addition of U937 cells prevented U937 binding in chain-like configurations, although binding of scattered individual cells persisted after hyaluronidase treatment. This was demonstrated after DAPI staining (figure 3.3B), and also following HA and U937 staining (figure 3.3G). Similarly, when cell monolayers were treated with testicular hyaluronidase after the addition of the monocytes, no binding of monocytes in chain-like configurations, and no HA cables were seen (data not shown).

It has been previously suggested that monocytes may interact with HA via monocyte cell surface CD44 [397]. Pre-incubation of U937 cells with anti-CD44 Ab, before adding them to an unstimulated HK-2 monolayer, markedly decreased binding of monocytes to HA cables (figure 3.3F). Addition of the CD44 antibody did not affect monocytes binding in the scattered pattern.

The nature of monocyte-PTC interaction was further examined by addition of radiolabelled monocytes to unstimulated confluent monolayers of HK-2 cells (figure 3.4). Bound radioactivity was reduced by either addition of soluble ICAM (200 ng/ml; R&D Systems) or addition of CD44 antibody (5 μg/ml; The Binding Site, UK) to the monocytes (prior to the binding phase of the experiment), although this was more prominent following CD44 blockade (about 20% reduction). Combined blockade of both ICAM ligands and CD44 receptors further reduced monocyte binding (about 40% reduction; $p<0.005$), thus suggesting that both HA-based interactions and ICAM-dependent interactions contribute to monocyte binding to unstimulated HK-2 cells.

The nature of monocyte-PTC interaction was studied in parallel by using hyaluronidase treatment. Removal of the HA cables by incubation with bovine testicular hyaluronidase prior to the addition of radiolabelled monocytes led to an increase in bound radioactivity, thus suggesting that HA cable-dependent monocyte binding may limit or block monocyte binding to cell surface ICAM by physically preventing the monocytes from reaching HK-2 cell ICAM receptors (figure 3.4).

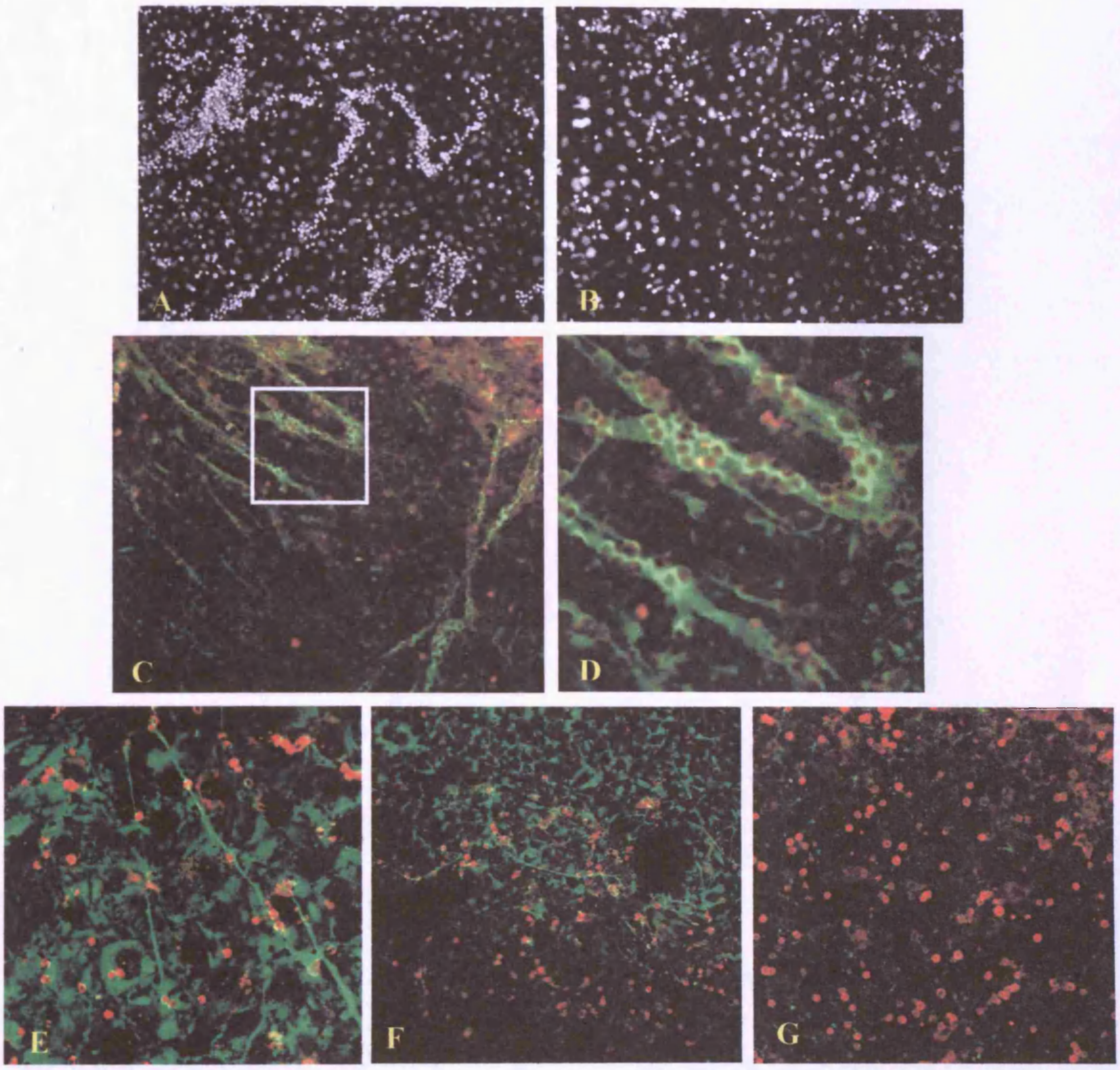

Figure 3.3: HA cables on confluent monolayers of HK-2 cells bind unstimulated monocytes.

Confluent monolayers of HK-2 cells were serum deprived for 48 h prior to the addition of unstimulated U937 cells at 37°C for 1 h prior to fixation. Localisation of monocytes was visualised by staining of cell nuclei with DAPI (**A** and **B**; magnification x 100). Binding of monocytes in chain like configurations can be seen **(A)**. This was abrogated when cells were treated with bovine testicular hyaluronidase at 37°C for 5 min prior to addition of monocytes **(B)**.
In parallel experiments **(C-G)**, HA (green) and monocytes (red) were visualised by addition of bioinylated HABP and anti-CD68 antibody respectively. U937 cells binding to HA cables on unstimulated HK-2 cells is shown in (**C**; magnification x 100) and (**D**; magnification x 300) while PBMC binding is shown in (**E**; magnification x 300).
The role of CD44 in monocyte binding was assessed by addition of anti-CD44 antibody (5 μg/ml) to monocytes for 1 h at 4°C prior to their addition to confluent un-stimulated HK-2 cells (**F**; magnification x 200). Monocyte binding was also assessed following treatment of HK-2 monolayers with bovine testicular hyaluronidase at 37°C for 5 min (**G**; magnification x 200).

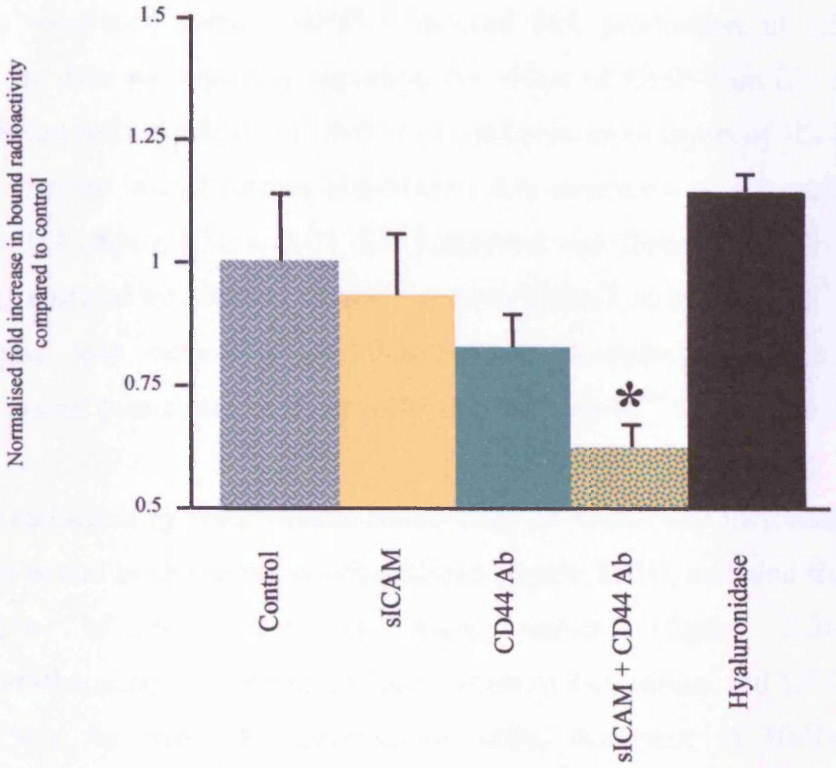

Figure 3.4: Quantification of monocyte binding to unstimulated HK-2 cells.

In control experiments, confluent monolayers of serum-deprived HK-2 cells were washed with PBS prior to addition of 1 x 10^6 ^{51}Cr-labelled U937 cells under serum-free conditions for 1 h at 37°C. Quantification of bound radioactivity was carried out as described in chapter two. Soluble ICAM (sICAM; 200 ng/ml) or anti-CD44 antibody (CD44; 5 µg/ml), were added to ^{51}Cr-labelled U937 cells for 1 h at 4°C prior to their addition to confluent monolayer of unstimulated HK-2 cells, or the monolayer was treated with bovine testicular hyaluronidase (200 µg/ml) at 37°C for 5 min prior to addition of monocytes. Bound radioactivity was subsequently quantified. Data represent mean ± SD of four individual experiments (* $p<0.005$).

3.2.3 BMP-7 stimulates HA cable formation and increases HA-dependent monocyte binding

As mentioned earlier, BMP-7 induced HA production in other systems. However, no data are available regarding the effect of BMP-7 on HA regulation in renal epithelial cells. Addition of BMP-7 to confluent monolayers of HK-2 cells led to a marked increase in cell surface HA-based cable structures as assessed by confocal imaging of HA (figure 3.5B and C). The functional significance of the increase in HA cables was assessed by addition of U937 cells to BMP-7 stimulated HK-2 cells. U937 cell binding was examined by fluorescence microscopy and quantified by determination of bound radioactivity following addition of ^{51}Cr-labelled U937 cells.

Examination by fluorescence microscopy demonstrated increased numbers of monocytes bound in chain-like configurations (figure 3.5H), and also showed thicker aggregations of monocytes in these cables (figure 3.5G). Double immunocytochemistry confirmed co-localisation of HA cables and U937 cell chains (figure 3.5F). As with the unstimulated cells, treatment of BMP-7-stimulated monolayers of cells with bovine testicular hyaluronidase prior to the addition of U937 cells removed the HA cables and also abrogated binding of U937 cells in chain-like configurations, although binding of individual cells was still seen.

Quantification of monocyte binding, following stimulation with BMP-7 for 24 h, confirmed that there was a significant increase in bound U937 cells at all doses of BMP-7 added (figure 3.6A). Following stimulation with BMP-7 (200 ng/ml) this represented a 118% increase of bound U937 cells over control, and for BMP-7 (800 ng/ml) a 160% increase ($p=0.0001$ for both). The increase in monocyte binding following stimulation with BMP-7 was attenuated (about 25% reduction; $p=0.0005$) when the monocytes were pre-incubated with anti-CD44 blocking antibody prior to the binding phase (figure 3.6B) suggesting that this increment in monocyte binding was mediated by interaction with HA.

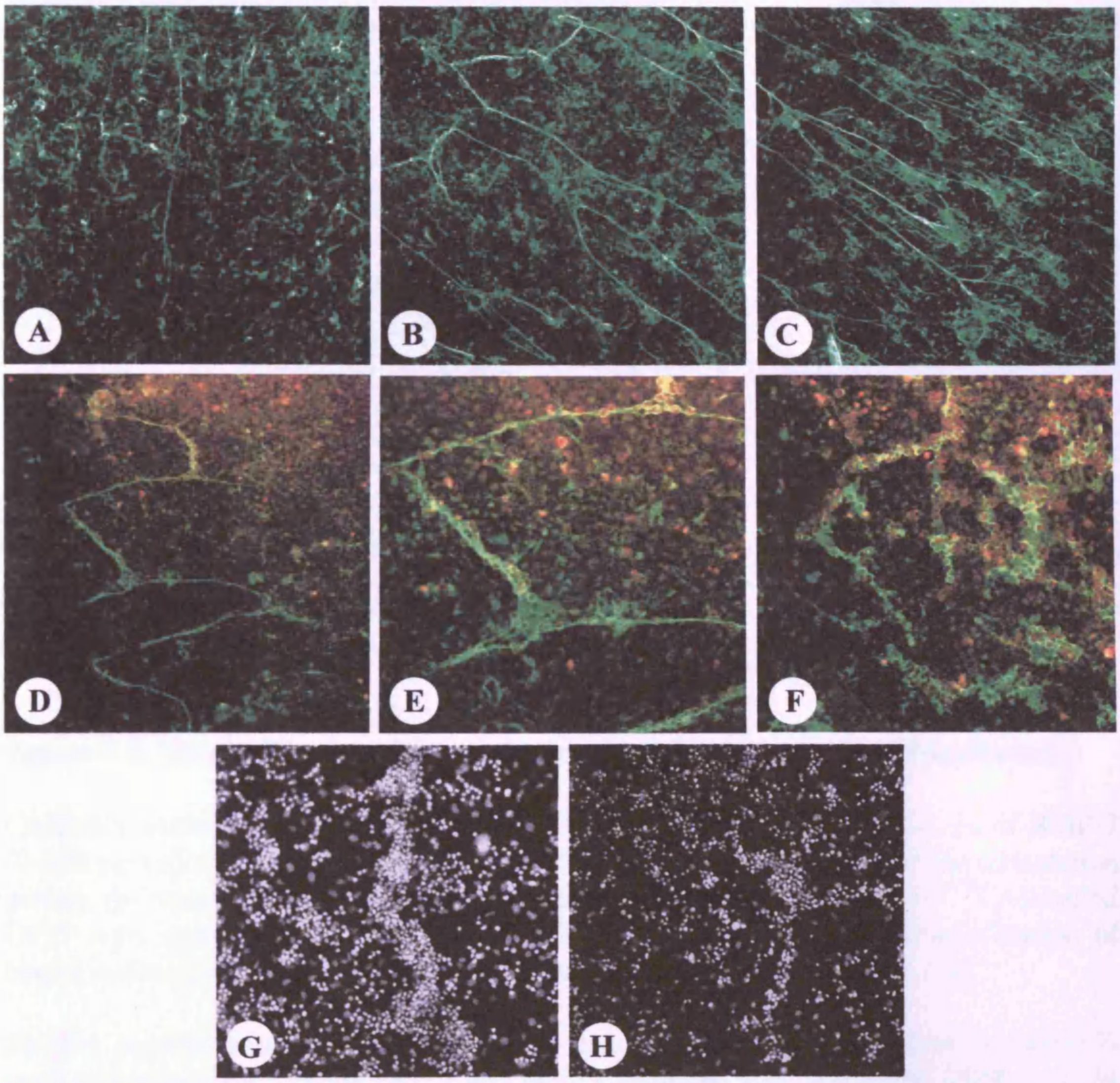

Figure 3.5: Induction of HA cables and monocyte binding by BMP-7.

Following 48 h of serum deprivation, BMP-7 (400 ng/ml) was added to confluent monolayers of HK-2 cells for 24 h under serum free conditions (**B** and **C**). In control cultures cells were exposed to serum-free medium alone (**A**). Following fixation HA was visualised by addition of biotinylated HABP and confocal imaging (magnification x 100).

In parallel experiments following BMP-7 stimulation (400 ng/ml), the monolayers were washed prior to addition of unstimulated U937 cells. Monocytes were visualised both by staining of cell nuclei with DAPI (**G**; magnification x 200 and **H**; magnification x 100), and double immunocytochemistry using biotinylated HABP and anti-CD68 antibody (**D**; magnification x 100, **E** and **F**; magnification x 200).

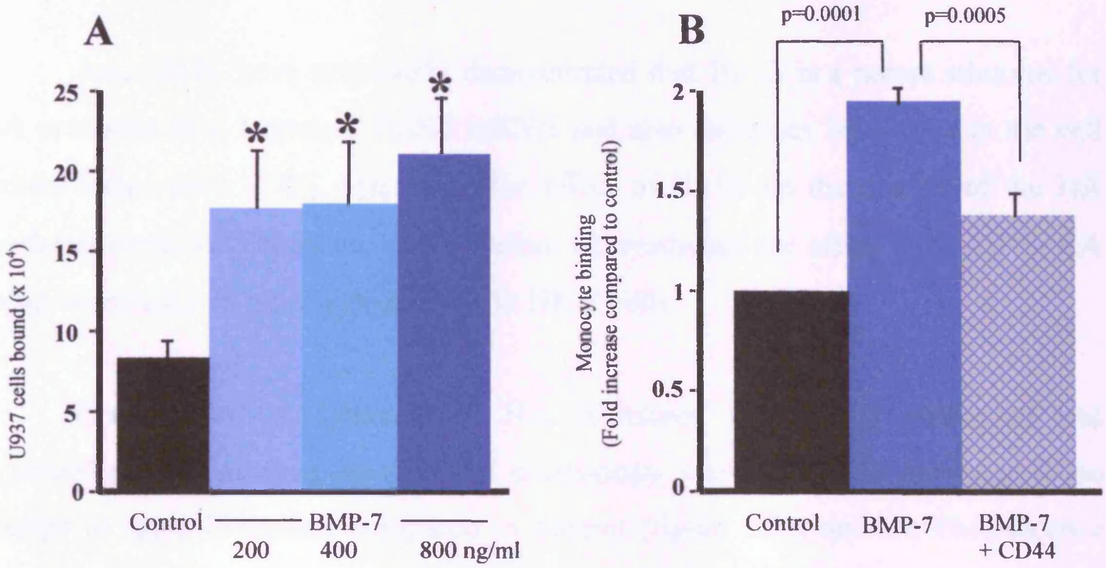

Figure 3.6: Quantification of monocyte binding following BMP-7 stimulation.

Confluent monolayers of HK-2 cells were stimulated with increasing doses of BMP-7 (0-800 ng/ml) under serum-free conditions for 24 h (**A**). At the end of the stimulation period, the monolayer was washed with PBS prior to addition of 1 x 10^6 ^{51}Cr-labelled U937 cells again under serum-free conditions for 1 h at 37°C. Quantification of bound radioactivity was carried out as described in chapter two (* $p<0.05$).

Parallel experiments were performed to determine the role of CD44 in BMP-7-mediated monocyte binding (**B**). Cells were stimulated with 400 ng/ml BMP-7 for 24 h. Anti-CD44 antibody (5 μg/ml) was added to ^{51}Cr-labelled U937 cells for 1 h at 4°C prior to their addition to confluent monolayers of stimulated HK-2 cells. Bound radioactivity was subsequently quantified. Data represent the mean ± SD of four individual experiments.

3.4 IL-1β increases HA synthesis but does not increase HA cable formation

Jones *et el.* have previously demonstrated that IL-1β is a potent stimulus for HA synthesis as it increases HAS2 mRNA and also increases HA levels in the cell culture supernatant [175]. However the effect of IL-1β on the quality of the HA produced remained unknown, and therefore I investigated the effect of IL-1β on HA cable formation and monocyte binding in HK-2 cells.

Comparison of extracellular HA structures between IL-1β-treated and untreated control cultures, by confocal microscopy, showed a slight reduction or no change in cable formation compared to control (figure 3.7A and B). Fluorescence microscopic examination of IL-1β stimulated monolayers demonstrated binding of individual U937 cells, but minimal binding in chain-like configurations (figure 3.7D).

To confirm microscopic observations, monocyte adhesion experiments were done. Stimulation of monolayers of HK-2 cells with IL-1β led to a dose-dependent increase in binding of ^{51}Cr-labelled U937 cells. IL-1β stimulated adhesion was significantly greater than binding of ^{51}Cr-labelled U937 cells to control monolayers of HK-2 cells at all doses. IL-1β at a dose of 1 ng/ml induced a 45% increase in bound U937 cells over control (p=0.0012), whilst at the highest dose of IL-1β used (100 ng/ml) a 76% increase in bound U937 cells was seen (p=0.0001) (figure 3.8A). In contrast to BMP-7-induced adhesion, IL-1β-induced monocyte binding was not affected by the addition of a blocking antibody to CD44 (figure 3.8B).

Since the increment in monocyte binding was not HA/CD44-dependent, I investigated the role of other monocyte adhesion molecules. ICAM-1 was the best candidate in here as ICAM-1 is expressed by PTCs [121] and can also be induced by various inflammatory cytokines including IL-1β [398, 399].

Addition of monocytes pre-treated with soluble ICAM-1 receptor to IL-β1-stimulated monolayers of HK-2 cells resulted in marked inhibition of the IL-1β-induced increase in monocyte binding (about 55%; p=0.0001, figure 3.8B). Similar results were obtained when the monocytes were incubated with an anti-LFA-1 Ab (ICAM-1 counter-ligand; data not shown).

The state of ICAM-1 RNA expression was also investigated to see whether it had a role in the increased monocyte binding seen following IL-1β stimulation. IL-1β , as reported by others [400, 401], increased the expression of ICAM-1 mRNA and this effect was most evident at 6 h (80% increase) but it is still noted after 24 and 48 h. BMP-7, as reported by Gould *et el.* [106], reduced ICAM-1 mRNA. This reduction was seen from 6 h (60% reduction) and it was most evident 24 h after stimulation (80% reduction). By 48 h, ICAM-1 mRNA levels were similar to that of control (figure 3.9).

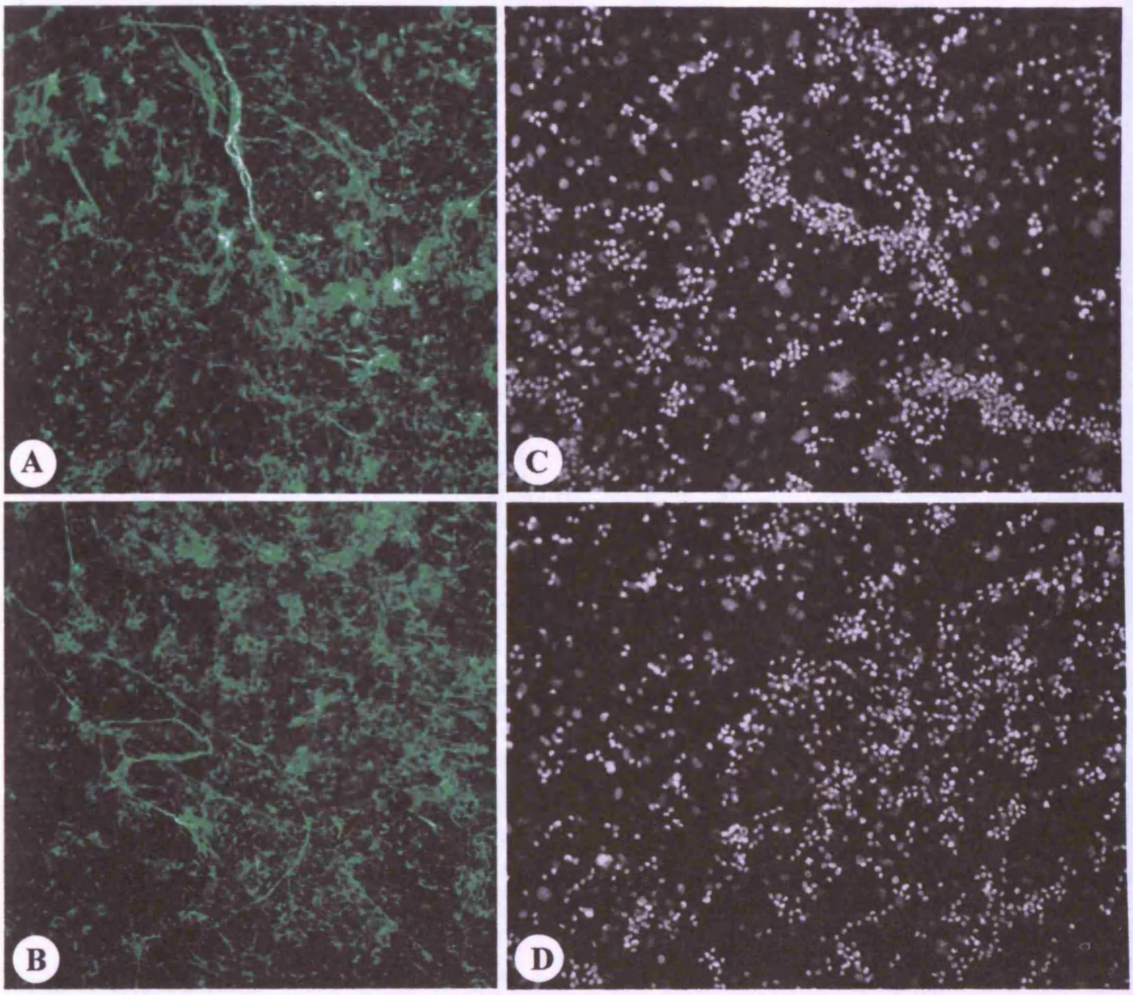

Figure 3.7: IL-1β did not induce HA cable formation.

Visualisation of HA and monocytes in control cells (**A** and **C**) and following IL-1β stimulation (**B** and **D**). Following 48 h of serum deprivation, IL-1β (1 ng/ml) was added to confluent monolayers of HK-2 cells for 24 h under serum-free conditions. In control experiments cells were exposed to serum-free medium alone. Following fixation HA was visualised after the addition of biotinylated HABP by confocal imaging (**A** and **B**; magnification x 100).

In parallel experiments following IL-1β stimulation, the monolayers were washed prior to addition of unstimulated U937 cell. In both IL-1β stimulated (**D**) and control (**C**) monolayers, monocytes were visualised by staining of cell nuclei with DAPI (magnification x 100).

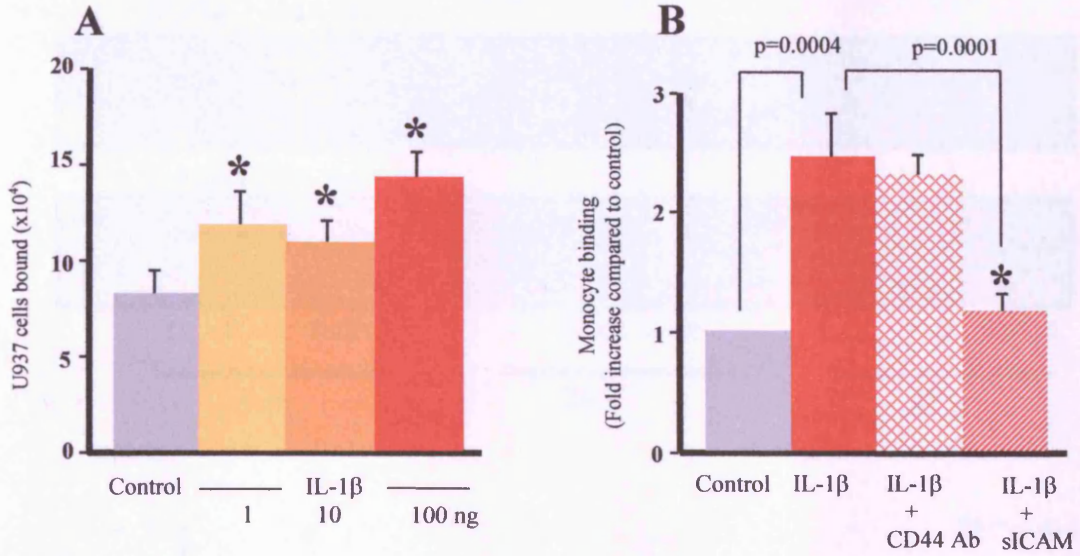

Figure 3.8: Quantification of monocyte binding following IL-1β stimulation.

Confluent monolayers of HK-2 cells were stimulated with increasing doses of IL-1β (0-100 ng/ml) under serum-free conditions for 24 h **(A)**. At the end of the stimulation period, the monolayer was washed with PBS prior to addition of ^{51}Cr-labelled U937 cells again under serum free conditions for 1 h at 37°C. Quantification of bound radioactivity was carried out as described in chapter two.

Parallel experiments were done to determine the role of CD44 and ICAM in IL-1β-mediated monocyte binding **(B)**. Cells were stimulated with 1 ng/ml IL-1β for 24 h. Anti-CD44 antibody (5 μg/ml), or soluble ICAM (200 ng/ml) was added to ^{51}Cr-labelled U937 cells for 1 h at 4°C prior to their addition to confluent monolayers of stimulated HK-2 cells. Bound radioactivity was subsequently quantified. Data represent mean ± SD of four individual experiments (* $p<0.05$).

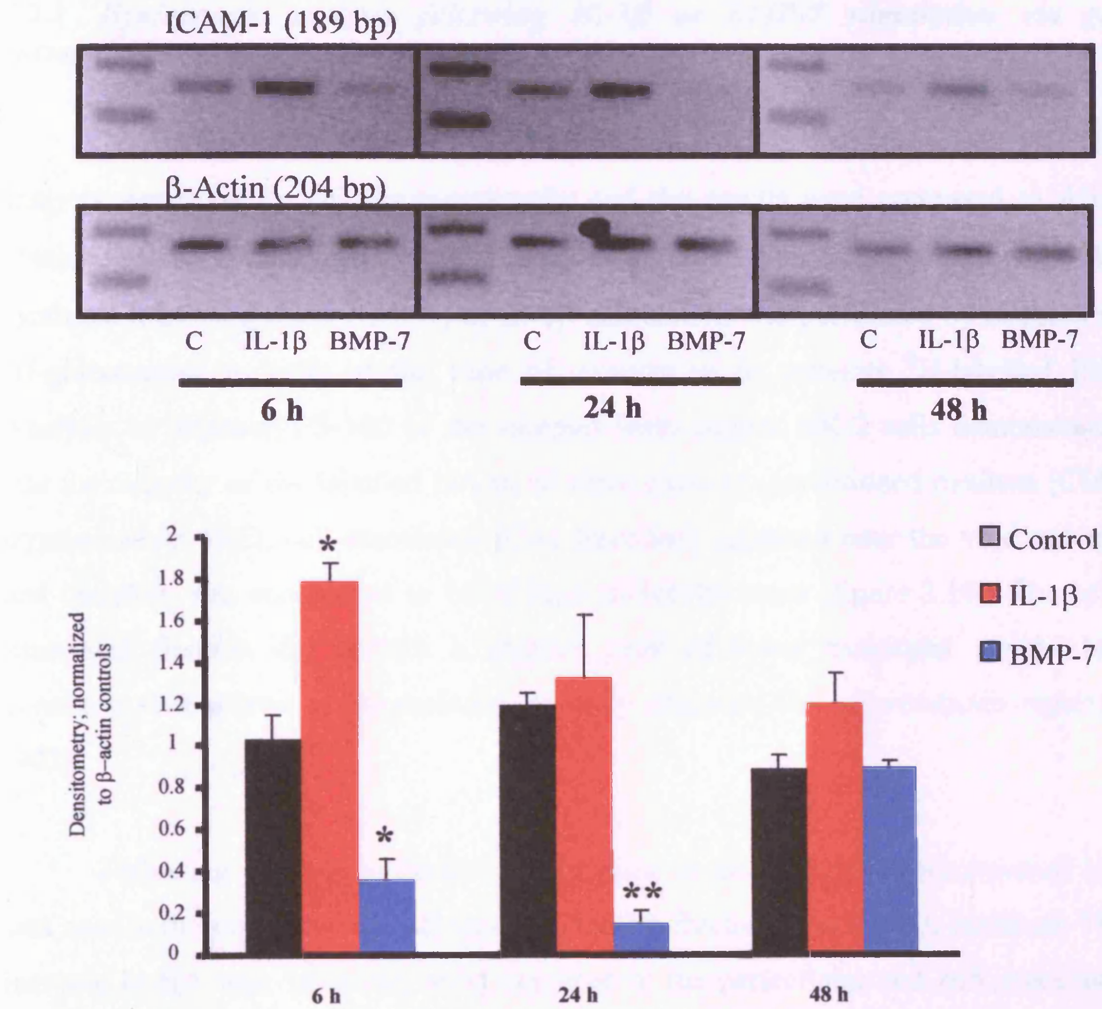

Figure 3.9: ICAM-1 mRNA expression in HK-2 cells.

Confluent monolayers of HK-2 cells were stimulated with either IL-1β (1 ng/ml) or BMP-7 (400 ng/ml) for 6, 24 or 48 h. In control (C) experiments, cells were exposed to serum-free medium only. At the end of the experimental period total cellular RNA was extracted and RT-PCR done as described in chapter two. Ethidium bromide-stained PCR products were separated on a 3% agarose gel. Densitometric ratios, normalised to the control value, of each of the genes of interest compared to the house-keeping gene, β-actin, of 4 individual experiments are shown in the graph. Data represents mean ± SD. *$p<0.05$, **$p=0.0001$ compared to the mean control ratio for each experiment.

3.2.5 Hyaluronan analysis following IL-1β or BMP-7 stimulation via gel chromatography

To further understand how BMP-7 influences HA regulation in PTC, HA analysis was done by gel chromatography and the results were compared to those obtained using unstimulated cells and after IL-1β stimulation. Characterisation of HA synthesis following either BMP-7, or IL-1β stimulation was performed by addition of ^{3}H-glucosamine to cells at the time of stimulation to generate ^{3}H-labelled HA. Analysis on Sephacryl S-500 of the samples from control HK-2 cells demonstrated that the majority of the labelled HA in all three extracts (conditioned medium [CM], trypsin extract [TE], cell-associated [CA] fractions) appeared near the void volume and therefore was considered to be of high molecular mass (figure 3.10). The cell-associated fraction did contain a smaller peak of lower molecular weight HA consistent with a pool of intracellular, partially degraded HA as previously reported [402].

Following addition of BMP-7, an increase in the amount of radiolabelled HA was seen in the supernatant (CM) fraction, the TE fraction, and the CA fractions. The increase in HA was, however, most apparent in the pericellular and cell associated fractions. Furthermore in the cell-associated fraction, there was an apparent increase in the molecular weight distribution of the second, lower molecular weight peak (figure 3.10). When the data were plotted in percentage graphs, low molecular weight HA constituted about 45% of total CA (figure 3.11 CA fraction) while BMP-7 reduced that percentage to about 22% in spite of increased total HA in the CA fraction. This suggested an altered HA catabolism in the BMP-7-treated sample.

Following IL-1β stimulation, there was also an increase in the amount of HA in all three cellular pools. However, in contrast to BMP-7-associated changes, IL-1β induced the largest change in the high molecular weight HA secreted into the cell culture supernatant (figure 3.10 and 3.11). Consistent with previous reports that showed increased intracellular and pericellular HA after IL-1β stimulation [219], IL-1β stimulation produced an increment of HA in both CA and TE fractions (figure 3.10 and 3.11).

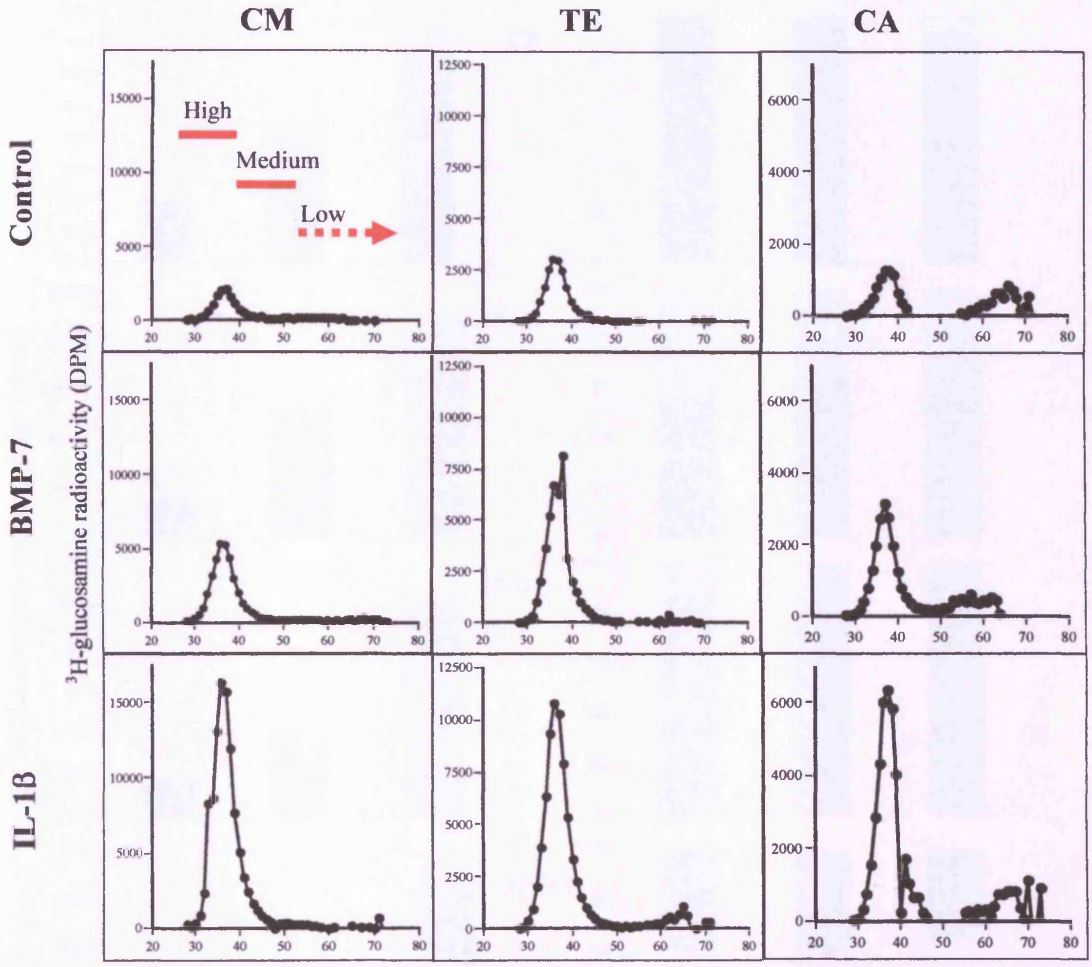

Figure 3.10: Analysis of ^{3}H-radiolabelled HA.

Confluent serum deprived monolayers of HK-2 cells were stimulated with BMP-7 (400 ng/ml) or IL-1β (1 ng/ml), or exposed to serum free medium (for Control) for 24 h in the presence of 20 μCi/ml ^{3}H-glucosamine. Subsequently conditioned medium **(CM)**, protein bound **(TE)** and cell-associated **(CA)** Hyaluronan fractions were prepared as described in chapter two. Radiolabelled HA was subsequently analysed by Sephacryl S-500 chromatography, followed by measurement of the radiolabel.

The bars labelled as high, medium and low represent molecular weight ranges (high molecular weight > 10^{6} Da, medium molecular weight between 10^{5}-10^{6} Da, low molecular weight < 10^{5} Da).

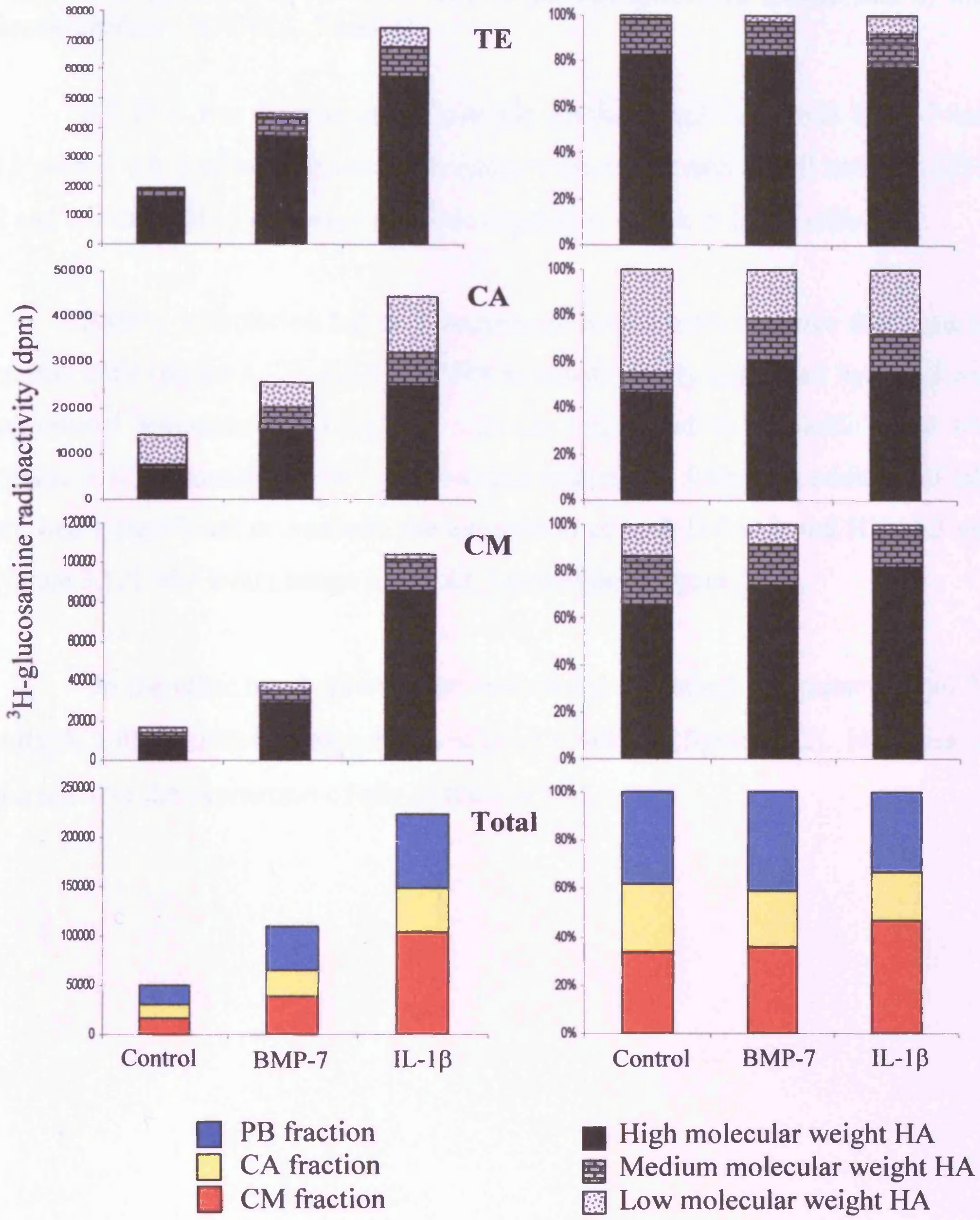

Figure 3.11: Analysis of ^{3}H-radiolabelled HA.

Confluent serum-deprived monolayers of HK-2 cells were stimulated with BMP-7 (400 ng/ml) or IL-1β (1 ng/ml), or exposed to serum free medium (as control) for 24 h in the presence of 20 μCi/ml ^{3}H-glucosamine. Subsequently conditioned medium **(CM)**, protein bound **(TE)** and cell associated **(CA)** Hyaluronan fractions were prepared and analysed as described in chapter two. The graphs on the left represent the absolute counts while the graphs on the right represent the percentage of different molecular weight HA in each fraction (High molecular weight > 10^6 Da, Low molecular weight < 10^5 Da). The lower left graph represent the total data from all 3 fractions plotted together and the percentage of each fraction.

3.2.6 The influence of IL-1β or BMP-7 on HA synthases (HAS2 and 3) and on hyaluronidases (HYAL1, 2 and 3)

RT-PCR was done to investigate the mechanism(s) by which BMP-7 and IL-1β altered HA profile. The candidate genes were HAS2 and HAS3 and also HYAL1, 2 and 3 because they represent the main regulators of HA in HK-2 cells.

BMP-7 stimulation led to induction of HAS2 mRNA above that seen in the control cells (figure 3.12). HAS3 mRNA is constitutively expressed by HK-2 cells as previously demonstrated [175], and was not influenced by the addition of BMP-7 (figure 3.12). Examination of hyaluronidase expression following addition of BMP-7 showed a significant decrease in the expression of both HYAL1 and HYAL2 mRNA (figure 3.12) with a no change in HYAL3 expression (figure 3.13).

On the other hand, stimulation with IL-1β increased the expression of HAS2 mRNA, without affecting expression of HAS 3 mRNA (figure 3.12). However, IL-1β did not alter the expression of any of the 3 HYALs.

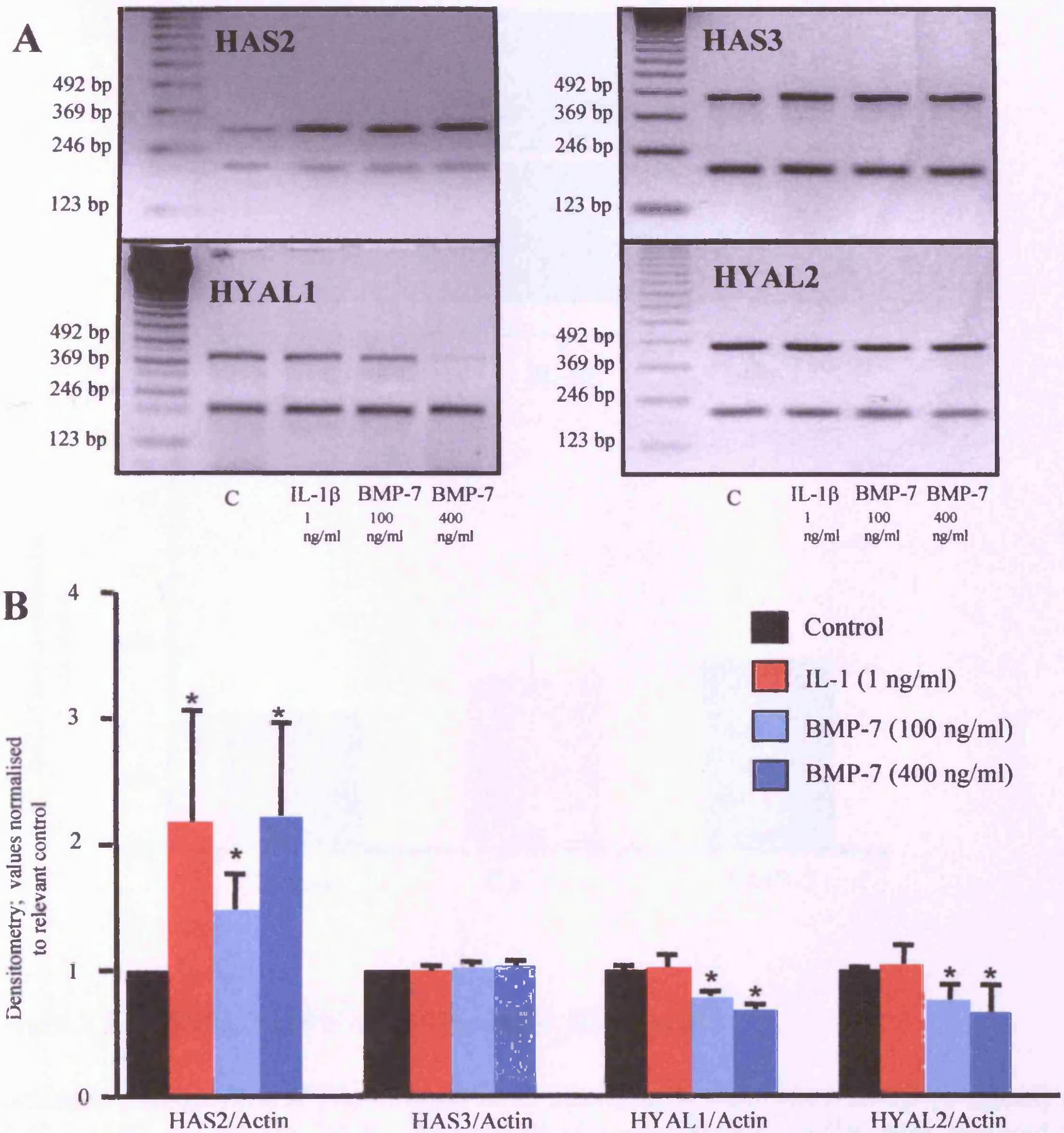

Figure 3.12: Expression of HA synthases (HAS2 and HAS3) mRNA and hyaluronidase (HYAL1 and HYAL2) mRNA.

(A) Confluent monolayers of HK-2 cells were stimulated with either IL-1β (1 ng/ml) or increasing doses of BMP-7 (0-800 ng/ml) for 24 h. In control (C) experiments, cells were exposed to serum-free medium only. At the end of the experimental period total cellular RNA was extracted and RT-PCR done as described in the chapter two. Ethidium bromide-stained PCR products were separated on a 3% agarose gel. Upper bands represent genes indicated in the picture; lower bands represent corresponding β-actin.

(B) Densitometric ratios, normalised to the control value, of each of the genes of interest compared to the house-keeping gene, β-actin, of 4 individual experiments are shown in the graph. Data represents mean ± SD. *$p<0.05$ compared to the mean control ratio for each experiment.

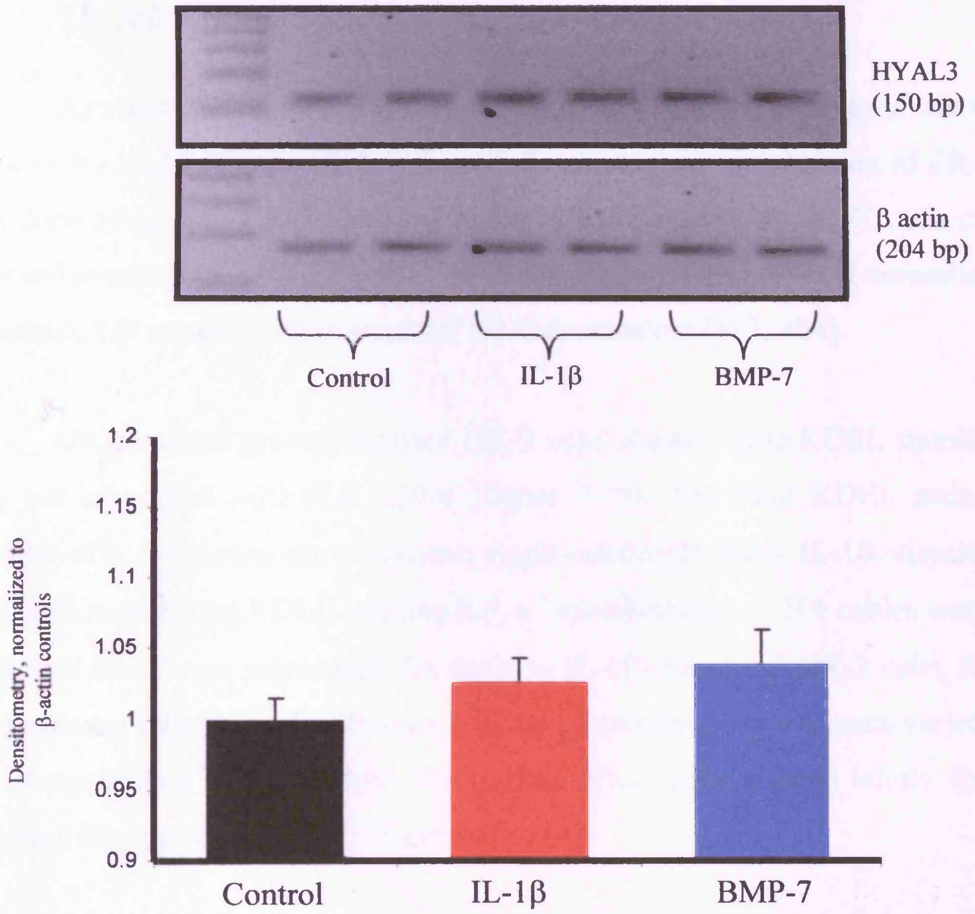

Figure 3.13: HYAL3 mRNA expression in HK-2 cells.

Confluent monolayers of HK-2 cells were stimulated with either IL-1β (1 ng/ml) or BMP-7 (400 ng/ml) for 24 h. In control (C) experiments, cells were exposed to serum-free medium only. At the end of the experimental period total cellular RNA was extracted and RT-PCR done as described in chapter two. Ethidium bromide-stained PCR products were separated on a 3% agarose gel. Densitometric ratios, normalised to the control value, of each of the genes of interest compared to the house-keeping gene, β-actin, of 4 individual experiments are shown in the graph. Data represents mean ± SD.

3.2.7 The role of ER stress in HA cable formation

As mentioned earlier, the association of ER stress and HA cables was reported recently by Majors *et al.* [170]. Using confocal imaging, visualisation of ER and HA was done using anti-KDEL antibody and b-HABP respectively. KDEL is a carboxyl-terminal tetrapeptide Lys-Asp-Glu-Leu that is found at the carboxyl terminus of a set of soluble ER proteins and is essential for their retention [403, 404].

Unstimulated growth-arrested HK-2 cells showed little KDEL staining and it was not associated with HA cables (figure 3.14). The faint KDEL staining is a possible effect of serum-starvation as it might induce ER stress. IL-1β-stimulated HK-2 cells showed strong KDEL staining but, as described earlier, HA cables were scarce. Although there were prominent HA coats in IL-1β-stimulated HK-2 cells, there was no consistent relation with ER stress (i.e. cells exhibiting big HA coats varied in their ER stress status). Finally, BMP-7-stimulated HK-2 cells stained faintly for KDEL although they produced more HA cables.

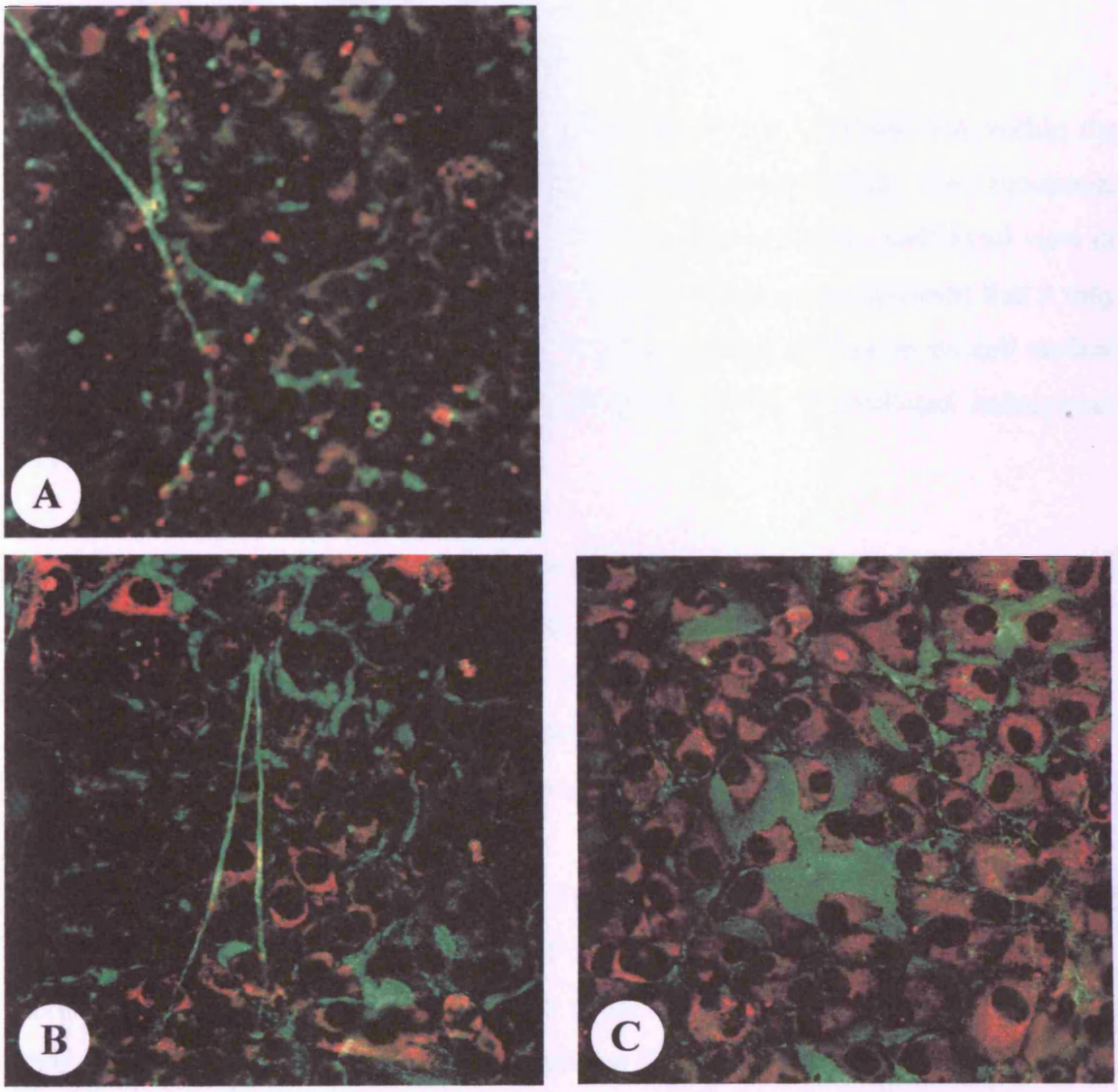

Figure 3.14: Visualisation of ER stress and HA.

Confluent growth-arrested HK-2 cells were stimulated with either serum-free medium as control (**A**), 400 ng/ml of BMP-7 (**B**) or 1 ng/ml IL-1β (**C**) for 24 h before fixation with 100% ice-cold methanol and staining with anti-KDEL Ab (Red) & b-HABP (Green) as described in chapter two (magnification x 300).

Discussion

Although numerous studies have demonstrated that increased HA within the kidney cortex is associated with different renal pathologies, the functional significance of these changes is not clear. What is clear is that the traditional view of HA being a structural scaffold is now being revised as it becomes apparent that it may function as a cellular signalling molecule, following either binding to its cell surface receptors (CD44 and RHAMM) or internalisation via CD44-mediated endocytosis [405].

In this chapter, it is been demonstrated that HA can mediate binding of monocytes to proximal tubular cells when HA coalesces into cable-like structures. These structures seem to originate from numerous different cells and form cables spanning several cell lengths (figure 1 and 2). HA cables present on unstimulated cells bind unstimulated monocytes, and their formation is up-regulated by BMP-7. As a consequence of increased HA cable formation, BMP-7 also increased HA-dependent monocyte binding. Increased HA cable formation following addition of BMP-7 was associated with induction of HAS2 mRNA, and an increase in newly synthesised cell associated HA was also observed. This would suggest a specific effect of BMP-7 on the assembly of pericellular HA structures in renal epithelial cells similar to the effect of BMP-7 on bovine articular cartilage chondrocytes [406].

Previous studies utilising colonic mucosal smooth muscle cells have suggested that the HCs of IαI are critical to the formation HA-based cables [258]. In my work, it was noted that there was a marked attenuation of HA cable formation in the absence of serum. All experiments described in this chapter were performed in the absence of serum. However, we have previously demonstrated that proximal tubular cells express bikunin and HC3 components of the IαI family constitutively [343]. This may, therefore, explain the ability of proximal tubular cells to generate stable HA-based cable structures in the absence of serum components. The role of IaI/preαI in the formation of HA cables will be discussed later in more detail (chapter five).

The specificity of the effect of BMP-7 was confirmed by data demonstrating that IL-1β, despite being a potent stimulus of HA synthesis, was unable to alter HA cable formation. IL-1β did however increase monocyte binding. This increase appeared to be unrelated to any alteration in formation of HA cables, but rather monocyte binding to HK-2 cells was mediated by other leukocyte adhesion molecules, in particular ICAM-1. Importantly, this data provides evidence that not only the quantity, but also the structure of HA is crucial for leukocyte binding.

In vitro studies shed some further light on the mechanistic basis of the mode of action of BMP-7. In mesangial cells, BMP-7 reduces TGF-β1-induced ECM effects [111] and *in vitro,* in proximal tubular cells, BMP-7 antagonises TNF-α-stimulated increases in expression of pro-inflammatory cytokines and chemokines [106]. There are no reports to date, apart from the work presented here, that relate the anti-inflammatory and anti-fibrotic effects of BMP-7 to increased HA production and the subsequent HA-mediated monocyte binding.

An important difference between BMP-7 and IL-1β in terms of their impact on HA turnover is their effects on hyaluronidase expression. Data in this chapter demonstrate down-regulation of hyaluronidase (HYAL1 and HYAL2) at the level of transcription by BMP-7 while IL-1β did not alter expression of either enzyme. The change in the molecular weight of the cell-associated HA following stimulation with BMP-7 is consistent with decreased intracellular degradation of HA due to reduced hyaluronidase activity. As yet there are no antibodies available to confirm that this was also paralleled by a decrease in protein expression and enzyme activity, but it is interesting to speculate that this difference between BMP-7- and IL-1β–mediated regulation of hyaluronidase may be key to understanding their differential effects on HA cable formation. HA synthesis occurs at or close to the cell membrane, and the growing HA chain is extruded through the membrane into the extracellular space [407]. At this stage, it is plausible to postulate that down-regulation of hyaluronidase activity by BMP-7 allows HA to remain associated with HAS, and that HA extruded through the cell membrane is anchored to HAS isoforms and associates with similarly anchored HA from neighbouring cell thus forming cables. In contrast, when hyaluronidase activity is unaffected, as seen following addition of IL-1β, extruded

HA is cleaved at the cell surface and secreted into the surrounding environment. In this study, this is reflected by the increased concentration of HA in the culture supernatant following addition of IL-1β, whilst BMP-7 led to a much smaller increase of HA in the culture supernatant, presumably due to less HA cleavage and release.

Binding interactions between leukocytes and other cells are best characterised in endothelial cells in which leukocyte integrins on their surface bind to their ligands such as ICAM-1 and VCAM-1 [408]. Similar mechanisms of binding have been demonstrated in resident renal cells such as PTCs [409] and fibroblasts [410]. Unstimulated PTCs express low levels of ICAM-1 with no VCAM-1 expression [121], and up-regulation of the adhesion molecules predict outcome in inflammatory renal disease [409]. Interaction of infiltrating inflammatory cells with PTCs through these adhesion molecules, stimulate the generation of several cytokine cascades [411]. It is likely that such as inflammatory loops, if not controlled appropriately, will turn into a chronic phase which leads to the development of progressive fibrosis characteristic of chronic renal disease. Data in this chapter show that BMP-7-induced monocyte binding is distinct from IL-1β-induced monocyte binding. We postulate that the HA cables keep the monocytes away from the pro-inflammatory receptors. This hypothesis is supported by the demonstration of increased monocyte binding to unstimulated cells when HA cables were removed by hyaluronidase treatment prior to the addition of the U937 cells. Our work also confirmed what previous studies have suggested [106], that BMP-7 may also influence ICAM/leukocyte interaction by down-regulation of ICAM expression in proximal tubular cells. In an *in vivo* setting, therefore, this would reduce the impact of any infiltrating monocytes, and prevent the development of a pro-inflammatory amplification loop, which may lead to progressive interstitial fibrosis.

This effect of cell-associated HA cables, in which HA is predominantly of high M_W, is in marked contrast to the reported effects of soluble low MW HA. Addition of HA of low MW is a potent stimulus for increased expression of ICAM-1 and VCAM-1 in tubular epithelial cells [412]. This together with increased expression of chemokines following addition of fragmented HA to PTCs [413], suggest that secreted HA, particularly when partially degraded, enhances leukocyte adhesion and subsequent cell activation, providing an amplification loop for pro-inflammatory effects of cytokines such as IL-1β. This reinforces the principle that, in general high MW HA represents the normal homeostatic state whereas the generation of low MW HA fragments signals a disruption of the normal homeostatic environment. More recently, high MW has been shown to inhibit monocytes population growth by the dual actions of impeding cell proliferation and inducing apoptosis [414]. This inhibition was mediated by interaction of HA with either CD44 or RHAMM expressed by U937 monocytes.

Although induction of ER stress in colonic fibroblasts is reported to induce HA deposition and subsequent HA-mediated leukocyte adhesion [170], confocal microscopy imaging did not reveal this relationship between an ER marker (KDEL) and HA cables in HK-2 cells and although IL-1β stimulated HA synthesis and induced ER stress, it failed to induce HA cable assembly. It is worth noting; however, that induction of ER stress *in vivo* is associated with increased HA deposition in mice colonic tissue and this association in also present in inflamed colonic tissue of human or mouse origin [170]. Moreover, HA-mediated monocyte binding is also increased after inducing ER stress in other cells such as lung mesenchymal cells and dermal fibroblasts (Majors A, unpublished observation). The differences in the cell types (epithelial cells versus fibroblasts) and in the stimulus used for ER induction (IL-1β versus tunicamycin) could be the reason behind the difference in the results.

The data presented in this chapter provide insight into how alterations in HA synthesis in the renal cortex may be involved in modulation of the interaction between infiltrating inflammatory cells and resident cells, and furthermore suggests a mechanism by which the known anti-inflammatory and anti-fibrotic effects of BMP-7 in renal disease may be mediated. We speculate that the presence of BMP-7 is an important determinant of the function of HA. Chronic renal impairment is associated with a relative deficiency of BMP-7 but increased HA in the kidney. Under these conditions, increased HA generation is unlikely to form HA-based cables and therefore may be contribute to the damaging fibrotic response. In the presence of BMP-7, however, the formation of HA cables would be beneficial with decreased interaction of infiltrating cells with resident cells surface adhesion molecules.

Chapter IV
The functional consequences of HAS2 over-expression and its effect on HA structures

4.1 Introduction

As outlined in chapter one, renal PTCs are important in the initiation of fibrosis. There is evidence that HA of low MW may have pro-inflammatory effects on PTCs [412, 413, 415, 416]. In contrast to these potential disease-promoting effects of HA, Ito *et al.* have demonstrated that binding of MW weight HA to its principle receptor, CD44 activates the MAP-kinase pathway and enhances PTC migration, suggesting that CD44 may be involved in the repair and restoration of PTC integrity following injury [417]. There is overwhelming evidence implicating TGF-β1 in progressive renal fibrosis. In PTCs, the interaction of HA with CD44 and crosstalk between the CD44 and TGF-β receptor leads to attenuation of TGF-β1 signalling [418], and increased trafficking of TGF-β receptors to lipid raft-associated pools [419], which facilitates increased receptor turnover [420]. These data therefore suggest that HA may also limit the pro-fibrotic response associated with progressive renal dysfunction.

Data presented in chapter three and data from previous work done in the department [175] have shown that HAS2 is the inducible isoform out of the two HAS isoforms expressed by the PTC. As mentioned in chapter one, three separate genes for human HA synthase (HAS) have been cloned and characterised, HAS1, HAS2 and HAS3 [421]. Previous work at the Institute of Nephrology examined the regulation of HA synthesis by renal PTCs *in vitro* [175] and demonstrated that stimulation of HA synthesis, by either IL-1β or high glucose, was associated with transcriptional activation of HAS2. HAS3 mRNA was constitutively expressed by PTCs but was not altered by stimuli increasing HA synthesis. HAS1 mRNA expression, on the other hand, was not detected in PTCs although on going work at the Institute suggests that induction of HAS1 may be a marker of terminal differentiation of myofibroblasts. Also, data from chapter three have demonstrated an association between stimulation of HA cables and induction of HAS2 mRNA in PTCs.

Several cell types surround themselves *in vitro* with HA in an organised pericellular matrix or "coat" [253, 422] in which, HA may be anchored to the surface of cells via an interaction with CD44 [423]. In chapter three, it is been shown that PTCs produce HA cable-like structures that bind mononuclear leukocytes via their cell surface CD44 receptors. Further to this, Zhang *et al.* have shown that binding of monocytes to these structures attenuates monocyte-dependent PTC generation of TGF-β1 [135]. Regulation of HA synthesis and assembly of extracellular HA-based structures, therefore, represents an important mechanism that regulates PTC function.

The aim of this chapter was to examine the functional consequences of HAS2-driven HA synthesis. For this, HAS2 ORF was cloned into an expression vector (pcDNA4/TO) which was used to generate a stable-transfected HK-2 cell line that would constitutively over-express HAS2 (detailed in chapter two). The HAS2-over-expressing cell line was then used, in comparison with mock-transfected cell line, to (*i*) study the alterations in HA synthesis and extracellular structures (HA quality and quantity), and to (*ii*) investigate the changes in two specific functions in the transfected cells, namely monocyte binding and cell migration.

4.2 Results

4.2.1 Confirmation of HAS2 over-expression in transfected HK-2 cells

After cloning of HAS2 ORF into pcDNA4/TO and generation of zeocin-resistant clones (detailed in chapter two). The next step was to confirm more HAS activity in these transfected cells. Several HK-2 clones were scanned for HA production in the supernatant by ELISA and one clone that showed a significant increase in HA production was picked for further analysis. All mock-transfected cells showed similar HA profiles and, therefore, one clone was selected as a control cell line.

Over-expression of HAS2 mRNA in the selected cell line was confirmed by RT-PCR (figure 4.1A). The specificity of HAS2 mRNA expression was demonstrated by examining the expression of HAS3 mRNA in both the HAS2 over-expressing cell line and in a stable cell line transfected with the empty vector (Mock). By scanning densitometry there was a 35% increase in HAS2 mRNA expression in the stable HAS2 cell line, with no significant change in HAS3 mRNA compared to the mock-transfected cell line (figure 4.1B).

HA generation by the cell lines was examined both by ELISA of the cell culture supernatant and also following ^{3}H-glucosamine labelling of HA and gel chromatography. Confluent monolayers of HAS2 over-expressing cells or mock-transfected cells were serum deprived for 48 h. Fresh serum-free medium was subsequently added for a further 24 h prior to collection and quantification of HA by ELISA (figure 4.1C). HA concentration in the culture supernatant was significantly greater in the HAS 2 over-expressing cell line. This represented a 70% increase in the HA over the mock transfected cells.

Analysis on Sephacryl S-500 of the ^{3}H-glucosamine-labelled HA samples from both the HAS2 over-expressing cell line and the mock transfected HK-2 cells demonstrated that the biggest difference in HA quantities was in the CM fraction (figure 4.1D). Also, the majority of the labelled HA in the conditioned medium and in the TE fraction appeared near the void volume and therefore was considered to be of high molecular mass (figure 4.2). In addition, in the HAS2 transfected cells, there was a marked increase in lower molecular weight HA in the CA fraction (representing more than 60% of this fraction) as compared to the mock-transfected cells (which had about 40% as low MW HA; figure 4.2).

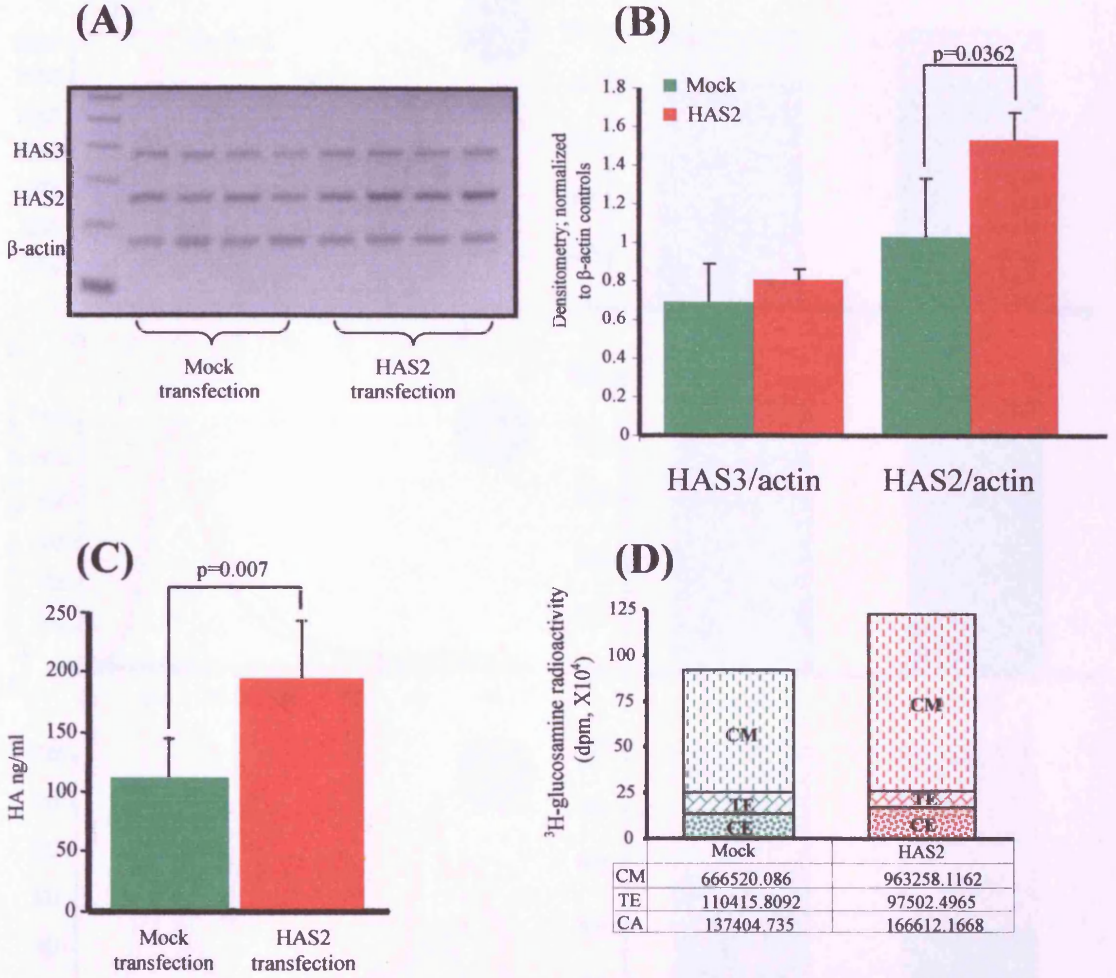

Figure 4.1: HAS2/HAS3 expression & HA production in HAS2-transfected HK-2 cells.

(A) Total mRNA was extracted from confluent, transfected monolayers after 48 h of serum deprivation. Ethidium bromide-stained PCR products were separated on a 3% agarose gel. Four representative PCR reactions are shown.

(B) densitometry data normalised to their respective actin bands.

In parallel experiments, supernatant samples were collected from confluent serum-deprived cells exposed to serum-free medium for 24 h after growth-arrest. HA was then quantified by ELISA **(C)**. Data represent mean ± SD of four separate experiments.

In **(D)**, the totals of the 3 fractions analysed by gel chromatography were plotted. The samples analysed were collected from either mock- or HAS2-transfected confluent serum-deprived monolayers that were exposed to serum-free medium for 24 h (CM; conditioned medium, TE; trypsin extract, CA; cell-associated. Detailed chromatography data are shown in figure 4.2.

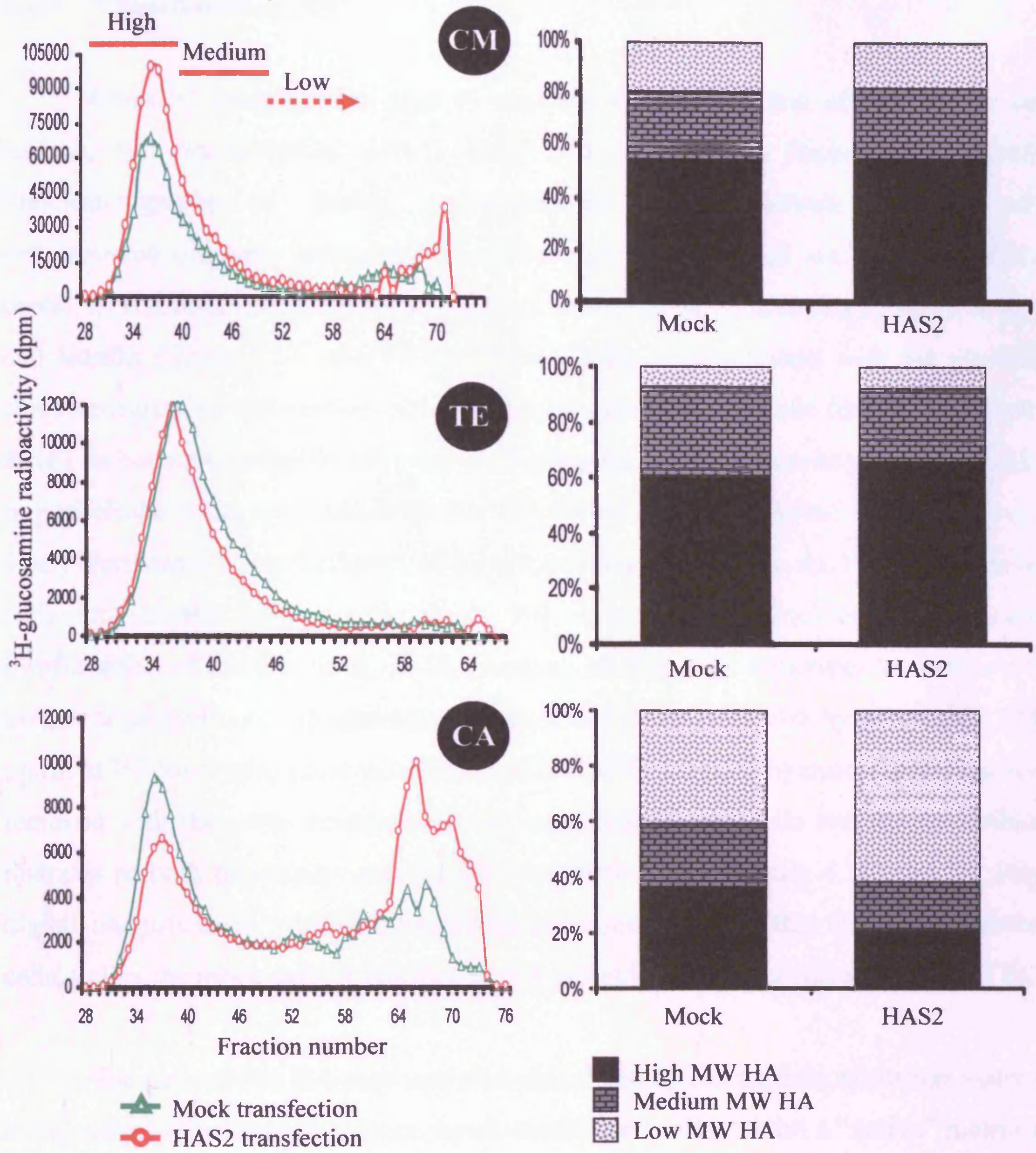

Figure 4.2: Analysis of HA in transfected HK-2 cells.

Confluent serum-deprived monolayers of HAS2 over-expressing cells or mock-transfected cells were exposed to serum-free conditions for 24 h in the presence of 20 μCi/ml ^{3}H-glucosamine. Subsequently, conditioned medium **(CM)**, trypsin extract **(TE)** and cell-associated **(CA)** HA fractions were prepared and analysed as described in chapter two. The bars labelled as High, Medium and Low represent MW ranges (high MW > 10^6 Da, medium MW from 10^5 to 10^6, low MW < 10^5 Da). The graphs on the right represent the percentage of different MW HA in each fraction.

4.2.2 Visualisation of HA

Confocal imaging was used to examine the organisation of HA on the cell surface. HA was identified with b-HABP and detected with fluorescent Avidin-D. Photomicrographs of fixed, growth-arrested mock-transfected HK-2 cells demonstrated diffusely arranged pericellular HA over the cell surface (pericellular coats). In addition, HA was demonstrated in cable-like structures that spanned several cell lengths (figure 4.3A and 4.4A). These results are consistent with the previous characterisation of cell surface HA in un-manipulated HK-2 cells (data from chapter three). In contrast, in the HAS2 over-expressing cell line HA was seen predominantly in pericellular coats with relatively few HA-based cables identified (figure 4.3B and 4.4B). Furthermore, the thickness of the pericellular HA coats in the HAS2 expressing cells was significantly greater than that seen in the mock-transfected cells. Confirmation of the nature of the HA content of the cable structures was shown by treatment of confluent monolayers of cells with bovine testicular hyaluronidase (200 μg/ml at RT for 5 min) prior to addition of b-HABP. Limited hyaluronidase digestion removed both the cable structures in the mock transfected cells and the pericellular matrices in both the mock- and HAS2- transfected cells (figure 4.3C and E). High digital magnification after hyaluronidase treatment showed that HAS2 transfected cells, unlike the mock cells, have foci of HA around their nuclei (figure 4.3D and F).

The pericellular HA coat was also visualised by the particle exclusion assay in living cells. Following sub-culture, mock-transfected cells exhibit a "native" matrix as demonstrated by a thin halo of exclusion of formalin-fixed horse erythrocytes (figure 4.4C). In contrast, HAS2-transfected cells assembled a much more prominent pericellular matrix (figure 4.4D).

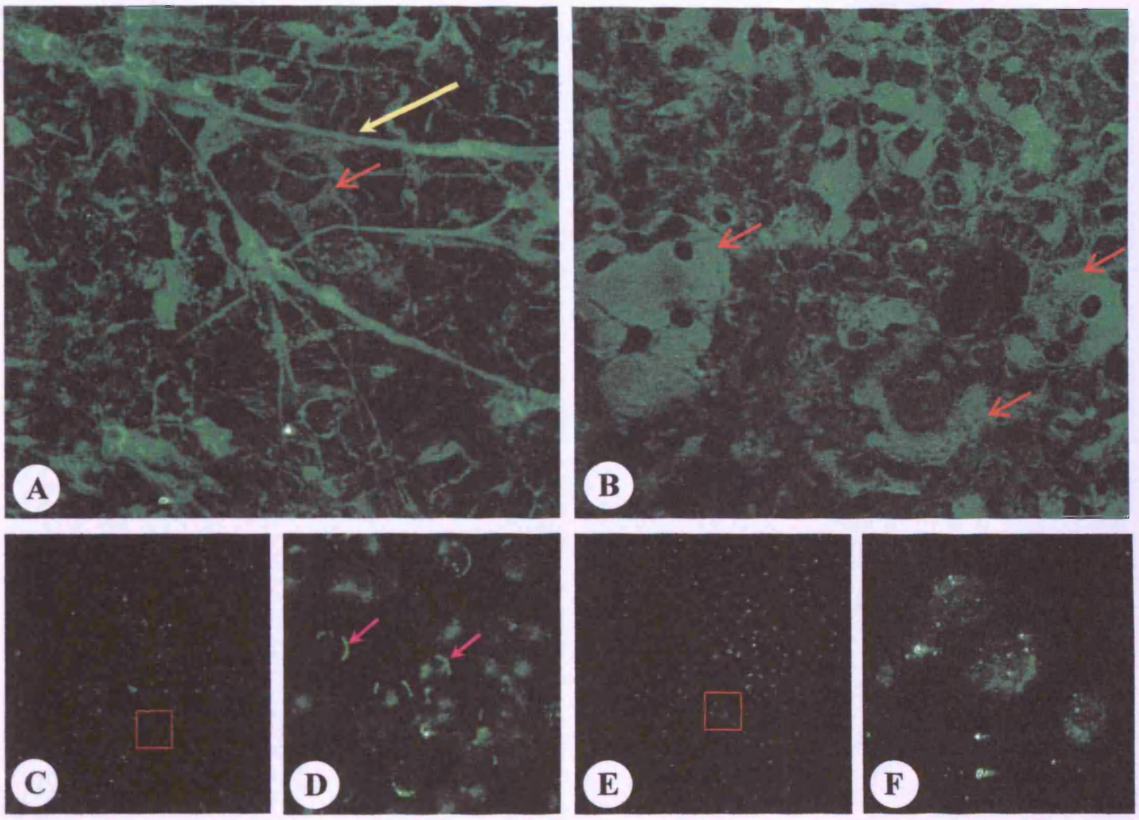

Figure 4.3: Visualisation of HA in transfected cells.

Confluent monolayers of mock-transfected **(A)** and HAS2 over-expressing **(B)** cells were serum deprived for 48 h prior to fixation with methanol and detection of HA by addition of biotinylated-HABP. Cells were imaged by confocal microscopy (magnification x 200). Pericellular coats are highlighted by red arrow heads and HA cables by yellow arrows.

To confirm the nature of HA staining, in parallel experiments, cells were treated with bovine testicular hyaluronidase (200 μg/ml) at 37°C for 5 min, prior to fixation and addition of b-HABP (Mock **(C)** and HAS2 **(E)**; magnification x 200). Red squares indicate areas that were digitally magnified (Mock **(D)** and HAS2 **(F)**). Pink arrows indicate the sites of membrane-bound HA (?CD44-bound), mostly evident in mock transfected cells **(D)**.

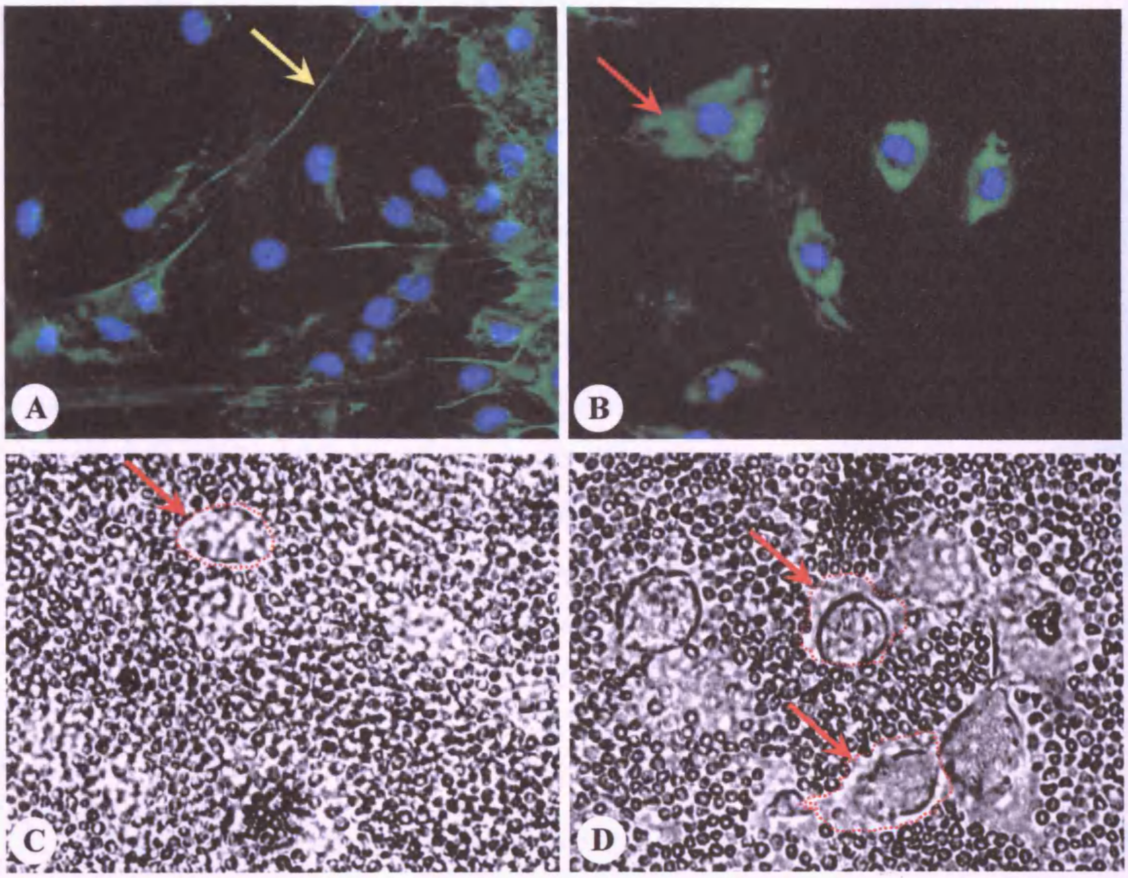

Figure 4.4: Visualisation of HA in transfected cells.

Sub-confluent mock-transfected **(A)** and HAS2 over-expressing **(B)** HK-2 cells were serum deprived for 48 h prior to fixation with methanol and detection of HA by addition of b-HABP. Sections were imaged by fluorescent microscopy (magnification x 200). Pericellular coats are highlighted by red arrows and HA cables by yellow arrows. Cell nuclei are visualised by DAPI staining (blue).

Functional pericellular matrix in the mock **(C)** and HAS2 over-expressing **(D)** cells was visualised by the particle exclusion assay. The zones of exclusion of formalin-fixed red blood cells in both cell lines are indicated by red arrows and dotted lines (magnification x 200).

4.2.3 HA-dependent monocyte binding

U937 monocytic cells were used to examine the binding capacity of inflammatory cells by either HAS2 over-expressing or mock-transfected HK-2 cells. Quantification of monocyte binding was done by determination of bound radioactivity following addition of ^{51}Cr-labelled U937 cells. In the mock-transfected cells, monocyte binding was significantly reduced by removal of cell surface HA by adding bovine testicular hyaluronidase (200 μg/ml) at 37°C for 5 min to the epithelial cell monolayers, prior to addition of monocytes. Despite increased HA generation in the HAS2 over-expressing cells, binding of labelled U937 cells was significantly greater in the mock-transfected cells (figure 4.5A). Addition of hyaluronidase to the HAS2 cell line did not significantly reduce the binding of labelled U937 cells. These data are therefore consistent with the marked difference in the expression of HA cables between the two cell lines.

Data in chapter three suggested that the increase in HA cables is associated with a down-regulation of hyaluronidase, suggesting that alteration in HA turnover may be involved in their generation. To further explore this possibility, hyaluronidase expression (HYAL1 and HYAL2) was examined by RT-PCR in the HAS2- and mock-transfected cells. Confluent cell monolayers were serum-deprived for 48 h prior to extraction of total mRNA. The marked decrease in HA cables in the HAS2 over-expressing cell line, and the increase in low molecular weight HA in the cell extract were associated with a significant increase in both HYAL1 and HYAL2 mRNA expression compared to mock-transfected cells (figure 4.5B and C).

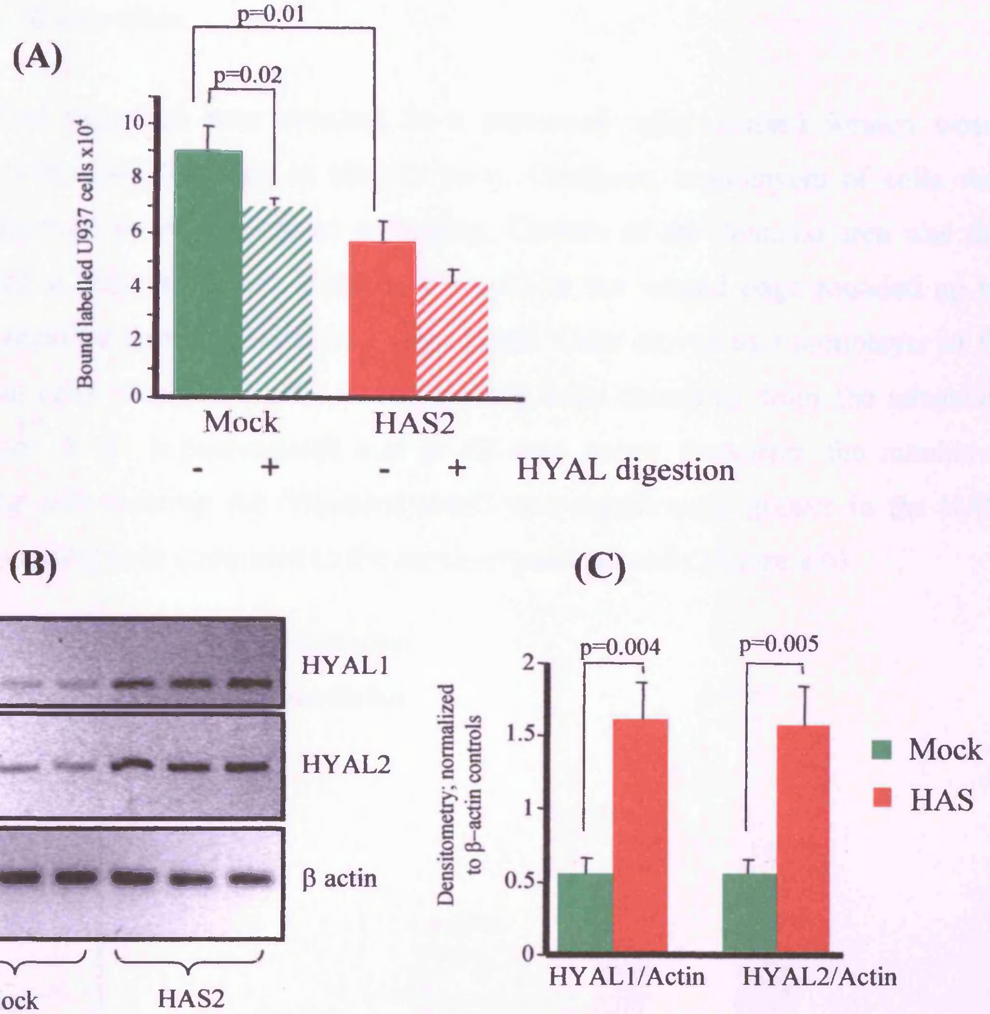

Figure 4.5: Reduced HA cable generation is associated with reduced monocyte binding and increased expression of hyaluronidases in HAS2 over-expressing cells.

(A) Quantification of monocyte binding: Confluent monolayers of serum-deprived cells were washed with PBS prior to addition of 1 x 10^6 ^{51}Cr-labelled U937 cells under serum-free conditions for 1 h at 37°C. Quantification of bound radioactivity was carried out as described in chapter two. To quantify HA-dependent binding, the monolayer was treated with bovine testicular hyaluronidase (200 μg/ml) at 37°C for 5 min prior to addition of monocytes. Data represent mean ± SD of four individual experiments.

(B) Expression of hyaluronidase (HYAL1 and HYAL2) mRNA. Total mRNA was extracted from confluent monolayers of mock-transfected and HAS2 over-expressing cells after 48 h of serum deprivation. Ethidium bromide-stained PCR products were separated on a 3% agarose gel. Three representative PCR reactions are shown.

(C) Densitometry data normalised to their respective actin bands.

4.2.4 *Cell migration*

Cell migration was assessed in a previously characterised scratch wound system [188, 354] (detailed in chapter two). Confluent monolayers of cells were serum deprived for 48 h prior to wounding. Closure of the denuded area was then monitored at different times. Initially, the cells at the wound edge rounded up but quickly regained their epithelial-like appearance. Cells moved as a monolayer of flat polygonal cells with some cells at the leading edge detaching from the advancing monolayer. At 24 h post-scratch and at all time points thereafter, the number of migrating cells entering the "denuded area" was significantly greater in the HAS2 over-expressing cells compared to the mock-transfected cells (figure 4.6).

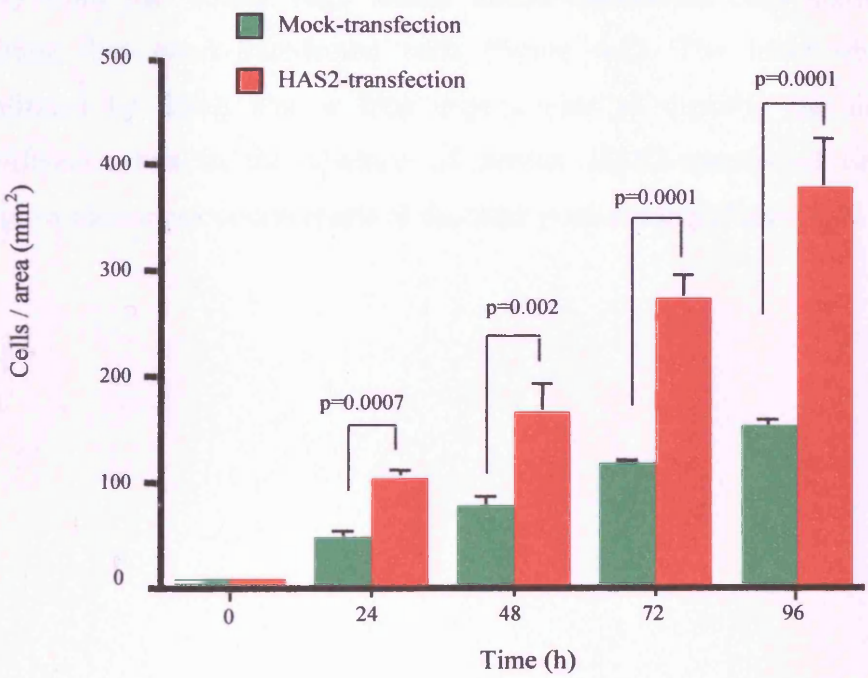

Figure 4.6: Quantification of cell migration.

Confluent serum-deprived monolayers of mock- or HAS2-transfected cells were scratched as described in chapter two to produce an intersecting area denuded of cells. Subsequently, following washing of the monolayer to remove detached cells, the rate of cell migration of each of the two cell lines was assessed by directly counting the number of cells migrating into the intersecting denuded area at the time points indicated. The data are expressed as the number of cells per denuded area. Data represent the mean ± SD of four individual experiments.

4.2.5 Enhanced cell migration is not due to an increased cell proliferation at the wound edge

The contribution of cell proliferation to the process of wound healing following mechanical injury was examined by incubating cells with BrdU followed by staining for BrdU. Figure 4.8 shows that almost no BrdU was incorporated into cells at/close to the wound edge in either mock- or HAS2-transfected cells at 24 h post wounding. Contrary to the observations at the wound edge, positive BrdU staining was detected in areas away from the wound edge (figure 4.7). BrdU incorporation experiments were repeated at 72 h post-wounding and no difference was seen between mock- or HAS2-transfected cells near the wound edge unlike areas away from the wound edge where HAS2-transfected cells showed more BrdU staining than mock-transfected cells (figure 4.7). The latter observations were confirmed by doing alamar blue experiments to quantify the difference in the proliferation rate in the absence of serum. HAS2-transfected cells significantly outgrow their mock counterparts at day four post-seeding (figure 4.8).

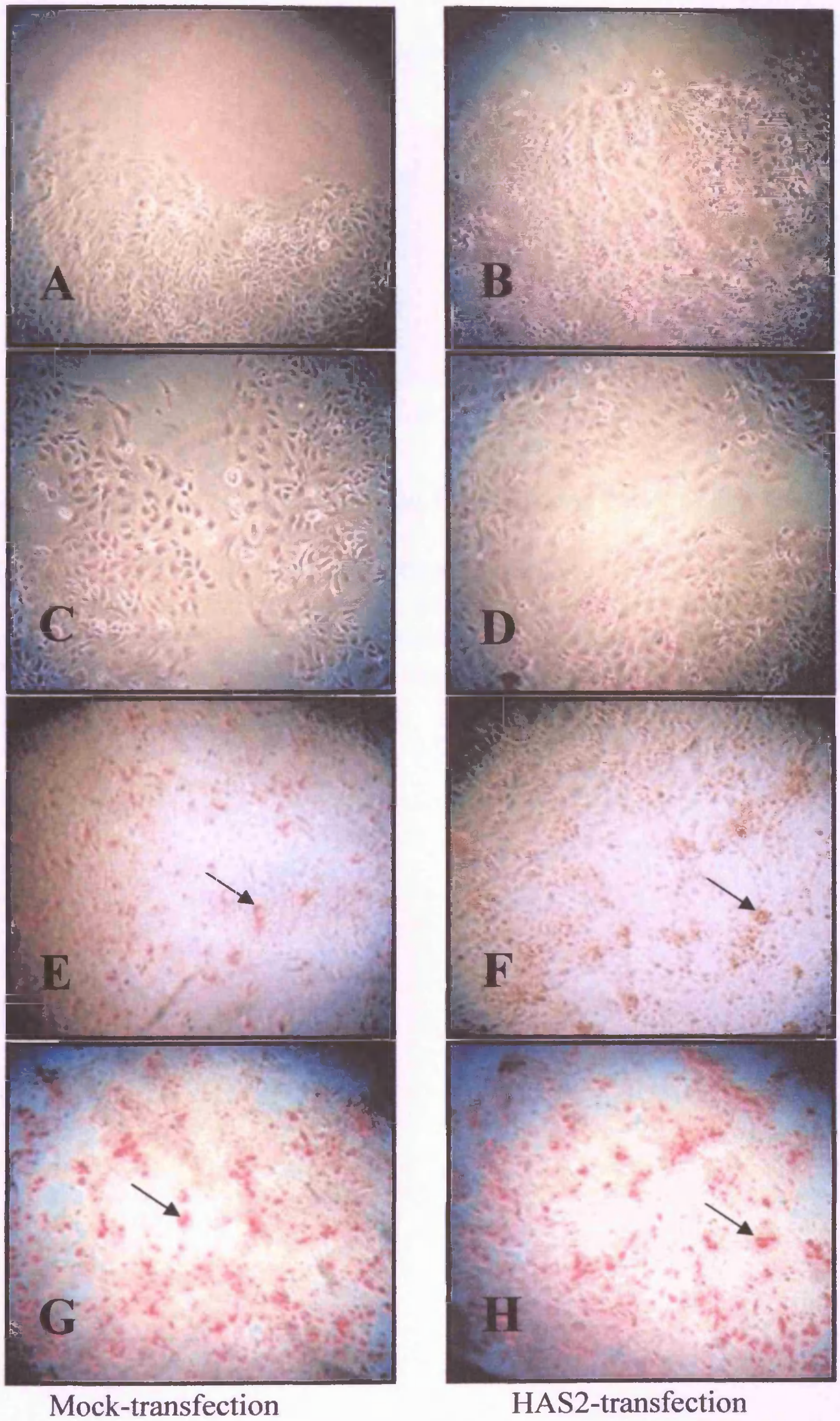

Figure 4.7: BrdU staining in transfected cells 24 and 72 h post-wounding.

Transfected HK-2 cells were wounded and incubated for 24 h (**A**, **B**, **E** and **F**) or 72 h (**C**, **D**, **G** and **H**) in serum-free medium. After that, medium was replaced with medium containing BrdU and incubated at 37°C for 5 h before fixing and staining as detailed in chapter two. (**A** and **C/B** and **D**) show mock-/HAS2-transfected cells at the wound edge. (**E** and **G/F** and **H**) show mock-/HAS2-transfected cells away from the wound edge (magnification x 100). Arrows indicate cells positively stained with BrdU.

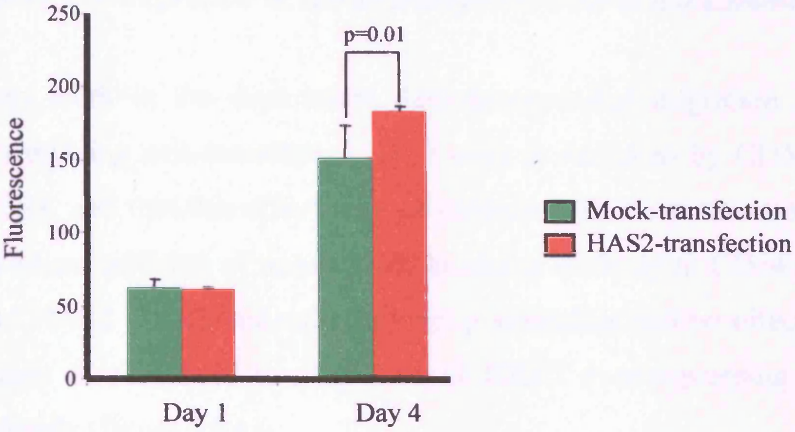

Figure 4.8: Growth profile in mock- and HAS2-transfected cells.

Transfected cells were seeded at low density with 10% FCS for 24 h. After 24 h, medium was replaced with serum-free medium containing 10% alamar blue and fluorescence measured after 1 h. After washing with PBS, cells were incubated with serum-free medium until the next alamar blue measurement (at day 4 post-seeding).

4.2.6 Enhanced cell migration in HAS2-transfected cells is not CD44-dependant

Previous work in the department demonstrated that migration in a scratch wound system utilising non-transfected HK-2 cells is mediated by CD44-dependent activation of ERK and that this effect may be enhanced by the addition of exogenous HA [188]. However, addition of monoclonal blocking antibody to CD44 (5 μg/ml) to a monolayer of HAS2 transfected cells following wounding had no effect on the rate of cell migration as compared to migration of HAS2 over-expressing cells in the absence of antibody (figure 4.9A).

Furthermore, reduction in the ERK activation was observed by immunoblot analysis of phosphorylated MAPK in the HAS2 over-expressing cells compared to mock-transfected cells (figure 4.10A). Cell surface CD44 expression was examined by flow cytometry and immunocytochemistry using an antibody to the common region of CD44. There was a marked decrease in cell surface expression of CD44 in the HAS2 over-expressing cells compared to the mock-transfected cells (figure 4.10B and C).

To demonstrate that migration in HAS2-transfected cells was related to the generation of HA, exogenous HA (MW 2 x 10^6 Da, 25 μg/ml) was added to the monolayer following the generation of a wound. Despite reduction in the expression of CD44, HAS2 over-expressing cells responded positively to exogenous HA and this represented a significant increase in migration at all time points beyond 48 h (figure 4.9B).

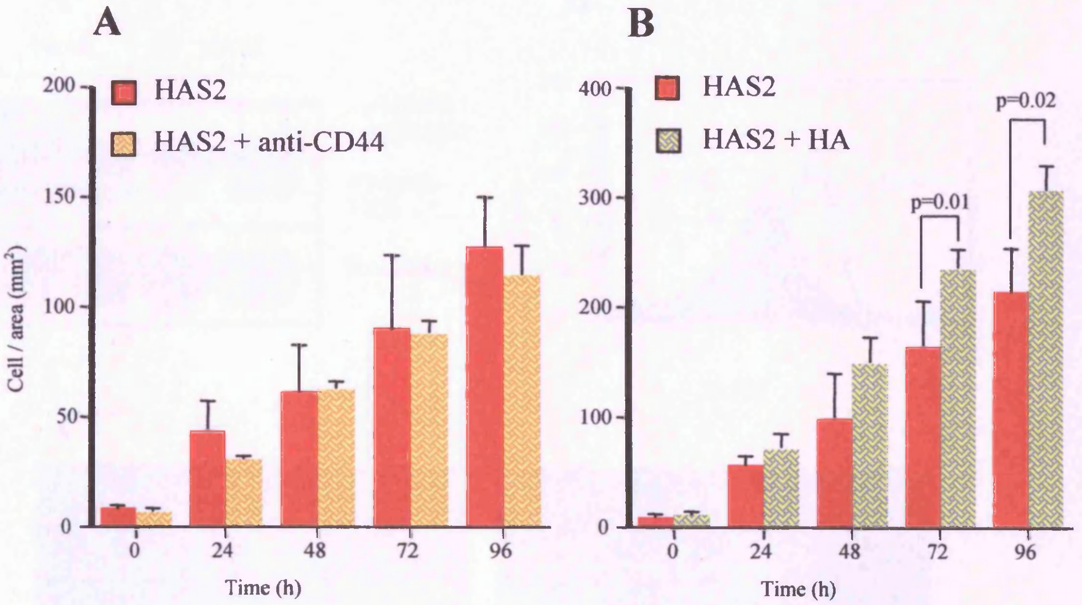

Figure 4.9: Role of CD44 in HAS2 over-expression-mediated enhanced cell migration.

Confluent HAS2-transfected cells were serum-deprived for 48 h prior to wounding. Migration was then assessed in **(A)** with or without CD44 blocking Ab and in **(B)** with or without HA (25 μg/ml; 2 x 10^6 kDa). No significant difference was noted at any of the time points between the 2 samples in **(A)**. Data represent the average of 4 individual experiments ±SD.

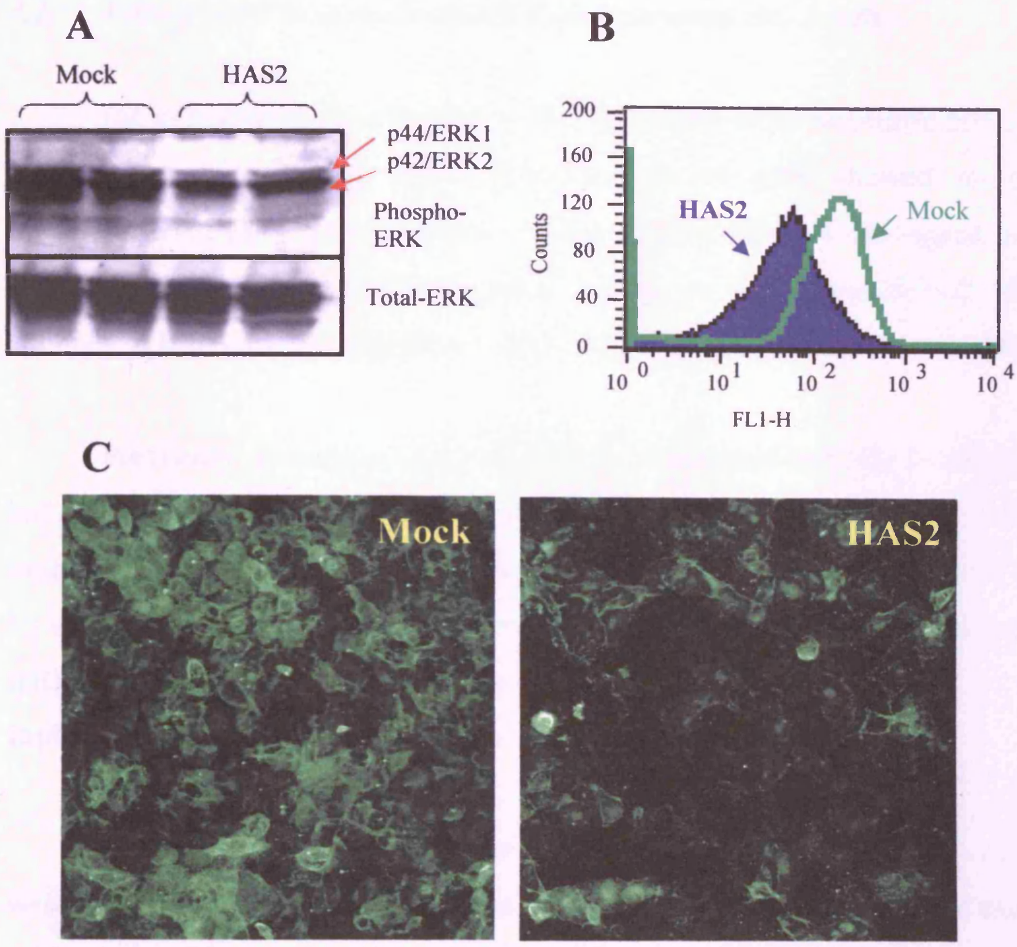

Figure 4.10: Reduced phosphor-ERK and CD44 expression in HAS2-transfected cells.

(A) Whole cell extracts from growth-arrested transfected cells were resolved by SDS-PAGE. The blots were probed with anti-phospho ERK (active ERK) before stripping and re-probing with anti-total ERK to ensure no change in the expression of whole cell ERK had occurred.

(B) CD44 expression assessed by FACS analysis in confluent growth-arrested cells. The graph shows a comparison between mock- and HAS2-transfected cells.

(C) CD44 expression shown by immunocytochemistry in growth-arrested mock- or HAS2-transfected HK-2 cells (magnification x 200).

4.2.7 Role of IαI/PαI in the migration of transfected HK-2 cells

IαI is known to be involved in the formation of extracellular HA structures (detailed in chapter one). Since HAS2-transfected cells showed an enhanced migratory rate, I wanted to investigate the importance of IαI in this regard. Following scratch wounding, incubation of either mock- or HAS2-transfected cells with antibody to IαI/PαI led to significant inhibition of cell migration (figure 4.11).

Previously, Janssen *et al.* [343] have demonstrated that HK-2 cells synthesise both HC3 and bikunin components of the IαI complex. Expression of HC3 was examined in the HAS2 over-expressing cells by RT-PCR and for protein expression by western analysis. In the HAS2 over-expressing cells there was a decrease in HC3 mRNA expression compared to mock-transfected cells (figure 4.12A) while bikunin expression was unaffected.

In addition, IαI/PαI protein expression in total cell lysates was analysed by western blotting (figure 4.12C). Western blot analysis detected many bands in the total extract of both mock- and HAS2-transfected cells where the highest molecular mass species are likely to correspond to IαI/PαI covalently attached to HA as previously described [424]. Duplicate samples were treated with *Streptomyces* hyaluronidase and this showed two major IαI positive bands. The lower MW species (~75 kDa) most likely represents HCs that were covalently bound to HA. The appearance of the upper band (~125 kDa) on hyaluronidase digestion and its sensitivity to NaOH treatment is similar to that described for the TSG-6·HC complexes in the murine cumulus-oocyte complex [346]. Also worth noting is that although HC3 mRNA expression was decreased, IαI/PαI-HA complex (figure 4.12C; lanes 1 and 4) was more prominent in HAS2-transfected cells which could mean that larger extracellular HA pools could act as a reservoir for secreted hyaladherins.

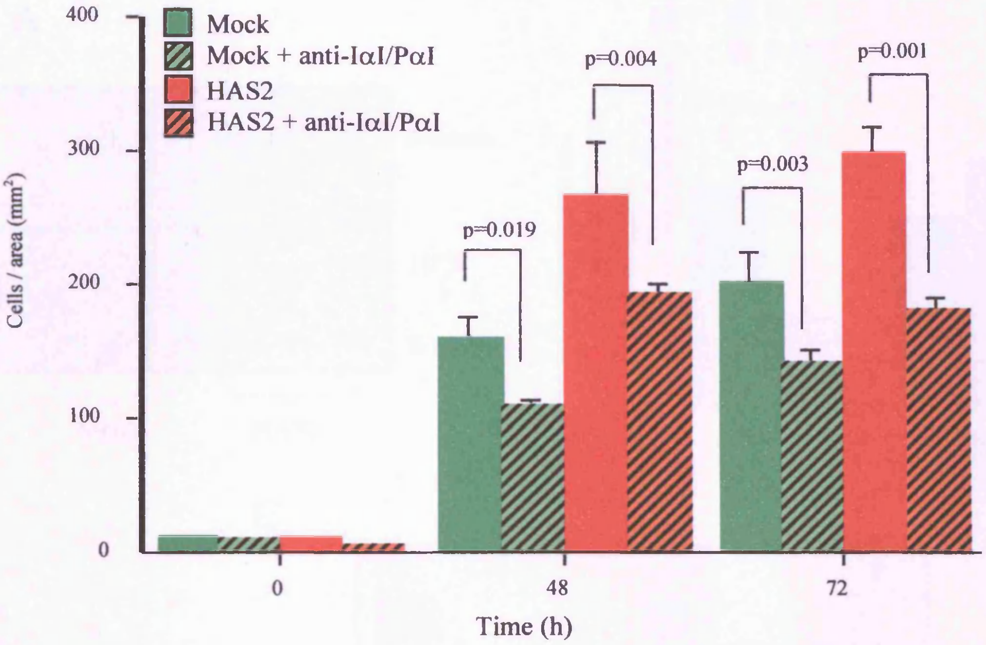

Figure 4.11: Ab to IαI/PαI reduced transfected HK-2 cells migration.

Confluent growth-arrested transfected HK-2 cells were mechanically scratched before addition of serum-free medium with or without polyclonal Ab to IαI/PαI (dilution 1/50). Wound closure was monitored as described in chapter two. Data represent the average of 4 individual experiments ± SD.

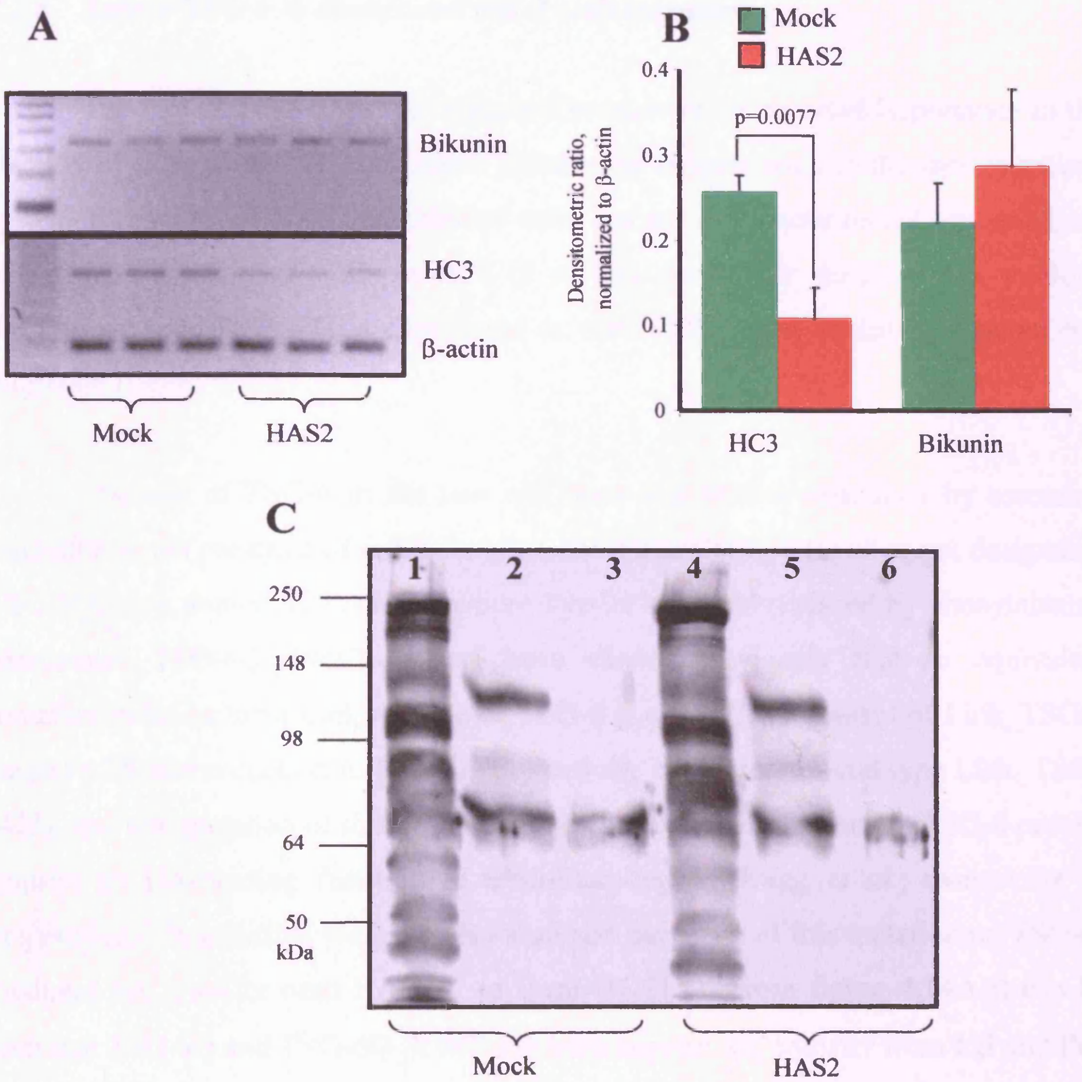

Figure 4.12: IαI/PαI mRNA and protein expression in transfected HK-2 cells.

Levels of mRNA expression of HC3 and bikunin in transfected HK-2 cells were assessed by RT-PCR after 48 h of serum-deprivation **(A)**. Ratios of band densities of HC3 and bikunin/β-actin were measured and plotted in **(B)**.

(C) Western blot analysis of IαI/PαI extracted from growth-arrested transfected HK-2 cells. 1=Total lysate (both cells and matrix), 2=HYAL-extracted matrix, and 3=NaOH-treated matrix (HYAL-extracted). Protein amounts loaded in lanes (1) were normalised to viable cell number (by alamar blue). The Ab used recognises intact IαI family members including: PαI (120-130 kDa), individual HCs (75-80 kDa), bikunin (35 kDa) and IαI associated with TSG-6 (TSG-6 molecular weight is 42 kDa).

4.2.8 Role of TSG-6 in transfected HK-2 cells migration

The role of TSG-6 was investigated because of its reported importance in the stability of extracellular HA structures (detailed in chapter one). In the scratch wound system, incubation of HAS2-transfected cells, but not mock-transfected cells, with rat anti-human monoclonal antibody A38 (5 μg/ml), previously demonstrated to block the formation of TSG-6-HCs complexes *in vitro* [278], significantly attenuated cell migration (figure 4.13).

The role of TSG-6 in the two cell lines was further examined by assessing migration in the presence of a full-length recombinant TSG-6 (Q allotype; designated TSG-6Q); or a mutant of TSG-6Q, where Tyr-94 has been replaced by phenylalanine (designated TSG-6Q_Y94F). It has been shown previously that an equivalent mutation in the isolated Link module of TSG-6 (i.e. the Y59F mutant of Link_TSG6) caused a 25-fold reduction in HA-binding activity compared to wild type Link_TSG6 [425], and that mutation of this residue in the context of the full-length TSG-6 protein impairs its HA-binding function to a similar degree (Rugg *et al.*, manuscript in preparation). In addition, we have also assessed the effect of this mutation on TSG-6-mediated HC transfer onto HA (i.e. to form HC·HA). From figure 4.14A it can be seen that TSG-6Q and TSG-6Q_Y94F can both support HC transfer from IαI and PαI onto HA, albeit with a slightly reduced activity of the mutant compared to wild type protein. Thus, it is possible to use a comparison of TSG-6Q and TSG-6Q_Y94F to differentiate between HA- and HC·HA-mediated effects. In this regard, both the TSG-6Q and TSG-6Q_Y94F significantly increased the migration of cells over-expressing HAS-2 (figure 4.14B). In contrast, addition of Link_TSG-6, which can bind to HA [426-428] but is unable to form stable complexes with HCs [317], had no effect of migration. From these experiments it is clear that TSG-6-mediated HC transfer is critical for the enhancement of migration of cells in which HA production is increased through over-expression of HAS2 mRNA. Furthermore, by using a monoclonal Ab that recognises TSG-6 link module epitopes [385], the presence of endogenous TSG-6 in the pericellular matrix was confirmed by immunocytochemistry revealing that TSG-6 co-localised with HA around the HAS2-transfected cells (figure 4.15).

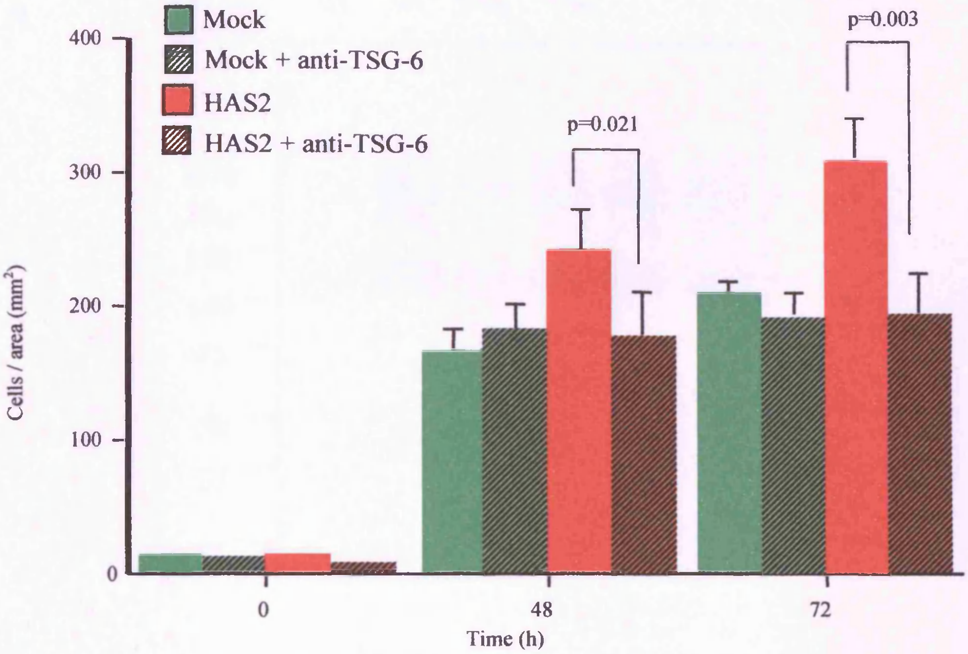

Figure 4.13: Effect of TSG-6 Ab on cell migration is exclusive to HAS2-transfected HK-2 cells.

Confluent growth-arrested transfected HK-2 cells were mechanically scratched before addition of serum-free medium with or without TSG-6 monoclonal Ab (clone A38; 5 μg/ml). Wound closure was monitored as described in chapter two. Data represent the average of 4 individual experiments ± SD.

A

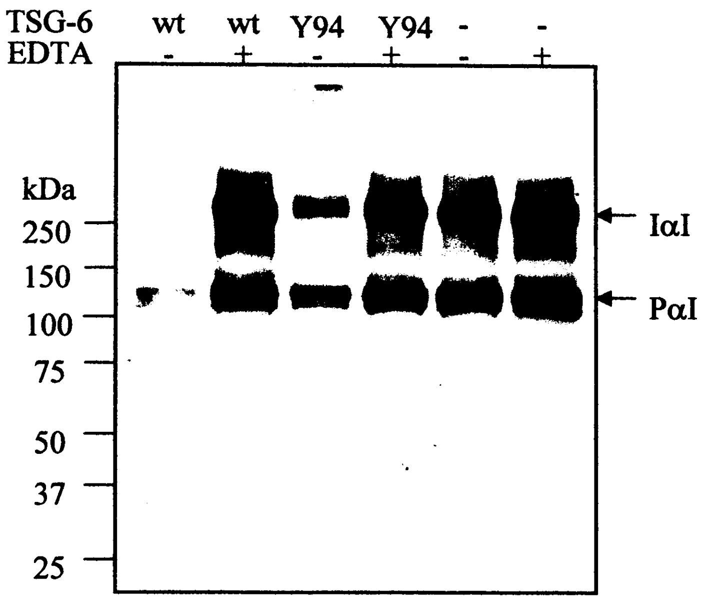

Figure 4.14A: Mechanism of TSG-6 effect on cell migration in HAS2-transfected cells.

Effect of mutation on TSG-6-mediated transfer of HCs onto HA. Mouse serum (as a source of IαI and PαI), high molecular mass HA and human recombinant TSG-6Q (wild type (wt) or TSG-6Q_Y94F mutant ('Y94F')) were incubated at 37°C in the absence or presence of EDTA. Samples were run on SDS-polyacrylamide gels and analysed by western blotting using a polyclonal antibody against IαI that also recognises PαI. The presence of EDTA (+) inhibits HC transfer and intense bands are seen for IαI and PαI, as described previously [429]. The absence of a band or a significant reduction in its intensity indicates that TSG-6-mediated HC transfer has taken place. TSG-6Q and 'Y94F' in the absence of EDTA (-) both give rise to a high level of HC transfer, however, if TSG-6 is not added then transfer does not occur. Whilst the 'Y94F' mutant leads to a significant amount of HC transfer it is somewhat less active than the wild type protein for the transfer of IαI and PαI HCs onto HA.

B

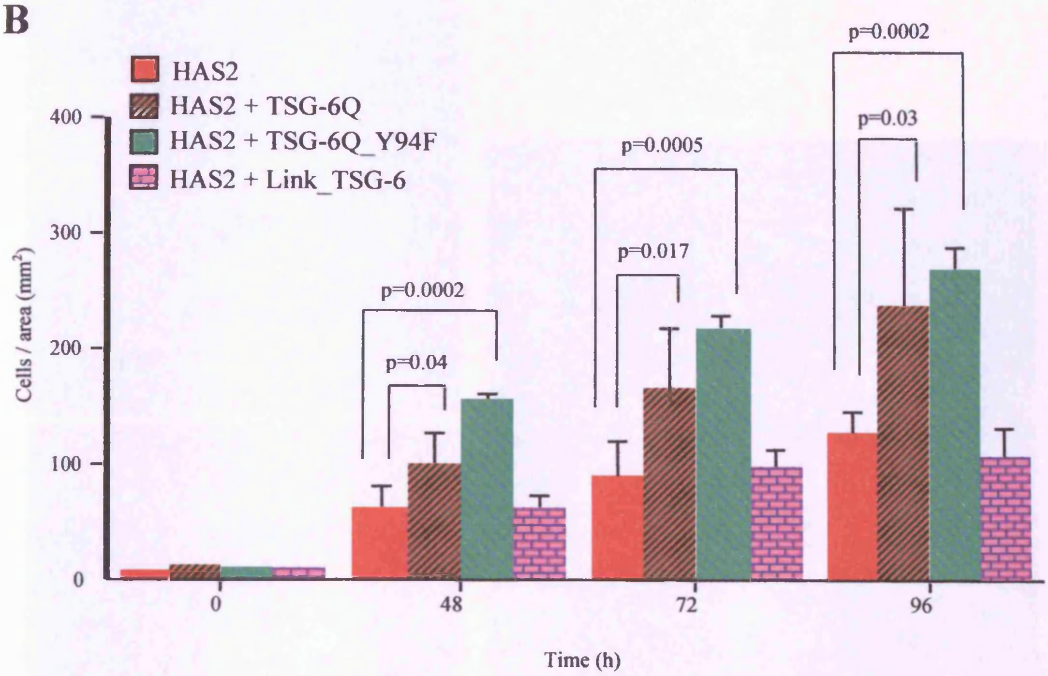

Figure 4.14B: Mechanism of TSG-6 effect on cell migration in HAS2-transfected cells.

Enhanced migration of HAS2 over-expressing cells is dependent on IαI/PαI transfer activity of TSG-6. Confluent growth-arrested HAS2-transfected HK-2 cells were mechanically scratched before addition of serum-free medium with or without TSG-6Q or TSG-6Q_Y94F or Link_TSG-6 (all at a final concentration of 5 μg/ml). Wound closure was monitored as described in chapter two. The data are expressed as the number of cells per mm2 of denuded area. Data represent the mean ± SD of four individual experiments.

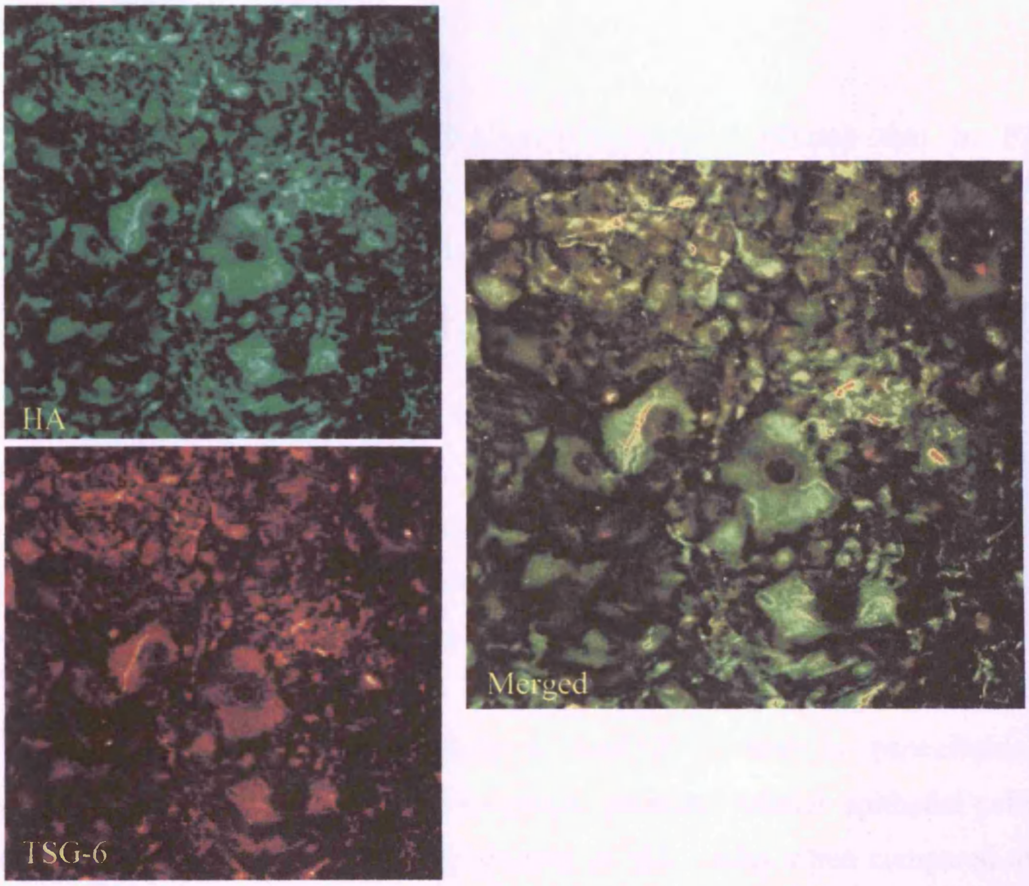

Figure 4.15: Co-localization of TSG-6 and extracellular HA.

Confluent monolayers of transfected HK-2 cells were serum deprived for 48 h prior to fixation with methanol and detection of either HA by addition of b-HABP (5 μg/ml) or TSG-6 using rat anti-human monoclonal antibody Q75 (5.3 μg/ml). Following overnight incubation, the slides were washed with PBS prior to incubation with either fluorescent Avidin-D (20 μg/ml) or anti-rat Texas red-conjugated antibody. Co-localisation of HA and TSG-6 was examined by merging of the two images.

4.3 Discussion

Previous studies in the department have demonstrated that in PTCs, stimulation of HA production is associated with induction of the HAS2 gene [175]. Data from chapter three have shown that induction of HAS2 is stimulus specific. Induction with BMP-7 led to an increase in the formation of HA cable-like structures whilst increased HA in response to IL-1β was most apparent in the culture medium. Furthermore, phenotypic alteration in renal epithelial cells may be driven by adenoviral expression of HAS2 [430]. In order to further examine the potential role of HAS2-driven HA synthesis in the alteration of epithelial cell function, the aim of the work presented in this chapter was to characterise alterations in HA and its consequences on cell functions following HAS2-driven HA synthesis in PTCs.

The data presented demonstrate a marked increase in pericellular HA following over-expression of HAS2 in human proximal tubular epithelial cells. In marked contrast, there was a striking absence of HA cables when compared to the mock-transfected cells. Data from chapter three have demonstrated that HA cables are associated with monocyte adhesion, which is consistent with the data presented in this chapter that the HAS2 over-expressing cells exhibit a reduction in HA-dependent monocyte binding. The big pericellular coats can also have a role in preventing monocyte adhesion via masking other receptors (like ICAM-1) and being unreceptive themselves to monocytes. This relative "un-reactivity" of the pericellular HA is also seen in other systems like colonic smooth muscle cells (De La Motte, CA – personal communication.). In chapter three, stimulation of cable formation following addition of BMP-7 was associated with decreased expression of both HYAL1 and HYAL2. In contrast to BMP-7, IL-1β did not influence HYAL expression and did not stimulate cable formation although it is a potent stimulus of HA synthesis. This led us to postulate that down-regulation of hyaluronidase activity by BMP-7 allowed HA to remain associated with HAS, and that HA extruded through the cell membrane is anchored to HAS isoforms and associates with similarly anchored HA from neighbouring cell thus forming cables. Data in this chapter are consistent with this hypothesis; a consequence of the up-regulation of hyaluronidase in the HAS2-transfected cells is that extruded HA is cleaved at the cell surface. Although we have only demonstrated alteration of HYAL1 and HYAL2 at the level of their mRNA, the increase in low molecular weight HA in the HAS2 cells suggest that this is also associated with increased HYAL enzyme activities.

The increase in the pericellular HA in the HAS2-transfected cells is consistent with the observation that inhibition of HAS2 activity has been demonstrated to inhibit pericellular matrix assembly in human articular chondrocytes [273]. The generation of such a pericellular matrix has been previously associated with the migratory capacity of cells [253] as was seen in the HAS2 over-expressing cells. Ito *et al.* have demonstrated that exogenous HA increased epithelial cell migration through CD44-dependent activation of the ERK MAPK pathway [188]. However, the enhanced migration seen in the HAS2-transfected cells is clearly not dependent on CD44 activation. Furthermore, a reduction of CD44 expression was seen in the HAS2 over-expressing cells. This would suggest that, in contrast to previous reports utilising articular chondrocytes [280], the pericellular HA matrix is not anchored by CD44 in this case. In certain cell types, HA is internalized for degradation by an endocytic pathway that requires CD44 function [431, 432]. A reduced endocytic capacity for HA as a consequence of reduced CD44 expression may therefore contribute to the accumulation of HA into the pericellular coats in our experimental system. Enhanced migration of the HAS2 over-expressing cells following addition of exogenous HA, however, demonstrates that they are still able to respond to alterations in HA. Other reports indicate that HA-dependent cell migration may be CD44 independent, but associated with another distinct HA cell surface receptor (like RHAMM) [247, 252]. More recent studies suggest that RHAMM compensates for CD44 in inflamed CD44-knockout mice [433]. It is interesting to speculate therefore that in the face of reduced CD44 expression in the HAS2 over-expressing epithelial cells, enhanced migration is related to preferential RHAMM activation. It is of note, however, that HA-induced transcription of metalloproteases has been demonstrated to be mediated via a cell surface receptor which is neither CD44 nor RHAMM [237], suggesting that further, as yet unidentified, cell surface receptors may mediate HA-dependent events.

In contrast to the lack of effect of the blocking antibody to CD44, antibodies to either IαI-related proteins or TSG-6 clearly attenuated migration of HAS2 over-expressing cells. Much of the work on the associations of IαI-related proteins with ECM has been done in the setting of the cumulus cell-oocyte complex (COC) [434]. In this system, it is clear that HA is the major structural component that determines the viscoelastic properties of the expanding matrix of the cumulus-oophorus. It is also well established that members of the IαI family are pivotal for the formation of the COC matrix, where covalent linkage of HCs of IαI (HC1 and HC2) and PαI (HC3) to HA has been demonstrated [279, 315], an interaction postulated to contribute to the stabilisation of the ECM [347, 435]. The localisation of HCs within the pericellular HA coat and the inhibition of migration of both mock- and HAS2-transfected cells by inclusion of an antibody to IαI/PαI therefore support the notion that addition of HCs to HA is an important mechanism by which the pericellular HA coat is stabilised in renal epithelial cells.

The data in this chapter also point to a critical role for TSG-6 in cell migration because inhibition of TSG-6 abrogated the migration of the HAS2 over-expressing cells, while addition of the full-length recombinant protein enhanced their migration. TSG-6, and its Link module domain, has been found to enhance the adhesion of leukocytes by increasing the affinity of HA binding to CD44 on the surface of lymphocyte cell lines [428]; this may occur by the TSG-6-mediated formation of cross-linked HA fibres that can lead to the clustering of multiple CD44 molecules. The lack of effect after the addition of Link_TSG6 would suggest that its action is independent of its HA-binding capacity, and again this is consistent with the decreased expression of CD44 in the HAS2-transfected cells. TSG-6 also forms covalent complexes with HCs from either IαI (HC1 or HC2) or PαI (HC3) that act as intermediates in their covalent transfer onto HA [429] thus stabilising extracellular matrices rich in HA [315]. In this regard, there are no HCs of either IαI or PαI incorporated into the cumulus matrix in the TSG-$6^{-/-}$ mouse and these animals are infertile due to an inability to expand their COCs [315]. There would, however, appear to be differences in the mechanism of transfer of HC1/HC2 and HC3, because TSG-6·HC complexes derived through HC transfer from IαI can be generated *in vitro* in the absence of serum [429], whilst TSG-6·HC3 complexes are only formed *in vitro* in the presence of serum [315, 429]. It has been proposed that the Link module of TSG-6 is directly involved in the formation of TSG-6·HC complexes since the A38 antibody, which has its epitope in the Link module [436], can inhibit this process and consequently block HC transfer onto HA [278, 429]. However, the Link module alone is unable to form covalent complexes with HCs [317]. In contrast to Link_TSG6, a mutated variant of the full-length protein, which has impaired HA binding but its ability to mediate the transfer of HCs from IαI and PαI is largely unaffected (figure 4.15), was able to augment cell migration in our system. These data therefore support the hypothesis that TSG-6-mediated transfer of HCs into the HA rich pericellular matrix is a critical regulator of cell migration.

Although the components of the IαI family are synthesised predominantly in hepatocytes, PTCs are known to express PαI, a member of the IαI family [343]. In the HK-2 cell culture model, cells were grown to confluence in the presence of serum. During this period of growth HCs may therefore be incorporated into the matrix from serum-derived IαI or PαI, or alternatively from endogenous PαI. However, the HCs incorporated during the period of migration following scratch wounding are mostly derived from endogenous PαI as all the experimental manipulations were performed under serum-free conditions. Interestingly, the anti-migratory effect of blocking TSG-6 was only apparent in the HAS2 over-expressing cells. This could be related to the decreased expression of HC3 chains in the HAS2 over-expressing cells. In these cells, given the relative deficiency of HCs, the presence of TSG-6, which co-localises to the HA in the pericellular coat, may be more critical for the formation of a stabilised pericellular matrix.

The data in this chapter demonstrate that the functional consequences of increased HA synthesis may not be directly related to the HA synthase isoform that drives its synthesis, and from it we postulate that the process of extracellular HA structure formation and assembly is determined by a complex series of mechanisms, which seem to affect the expression patterns of HA degrading enzymes as well as some hyaladherins.

Chapter V

Further characterisation of HA cables: the role of hyaladherins and HAS3-overexpression

5.1 Introduction

The aim of this chapter is to examine two aspects of HA structures produced by PTCs: the first is the structural components of HA cables, and the second is the role of the constitutive HAS isoform expressed by PTCs – namely HAS3.

To date, few studies have been done to analyse the components of HA cables [170, 258]. All these studies have examined the composition of HA cables produced by colonic smooth muscle cells. There are no studies about the structural components of HA cables in the kidney.

Work in chapter four focused on the role of inducible HAS isoform in PTCs (i.e. HAS2), work in this chapter focused on the role of the constitutive HAS isoform (HAS3) and its role in regulating extracellular HA structures produced by PTCs. The study of HAS3 functionality became more important after HAS2-overexpression did not enhance cable synthesis which was shown to be part of the anti-inflammatory response of PTCs.

The specific aims in this chapter were to:

1. Further analyse the structural components of HA cables.

2. Clone HAS3 ORF into the expression vector (pcDNA4/TO) that was tested in chapter four.

3. Study the alterations in HA synthesis and extracellular structures (HA quantity and quality) following HAS3-overexpression.

4. Investigate the changes in two specific functions in the HAS3-transfected cells, namely monocyte binding and cell migration.

5.2 Results

5.2.1 Characterisation of HA cables in HK-2 cells: the role of serum, IαI, TSG-6, versican.

5.2.1.1 The role of serum: Work done by the Cleveland group demonstrated that in colonic smooth muscle cells, HA cables are only formed in the presence of serum [258], therefore, the role of FCS in HA cable formation by PTC was investigated. For this, HK-2 cells were grown to confluence before growth-arresting for 48 h which was followed by replacement of culture medium with either serum-free medium or medium containing 2% FCS for 24 h. Confocal microscopy was used to examine the organisation of hyaluronan on the cell surface. As with previous experiments, HA was identified with b-HABP and detected with fluorescent Avidin-D. Photomicrographs of fixed, growth-arrested HK-2 cells demonstrated diffusely arranged pericellular HA over the cell surface in addition to cable-like structures that spanned several cell lengths (figure 5.1A), as previously described in chapter three. Culture of HK-2 cells in the presence of FCS (2%) showed a markedly increased number of HA cables on their surface (figure 5.1B). The HA content of these structures was confirmed by 5 min treatment of bovine testicular hyaluronidase which removed all the cables (figure 5.1C).

Monocyte binding was also altered following incubation with FCS. Confluent, growth-arrested HK-2 cells were incubated with either serum-free medium or medium containing 2% FCS for 24 h before addition of radiolabelled monocytes. FCS-treated HK-2 cells bound more monocytes than unstimulated HK-2 cells (120% increase; p=0.0046; figure 5.3).

5.2.1.2 The role of IαI: previous studies have shown that the HCs from the IαI family are important in the formation of pericellular HA coats [344]. Studies in smooth muscle cells have also demonstrated that HCs are an important structural component of HA cables in this cell type [258]. The IαI antibody used recognises all components of IαI (HC1, HC2 and bikunin) as well as intact PαI, but not HC3 [437]. Using this antibody, confocal microscopy of HK-2 cells grown in the absence of serum revealed co-localisation of IαI staining with the HA cables and coats (figure

5.2). This suggests that components of the IαI family are incorporated into the extracellular HA structures, although it was not possible to distinguish between IαI HC1/HC2 and PαI.

Incubation of cells under serum-free conditions in the presence of the IαI/PαI antibody resulted in severe truncation of the HA cables, and at higher antibody concentration complete absence of HA cable formation (figure 5.1D and E). The effect of the antibody was not apparent when the antibody was added in the presence of 2% FCS (figure 5.1F). Under these conditions it is likely that serum-derived HCs are in excess and thus overcome the inhibitory action of the antibody.

Data from chapter three have demonstrated that monocyte binding is dependent on cell surface HA cables. Having demonstrated reduced cable formation in the presence of antibody to IαI/PαI, I subsequently examined the effect of the antibody on monocyte adhesion to HK-2 cells. Reduction of HA cable formation by antibody to IαI was accompanied by significant attenuation of monocyte binding (figure 5.3). This represented about 25% reduction in bound monocytes compared to control ($p=0.01$).

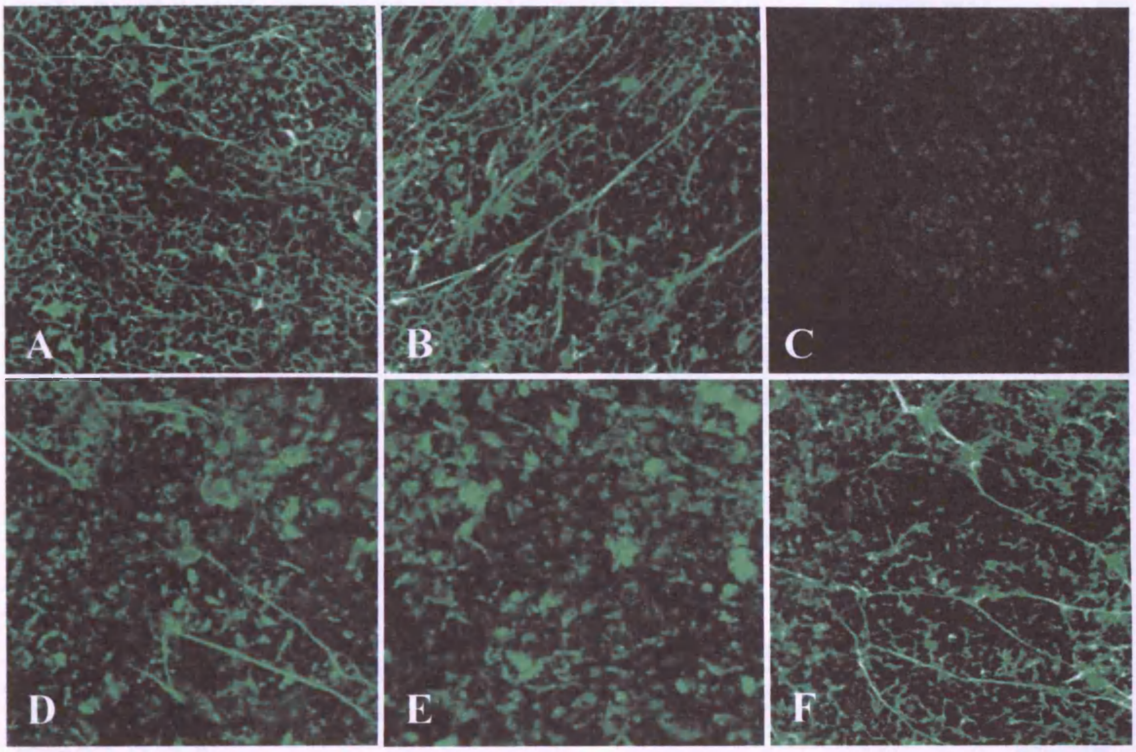

Figure 5.1: Effect of FCS and IαI blockade on HA cable formation.

Confluent monolayers HK-2 cells were serum-deprived for 48 h prior to addition of serum-free medium only **(A** and **C)**, or medium containing FCS (2%) **(B)**, or serum-free medium with IαI Ab (1/200) **(D)**, or serum-free medium with IαI Ab (1/50) **(E)**, or medium with IαI Ab (1/50) containing FCS (2%) in **(F)**. 24 h later, fixation done with methanol and detection of HA by addition of b-HABP (magnification x 100).

In **(C)**, HK-2 cells were treated with bovine testicular hyaluronidase (200 μg/ml) at 37°C for 5 min prior to labelling with b-HABP, to confirm the specificity of HA staining.

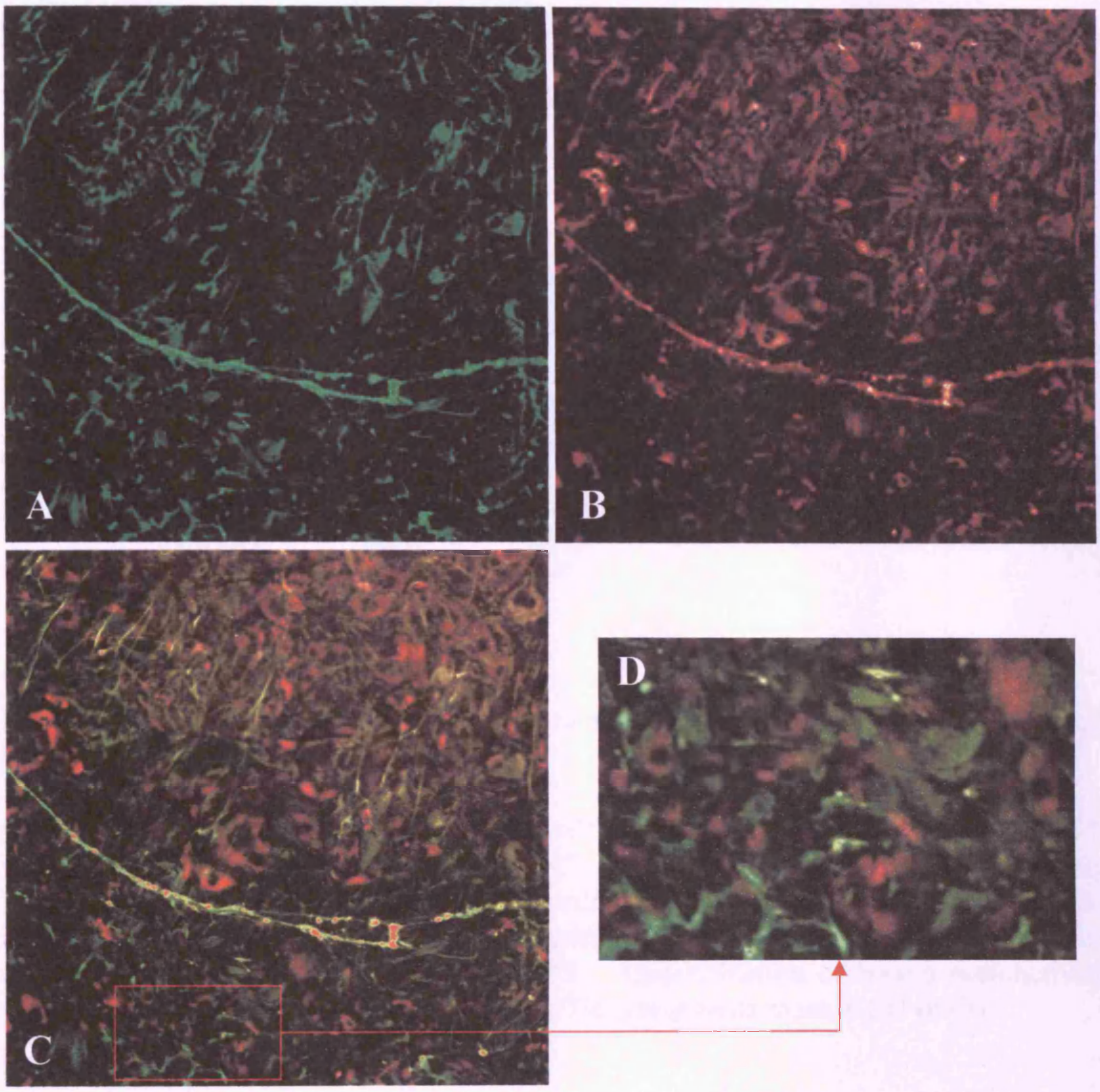

Figure 5.2: Localisation of IαI/PαI.

Confluent monolayers of HK-2 cells were growth-arrested for 48 h prior to fixation with methanol. HA was detected by addition of b-HABP and fluorescent Avidin-D **(A)**, and IαI/PαI detected by addition of polyclonal antibody to IαI/PαI and anti-rat Texas red conjugated antibody **(B)**. Co-localisation of HA and IαI/PαI was examined by merging individual images **(C)** (magnification x 100). The red square area in C was enlarged to show intracellular IαI/PαI staining **(D)**.

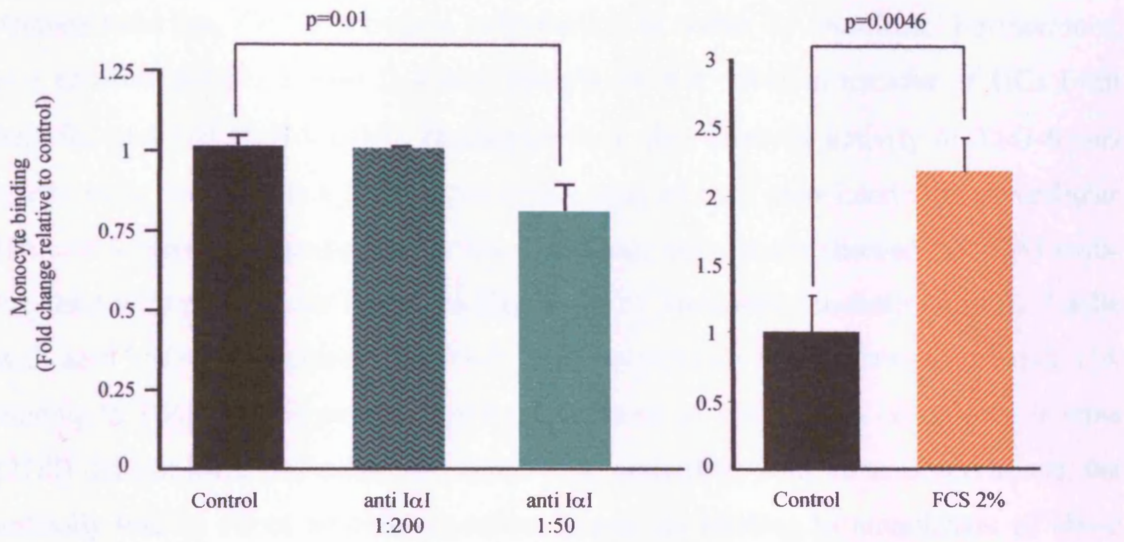

Figure 5.3: Monocyte binding is decreased after IαI blockade and increased after FCS supplementation.

Confluent monolayers of HK-2 cells were serum-deprived for 48 h before incubation with either polyclonal antibody to IαI/PαI (1:200 or 1:50) or with medium containing 2% FCS or with serum-free medium for further 24 h (as control). Subsequently, the monolayer was washed with PBS prior to addition of 1 x 10^6 ^{51}Cr-labelled U937 cells under serum-free conditions for 1 h at 37°C. Quantification of bound radioactivity was carried out as described in chapter two. Data represent mean ± SD (n=3).

5.2.1.3 The role of TSG-6: Studies utilizing the TSG-6$^{-/-}$ mouse have demonstrated that TSG-6 is critical in formation of stable HA matrices. Furthermore, in a cell-free system TSG-6 is a key catalyst for the covalent transfer of HCs from both IαI and PαI to HA [438]. In chapter four, this catalytic activity of TSG-6 was shown to be involved in a pro-migratory function of cells associated with pericellular HA coat formation. Also in chapter four, confocal microscopy showed that TSG-6 co-localised with pericellular HA coats (figure 4.15). However, incubation of HK-2 cells with anti TSG-6 monoclonal antibody A38 (previously demonstrated to block HA binding to TSG-6 [385] and prevent the formation of TSG-6-HCs complexes *in vitro* [278]) did not influence cable formation and, consistent with these observations, the antibody had no effect on HA-dependent monocyte binding to monolayers of HK-2 cells (figure 5.4).

These results therefore suggest that TSG-6 is not involved in the stabilisation of HA cables by transfer of IαI family components or that transfer of HCs to HA cables is not solely dependent on the effect of TSG-6.

5.2.1.4 The role of versican: Versican is also reported to be important in the formation of extracellular HA structures [253]. Results from other laboratories have shown its localisation with both HA coats and cables (De La Motte, CA – personal communication). Using confocal imaging, versican showed positive co-localisation with HA in the matrix with little or no positive staining intracellularly (figure 5.5).

The effect of blocking versican on extracellular HA structures was examined by incubating HK-2 cells with anti-versican antibody for 24 h before staining for HA. Confocal imaging showed no difference between control cultures and antibody-treated cultures (figure 5.6A and B). In addition, HK-2 cells incubated with versican Ab for 24 h did not differ significantly from untreated HK-2 cells in terms of monocyte binding capacity (figure 5.6C).

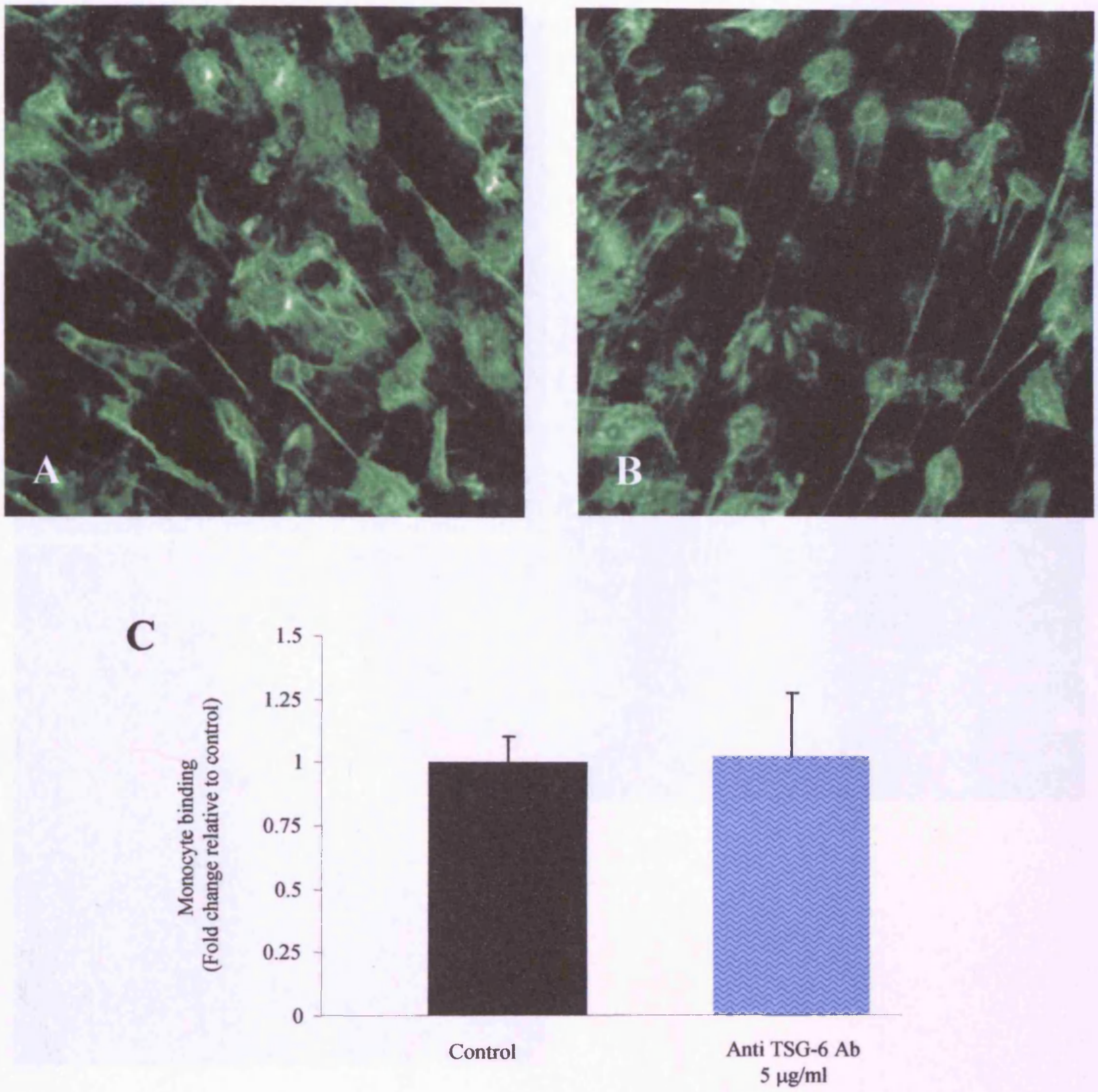

Figure 5.4: Effect of TSG-6 blockade on HA cable formation and monocyte binding.

HK-2 cells were grown in the presence of 10% FCS and then serum-deprived for 48 h prior to the addition serum-free medium as control **(A)** or serum-free medium containing anti-TSG-6 antibody (clone A38; 5 μg/ml) for 24 h **(B)** . Cells were then fixed with 100% ice-cold methanol and labelled with HABP for HA detection (magnification x 200).

In **(C)**, confluent HK-2 cells were serum-deprived for 48 h prior to the addition of serum-free medium as control, or serum-free medium containing anti-TSG-6 antibody (clone A38; 5 μg/ml) for 24 h. Subsequently, the monolayer was washed with PBS prior to addition of 1 x 10^6 ^{51}Cr-labelled U937 cells again under serum-free conditions for 1 h at 37°C. Quantification of bound radioactivity was carried out as described in chapter two. Data represent mean ± SD of three experiments.

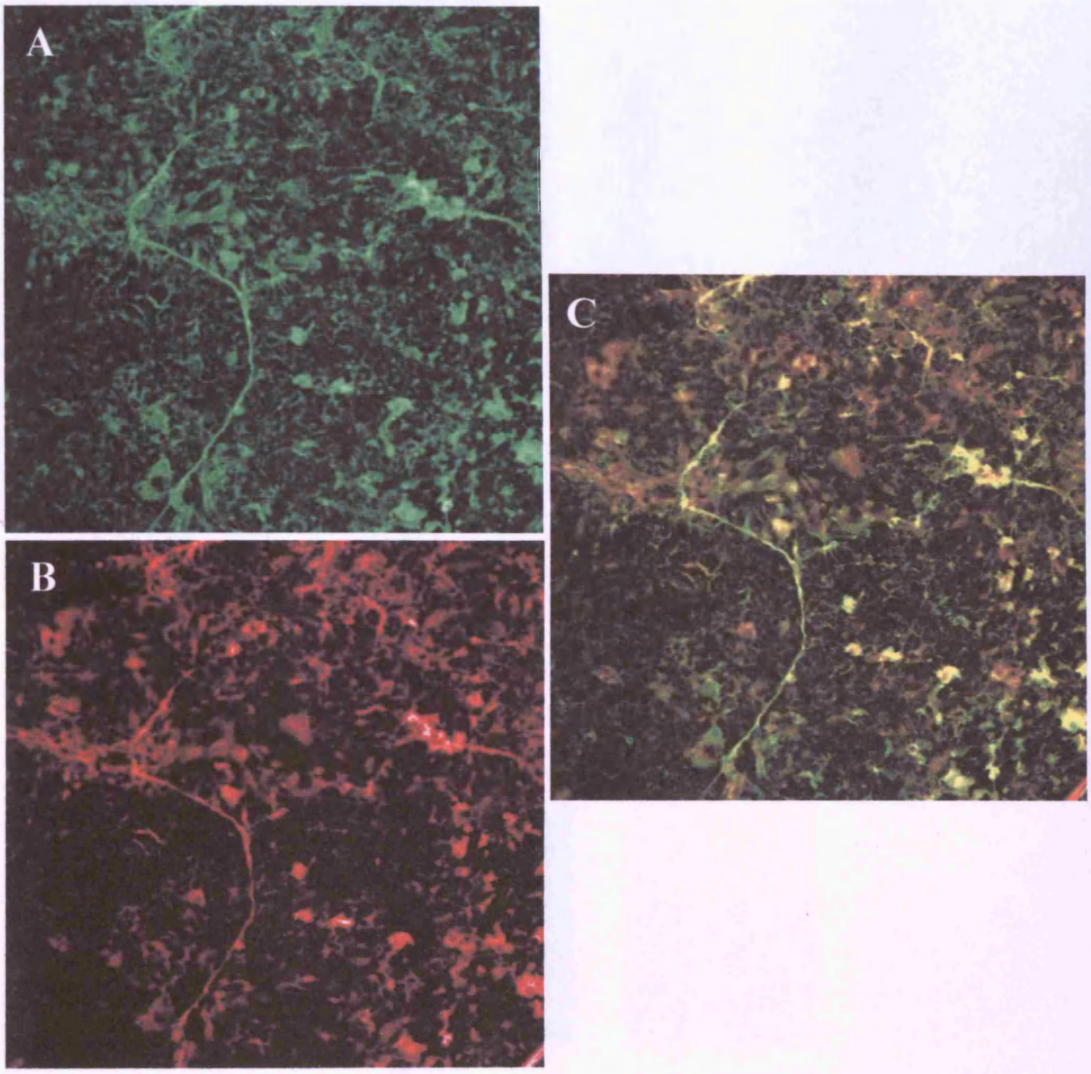

Figure 5.5: Co-localisation of versican and HA.

Confluent monolayers of HK-2 cells were growth-arrested for 48 h prior to fixation with methanol. HA was detected by addition of biotinylated HABP and fluorescent Avidin-D **(A)**, and versican detected by addition of monoclonal antibody to versican 2-B-1 and secondary Texas red-conjugated antibody **(B)**. Co-localisation of HA and versican was examined by merging of individual images **(C)** (magnification x 100).

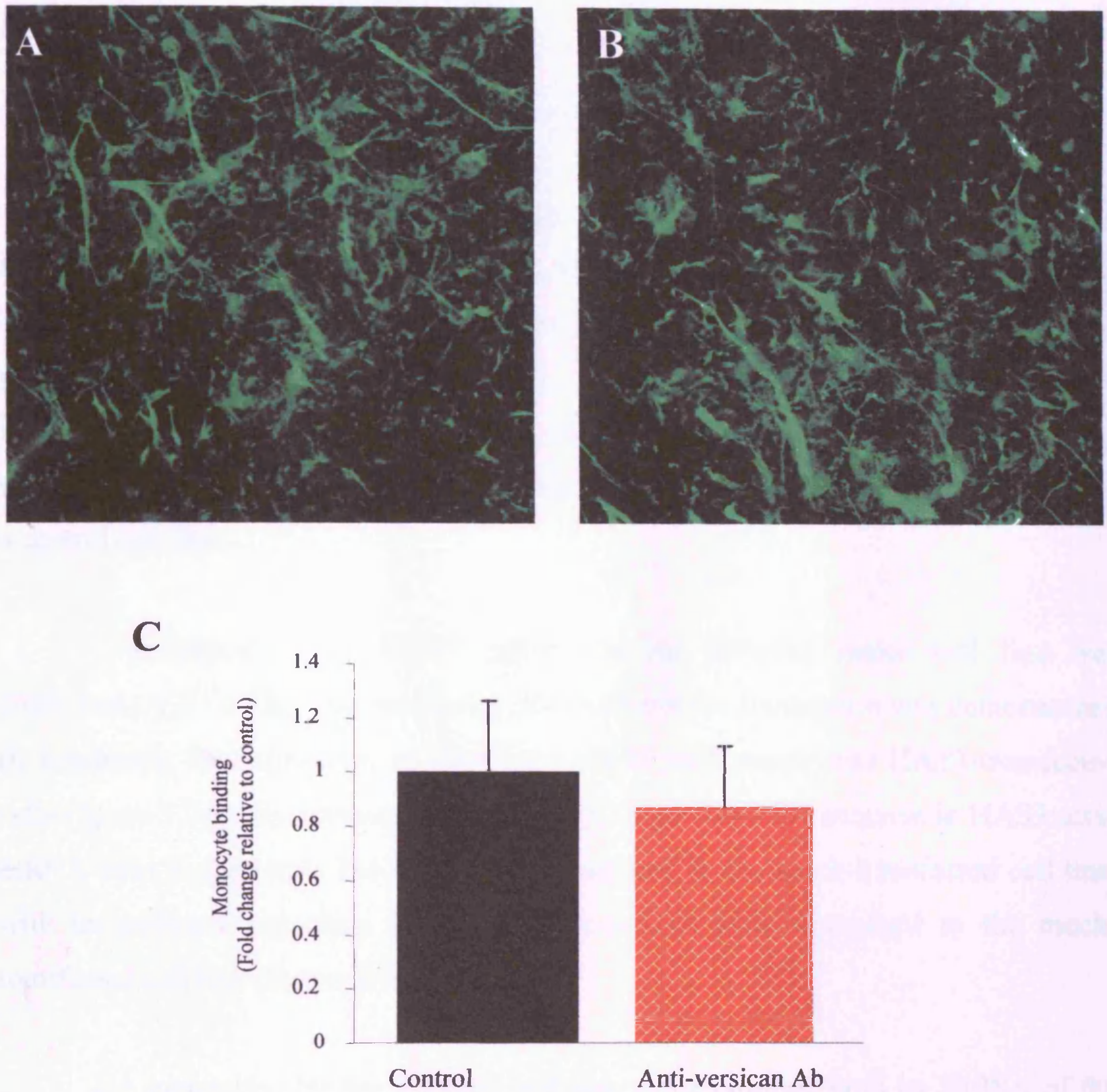

Figure 5.6: Effect of anti-versican antibody on HA cable formation and monocytes binding.

HK-2 cells were grown in the presence of 10% FCS and then serum-deprived for 48 h prior to the addition serum-free medium as control **(A)** or serum-free medium containing anti-versican (dilution 1/100) antibody for 24 h **(B)** . Cells were then fixed by 100% ice-cold methanol and labelled with HABP for HA detection (magnification x 100).

In **(C)**, confluent HK-2 cells were serum-deprived for 48 h prior to the addition of serum-free medium as control, or serum-free medium containing anti-versican antibody (dilution 1/100) for 24 h. Subsequently, the monolayer was washed with PBS prior to addition of 1 x 10^6 ^{51}Cr-labelled U937 cells under serum-free conditions for 1 h at 37°C. Quantification of bound radioactivity was carried out as described in chapter two. Data represent mean ± SD of three experiments.

5.2.2 HAS3 over-expression

5.2.2.1 Confirmation of HAS3 over-expression in transfected HK-2 cells

After cloning of HAS3 ORF into pcDNA4/TO and generation of zeocin-resistant clones (detailed in chapter two), the next step was to confirm more HAS3 activity in these transfected cells. Several HK-2 clones were scanned for HA production in the supernatant by ELISA and one clone that showed a significant increase in HA production (figure 5.7C) was picked for further analysis. All mock-transfected cells showed similar HA profiles and, therefore, one clone was selected as a control cell line.

Over-expression of HAS3 mRNA in the selected stable cell line was confirmed by RT-PCR. The specificity of HAS3 mRNA expression was demonstrated by examining the expression of HAS2 mRNA in both mock- and HAS3-transfected cells (figure 5.7A). By scanning densitometry, there was 25% increase in HAS3:actin mRNA ratio in the stable HAS3 cell line compared to the mock-transfected cell line, with insignificant reduction in HAS2:actin mRNA ratio compared to the mock-transfected cell line (figure 5.7B).

HA generation by the selected cell line was examined both by ELISA of the cell culture supernatant and by ^{3}H-glucosamine labelling of HA. Confluent monolayers of HAS3- or mock-transfected cells were serum-deprived for 48 h. Fresh serum-free medium was subsequently added for a further 24 h prior to collection and quantification of HA by ELISA (figure 5.7C). HA concentration in the culture supernatant was significantly greater in the HAS3 expressing cell line. This represented a 32% increase in the HA over the mock-transfected cells ($p=0.004$).

Analysis on Sephacryl S-500 of the ^{3}H-glucosamine-labelled HA samples from both the HAS3- and the mock-transfected HK-2 cells demonstrated that the majority of the labelled HA appeared near the void volume and therefore was considered to be of high molecular mass (figure 5.8). In addition, there was a marked increase in the generation of medium and low molecular weight HA in the CM and the TE of the HAS3 over-expressing cells as compared to the mock-transfected cells.

An unexpected reduction (57%) in the CA radiolabelled HA was seen in the HAS3-transfected cells compared to the mock-transfected cells. This reduction was seen in all the molecular weight fractions (high, medium and low). Of note also is that there were smaller HA fragments in the CA fraction of the HAS3 sample which is suggestive of increased HA degradative activity (figure 5.8 CA).

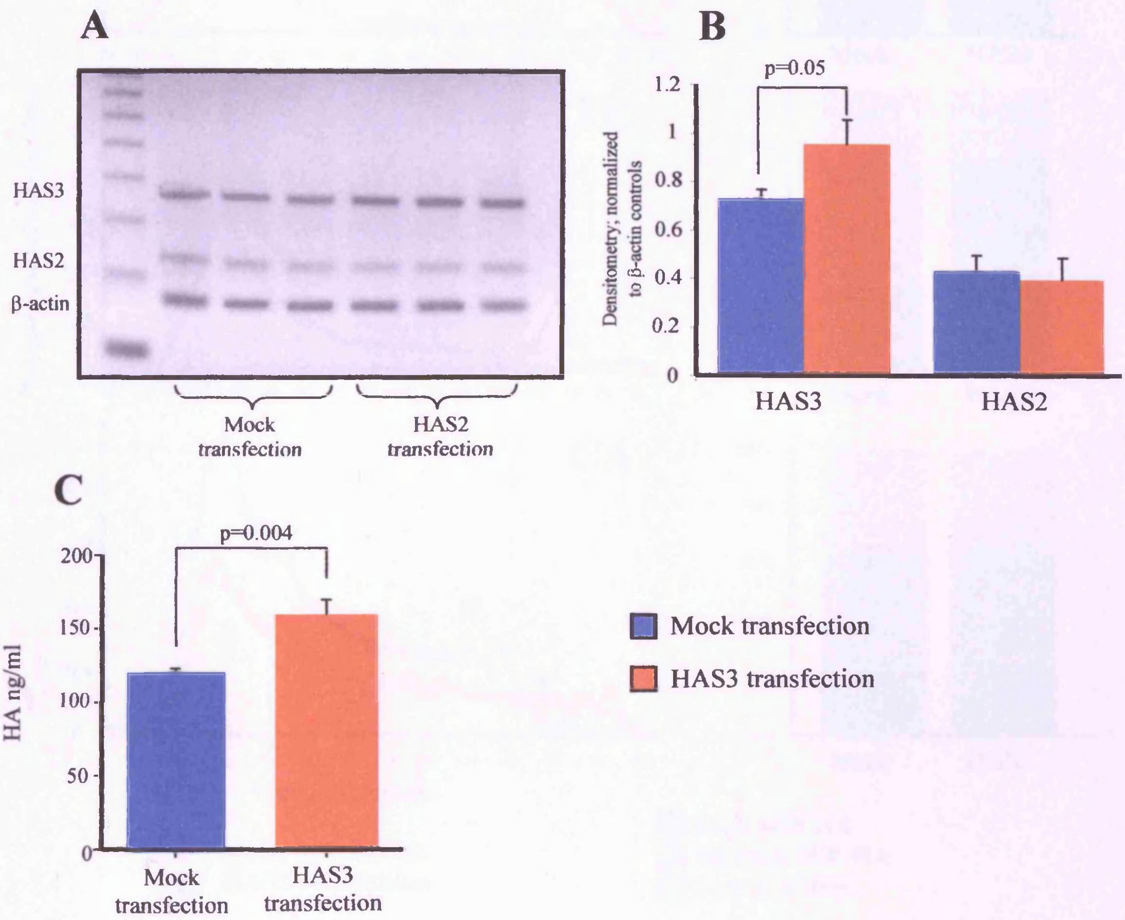

Figure 5.7: HAS2/HAS3 expression and HA production in transfected HK-2 cells.

(A) Total mRNA was extracted from confluent, transfected monolayers after 48 h of serum deprivation. Ethidium bromide stained PCR products were separated on a 3% agarose gel. Three representative PCR reactions are shown.

In **(B)**, densitometry data of the gel bands are plotted normalised to their respective actin bands.

In parallel experiments, supernatant samples were collected from confluent serum-deprived cells exposed to serum-free medium for 24 h after growth-arrest. HA was then quantified by ELISA **(C)**. Data represent mean ± SD of four separate experiments.

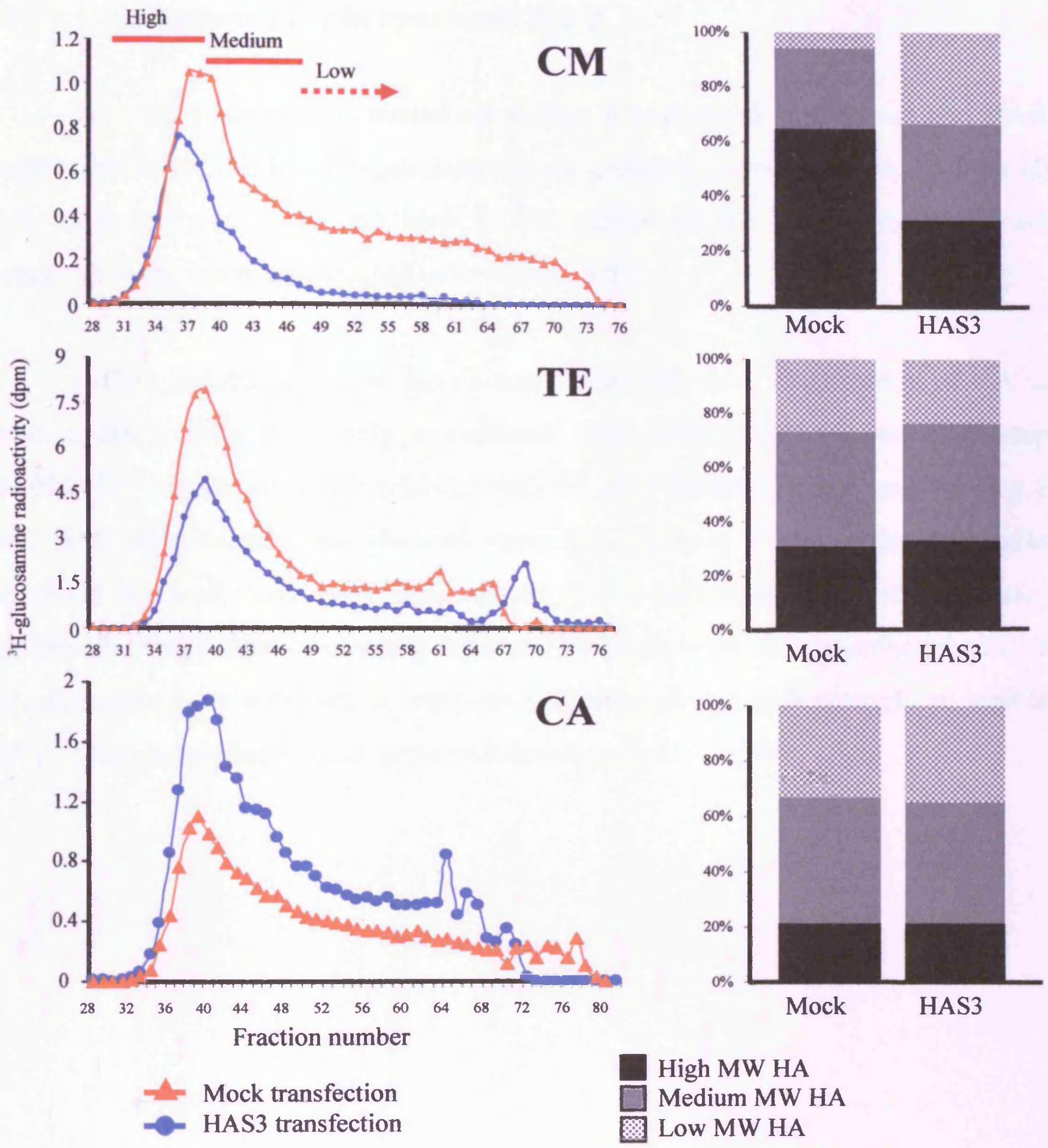

Figure 5.8: Analysis of HA in transfected HK-2 cells.

Confluent serum-deprived monolayers of HAS3- or mock-transfected cells were exposed to serum-free conditions for 24 h in the presence of 20 μCi/ml ^{3}H-glucosamine. Subsequently, conditioned medium **(CM)**, trypsin extract **(TE)** and cell-associated **(CA)** HA fractions were prepared and analysed as described in chapter two. The bars labelled as High, Medium and Low represent molecular weight ranges (High MW > 10^6 Da, Low MW < 10^5 Da). The graphs on the right represent the percentage of different MW HA in each fraction.

5.2.2.2 Visualisation of HA in transfected HK-2

HA was visualised as described earlier in both mock-transfected and HAS3-transfected cells. Confocal images demonstrate a marked increase in extracellular HA, both in pericellular coats and also in HA cables in the HAS3-transfected cells compared to the mock-transfected cells (figure 5.9).

Before isolating a stable HAS3-transfected cell line, visualisation of HA was done in HK-2 cells transiently transfected with HAS3/pcDNA4 vector or empty pcDNA4/TO vector (as mock transfection) for 24 h before fixation and staining for HA. HAS3-transfected cells showed more HA, in both forms: coats and cables, compared to mock-transfected cells (figure 5.10). Although it was not possible to confirm that these cable-producing cells are the positive HAS-3 transfected cells, the data generated from both stable- and transiently-transfected cells strongly suggest that HAS3-over-expression is associated with increase in HA cables.

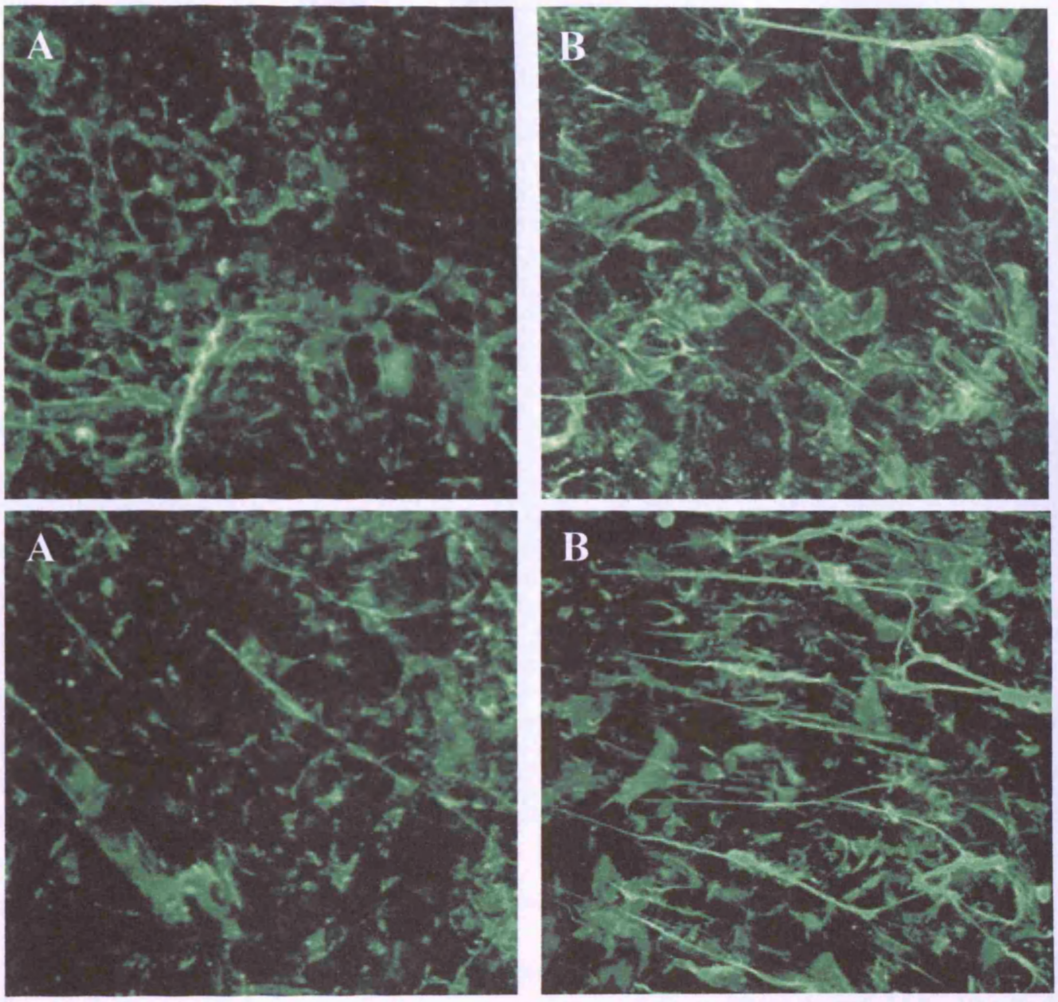

Figure 5.9: Visualisation of HA in stable-transfected cells.

Confluent monolayers of mock- **(A)** and HAS3- **(B)** transfected cells were serum-deprived for 48 h prior to fixation with methanol and detection of HA by addition of b-HABP. Sections were imaged by confocal microscopy (magnification x 200).

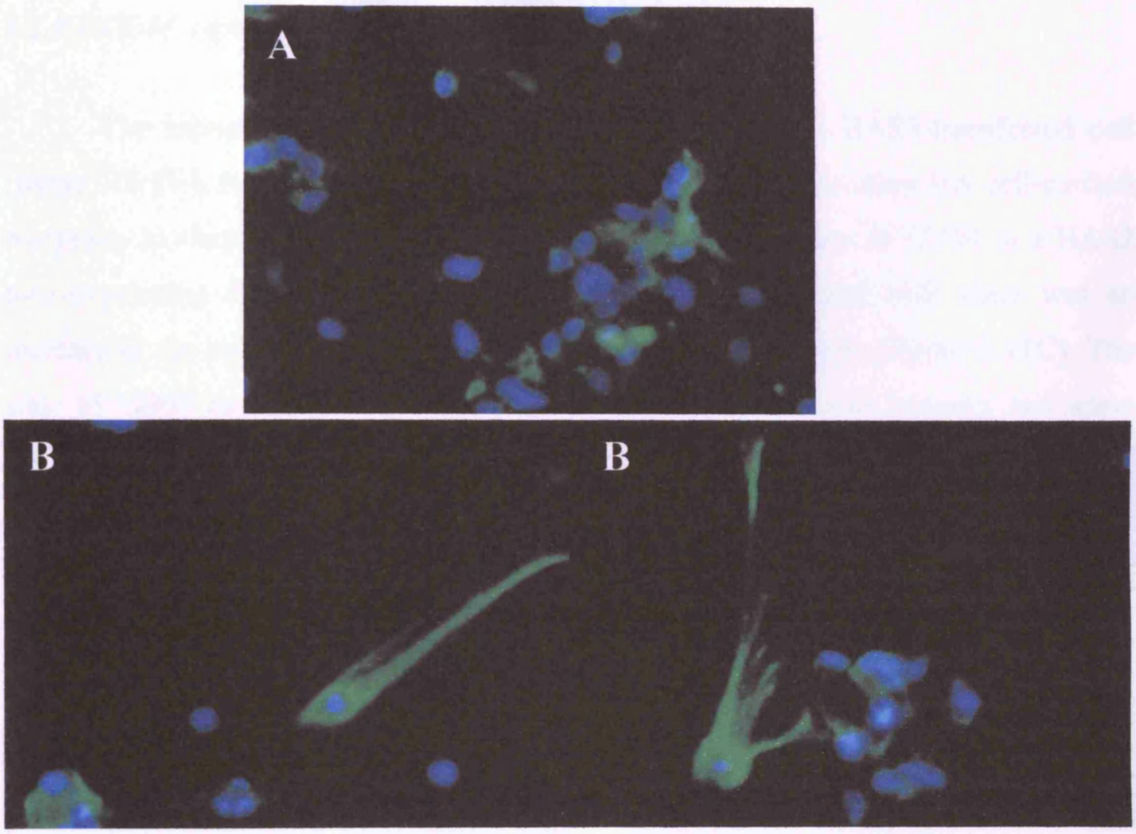

Figure 5.10: Visualisation of HA in transiently-transfected cells.

Sub-confluent HK-2 cells were serum-deprived for 48 h prior to mock- **(A)** or HAS3- **(B)** transfection. 24 h later, fixation was done with methanol and HA detected by addition of b-HABP. Sections were imaged by fluorescence microscopy (magnification x 200). Cell nuclei are visualised by DAPI staining (blue).

5.2.2.3 CD44 expression in HAS3-over-expressing cells

The increased HA in the trypsin extract fraction, in HAS3-transfected cell (figure 5.8 TE), is suggestive of increased CD44 expression or other HA cell-surface receptors. In chapter four, data have shown reduced expression of CD44 in a HAS2 over-expressing cell line. In contrast, in the HAS3-transfected cells there was an increase in the cell surface CD44 as assessed by FACS analysis (figure 5.11C). The state of CD44 expression was also investigated using confocal imaging and again HAS3-transfected cells showed stronger CD44 staining than mock-transfected cells (figure 5.11D and E).

5.2.2.4 Expression of relevant HA regulators/structural components after HAS3-overexpression: Hyaluronidases and PαI

Data from both chapters three and four pointed to a role of hyaluronidases in HA cable formation. Also, in HAS2-transfected cells (where less cables were seen), there was a marked reduction in HC3 of PαI. RT-PCR was done to investigate the expression of HYALs (HYAL1 and HYAL2) and PαI (bikunin and HC3) mRNA in mock- and HAS3-transfected cells. Both HYAL1 and HYAL2 were up-regulated in the HAS3-transfected cells (figure 5.12). Densitometry data showed that the increase was about 250% in HYAL1/actin ratio ($p=0.0006$) and about 200% in HYAL2/actin ratio ($p=0.0011$).

In addition, there was up-regulation of both components of the PαI: bikunin and to a lesser extent HC3. The increase was about 150% in bikunin/actin ratio ($p=0.0481$) and about 15% in HC3/actin ratio (p=n/s).

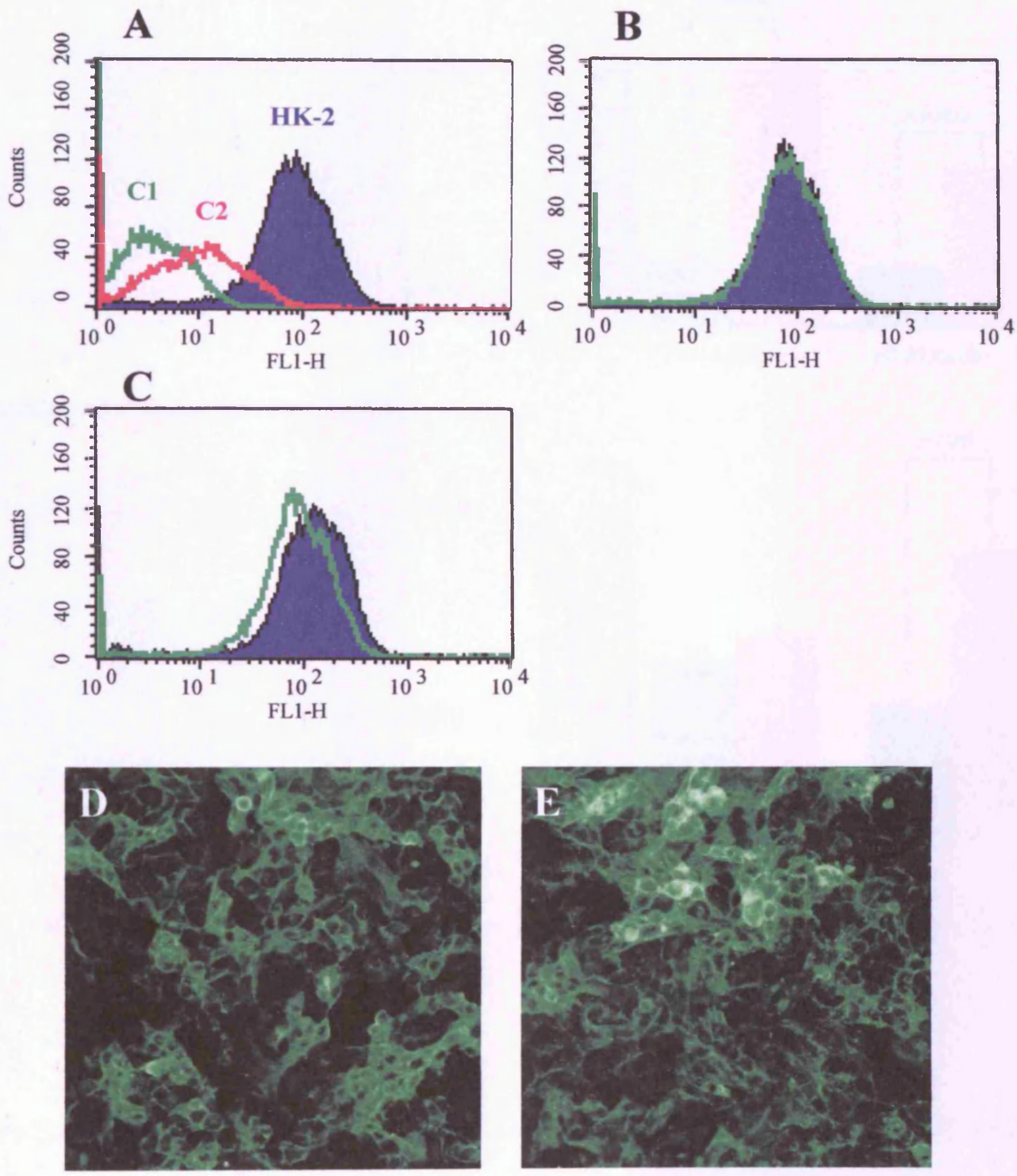

Figure 5.11: CD44 expression in control and transfected HK-2 cells.

Confluent growth-arrested HK-2 cells were analysed by flow cytometry using anti-CD44 Ab. **(A)** Shows untransfected HK-2 cells with two controls: C1 is unlabelled cells while C2 is cells labelled with secondary FITC-conjugated Ab only. **(B)** Shows a comparison between untransfected (green line) and mock-transfected (violet area) HK-2 cells and **(C)** between mock- (green line) and HAS3- (violet area) transfected cells.

CD44 expression is shown by immunocytochemistry in growth-arrested mock- **(D)** or HAS3- **(E)** transfected HK-2 cells (magnification x 200).

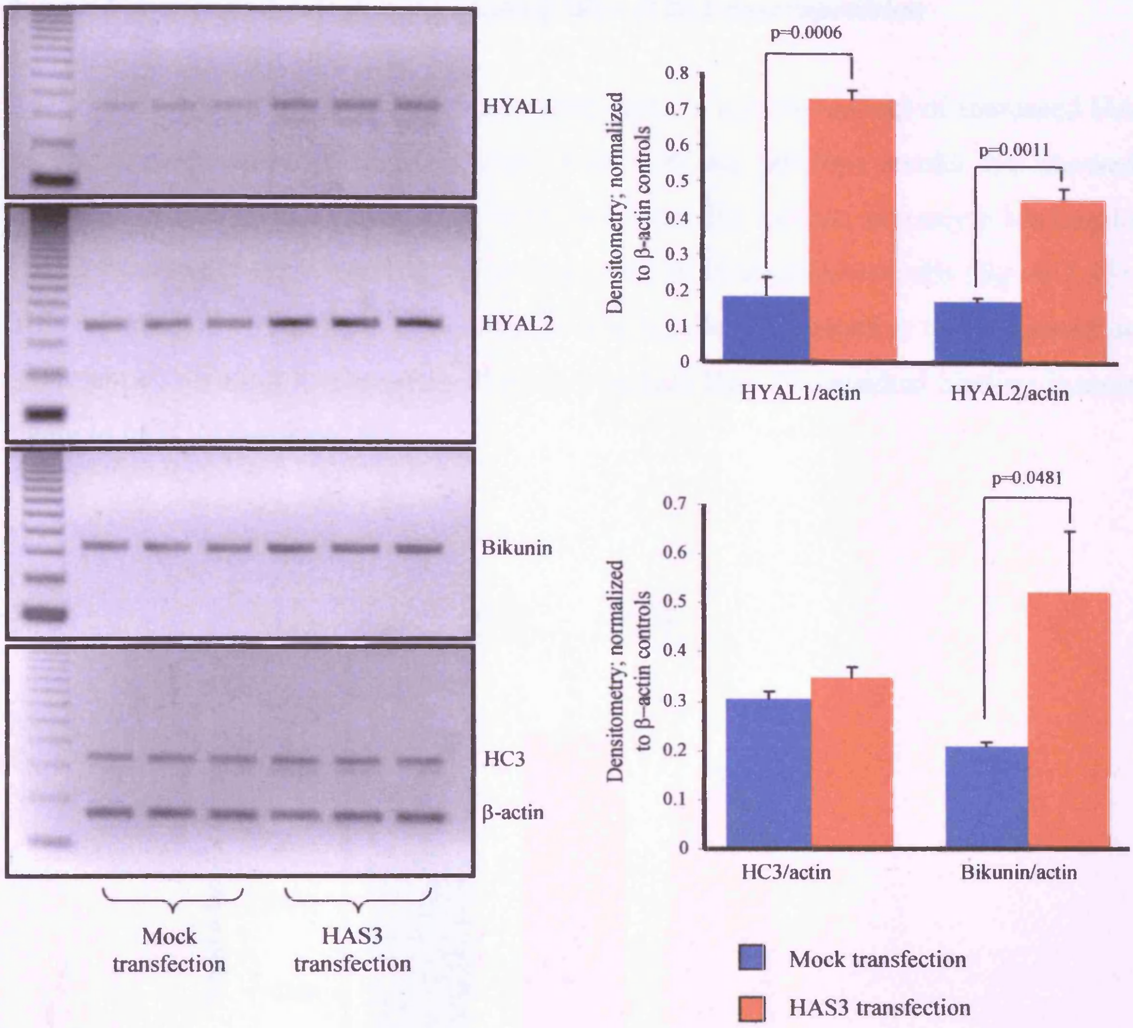

Figure 5.12: mRNA expression of HYAL1/2 and PαI components (Bikunin and HC3).

Total mRNA was extracted from confluent monolayers of mock- and HAS3-transfected cells after 48 h of serum deprivation. PCR performed for various cycles as detailed in chapter two. Ethidium bromide-stained PCR products were separated on a 3% agarose gel. Three representative PCR reactions are shown. Densitometric ratios of the gene of interest compared to the house-keeping gene β-actin of 3 individual experiments are shown with the data representing mean ± SD.

5.2.2.6 Cell migration after HAS3-overexpression

Cell migration was assessed in mock- and HAS3-transfected cell lines as described in chapter two. Confluent monolayers of cells were serum-deprived for 48 h prior to generation of an intersecting area of denuded cells by scraping with sterile 1000 μl pipette tip. Closure of the denuded area was then monitored at different times. Cell migration was increased in HAS3-transfected cells compared mock-transfected cells and this increase was significant 48 h after scratching and all the time points that followed (figure 5.14).

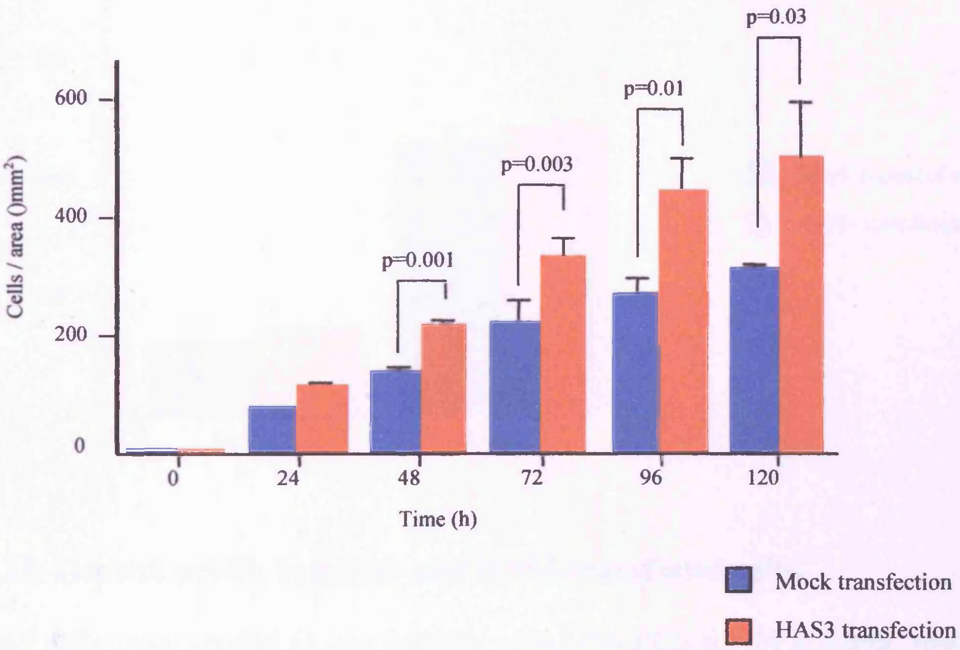

Figure 5.14: Quantification of cell migration.

Confluent serum-deprived monolayers of mock- or HAS3-transfected cells were scratched to produce an intersecting area of denuded cells. Subsequently, following washing of the monolayer to remove detached cells, the rate of cell migration of each of the two cell lines was assessed by directly counting the number of cells migrating into the intersecting denuded area at each of the time points indicated. The data are expressed as the number of cells per denuded area. Data represent the mean ± of four individual experiments.

5.2.2.7 Enhanced cell migration after HAS3-transfection is independent of cellular proliferation

Cellular proliferation in the transfected cells was assessed by alamar blue as described in chapter two. The rationale for doing proliferation measurement was to check whether the increased migratory rate in the HAS3-transfected cells is caused by increased proliferation rate. Following 96 h of serum-starvation, there was no significant difference between mock- and HAS3-transfected cells (figure 5.15).

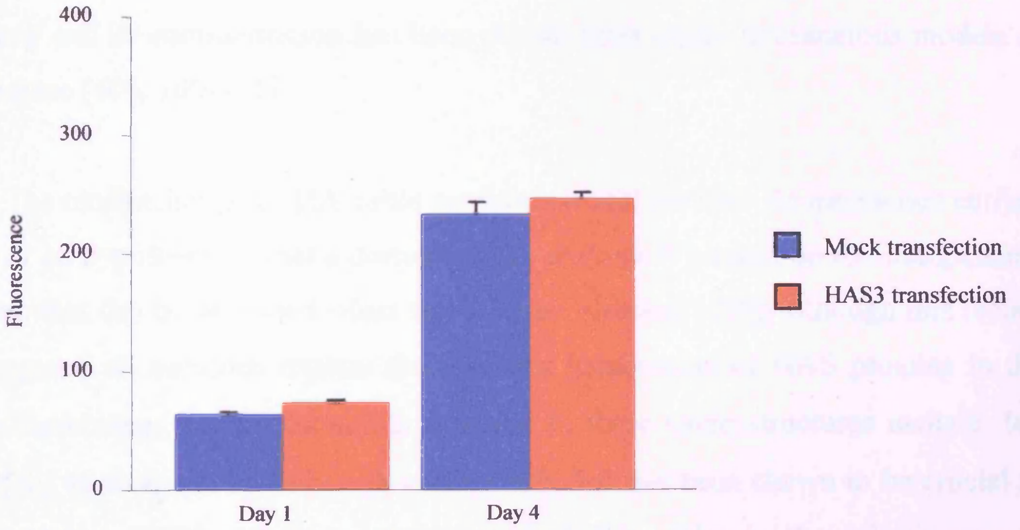

Figure 5.15: Growth profile in mock- and HAS3-transfected cells.

Transfected cells were seeded at low density with 10% FCS for 24 h. Later, medium was replaced with serum-free medium containing 10% alamar blue and a fluorescence measurement was taken after 1 h. After washing with PBS, cells were re-incubated with serum-free medium until the next alamar blue measurement (at day 4 post-seeding).

5.3 Discussion

Data from chapter three have shown that in addition to pericellular HA coats, PTCs form HA in cable-like structures which support interactions with monocytes, via their cell surface CD44 receptors. The monocyte-HA interaction prevents monocytes-PTCs direct interaction which drive ICAM-dependent TGF-β1 generation [135, 363]. This suggests that synthesis of HA cables may limit renal injury. Consistent with this hypothesis is our observation that cable formation is stimulated by BMP-7. Chronic renal failure has been postulated to be a state of BMP-7 deficiency and its administration has been shown limit injury in numerous models of renal disease [104, 109-111].

The mechanism(s) of HA cable synthesis is still unclear. As mentioned earlier, Majors *et al.* hypothesised that a dormant HAS isoform is located on the endoplasmic reticulum that can be activated when the cells are stressed [170], although this theory stands against all previous reports that showed localization of HAS proteins in the cellular membrane. The hyaladherins reported in these cable structures include: IαI [170, 258], versican [170], although to date only IαI has been shown to be crucial to cable formation [258]. All these reports studied HA-cables in the colonic smooth muscle cells. There are no studies, to date, analysing the components of these structures in the kidney. In this chapter, the nature and structure of HA cables produced by PTCs was characterized in detail.

An important observation from the data in this chapter is the incorporation of components of the IαI family of proteins into the HA cables and the demonstration of their importance in cable assembly. Both cable assembly and HA-dependent monocyte binding to PTCs was inhibited by an antibody to IαI/PαI. Another observation is that in PTCs, HA cables are formed in the absence of serum unlike colonic smooth muscle cell in which HA cables were first described only in the presence of serum. However, addition of serum enhanced HA cable formation by PTCs and caused more monocyte adhesion. The IαI family includes four plasma proteins; these are free bikunin, IαI, PαI and IαLI. Although the components of the IαI family are synthesised predominantly in hepatocytes, PTCs generate the PαI variant of the IαI family [343]. This may therefore explain the generation of cables by PTC in the absence of serum, which is the source of IαI family protein components for colonic smooth muscle cells. This hypothesis is further supported by the demonstration of HA cables in the HAS3 over-expressing cell line. This is in contrast to the reduction in HA cables seen in a HAS2 over-expressing (data from chapter four). One difference between the two cell lines is the expression of HC3 mRNA which is markedly down-regulated in the HAS2 cell line while abundantly expressed in the HAS3 cell line. Future work in the department is aimed at clarifying the role of endogenous PαI in the assembly of pericellular HA by PTCs. This can be investigated by inhibition of protein synthesis using siRNA technology.

TSG-6 is an inflammation-associated secreted protein composed of contiguous Link and CUB domains (detailed in chapter one). It may bind to HA directly through its link module [428], and has also been demonstrated to play an important role in the transfer of HCs from IαI onto HA [278, 438]. This reaction can be visualised in a cell-free system utilising purified IαI, HA and TSG-6 in the absence of serum [315]. TSG-6 role in transfer of HC3 from PαI is less well understood. In an *in vitro* assay in the absence of serum TSG-6 does not support the transfer of HC3 from PαI to HA (Day AJ – unpublished observation), although studies in the TSG-6$^{-/-}$ mouse do suggest that TSG-6 *in vivo* may be involved in HC3 transfer [315]. Data from chapter four demonstrated that the transfer of HCs of IαI/PαI to HA by TSG-6 is involved in the formation of pericellular HA coats. In contrast, the data presented in this chapter suggest that TSG-6 is not such a key event in the incorporation of IαI/PαI components into HA cables. This observation that TSG-6 is not a critical factor in the formation of HA cables is also consistent with previous work which demonstrated that IL-1β stimulates PTC TSG-6 synthesis [343], decreases formation of HA cables and HA-dependent monocyte binding (chapter three), despite being a potent stimulus of PTC HA generation [175]. Taken together these data suggest that up-regulation of TSG-6 during inflammation may represent a harmful effect as it enhances the build-up of HA coats by facilitating the transfer of IαI/PαI into pericellular HA coats which: (*i*) negatively affect HA cable formation that may suppress the impact of infiltrating inflammatory cells, and (*ii*) stimulates a migratory phenotype in the PTC that is shown to be associated with epithelial transdifferentiation and renal fibrosis.

Another hyaladherin that was identified as a component of HA cables is the large chondroitin sulphate proteoglycan, versican. Data generated using colonic smooth muscle cells suggest that versican is important in binding leukocytes to HA cables, although the counter-receptor on the leukocyte has not been fully characterised [258]. The Ab used for versican detection (monoclonal AB, clone 2B1) reacts with the intact molecule of the proteoglycan and the chondroitinase ABC-treated core molecule [439]. Experiments by the Cleveland group have shown that this anti-versican Ab reacts with the G3 domain of the proteoglycan and not with the G1 domain, which can bind to HA and CD44 [440](De La Motte, CA – unpublished observation). In the light of the above observation, our results (figure 5.5B) can be explained but also fails to confirm whether versican is essential to cable formation or not.

IL-1β, which abrogates PTC cable formation, is a known inhibitor of versican synthesis [441] in other cell systems. Interestingly chondroitin sulphate competes efficiently with immobilized HA for the binding of full length TSG-6 at physiological pH [442]. In addition, overlapping sites in the G1 domain of versican bind HA and TSG-6 link module [443] whilst overlapping sites on the link module of TSG-6 mediate binding to HA and chondroitin-4-sulphate [314]. Versican has been shown to bind HCs of the IαI family and also has been demonstrated to support the transfer of HCs onto HA [444]. This raises the possibility that TSG-6/Versican counter-regulatory mechanisms exist which modulate HA assembly altering the balance between HA coat and cable formation. In addition to its structural role in HA cables, it is therefore interesting to speculate that induction of versican may result in abrogation of TSG-6 HCs transfer activity thus hampering coat formation and favouring cable assembly. This role for versican, in the assembly of HA cables, is also consistent with studies demonstrating an anti-inflammatory effect, as versican can bind specific chemokines and this binding tends to down-regulate chemokines function [445].

BMP-7 stimulation leads to an increase in HA cable formation (data from chapter three). This observation was associated with down-regulation of hyaluronidase expression (HYAL1 and 2). Furthermore, decreased HA cable formation in HAS2 over-expressing cells was associated with an increase in hyaluronidase expression. This led us to postulate that hyaluronidase expression may be causally related to HA cable formation, and that down-regulation of hyaluronidase activity may help HA to remain associated with its synthesizing enzyme, and that HA extruded through the cell membrane is anchored to HAS isoforms and associates with similarly anchored HA from neighbouring cell thus forming cables. The data in this chapter, however, would suggest that this is not the case as increased HA cable formation in the HAS3 over-expressing cells occurred despite an increase in hyaluronidase activity. This suggests that the increase in hyaluronidase expression in both the HAS2 and HAS3 over-expressing cells represents a feedback response of the cell when it encounters a huge excess of HA and is therefore not causally related to the absence of cables in HAS2 over-expressing cells.

An alternative explanation put forward to explain the absence of cables in HAS2 cells is related to organisation of HAS2, and that competition for the UDP-sugar substrates between cable forming and non-cable forming HAS may limit cable formation. Cable forming HAS may, therefore, have specific membrane organisation which require additional structural components not present in the transfected cells which therefore limit cable formation in these cells. The ability of HAS3 transfected cells to form cables would, however, suggest that the expression of the specific isoforms of the HAS enzyme is the critical issue in HA cable formation.

PTCs express two of the three known HAS isoforms [175], HAS2 and HAS3, as mentioned earlier, although HAS2 represents the main HA synthase as more mRNA copies are expressed by PTCs compared to HAS3. Research done by others have shown that HAS3 can be up-regulated by different stimuli along with or independent of other HAS isoforms, and in different cell types such as skin fibroblasts [181], embryonic chondrocytes [186], keratinocytes [302, 446], and periodontal ligament cells [180]. HAS3 is also up-regulated in metastatic colon carcinoma cells [447], where its inhibition by anti-sense HAS3 transfection leads to a reduction of tumour growth. HAS3. HAS3 expression has also been linked to prostate cancer cell growth [191], but not to their metastatic ability. The HA produced by the HAS3 isoform is of smaller molecular weight compared to that produced by HAS2 [448, 449], however, it is still in the range of high molecular weight HA (between 2 x 10^5-2 x 10^6) and, as other HAS isoforms, participate in the formation of the pericellular matrix.

Over-expression of HAS3 lead also to an increase in pericellular HA coats and PTC wound re-epithelialization (migration). Although, the effect on cell migration was significant 48 h after wounding and thereafter, the enhanced migration was less prominent than that seen in the HAS2-transfected cells. The reason behind this variation could be the difference in the arrangement of pericellular HA in the cell lines but also could be due to more complex factors such as differences in HA profile (molecular weight and distribution) and the expression of HA receptors involved in the migratory process as CD44 (which is increased in HAS3-transfected cell), and RHAMM. It would be interesting to investigate the role of RHAMM in PTCs migration as it is still an unexplored issue.

In summary, the data suggest that regulation of hyaladherins in the face of constitutive HA generation, may be the key to cable assembly rather than induction of HA synthesis *per se*. Also, the data points toward differences between HAS3 and HAS2 isoforms in many aspects such as the quality and distribution of HA produced, effects on important biological functions, all of which could be due to different enzyme localization.

Chapter VI

General discussion

When HA was discovered about 70 years ago, it was viewed as an inert viscoelastic structure involved in soft tissue lubrication and tissue hydration. The view of HA has been modified as it is now known that HA participates in a wide range of biological events in both normal and disease status. Although very simple in structure as a glycoaminoglycan, the diverse role of HA in matrix biology stems partially from this simple structure as it allows HA to interact with a wide range of molecules. Work presented in this thesis and from other groups have shown that different hyaladherins are involved in different extracellular HA structures (TSG6 in pericellular coats, versican in cables and IαI in both) and these HA structures differ in their impact on their environment.

It is now clear that pericellular/cell-associated HA differs from soluble extracellular HA which binds to cell surface HA receptors inducing a wide range of biological activities which is partially due to the wide range of HA molecular weight (from 5000 to 30000 disaccharide units). Several workers have reported that HA-oligosaccharides may stimulate gene expression and protein synthesis of chemokines [450] and interstitial collagens [451]. In contrast, high MW HA inhibits the "bio-activity" of TGF-β and stimulates the secretion of tissue inhibitors of metalloproteinases [452, 453]. Furthermore, high molecular weight HA reduced T-cell-mediated liver injury by reducing pro-inflammatory cytokines such as TNF-α and IF-γ, an effect that was not produced by low MW HA [454]. These observations, therefore, suggest that high molecular weight HA may be "anti-fibrotic" whereas, if unabated, the generation of low MW HA fragments may disrupt the normal balance between cells and matrix and contribute to the pathophysiology of chronic tissue inflammation and fibrosis.

The work outlined in this thesis focused mainly on extracellular HA structures, their regulation by PTCs and their function. In chapter three, the discovery of HA cable formation by unstimulated PTCs represented a novel finding in two aspects as no reports had investigated the potential for HA cable production by epithelial cells (all studies were done in cells of mesenchymal origin like smooth muscle cells and mesangial cells), and HA cables (in other systems) were noted only in disease-mimicking conditions (like diabetes mellitus and inflammatory bowel disease) and also were formed only in the presence of serum (which is a rich source of hyaladherins). Because PTCs have the ability to produce HA cables in resting conditions, this suggested that their function is possibly different from those produced in disease-mimicking conditions. This hypothesis is supported by work which was performed by a fellow researcher during my studies (discussed below).

In the context of PTC pathophysiology, HA cables seem to play an anti-inflammatory, anti-fibrotic role in that the presence of HA cables around PTCs reduces the generation of TGF-β1 by these cells when exposed to monocytes [135]. Zhang *et al.* have illustrated that monocytes can interact with ICAM on PTCs. This direct interaction between monocytes and PTCs results in PTC "activation" and stimulates TGF-β1 generation by PTCs. In the presence of HA cables, however, monocyte access to ICAM receptors is minimized and so less ICAM-dependant TGF-β1 generation is seen.

BMP-7 has emerged recently as a new therapeutic agent for renal pathologies. It is well-established now that chronic renal diseases represent a state of BMP-7 deficiency, and many animal studies have shown a recovery response from the injured kidney after BMP-7 administration. Many studies have been done to elucidate the real mechanism through which BMP-7 exerts its healing effect. Most notably, Zeisberg *et al.* have shown that BMP-7 counteracts TGF-β1-induced epithelial-to-mesenchymal differentiation [109]. A second mechanism was suggested by Gould *et al.* as they showed that BMP-7 stimulation of epithelial cells decreases mRNA expression for endothelin-2 (ET-2; a vasoconstrictor), and increases mRNA expression for heme oxygenase (HO-1; a vasodilator) [106], this effect is beneficial to the kidney in the post-injury phase as it helps in increasing blood supply to the damaged tissue. The previous study also showed that BMP-7 stimulation resulted in decreased basal and TNF-α-stimulated expression of some pro-inflammatory cytokines such as IL-1β and IL-6. Another mechanism for mode of action of BMP-7 was suggested by the candidate (date from chapter three) and this mechanism was related to the BMP-7 effect on HA regulation. Again this concept was supported by work done at the Institute by Zhang XL (discussed below).

The relationship between HA and BMP-7 was first reported by Nishida *et al.* in 2000 [179]. In that report, BMP-7 stimulation of chondrocytes led to induction of HAS2 mRNA together with up-regulation of CD44 and aggrecan (a member of the hyaladherins) mRNA resulting in an increase in the size of the pericellular matrices in these cells. Further work done by the same group has revealed that this matrix-regaining effect (via HAS2 and aggrecan up-regulation) of BMP-7 is beneficial in the HA hexasaccharide-induced matrix-depletion model of osteoarthritis [275]. Interestingly, IL-1α stimulation of chondrocytes led to a decrease in pericellular matrix although it enhanced HAS2 mRNA expression. This is thought to be caused by both CD44 mRNA up-regulation (which increases HA internalization) and inhibition of aggrecan expression (which might promote the stability of extracellular HA structures)[178].

In chapter three, BMP-7 was shown to increase HA cable generation by PTCs. This increase in HA cables was associated with an increase in HAS2 mRNA and down-regulation of both HYAL1 and 2 mRNA. Further work by Zhang *et al.* has illustrated clearly that the BMP-7-mediated increase in cable generation is important in down-regulating the impact of incoming monocytes *i.e.* decreased PTC TGF-β1 generation [363]. The same work also showed that the effect of increased ICAM-1 expression (through TNF-α stimulation) can be masked by HA cables as BMP-7 treatment reduced PTCs-monocyte direct interaction (and subsequent TGF-β1 generation). This effect of BMP-7 on HA cables and how it may mask PTCs surface-receptors is illustrated in figure 6.1. Thus, in normal physiological conditions the presence of BMP-7 will lessen the impact of any tissue macrophages, while in renal pathology the reduction in BMP-7 levels may translate into a reduction of HA cables and hence an increase in the inflammatory potential of the incoming monocytes.

In contrast to the view presented in this thesis, HA cables are also viewed as pro-inflammatory, pro-fibrotic structures. Work done on colonic smooth muscle cells [170, 258] and mesangial cells [282] showed that various stimuli (such as high glucose and viral infections) can induce the formation of HA cables in these systems and these HA cables are suggested to be important in initiating/maintaining the inflammatory reaction associated with inflammatory diseases like ulcerative colitis and diabetic nephropathy. Further work done at the Institute of Nephrology, however, would support the hypothesis that HA deposits do not drive inflammation in diabetic nephropathy (Lewis, A – M.D. thesis 2006). In that study, renal biopsies from human patients with/without DN showed that although HA was increased in DN, HA could not be established as a predictor of outcome and no correlation was found between HA and the extent of inflammatory infiltrate (monocytes and macrophages).

The above hypothesis is further supported by data generated following examination of IL-1β effect on HA structures (chapter three) which highlighted the specificity of HA cables as IL-1β is a potent stimulus of HA production. Previous work in the department showed that IL-1β not only increases HAS2 mRNA expression [175] but also increased TSG-6 mRNA expression [343], however, IL-1β does not alter the expression of IαI in PTCs. In addition, IL-1β was shown to increase the expression of functionally active CD44 [219] and increase HA/CD44 interaction. The increase in CD44 functionality was not the result of increased CD44 mRNA expression but the result of increased post-translational O-glycosylation of CD44. This increase in CD44 activity could be attributed to conformational changes mediated by carbohydrates which might restrict cell surface mobility of CD44 or cause charge repulsion between neighbouring CD44 molecules thus preventing the formation of functional multivalent aggregated receptors. The increase in pericellular HA coats (figure 3.14) in PTCs after IL-1β stimulation can, therefore, be the result of the above mentioned changes *i.e.* increased HAS2 mRNA (increase in crude HA), increased CD44 functionality (increase in pericellular HA assembly) and increased TSG-6 expression (which is crucial in stabilising pericellular HA coats), moreover, these factors could be preferentially increasing HA coats at the expense of HA cable formation. The increased pericellular HA, as shown in chapter four, induces epithelial cell migration and therefore can be viewed as an inflammatory response.

IL-1β treatment of PTCs resulted in increased ICAM-1 mRNA expression which led to increased monocyte binding that was mostly ICAM-1 dependent (data from chapter three). Direct cell-to-cell contact is thought to be an important feature of a variety of biological processes. *De novo* tubular expression of ICAM-1 and increased expression by interstitial cells occurs in various human renal diseases and in general, the intensity of ICAM staining correlates with disease activity [455]. Furthermore, administration of antibody to ICAM-1 has been proposed as a possible therapeutic option to preserve renal function, at least in a model of ischaemic renal injury [456]. Work done by Zhang *et al.* has demonstrated that in PTCs, the interaction of ICAM-1 with leukocytes plays a key role in the subsequent pathological events. The direct interaction between leukocytes and PTCs through ICAM-1 leads to increased TGF-β1 generation by PTCs and the effect of this interaction (on TGF-β1 generation) was reduced when this ICAM-1 dependent cell-to-cell interaction was inhibited (by blocking leukocyte ICAM-1 receptor via either CD11a/CD18 Ab or by soluble ICAM-1 receptors), moreover blocking monocyte-HA cable interactions (via CD44 Ab) resulted in increased TGF-β1 generation, possibly by increasing direct cell-to-cell contact (Zhang, XL – M.D. thesis 2005).

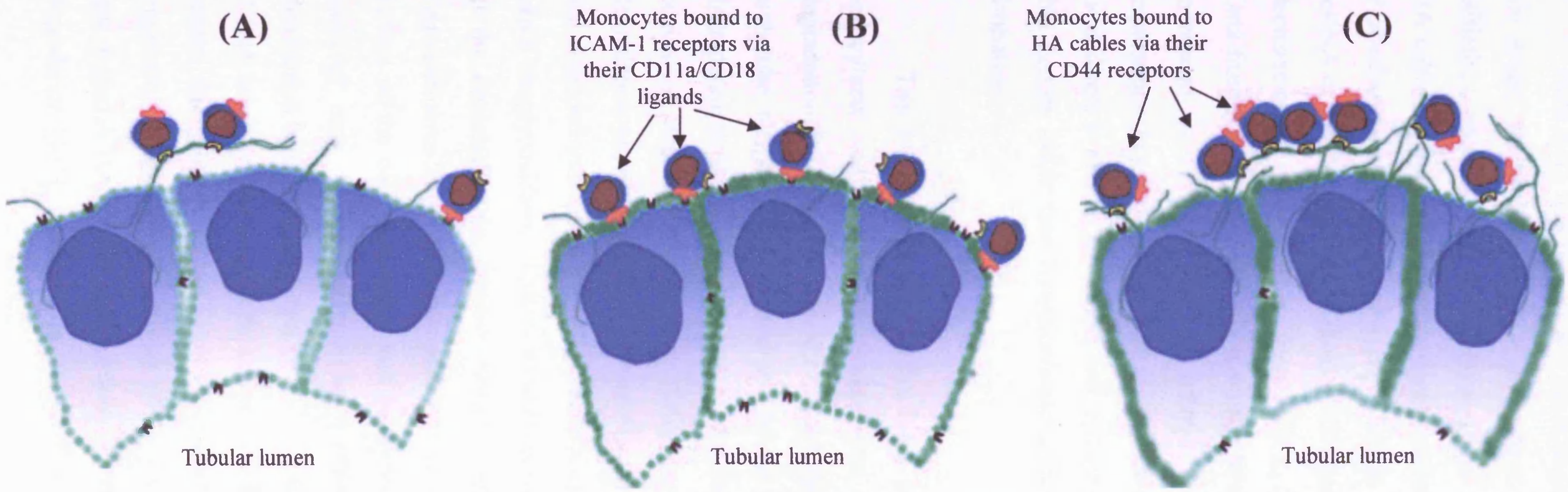

Figure 6.1: Schematic diagram depicting the proposed mechanism by which IL-1β or BMP-7 might affect the interaction of monocytes with adhesion molecules expressed by PTCs.

(A) Under normal physiological conditions, few monocytes are present in the renal interstitium. With an intact basement membrane and the presence of HA cables, very few monocytes might interact directly with PTCs ICAM-1 receptors.

(B) Although ICAM-1 is known to be expressed predominantly on the luminal aspect of PTCs, under pro-inflammatory conditions (represented by IL-1β stimulation in this study) it may also be expressed and up-regulated on the basal aspect of the cell (Zhang, XL – M.D. thesis 2005). Under such conditions, which are usually associated with damage to the basement membrane, infiltrating monocytes gain access to cell surface ICAM-1, which subsequently triggers the generation of a pro-fibrotic response, by stimulating TGF-β1 generation.

(C) In contrast, following stimulation by BMP-7, PTCs generate HA cable structures which preferentially bind infiltrating monocytes by engagement of monocyte CD44. This interaction subsequently prevents/retards migration of monocytes onto the PTC cell surface, thus preventing their interaction with PTC ICAM-1.

Data from this thesis have confirmed the concept that HA cable formation is not single factor-dependent; like increased synthesis or decreased degradation. Initially, a potential role for hyaluronidases was thought to be an important factor in HA cable regulation. This was supported by data from BMP-7 experiments (which showed a concomitant increase in HA cables with a reduction in HYAL1 and HYAL2 mRNA expression) and data from HAS2-transfections (which showed a concomitant decrease in HA cables with an increment in HYAL1 and HYAL2 mRNA expression). Data from HAS3-transfections, however, showed increased HA cables along with an increment in HYAL1 and 2 mRNA expressions. Also, increases in mRNA expressions do not necessarily translate into more protein activity and currently, there is no direct evidence to support cell surface degradation of HA in PTCs. This meant that factors, other than hyaluronidase activity, could be more crucial to HA cable formation.

The degradation of HA has been proposed to occur via receptor-mediated endocytosis and subsequent degradation within lysosomes and generally, HA degradation is considered as an intracellular process. Initially, extracellular high molecular weight HA is bound to plasma membrane via CD44 or RHAMM. The degradation of HA is initiated by HYAL2, however, it is unclear whether degradation begins at the cell-surface or following receptor-mediated endocytosis. The degradation products of HYAL2 are then transferred via endosomes into lysosomes and degraded into small oligosaccharides by the co-ordinated action of HYAL1 and two β-exoglycosidases. This proposed mechanism is supported by recent work done in the department on smooth muscle cells (Jenkins RH – Ph.D. thesis 2005). Immunofluorescence experiments showed that HYAL2 is localised to the inner surface of the cell membrane and to intracellular compartments, while HYAL1 is localised only to intracellular compartments. Interestingly, there was no co-localisation between CD44 and HYAL2 in the cell membrane of smooth muscle cells (CD44 being on the outer side and HYAL2 on the inner side). There are, however, reports that propose an extracellular mechanism for HA degradation. Mechanisms suggested include limited activity of HYAL2 in sub-optimal pH of 7.4 which binds and degrades HA at the cell surface before subsequent internalisation and further degradation [457]. Also, the presence of acidic extracellular microenvironments for

HA degradation was suggested [458]. For all that, more work is needed to establish the role of HYALs in HA cable formation. This could be achieved, for example, by using a pure hyaluronidase inhibitor (yet to be identified) in control/stimulated/transfected cells. Indomethacin (a non-steroidal anti-inflammatory agent), which is considered as a HYAL inhibitor [459], could be used in initial experiments. Also, transfecting cells with vectors containing HYAL1 or HYAL2 constructs (cloned successfully in the Institute of Nephrology) would be another useful approach to elucidate the role of HYALs.

Although HAS3 was initially viewed as the constitutive generator of HA by PTCs [175], HAS3 over-expression was associated with increased HA cables which, in turn, increased monocyte adherence. Similar findings *i.e.* HA cable induction after HAS3 over-expression were reported in other laboratories (Tammi, M – unpublished data) although the potential of these HA structures to bind monocytes was not tested. The reduction in HA cables seen after HAS2 over-expression supports the concept that HA cables are HAS3-dependent. Several points should be considered to better understand the mechanism of formation of extracellular HA structures, including: (*i*) Substrate competition between different HAS isoforms: over-expression of HAS2 might lead to substrate deficiency for the cable-producing HAS3. (*ii*) Differences in enzyme localisation: HAS activity has been linked to its plasma membrane localisation [460]. This work by the Finland group shows that latent HAS2 and HAS3 are present in the ER-Golgi pathway and this pool can be rapidly mobilized and activated by insertion in the plasma membrane. Furthermore, it shows that substrate starvation of HAS can result in its exclusion from the plasma membrane and finally its inactivation. (*iii*) Differences in PαI (and other hyaladherins) expression (discussed below)

IαI has been identified to be an important component of HA cables and its expression is now known to be a crucial factor in HA cable formation. In others' work as well as data from this thesis, blockade of IαI resulted in severe truncation of HA cables and reduced monocyte-HA interaction. One of the main differences noted between the HAS2 and HAS3 over-expressing cells was their PαI expression. In the HAS2-transfected cells, HC3 expression was decreased while it is unchanged or slightly increased in the HAS3-transfected cells. The down-regulation of HC3 mRNA in HAS2-transfected HK-2 cells is intriguing but one can speculate that because HAS2 over-expression resulted in increased cell-associated HA, the cells, attempting to clear intracellular HA, try to down-regulate hyaladherins to facilitate HA degradation and/or expulsion. This explanation is supported by western blot experiments that showed positive intracellular HA-IαI interaction (data from chapter four). It is also supported by data from HAS3 over-expression where cell-associated HA was decreased and IαI mRNA levels were unchanged (data from chapter five).

Mia *et al.* [459] suggested that the circulating HYAL inhibitor is a member of the IαI family, with the PαI as the most likely candidate as observed from reverse HA-substrate gel zymography experiments. The circulating inhibitor, yet to be properly identified, is ineffective against *Streptomyces* hyaluronidase which suggests that protection of HA substrate is not the entire mechanism of action of the hyaluronidase inhibition. Data from this thesis supports this HA-protective ability of PαI: (*i*) IαI/PαI Ab (which is reported to reverse the PαI HYAL inhibitory effect) in chapter five resulted in dramatic decrease in HA cable formation. (*ii*) Reduction in HC3 expression in HAS2-transfected cells was associated with decreased cable formation, although overall HA content was increased. While the stable expression of HC3 following HAS3 over-expression was associated with increased cable formation although HYAL1 and 2 mRNA expression increased. This role of IαI in PTCs represents an interesting area to investigate. This could be done for example by using inhibitory methods like siRNA or antisense transfection after stimulating cable formation (with BMP-7 stimulation or HAS3 transfection).

TSG-6 has been shown to be crucial in stabilising pericellular HA coats via catalysing the transfer of IαI/PαI HCs onto HA chains (data from chapter four). However, the role of TSG-6 as the major catalyst of HC-HA cable interaction is not well-established as Ab blocking experiments failed to inhibit HA cable formation and did not alter HA-dependent monocyte binding. Concurring with this are the data obtained from $TSG^{-/-}$ mouse mesenchymal cells which showed that, upon stimulation, these knock-out cells produce monocyte-binding HA cables as effectively as cells isolated from wild-type mice (De La Motte, CA – Ph.D. thesis 2004). Taken together, these data strongly suggest that TSG-6 is not crucial to HA cable formation nor to HA-dependent monocyte binding.

The role of versican in the formation of HA cables was investigated in chapter three and the results showed positive co-localisation of extracellular HA and versican. How crucial versican is for the formation of these cables is still a question without a clear answer. However, work from the Cleveland group has shown, in addition to HA-versican co-localisation, that using L-selectin blocking Ab (which interacts with the G3 domain of versican [330]) to treat stimulated smooth muscle cells (with higher HA cables content) caused a 70% reduction in monocyte binding (De La Motte, CA – Ph.D. thesis 2004). Interestingly, smooth muscle cells cultured in sulphate-free medium were shown to produce HA cables that do not bind monocytes. These HA cables showed positive IαI incorporation in them, however their versican content was reduced (De La Motte, CA – personal communication). From these observations it is proposed that: (*i*) Resting monocytes adhere first via their L-selectin receptors before interacting with HA via their CD44 receptors. (*ii*) Versican incorporation into HA cables is crucial to their function (monocyte adherence) but not to its formation, although much work is still needed in this regard to prove these concepts and to establish the importance of versican in HA cables.

Data from this thesis suggest that HA cables and pericellular coats are different in at least two respects: differences in sub-cellular origins (perinuclear for HA cables while HA coats are closely related to plasma membrane) and differences in their physiological impact; with HA cables representing an anti-inflammatory response while HA coats have a role in enhancing cell migration which can be viewed either as a pro-fibrotic role (facilitating epithelial-to-mesenchymal transformation in the interstitium) or as a healing role (facilitating the replacement of damaged tubular cells).

Finally, the work presented here gives detailed insights into the metabolism of HA in the PTCs. A new mechanism of action is suggested for the renal-protective agent BMP-7. A new form of extracellular HA was examined in detail along with its main regulators: HAS2 and HAS3. The potential role of different hyaladherins in the extracellular HA structures was examined. Ultimately, this work addressed an important matrix molecule in renal pathophysiology that still requires more research to understand its full potential.

Chapter VII

References

1. Cameron, J.S., et al., *Oxford Textbook of Clinical Nephrology.* 1992.
2. Rubin-Kelley, V.E. and A.M. Jevnikar, *Antigen presentation by renal tubular epithelial cells.* J Am Soc Nephrol, 1991. **2**(1): p. 13-26.
3. Herrera, M.B., et al., *Mesenchymal stem cells contribute to the renal repair of acute tubular epithelial injury.* Int J Mol Med, 2004. **14**(6): p. 1035-41.
4. Okada, H., et al., *Early role of Fsp1 in epithelial-mesenchymal transformation.* Am J Physiol, 1997. **273**(4 Pt 2): p. F563-74.
5. Longmore, M., I. Wilkinson, and E. Torok, *Oxford handbook of clinical medicine.* Oxford University Press, Oxford, 2001.
6. Schainuck, L.I., et al., *Structural-functional correlations in renal disease. II. The correlations.* Hum Pathol, 1970. **1**(4): p. 631-41.
7. Risdon, R.A., J.C. Sloper, and H.E. De Wardener, *Relationship between renal function and histological changes found in renal-biopsy specimens from patients with persistent glomerular nephritis.* Lancet, 1968. **2**(7564): p. 363-6.
8. Mauer, S.M., et al., *Structural-functional relationships in diabetic nephropathy.* J Clin Invest, 1984. **74**(4): p. 1143-55.
9. Bader, R., et al., *Structure and function of the kidney in diabetic glomerulosclerosis. Correlations between morphological and functional parameters.* Pathol Res Pract, 1980. **167**(2-4): p. 204-16.
10. Bohle, A., et al., *The pathogenesis of chronic renal failure in diabetic nephropathy. Investigation of 488 cases of diabetic glomerulosclerosis.* Pathol Res Pract, 1991. **187**(2-3): p. 251-9.
11. Bohle, A., et al., *The role of the interstitium of the renal cortex in renal disease.* Contrib Nephrol, 1979. **16**: p. 109-14.
12. Mackensen, S., et al., *Influence of the renal cortical interstitium on the serum creatinine concentration and serum creatinine clearance in different chronic sclerosing interstitial nephritides.* Nephron, 1979. **24**(1): p. 30-4.
13. von Gise, H., et al., *Correlations between the morphological and clinical findings in a patient recovering from secondary generalised amyloidosis with renal involvement. Light- and electron microscopic investigations on serial biopsies.* Virchows Arch A Pathol Anat Histol, 1978. **379**(2): p. 119-29.
14. Saito, T. and R.C. Atkins, *Contribution of mononuclear leucocytes to the progression of experimental focal glomerular sclerosis.* Kidney Int, 1990. **37**(4): p. 1076-83.

15. Cordonnier, D.J., et al., *Expansion of cortical interstitium is limited by converting enzyme inhibition in type 2 diabetic patients with glomerulosclerosis. The Diabiopsies Group.* J Am Soc Nephrol, 1999. **10**(6): p. 1253-63.

16. Eddy, A.A., *Molecular basis of renal fibrosis.* Pediatr Nephrol, 2000. **15**(3-4): p. 290-301.

17. Rocco, M.V., et al., *Elevated glucose stimulates TGF-beta gene expression and bioactivity in proximal tubule.* Kidney Int, 1992. **41**(1): p. 107-14.

18. Kohan, D.E., *Endothelin synthesis by rabbit renal tubule cells.* Am J Physiol, 1991. **261**(2 Pt 2): p. F221-6.

19. Yard, B.A., et al., *IL-1 alpha stimulated TNF alpha production by cultured human proximal tubular epithelial cells.* Kidney Int, 1992. **42**(2): p. 383-9.

20. Frank, J., et al., *Human renal tubular cells as a cytokine source: PDGF-B, GM-CSF and IL-6 mRNA expression in vitro.* Exp Nephrol, 1993. **1**(1): p. 26-35.

21. Schmouder, R.L., R.M. Strieter, and S.L. Kunkel, *Interferon-gamma regulation of human renal cortical epithelial cell-derived monocyte chemotactic peptide-1.* Kidney Int, 1993. **44**(1): p. 43-9.

22. Schmouder, R.L., et al., *In vitro and in vivo interleukin-8 production in human renal cortical epithelia.* Kidney Int, 1992. **41**(1): p. 191-8.

23. Norman, J., et al., *EGF-induced mitogenesis in proximal tubular cells: potentiation by angiotensin II.* Am J Physiol, 1987. **253**(2 Pt 2): p. F299-309.

24. Zhang, G.H., et al., *Regulation of rat proximal tubule epithelial cell growth by fibroblast growth factors, insulin-like growth factor-1 and transforming growth factor-beta, and analysis of fibroblast growth factors in rat kidney.* J Cell Physiol, 1991. **148**(2): p. 295-305.

25. Cui, S., et al., *IGF-II/Man-6-P receptors in rat kidney: apical localization in proximal tubule cells.* Kidney Int, 1993. **43**(4): p. 796-807.

26. Humes, H.D., et al., *Effects of transforming growth factor-beta, transforming growth factor-alpha, and other growth factors on renal proximal tubule cells.* Lab Invest, 1991. **64**(4): p. 538-45.

27. Wang, S.N., J. Lapage, and R. Hirschberg, *Glomerular ultrafiltration and apical tubular action of IGF-I, TGF-beta, and HGF in nephrotic syndrome.* Kidney Int, 1999. **56**(4): p. 1247-51.

28. Phillips, A., U. Janssen, and J. Floege, *Progression of diabetic nephropathy. Insights from cell culture studies and animal models.* Kidney Blood Press Res, 1999. **22**(1-2): p. 81-97.

29. Phillips, A.O., et al., *Exposure of human renal proximal tubular cells to glucose leads to accumulation of type IV collagen and fibronectin by decreased degradation.* Kidney Int, 1997. **52**(4): p. 973-84.

30. Jernigan, S.M. and A.A. Eddy, *Experimental insights into the mechanism of tubulo-interstitial scarring. In: El Nahas M, Harris K, Anderson S (eds) Mechanisms and clinical management of chronic renal failure.* Oxford University Press, Oxford, 2000: p. 104-145.

31. Lawrence, M.B. and T.A. Springer, *Leukocytes roll on a selectin at physiologic flow rates: distinction from and prerequisite for adhesion through integrins.* Cell, 1991. **65**(5): p. 859-73.

32. von Andrian, U.H., et al., *Two-step model of leukocyte-endothelial cell interaction in inflammation: distinct roles for LECAM-1 and the leukocyte beta 2 integrins in vivo.* Proc Natl Acad Sci U S A, 1991. **88**(17): p. 7538-42.

33. Ricardo, S.D., et al., *Expression of adhesion molecules in rat renal cortex during experimental hydronephrosis.* Kidney Int, 1996. **50**(6): p. 2002-10.

34. Morrissey, J.J. and S. Klahr, *Differential effects of ACE and AT1 receptor inhibition on chemoattractant and adhesion molecule synthesis.* Am J Physiol, 1998. **274**(3 Pt 2): p. F580-6.

35. Okada, H., et al., *Inhibition of monocyte chemoattractant protein-1 expression in tubular epithelium attenuates tubulointerstitial alteration in rat Goodpasture syndrome.* Kidney Int, 2000. **57**(3): p. 927-36.

36. Ophascharoensuk, V., et al., *Obstructive uropathy in the mouse: role of osteopontin in interstitial fibrosis and apoptosis.* Kidney Int, 1999. **56**(2): p. 571-80.

37. Nathan, C.F., *Secretory products of macrophages.* J Clin Invest, 1987. **79**(2): p. 319-26.

38. Lan, H.Y., et al., *Local macrophage proliferation in the progression of glomerular and tubulointerstitial injury in rat anti-GBM glomerulonephritis.* Kidney Int, 1995. **48**(3): p. 753-60.

39. Wang, Y., et al., *Induction of monocyte chemoattractant protein-1 by albumin is mediated by nuclear factor kappaB in proximal tubule cells.* J Am Soc Nephrol, 1999. **10**(6): p. 1204-13.
40. Grandaliano, G., et al., *Monocyte chemotactic peptide-1 expression in acute and chronic human nephritides: a pathogenetic role in interstitial monocytes recruitment.* J Am Soc Nephrol, 1996. **7**(6): p. 906-13.
41. Tang, W.W., et al., *Chemokine expression in experimental tubulointerstitial nephritis.* J Immunol, 1997. **159**(2): p. 870-6.
42. Tesch, G.H., et al., *Monocyte chemoattractant protein 1-dependent leukocytic infiltrates are responsible for autoimmune disease in MRL-Fas(lpr) mice.* J Exp Med, 1999. **190**(12): p. 1813-24.
43. Biancone, L., et al., *Alternative pathway activation of complement by cultured human proximal tubular epithelial cells.* Kidney Int, 1994. **45**(2): p. 451-60.
44. Tang, S., et al., *Apical proteins stimulate complement synthesis by cultured human proximal tubular epithelial cells.* J Am Soc Nephrol, 1999. **10**(1): p. 69-76.
45. Rampino, T., et al., *Macrophage-stimulating protein is produced by tubular cells and activates mesangial cells.* J Am Soc Nephrol, 2002. **13**(3): p. 649-57.
46. Leonard, E.J. and A. Skeel, *A serum protein that stimulates macrophage movement, chemotaxis and spreading.* Exp Cell Res, 1976. **102**(2): p. 434-8.
47. Skeel, A., et al., *Macrophage stimulating protein: purification, partial amino acid sequence, and cellular activity.* J Exp Med, 1991. **173**(5): p. 1227-34.
48. Kees-Folts, D., J.L. Sadow, and G.F. Schreiner, *Tubular catabolism of albumin is associated with the release of an inflammatory lipid.* Kidney Int, 1994. **45**(6): p. 1697-709.
49. Eddy, A.A., *Interstitial fibrosis in hypercholesterolemic rats: role of oxidation, matrix synthesis, and proteolytic cascades.* Kidney Int, 1998. **53**(5): p. 1182-9.
50. Alpers, C.E., et al., *Human renal cortical interstitial cells with some features of smooth muscle cells participate in tubulointerstitial and crescentic glomerular injury.* J Am Soc Nephrol, 1994. **5**(2): p. 201-9.
51. Goumenos, D.S., et al., *Myofibroblasts, predictors of progression of mesangial IgA nephropathy?* Nephrol Dial Transplant, 1994. **9**(10): p. 1418-25.

52. Roberts, I.S., et al., *Interstitial myofibroblasts: predictors of progression in membranous nephropathy.* J Clin Pathol, 1997. **50**(2): p. 123-7.
53. Jenkins, R.H., et al., *Myofibroblastic differentiation leads to hyaluronan accumulation through reduced hyaluronan turnover.* J Biol Chem, 2004. **279**(40): p. 41453-60.
54. Evans, R.A., et al., *TGF-beta1-mediated fibroblast-myofibroblast terminal differentiation-the role of Smad proteins.* Exp Cell Res, 2003. **282**(2): p. 90-100.
55. Fan, J.M., et al., *Transforming growth factor-beta regulates tubular epithelial-myofibroblast transdifferentiation in vitro.* Kidney Int, 1999. **56**(4): p. 1455-67.
56. Ito, Y., et al., *Expression of connective tissue growth factor in human renal fibrosis.* Kidney Int, 1998. **53**(4): p. 853-61.
57. Riser, B.L., et al., *Regulation of connective tissue growth factor activity in cultured rat mesangial cells and its expression in experimental diabetic glomerulosclerosis.* J Am Soc Nephrol, 2000. **11**(1): p. 25-38.
58. Harris, R.C. and H.F. Cheng, *The intrarenal renin-angiotensin system: a paracrine system for the local control of renal function separate from the systemic axis.* Exp Nephrol, 1996. **4 Suppl 1**: p. 2-7.
59. Wolf, G. and E.G. Neilson, *Angiotensin II as a renal growth factor.* J Am Soc Nephrol, 1993. **3**(9): p. 1531-40.
60. Zoja, C., et al., *Proximal tubular cell synthesis and secretion of endothelin-1 on challenge with albumin and other proteins.* Am J Kidney Dis, 1995. **26**(6): p. 934-41.
61. Kliem, V., et al., *Mechanisms involved in the pathogenesis of tubulointerstitial fibrosis in 5/6-nephrectomized rats.* Kidney Int, 1996. **49**(3): p. 666-78.
62. Fellstrom, B., et al., *Platelet-derived growth factor receptors in the kidney--upregulated expression in inflammation.* Kidney Int, 1989. **36**(6): p. 1099-102.
63. Gesualdo, L., et al., *Expression of platelet-derived growth factor receptors in normal and diseased human kidney. An immunohistochemistry and in situ hybridization study.* J Clin Invest, 1994. **94**(1): p. 50-8.
64. Prieto, J., A. Eklund, and M. Patarroyo, *Regulated expression of integrins and other adhesion molecules during differentiation of monocytes into macrophages.* Cell Immunol, 1994. **156**(1): p. 191-211.

65. Morita, H., et al., *Basic fibroblast growth factor-binding domain of heparan sulfate in the human glomerulosclerosis and renal tubulointerstitial fibrosis.* Lab Invest, 1994. **71**(4): p. 528-35.

66. Guo, G., et al., *Role of TNFR1 and TNFR2 receptors in tubulointerstitial fibrosis of obstructive nephropathy.* Am J Physiol, 1999. **277**(5 Pt 2): p. F766-72.

67. Lan, H.Y., et al., *Suppression of experimental crescentic glomerulonephritis by the interleukin-1 receptor antagonist.* Kidney Int, 1993. **43**(2): p. 479-85.

68. Eddy, A.A., et al., *Interstitial fibrosis in mice with overload proteinuria: deficiency of TIMP-1 is not protective.* Kidney Int, 2000. **58**(2): p. 618-28.

69. Phillips, A.O., et al., *Elevated D-glucose concentrations modulate TGF-beta 1 synthesis by human cultured renal proximal tubular cells. The permissive role of platelet-derived growth factor.* Am J Pathol, 1995. **147**(2): p. 362-74.

70. Morrisey, K., et al., *Translational regulation of renal proximal tubular epithelial cell transforming growth factor-beta1 generation by insulin.* Am J Pathol, 2001. **159**(5): p. 1905-15.

71. Chua, C.C., et al., *Angiotensin II induces TGF-beta 1 production in rat heart endothelial cells.* Biochim Biophys Acta, 1994. **1223**(1): p. 141-7.

72. Wolf, G., *Link between angiotensin II and TGF-beta in the kidney.* Miner Electrolyte Metab, 1998. **24**(2-3): p. 174-80.

73. Kopp, J.B., et al., *Transgenic mice with increased plasma levels of TGF-beta 1 develop progressive renal disease.* Lab Invest, 1996. **74**(6): p. 991-1003.

74. Clouthier, D.E., S.A. Comerford, and R.E. Hammer, *Hepatic fibrosis, glomerulosclerosis, and a lipodystrophy-like syndrome in PEPCK-TGF-beta1 transgenic mice.* J Clin Invest, 1997. **100**(11): p. 2697-713.

75. Shinozaki, M., et al., *Marked suppression of interstitial fibrosis with adenovirus-mediated in vivo gene transfer of soluble TGF-beta type II receptor in experimental hydronephrosis (Abstract).* J Am Soc Nephrol, 1998. **9**: p. 527A.

76. Mizuno, S., et al., *Hepatocyte growth factor prevents renal fibrosis and dysfunction in a mouse model of chronic renal disease.* J Clin Invest, 1998. **101**(9): p. 1827-34.

77. Takayama, H., et al., *Renal tubular hyperplasia, polycystic disease, and glomerulosclerosis in transgenic mice overexpressing hepatocyte growth factor/scatter factor.* Lab Invest, 1997. **77**(2): p. 131-8.

78. Chevalier, R.L., et al., *Renal tubulointerstitial injury from ureteral obstruction in the neonatal rat is attenuated by IGF-1.* Kidney Int, 2000. **57**(3): p. 882-90.

79. Hirschberg, R., *Bioactivity of glomerular ultrafiltrate during proteinuria may contribute to renal tubulo-interstitial lesions. Evidence for a role for insulin-like growth factor 1.* J Clin Invest, 1996. **98**: p. 116-124.

80. Tang, W.W., G.Y. Van, and M. Qi, *Myofibroblast and alpha 1 (III) collagen expression in experimental tubulointerstitial nephritis.* Kidney Int, 1997. **51**(3): p. 926-31.

81. Johnson, T.S., et al., *Transglutaminase transcription and antigen translocation in experimental renal scarring.* J Am Soc Nephrol, 1999. **10**(10): p. 2146-57.

82. Diamond, J.R., et al., *Increased expression of decorin in experimental hydronephrosis.* Kidney Int, 1997. **51**(4): p. 1133-9.

83. Schaefer, L., et al., *Decorin, biglycan and their endocytosis receptor in rat renal cortex.* Kidney Int, 1998. **54**(5): p. 1529-41.

84. Stokes, M.B., et al., *Expression of decorin, biglycan, and collagen type I in human renal fibrosing disease.* Kidney Int, 2000. **57**(2): p. 487-98.

85. Jones, C.L., et al., *Renal extracellular matrix accumulation in acute puromycin aminonucleoside nephrosis in rats.* Am J Pathol, 1992. **141**(6): p. 1381-96.

86. Fioretto, P., et al., *Reversal of lesions of diabetic nephropathy after pancreas transplantation.* N Engl J Med, 1998. **339**(2): p. 69-75.

87. Gonzalez-Avila, G., F. Vadillo-Ortega, and R. Perez-Tamayo, *Experimental diffuse interstitial renal fibrosis. A biochemical approach.* Lab Invest, 1988. **59**(2): p. 245-52.

88. McCawley, L.J. and L.M. Matrisian, *Matrix metalloproteinases: they're not just for matrix anymore!* Curr Opin Cell Biol, 2001. **13**(5): p. 534-40.

89. Egeblad, M. and Z. Werb, *New functions for the matrix metalloproteinases in cancer progression.* Nat Rev Cancer, 2002. **2**(3): p. 161-74.

90. Zaoui, P., et al., *Role of metalloproteases and inhibitors in the occurrence and progression of diabetic renal lesions.* Diabetes Metab, 2000. **26 Suppl 4**: p. 25-9.

91. Visse, R. and H. Nagase, *Matrix metalloproteinases and tissue inhibitors of metalloproteinases: structure, function, and biochemistry.* Circ Res, 2003. **92**(8): p. 827-39.

92. Seron, D., et al., *Number of interstitial capillary cross-sections assessed by monoclonal antibodies: relation to interstitial damage.* Nephrol Dial Transplant, 1990. **5**(10): p. 889-93.

93. Marcussen, N., *Atubular glomeruli and the structural basis for chronic renal failure.* Lab Invest, 1992. **66**(3): p. 265-84.

94. Orphanides, C., L.G. Fine, and J.T. Norman, *Hypoxia stimulates proximal tubular cell matrix production via a TGF-beta1-independent mechanism.* Kidney Int, 1997. **52**(3): p. 637-47.

95. von Bubnoff, A. and K.W. Cho, *Intracellular BMP signaling regulation in vertebrates: pathway or network?* Dev Biol, 2001. **239**(1): p. 1-14.

96. Dudley, A.T., K.M. Lyons, and E.J. Robertson, *A requirement for bone morphogenetic protein-7 during development of the mammalian kidney and eye.* Genes Dev, 1995. **9**(22): p. 2795-807.

97. Godin, R.E., et al., *Regulation of BMP7 expression during kidney development.* Development, 1998. **125**(17): p. 3473-82.

98. Kingsley, D.M., *The TGF-beta superfamily: new members, new receptors, and new genetic tests of function in different organisms.* Genes Dev, 1994. **8**(2): p. 133-46.

99. Griffith, D.L., et al., *Three-dimensional structure of recombinant human osteogenic protein 1: structural paradigm for the transforming growth factor beta superfamily.* Proc Natl Acad Sci U S A, 1996. **93**(2): p. 878-83.

100. Lyons, K.M., B.L. Hogan, and E.J. Robertson, *Colocalization of BMP 7 and BMP 2 RNAs suggests that these factors cooperatively mediate tissue interactions during murine development.* Mech Dev, 1995. **50**(1): p. 71-83.

101. Luo, G., et al., *BMP-7 is an inducer of nephrogenesis, and is also required for eye development and skeletal patterning.* Genes Dev, 1995. **9**(22): p. 2808-20.

102. Vukicevic, S., et al., *Induction of nephrogenic mesenchyme by osteogenic protein 1 (bone morphogenetic protein 7).* Proc Natl Acad Sci U S A, 1996. **93**(17): p. 9021-6.

103. Dudley, A.T., R.E. Godin, and E.J. Robertson, *Interaction between FGF and BMP signaling pathways regulates development of metanephric mesenchyme.* Genes Dev, 1999. **13**(12): p. 1601-13.

104. Vukicevic, S., et al., *Osteogenic protein-1 (bone morphogenetic protein-7) reduces severity of injury after ischemic acute renal failure in rat.* J Clin Invest, 1998. **102**(1): p. 202-14.

105. Simon, M., et al., *Expression of bone morphogenetic protein-7 mRNA in normal and ischemic adult rat kidney.* Am J Physiol, 1999. **276**(3 Pt 2): p. F382-9.

106. Gould, S.E., et al., *BMP-7 regulates chemokine, cytokine, and hemodynamic gene expression in proximal tubule cells.* Kidney Int, 2002. **61**(1): p. 51-60.

107. Zeisberg, M., G.A. Muller, and R. Kalluri, *Are there endogenous molecules that protect kidneys from injury? The case for bone morphogenic protein-7 (BMP-7).* Nephrol Dial Transplant, 2004. **19**(4): p. 759-61.

108. Hruska, K.A., et al., *Osteogenic protein-1 prevents renal fibrogenesis associated with ureteral obstruction.* Am J Physiol Renal Physiol, 2000. **279**(1): p. F130-43.

109. Zeisberg, M., et al., *BMP-7 counteracts TGF-beta1-induced epithelial-to-mesenchymal transition and reverses chronic renal injury.* Nat Med, 2003. **9**(7): p. 964-8.

110. Klahr, S., et al., *New approaches to delay the progression of chronic renal failure.* Kidney Int Suppl, 2002(80): p. 23-6.

111. Wang, S. and R. Hirschberg, *BMP7 antagonizes TGF-beta -dependent fibrogenesis in mesangial cells.* Am J Physiol Renal Physiol, 2003. **284**(5): p. F1006-13.

112. Bosukonda, D., et al., *Characterization of receptors for osteogenic protein-1/bone morphogenetic protein-7 (OP-1/BMP-7) in rat kidneys.* Kidney Int, 2000. **58**(5): p. 1902-11.

113. Mackensen-Haen, S., et al., *The consequences for renal function of widening of the interstitium and changes in the tubular epithelium of the renal cortex*

and outer medulla in various renal diseases. Clin Nephrol, 1992. **37**(2): p. 70-7.

114. Bohle, A., S. Mackensen-Haen, and H. von Gise, *Significance of tubulointerstitial changes in the renal cortex for the excretory function and concentration ability of the kidney: a morphometric contribution.* Am J Nephrol, 1987. **7**(6): p. 421-33.
115. Bohle, A., et al., *Correlation between relative interstitial volume of the renal cortex and serum creatinine concentration in minimal changes with nephrotic syndrome and in focal sclerosing glomerulonephritis.* Virchows Arch A Pathol Anat Histol, 1977. **376**(3): p. 221-32.
116. Wang, S.N., J. Lapage, and R. Hirschberg, *Loss of tubular bone morphogenetic protein-7 in diabetic nephropathy.* J Am Soc Nephrol, 2001. **12**(11): p. 2392-9.
117. Dustin, M.L. and T.A. Springer, *Role of lymphocyte adhesion receptors in transient interactions and cell locomotion.* Annu Rev Immunol, 1991. **9**: p. 27-66.
118. Carlos, T.M. and J.M. Harlan, *Leukocyte-endothelial adhesion molecules.* Blood, 1994. **84**(7): p. 2068-101.
119. Williams, A.F., *Surface molecules and cell interactions.* J Theor Biol, 1982. **98**(2): p. 221-34.
120. Dustin, M.L., et al., *Induction by IL 1 and interferon-gamma: tissue distribution, biochemistry, and function of a natural adherence molecule (ICAM-1).* J Immunol, 1986. **137**(1): p. 245-54.
121. Weinreich, T., et al., *Suppression of ICAM-1 expression in renal proximal tubular cells by 1,25-dihydroxyvitamin D3.* Kidney Blood Press Res, 2001. **24**(2): p. 92-8.
122. Harning, R., et al., *Serum levels of circulating intercellular adhesion molecule 1 in human malignant melanoma.* Cancer Res, 1991. **51**(18): p. 5003-5.
123. Staunton, D.E., et al., *The arrangement of the immunoglobulin-like domains of ICAM-1 and the binding sites for LFA-1 and rhinovirus.* Cell, 1990. **61**(2): p. 243-54.
124. Marlin, S.D. and T.A. Springer, *Purified intercellular adhesion molecule-1 (ICAM-1) is a ligand for lymphocyte function-associated antigen 1 (LFA-1).* Cell, 1987. **51**(5): p. 813-9.

125. Diamond, M.S., et al., *Binding of the integrin Mac-1 (CD11b/CD18) to the third immunoglobulin-like domain of ICAM-1 (CD54) and its regulation by glycosylation.* Cell, 1991. **65**(6): p. 961-71.
126. Braun, M., et al., *Cellular adhesion molecules on vascular smooth muscle cells.* Cardiovasc Res, 1999. **41**(2): p. 395-401.
127. Barks, J.L., J.J. McQuillan, and M.F. Iademarco, *TNF-alpha and IL-4 synergistically increase vascular cell adhesion molecule-1 expression in cultured vascular smooth muscle cells.* J Immunol, 1997. **159**(9): p. 4532-8.
128. Panettieri, R.A., Jr., et al., *Activation of cAMP-dependent pathways in human airway smooth muscle cells inhibits TNF-alpha-induced ICAM-1 and VCAM-1 expression and T lymphocyte adhesion.* J Immunol, 1995. **154**(5): p. 2358-65.
129. Elices, M.J., et al., *VCAM-1 on activated endothelium interacts with the leukocyte integrin VLA-4 at a site distinct from the VLA-4/fibronectin binding site.* Cell, 1990. **60**(4): p. 577-84.
130. Ruegg, C., et al., *Role of integrin alpha 4 beta 7/alpha 4 beta P in lymphocyte adherence to fibronectin and VCAM-1 and in homotypic cell clustering.* J Cell Biol, 1992. **117**(1): p. 179-89.
131. Musso, A., et al., *Regulation of ICAM-1-mediated fibroblast-T cell reciprocal interaction: implications for modulation of gut inflammation.* Gastroenterology, 1999. **117**(3): p. 546-56.
132. Pigott, R. and C. Power, *The adhesion molecule facts book.* Academic Press, London, UK., 1993.
133. Sims, T.N. and M.L. Dustin, *The immunological synapse: integrins take the stage.* Immunol Rev, 2002. **186**: p. 100-17.
134. Larson, R.S. and T.A. Springer, *Structure and function of leukocyte integrins.* Immunol Rev, 1990. **114**: p. 181-217.
135. Zhang, X.L., et al., *Renal proximal tubular epithelial cell transforming growth factor-beta1 generation and monocyte binding.* Am J Pathol, 2004. **165**(3): p. 763-73.
136. Harlan, J.M., et al., *The role of neutrophil membrane glycoprotein GP-150 in neutrophil adherence to endothelium in vitro.* Blood, 1985. **66**(1): p. 167-78.
137. Arnaout, M.A., L.L. Lanier, and D.V. Faller, *Relative contribution of the leukocyte molecules Mo1, LFA-1, and p150,95 (LeuM5) in adhesion of*

granulocytes and monocytes to vascular endothelium is tissue- and stimulus-specific. J Cell Physiol, 1988. **137**(2): p. 305-9.

138. Ross, G.D., *Role of the lectin domain of Mac-1/CR3 (CD11b/CD18) in regulating intercellular adhesion.* Immunol Res, 2002. **25**(3): p. 219-27.

139. Kawashima, H., et al., *Binding of a large chondroitin sulfate/dermatan sulfate proteoglycan, versican, to L-selectin, P-selectin, and CD44.* J Biol Chem, 2000. **275**(45): p. 35448-56.

140. Griffin, J.D., et al., *Granulocyte-macrophage colony-stimulating factor and other cytokines regulate surface expression of the leukocyte adhesion molecule-1 on human neutrophils, monocytes, and their precursors.* J Immunol, 1990. **145**(2): p. 576-84.

141. Tedder, T.F., et al., *Expression of the human leukocyte adhesion molecule, LAM1. Identity with the TQ1 and Leu-8 differentiation antigens.* J Immunol, 1990. **144**(2): p. 532-40.

142. DeGrendele, H.C., et al., *CD44 and its ligand hyaluronate mediate rolling under physiologic flow: a novel lymphocyte-endothelial cell primary adhesion pathway.* J Exp Med, 1996. **183**(3): p. 1119-30.

143. Meyer, K. and J.W. Palmer, *The polysaccharide of the vitreous humor.* J Biol Chem, 1934. **107**: p. 629-34.

144. Weissmann, B., et al., *Isolation of oligosaccharides enzymatically produced from hyaluronic acid.* J Biol Chem, 1954. **208**(1): p. 417-29.

145. Butler, J., N.W. Rydell, and E.A. Balazs, *Hyaluronic acid in synovial fluid. VI. Effect of intra-articular injection of hyaluronic acid on the clinical symptoms of arthritis in track horses.* Acta Vet Scand, 1970. **11**(2): p. 139-55.

146. Miller, D. and R. Stegmann, *Use of sodium hyaluronate in human IOL implantation.* Ann Ophthalmol, 1981. **13**(7): p. 811-5.

147. Miller, D. and R. Stegmann, *Secondary intraocular lens implantation using sodium hyaluronate.* Ann Ophthalmol, 1982. **14**(7): p. 621-3.

148. Fraser, J.R., T.C. Laurent, and U.B. Laurent, *Hyaluronan: its nature, distribution, functions and turnover.* J Intern Med, 1997. **242**(1): p. 27-33.

149. Hascall, V. and T. Laurent, *Hyaluronan: Stucture and physical properties.* Science of Hyaluronan Today [online], 1997. <**http://www.glycoforum.gr.jp/science/hyaluronan/HA01/HA01E.html**>.

150. Reed, R.K., K. Lilja, and T.C. Laurent, *Hyaluronan in the rat with special reference to the skin.* Acta Physiol Scand, 1988. **134**(3): p. 405-11.

151. Laurent, U.B., et al., *Hyaluronan in human cerebrospinal fluid.* Acta Neurol Scand, 1996. **94**(3): p. 194-206.

152. Fraser, J.R., et al., *Plasma clearance, tissue distribution and metabolism of hyaluronic acid injected intravenously in the rabbit.* Biochem J, 1981. **200**(2): p. 415-24.

153. Fraser, J.R., et al., *Elimination of hyaluronic acid from the blood stream in the human.* Clin Exp Pharmacol Physiol, 1984. **11**(1): p. 17-25.

154. Hansell, P., et al., *Hyaluronan content in the kidney in different states of body hydration.* Kidney Int, 2000. **58**(5): p. 2061-8.

155. Philipson, L.H. and N.B. Schwartz, *Subcellular localization of hyaluronate synthetase in oligodendroglioma cells.* J Biol Chem, 1984. **259**(8): p. 5017-23.

156. Prehm, P., *Hyaluronate is synthesized at plasma membranes.* Biochem J, 1984. **220**(2): p. 597-600.

157. Barland, P., C. Smith, and D. Hamerman, *Localization of hyaluronic acid in synovial cells by radioautography.* J Cell Biol, 1968. **37**(1): p. 13-26.

158. Mitchell, D. and T. Hardingham, *Monensin inhibits synthesis of proteoglycan, but not of hyaluronate, in chondrocytes.* Biochem J, 1982. **202**(1): p. 249-54.

159. Sugahara, K., N.B. Schwartz, and A. Dorfman, *Biosynthesis of hyaluronic acid by Streptococcus.* J Biol Chem, 1979. **254**(14): p. 6252-61.

160. Ishimoto, N. and J.L. Strominger, *Uridine diphosphate as the sole uridine nucleotide product of hyaluronic acid synthetase in group A streptococci.* Biochim Biophys Acta, 1967. **148**(1): p. 296-7.

161. Mapleson, J.L. and M. Buchwald, *Effect of cycloheximide and dexamethasone phosphate on hyaluronic acid synthesis and secretion in cultured human skin fibroblasts.* J Cell Physiol, 1981. **109**(2): p. 215-22.

162. Hopwood, J.J. and A. Dorfman, *Glycosaminoglycan synthesis by cultured human skin fibroblasts after transformation with simian virus 40.* J Biol Chem, 1977. **252**(14): p. 4777-85.

163. Hart, G.W. and W.J. Lennarz, *Effects of tunicamycin on the biosynthesis of glycosaminoglycans by embryonic chick cornea.* J Biol Chem, 1978. **253**(16): p. 5795-801.

164. Goldberg, R.L. and B.P. Toole, *Monensin inhibition of hyaluronate synthesis in rat fibrosarcoma cells.* J Biol Chem, 1983. **258**(11): p. 7041-6.
165. Shyjan, A.M., et al., *Functional cloning of the cDNA for a human hyaluronan synthase.* J Biol Chem, 1996. **271**(38): p. 23395-9.
166. Watanabe, K. and Y. Yamaguchi, *Molecular identification of a putative human hyaluronan synthase.* J Biol Chem, 1996. **271**(38): p. 22945-8.
167. Spicer, A.P., J.S. Olson, and J.A. McDonald, *Molecular cloning and characterization of a cDNA encoding the third putative mammalian hyaluronan synthase.* J Biol Chem, 1997. **272**(14): p. 8957-61.
168. Prehm, P., *Synthesis of hyaluronate in differentiated teratocarcinoma cells. Mechanism of chain growth.* Biochem J, 1983. **211**(1): p. 191-8.
169. Weigel, P.H., *Bacterial Hyaluronan Synthase - An Update.* Science of Hyaluronan Today [online], 2004. <http://www.glycoforum.gr.jp/science/hyaluronan/HA06a/HA06aE.html> .
170. Majors, A.K., et al., *Endoplasmic reticulum stress induces hyaluronan deposition and leukocyte adhesion.* J Biol Chem, 2003. **278**(47): p. 47223-31.
171. Weigel, P.H., V.C. Hascall, and M. Tammi, *Hyaluronan synthases.* J Biol Chem, 1997. **272**(22): p. 13997-4000.
172. Prehm, P., *Synthesis of hyaluronate in differentiated teratocarcinoma cells. Characterization of the synthase.* Biochem J, 1983. **211**(1): p. 181-9.
173. Mian, N., *Characterization of a high-Mr plasma-membrane-bound protein and assessment of its role as a constituent of hyaluronate synthase complex.* Biochem J, 1986. **237**(2): p. 343-57.
174. Itano, N., et al., *Three isoforms of mammalian hyaluronan synthases have distinct enzymatic properties.* J Biol Chem, 1999. **274**(35): p. 25085-92.
175. Jones, S. and A.O. Phillips, *Regulation of renal proximal tubular epithelial cell hyaluronan generation: implications for diabetic nephropathy.* Kidney Int, 2001. **59**(5): p. 1739-49.
176. Sugiyama, Y., et al., *Putative hyaluronan synthase mRNA are expressed in mouse skin and TGF-beta upregulates their expression in cultured human skin cells.* J Invest Dermatol, 1998. **110**(2): p. 116-21.

177. Kennedy, C.I., et al., *Proinflammatory cytokines differentially regulate hyaluronan synthase isoforms in fetal and adult fibroblasts.* J Pediatr Surg, 2000. **35**(6): p. 874-9.

178. Nishida, Y., et al., *Stimulation of hyaluronan metabolism by interleukin-1alpha in human articular cartilage.* Arthritis Rheum, 2000. **43**(6): p. 1315-26.

179. Nishida, Y., et al., *Osteogenic protein 1 stimulates cells-associated matrix assembly by normal human articular chondrocytes: up-regulation of hyaluronan synthase, CD44, and aggrecan.* Arthritis Rheum, 2000. **43**(1): p. 206-14.

180. Ijuin, C., et al., *Regulation of hyaluronan synthase gene expression in human periodontal ligament cells by tumour necrosis factor-alpha, interleukin-1beta and interferon-gamma.* Arch Oral Biol, 2001. **46**(8): p. 767-72.

181. Kuroda, K., et al., *Up-regulation of putative hyaluronan synthase mRNA by basic fibroblast growth factor and insulin-like growth factor-1 in human skin fibroblasts.* J Dermatol Sci, 2001. **26**(2): p. 156-60.

182. Sayo, T., et al., *Hyaluronan synthase 3 regulates hyaluronan synthesis in cultured human keratinocytes.* J Invest Dermatol, 2002. **118**(1): p. 43-8.

183. Pienimaki, J.P., et al., *Epidermal growth factor activates hyaluronan synthase 2 in epidermal keratinocytes and increases pericellular and intracellular hyaluronan.* J Biol Chem, 2001. **276**(23): p. 20428-35.

184. Yamada, Y., et al., *The gene structure and promoter sequence of mouse hyaluronan synthase 1.* Biochem J, 1998. **330 (Pt 3)**: p. 1223-7.

185. Yung, S., G.J. Thomas, and M. Davies, *Induction of hyaluronan metabolism after mechanical injury of human peritoneal mesothelial cells in vitro.* Kidney Int, 2000. **58**(5): p. 1953-62.

186. Dowthwaite, G.P., et al., *The effect of mechanical strain on hyaluronan metabolism in embryonic fibrocartilage cells.* Matrix Biol, 1999. **18**(6): p. 523-32.

187. Recklies, A.D., et al., *Differential regulation and expression of hyaluronan synthases in human articular chondrocytes, synovial cells and osteosarcoma cells.* Biochem J, 2001. **354**(Pt 1): p. 17-24.

188. Ito, T., et al., *Hyaluronan and proximal tubular cell migration.* Kidney Int, 2004. **65**(3): p. 823-33.

189. Camenisch, T.D., et al., *Disruption of hyaluronan synthase-2 abrogates normal cardiac morphogenesis and hyaluronan-mediated transformation of epithelium to mesenchyme.* J Clin Invest, 2000. **106**(3): p. 349-60.
190. Kosaki, R., K. Watanabe, and Y. Yamaguchi, *Overproduction of hyaluronan by expression of the hyaluronan synthase Has2 enhances anchorage-independent growth and tumorigenicity.* Cancer Res, 1999. **59**(5): p. 1141-5.
191. Liu, N., et al., *Hyaluronan synthase 3 overexpression promotes the growth of TSU prostate cancer cells.* Cancer Res, 2001. **61**(13): p. 5207-14.
192. Itano, N., et al., *Relationship between hyaluronan production and metastatic potential of mouse mammary carcinoma cells.* Cancer Res, 1999. **59**(10): p. 2499-504.
193. Enegd, B., et al., *Overexpression of hyaluronan synthase-2 reduces the tumorigenic potential of glioma cells lacking hyaluronidase activity.* Neurosurgery, 2002. **50**(6): p. 1311-8.
194. Simpson, M.A., et al., *Manipulation of hyaluronan synthase expression in prostate adenocarcinoma cells alters pericellular matrix retention and adhesion to bone marrow endothelial cells.* J Biol Chem, 2002. **277**(12): p. 10050-7.
195. Laurent, U.B. and T. Laurent, *On the origin of Hayluronate in blood.* Biochem Int, 1981. **2**: p. 195-9.
196. Laurent, U.B., J.R. Fraser, and T.C. Laurent, *An experimental technique to study the turnover of concentrated hyaluronan in the anterior chamber of the rabbit.* Exp Eye Res, 1988. **46**(1): p. 49-58.
197. Reed, R.K., et al., *Removal rate of [3H]hyaluronan injected subcutaneously in rabbits.* Am J Physiol, 1990. **259**(2 Pt 2): p. H532-5.
198. Brown, T.J., U.B. Laurent, and J.R. Fraser, *Turnover of hyaluronan in synovial joints: elimination of labelled hyaluronan from the knee joint of the rabbit.* Exp Physiol, 1991. **76**(1): p. 125-34.
199. Fraser, J.R. and T.C. Laurent, *Turnover and metabolism of hyaluronan.* Ciba Found Symp, 1989. **143**: p. 41-53; discussion 53-9, 281-5.
200. Schenck, P., et al., *Synthesis and degradation of hyaluronate by synovia from patients with rheumatoid arthritis.* J Rheumatol, 1995. **22**(3): p. 400-5.
201. Li, M., et al., *Degradation of hyaluronan by peroxynitrite.* Arch Biochem Biophys, 1997. **341**(2): p. 245-50.

202. Csoka, A.B., S.W. Scherer, and R. Stern, *Expression analysis of six paralogous human hyaluronidase genes clustered on chromosomes 3p21 and 7q31.* Genomics, 1999. **60**(3): p. 356-61.

203. Lokeshwar, V.B., et al., *Regulation of hyaluronidase activity by alternative mRNA splicing.* J Biol Chem, 2002. **277**(37): p. 33654-63.

204. Rai, S.K., et al., *Candidate tumor suppressor HYAL2 is a glycosylphosphatidylinositol (GPI)-anchored cell-surface receptor for jaagsiekte sheep retrovirus, the envelope protein of which mediates oncogenic transformation.* Proc Natl Acad Sci U S A, 2001. **98**(8): p. 4443-8.

205. Chang, N.S., *Transforming growth factor-beta1 blocks the enhancement of tumor necrosis factor cytotoxicity by hyaluronidase Hyal-2 in L929 fibroblasts.* BMC Cell Biol, 2002. **3**(1): p. 8.

206. Ji, L., et al., *Expression of several genes in the human chromosome 3p21.3 homozygous deletion region by an adenovirus vector results in tumor suppressor activities in vitro and in vivo.* Cancer Res, 2002. **62**(9): p. 2715-20.

207. Lepperdinger, G., J. Mullegger, and G. Kreil, *Hyal2--less active, but more versatile?* Matrix Biol, 2001. **20**(8): p. 509-14.

208. Stern, R., *Devising a pathway for hyaluronan catabolism: are we there yet?* Glycobiology, 2003. **13**(12): p. 105R-115R.

209. Roden, L., et al., *Enzymic pathways of hyaluronan catabolism.* Ciba Found Symp, 1989. **143**: p. 60-76; discussion 76-86, 281-5.

210. Afify, A.M., et al., *Purification and characterization of human serum hyaluronidase.* Arch Biochem Biophys, 1993. **305**(2): p. 434-41.

211. Csoka, A.B., et al., *Purification and microsequencing of hyaluronidase isozymes from human urine.* FEBS Lett, 1997. **417**(3): p. 307-10.

212. Triggs-Raine, B., et al., *Mutations in HYAL1, a member of a tandemly distributed multigene family encoding disparate hyaluronidase activities, cause a newly described lysosomal disorder, mucopolysaccharidosis IX.* Proc Natl Acad Sci U S A, 1999. **96**(11): p. 6296-300.

213. Flannery, C.R., et al., *Expression and activity of articular cartilage hyaluronidases.* Biochem Biophys Res Commun, 1998. **251**(3): p. 824-9.

214. Nicoll, S.B., et al., *Hyaluronidases and CD44 undergo differential modulation during chondrogenesis.* Biochem Biophys Res Commun, 2002. **292**(4): p. 819-25.

215. Cherr, G.N., A.I. Yudin, and J.W. Overstreet, *The dual functions of GPI-anchored PH-20: hyaluronidase and intracellular signaling.* Matrix Biol, 2001. **20**(8): p. 515-25.

216. Deng, X., Y. He, and P.A. Martin-Deleon, *Mouse Spam1 (PH-20): evidence for its expression in the epididymis and for a new category of spermatogenic-expressed genes.* J Androl, 2000. **21**(6): p. 822-32.

217. Zhang, H. and P.A. Martin-DeLeon, *Mouse Spam1 (PH-20) is a multifunctional protein: evidence for its expression in the female reproductive tract.* Biol Reprod, 2003. **69**(2): p. 446-54.

218. Beech, D.J., A.K. Madan, and N. Deng, *Expression of PH-20 in normal and neoplastic breast tissue.* J Surg Res, 2002. **103**(2): p. 203-7.

219. Jones, S.G., T. Ito, and A.O. Phillips, *Regulation of proximal tubular epithelial cell CD44-mediated binding and internalisation of hyaluronan.* Int J Biochem Cell Biol, 2003. **35**(9): p. 1361-77.

220. Forteza, R., et al., *Hyaluronan serves a novel role in airway mucosal host defense.* Faseb J, 2001. **15**(12): p. 2179-86.

221. Lesley, J., R. Hyman, and P.W. Kincade, *CD44 and its interaction with extracellular matrix.* Adv Immunol, 1993. **54**: p. 271-335.

222. Bourguignon, L.Y., et al., *CD44 interaction with tiam1 promotes Rac1 signaling and hyaluronic acid-mediated breast tumor cell migration.* J Biol Chem, 2000. **275**(3): p. 1829-38.

223. Bourguignon, L.Y., et al., *A CD44-like endothelial cell transmembrane glycoprotein (GP116) interacts with extracellular matrix and ankyrin.* Mol Cell Biol, 1992. **12**(10): p. 4464-71.

224. Lokeshwar, V.B., N. Iida, and L.Y. Bourguignon, *The cell adhesion molecule, GP116, is a new CD44 variant (ex14/v10) involved in hyaluronic acid binding and endothelial cell proliferation.* J Biol Chem, 1996. **271**(39): p. 23853-64.

225. Lokeshwar, V.B., N. Fregien, and L.Y. Bourguignon, *Ankyrin-binding domain of CD44(GP85) is required for the expression of hyaluronic acid-mediated adhesion function.* J Cell Biol, 1994. **126**(4): p. 1099-109.

226. Sleeman, J., et al., *Regulated clustering of variant CD44 proteins increases their hyaluronate binding capacity.* J Cell Biol, 1996. **135**(4): p. 1139-50.

227. Oliferenko, S., et al., *Hyaluronic acid (HA) binding to CD44 activates Rac1 and induces lamellipodia outgrowth.* J Cell Biol, 2000. **148**(6): p. 1159-64.

228. Kamikura, D.M., et al., *Enhanced transformation by a plasma membrane-associated met oncoprotein: activation of a phosphoinositide 3'-kinase-dependent autocrine loop involving hyaluronic acid and CD44.* Mol Cell Biol, 2000. **20**(10): p. 3482-96.

229. Bourguignon, L.Y., et al., *Interaction between the adhesion receptor, CD44, and the oncogene product, p185HER2, promotes human ovarian tumor cell activation.* J Biol Chem, 1997. **272**(44): p. 27913-8.

230. Bourguignon, L.Y., et al., *CD44 interaction with c-Src kinase promotes cortactin-mediated cytoskeleton function and hyaluronic acid-dependent ovarian tumor cell migration.* J Biol Chem, 2001. **276**(10): p. 7327-36.

231. McKee, C.M., et al., *Hyaluronan fragments induce nitric-oxide synthase in murine macrophages through a nuclear factor kappaB-dependent mechanism.* J Biol Chem, 1997. **272**(12): p. 8013-8.

232. Fitzgerald, K.A., et al., *Ras, protein kinase C zeta, and I kappa B kinases 1 and 2 are downstream effectors of CD44 during the activation of NF-kappa B by hyaluronic acid fragments in T-24 carcinoma cells.* J Immunol, 2000. **164**(4): p. 2053-63.

233. Zhu, D. and L.Y. Bourguignon, *Interaction between CD44 and the repeat domain of ankyrin promotes hyaluronic acid-mediated ovarian tumor cell migration.* J Cell Physiol, 2000. **183**(2): p. 182-95.

234. Yonemura, S., et al., *Ezrin/radixin/moesin (ERM) proteins bind to a positively charged amino acid cluster in the juxta-membrane cytoplasmic domain of CD44, CD43, and ICAM-2.* J Cell Biol, 1998. **140**(4): p. 885-95.

235. Spessotto, P., et al., *Hyaluronan-CD44 interaction hampers migration of osteoclast-like cells by down-regulating MMP-9.* J Cell Biol, 2002. **158**(6): p. 1133-44.

236. Ohno-Nakahara, M., et al., *Induction of CD44 and MMP expression by hyaluronidase treatment of articular chondrocytes.* J Biochem (Tokyo), 2004. **135**(5): p. 567-75.

237. Fieber, C., et al., *Hyaluronan-oligosaccharide-induced transcription of metalloproteases.* J Cell Sci, 2004. **117**(Pt 2): p. 359-67.

238. Hall, C.L., et al., *pp60(c-src) is required for cell locomotion regulated by the hyaluronanreceptor RHAMM.* Oncogene, 1996. **13**(10): p. 2213-24.

239. Zhang, S., et al., *The hyaluronan receptor RHAMM regulates extracellular-regulated kinase.* J Biol Chem, 1998. **273**(18): p. 11342-8.

240. Assmann, V., et al., *The intracellular hyaluronan receptor RHAMM/IHABP interacts with microtubules and actin filaments.* J Cell Sci, 1999. **112 (Pt 22)**: p. 3943-54.

241. Lynn, B.D., et al., *Identification of sequence, protein isoforms, and distribution of the hyaluronan-binding protein RHAMM in adult and developing rat brain.* J Comp Neurol, 2001. **439**(3): p. 315-30.

242. Entwistle, J., C.L. Hall, and E.A. Turley, *HA receptors: regulators of signalling to the cytoskeleton.* J Cell Biochem, 1996. **61**(4): p. 569-77.

243. Lokeshwar, V.B. and M.G. Selzer, *Differences in hyaluronic acid-mediated functions and signaling in arterial, microvessel, and vein-derived human endothelial cells.* J Biol Chem, 2000. **275**(36): p. 27641-9.

244. Wang, C., et al., *The overexpression of RHAMM, a hyaluronan-binding protein that regulates ras signaling, correlates with overexpression of mitogen-activated protein kinase and is a significant parameter in breast cancer progression.* Clin Cancer Res, 1998. **4**(3): p. 567-76.

245. Mohapatra, S., et al., *Soluble hyaluronan receptor RHAMM induces mitotic arrest by suppressing Cdc2 and cyclin B1 expression.* J Exp Med, 1996. **183**(4): p. 1663-8.

246. Turley, E.A., P.W. Noble, and L.Y. Bourguignon, *Signaling properties of hyaluronan receptors.* J Biol Chem, 2002. **277**(7): p. 4589-92.

247. Savani, R.C., et al., *Differential involvement of the hyaluronan (HA) receptors CD44 and receptor for HA-mediated motility in endothelial cell function and angiogenesis.* J Biol Chem, 2001. **276**(39): p. 36770-8.

248. Masellis-Smith, A., et al., *Hyaluronan-dependent motility of B cells and leukemic plasma cells in blood, but not of bone marrow plasma cells, in multiple myeloma: alternate use of receptor for hyaluronan-mediated motility (RHAMM) and CD44.* Blood, 1996. **87**(5): p. 1891-9.

249. Kaya, G., et al., *Selective suppression of CD44 in keratinocytes of mice bearing an antisense CD44 transgene driven by a tissue-specific promoter disrupts hyaluronate metabolism in the skin and impairs keratinocyte proliferation.* Genes Dev, 1997. **11**(8): p. 996-1007.

250. Teder, P., et al., *Resolution of lung inflammation by CD44.* Science, 2002. **296**(5565): p. 155-8.

251. Margolis, R.K., et al., *Glycosaminoglycans and glycoproteins associated with rat brain nuclei.* Biochim Biophys Acta, 1976. **451**(2): p. 465-9.

252. Collis, L., et al., *Rapid hyaluronan uptake is associated with enhanced motility: implications for an intracellular mode of action.* FEBS Lett, 1998. **440**(3): p. 444-9.

253. Evanko, S.P., J.C. Angello, and T.N. Wight, *Formation of hyaluronan- and versican-rich pericellular matrix is required for proliferation and migration of vascular smooth muscle cells.* Arterioscler Thromb Vasc Biol, 1999. **19**(4): p. 1004-13.

254. Assmann, V., et al., *The human hyaluronan receptor RHAMM is expressed as an intracellular protein in breast cancer cells.* J Cell Sci, 1998. **111 (Pt 12)**: p. 1685-94.

255. Hofmann, M., et al., *Identification of IHABP, a 95 kDa intracellular hyaluronate binding protein.* J Cell Sci, 1998. **111 (Pt 12)**: p. 1673-84.

256. Huang, L., et al., *Molecular characterization of a novel intracellular hyaluronan-binding protein.* J Biol Chem, 2000. **275**(38): p. 29829-39.

257. Evanko, S.P. and T.N. Wight, *Intracellular localization of hyaluronan in proliferating cells.* J Histochem Cytochem, 1999. **47**(10): p. 1331-42.

258. de la Motte, C.A., et al., *Mononuclear leukocytes bind to specific hyaluronan structures on colon mucosal smooth muscle cells treated with polyinosinic acid:polycytidylic acid: inter-alpha-trypsin inhibitor is crucial to structure and function.* Am J Pathol, 2003. **163**(1): p. 121-33.

259. Pitcock, J.A., et al., *Glycosaminoglycans of the rat renomedullary interstitium: ultrastructural and biochemical observations.* Exp Mol Pathol, 1988. **49**(3): p. 373-87.

260. Mahadevan, P., et al., *Increased hyaluronan production in the glomeruli from diabetic rats: a link between glucose-induced prostaglandin production and reduced sulphated proteoglycan.* Diabetologia, 1995. **38**(3): p. 298-305.

261. Mahadevan, P., et al., *Effect of prostaglandin E2 and hyaluronan on mesangial cell proliferation. A potential contribution to glomerular hypercellularity in diabetes.* Diabetes, 1996. **45**(1): p. 44-50.

262. Sibalic, V., et al., *Upregulated renal tubular CD44, hyaluronan, and osteopontin in kdkd mice with interstitial nephritis.* Nephrol Dial Transplant, 1997. **12**(7): p. 1344-53.

263. Lewington, A.J., et al., *Expression of CD44 in kidney after acute ischemic injury in rats.* Am J Physiol Regul Integr Comp Physiol, 2000. **278**(1): p. R247-54.

264. Wells, A., et al., *Increased hyaluronan in acutely rejecting human kidney grafts.* Transplantation, 1993. **55**(6): p. 1346-9.

265. Wells, A.F., et al., *The localization of hyaluronan in normal and rejected human kidneys.* Transplantation, 1990. **50**(2): p. 240-3.

266. Wells, A., et al., *Role of hyaluronan in chronic and acutely rejecting kidneys.* Transplant Proc, 1993. **25**(2): p. 2048-9.

267. Sano, N., K. Kitazawa, and T. Sugisaki, *Localization and roles of CD44, hyaluronic acid and osteopontin in IgA nephropathy.* Nephron, 2001. **89**(4): p. 416-21.

268. Beck-Schimmer, B., et al., *Hyaluronan induces monocyte chemoattractant protein-1 expression in renal tubular epithelial cells.* J Am Soc Nephrol, 1998. **9**(12): p. 2283-90.

269. Oertli, B., et al., *Mechanisms of hyaluronan-induced up-regulation of ICAM-1 and VCAM-1 expression by murine kidney tubular epithelial cells: hyaluronan triggers cell adhesion molecule expression through a mechanism involving activation of nuclear factor-kappa B and activating protein-1.* J Immunol, 1998. **161**(7): p. 3431-7.

270. Knepper, M.A., et al., *Concentration of solutes in the renal inner medulla: interstitial hyaluronan as a mechano-osmotic transducer.* Am J Physiol Renal Physiol, 2003. **284**(3): p. F433-46.

271. Lee, G.M., et al., *The dynamic structure of the pericellular matrix on living cells.* J Cell Biol, 1993. **123**(6 Pt 2): p. 1899-907.

272. Knudson, W., E. Bartnik, and C.B. Knudson, *Assembly of pericellular matrices by COS-7 cells transfected with CD44 lymphocyte-homing receptor genes.* Proc Natl Acad Sci U S A, 1993. **90**(9): p. 4003-7.

273. Nishida, Y., et al., *Antisense inhibition of hyaluronan synthase-2 in human articular chondrocytes inhibits proteoglycan retention and matrix assembly.* J Biol Chem, 1999. **274**(31): p. 21893-9.

274. Toole, B.P., *Hyaluronan is not just a goo!* J Clin Invest, 2000. **106**(3): p. 335-6.
275. Nishida, Y., C.B. Knudson, and W. Knudson, *Osteogenic Protein-1 inhibits matrix depletion in a hyaluronan hexasaccharide-induced model of osteoarthritis.* Osteoarthritis Cartilage, 2004. **12**(5): p. 374-82.
276. Evanko, S.P., et al., *Platelet-derived growth factor stimulates the formation of versican-hyaluronan aggregates and pericellular matrix expansion in arterial smooth muscle cells.* Arch Biochem Biophys, 2001. **394**(1): p. 29-38.
277. Salustri, A., et al., *PTX3 plays a key role in the organization of the cumulus oophorus extracellular matrix and in in vivo fertilization.* Development, 2004. **131**(7): p. 1577-86.
278. Ochsner, S.A., et al., *Disrupted function of tumor necrosis factor-alpha-stimulated gene 6 blocks cumulus cell-oocyte complex expansion.* Endocrinology, 2003. **144**(10): p. 4376-84.
279. Zhuo, L., et al., *Defect in SHAP-hyaluronan complex causes severe female infertility. A study by inactivation of the bikunin gene in mice.* J Biol Chem, 2001. **276**(11): p. 7693-6.
280. Knudson, W., et al., *CD44-anchored hyaluronan-rich pericellular matrices: an ultrastructural and biochemical analysis.* Exp Cell Res, 1996. **228**(2): p. 216-28.
281. de La Motte, C.A., et al., *Mononuclear leukocytes preferentially bind via CD44 to hyaluronan on human intestinal mucosal smooth muscle cells after virus infection or treatment with poly(I.C).* J Biol Chem, 1999. **274**(43): p. 30747-55.
282. Wang, A. and V.C. Hascall, *Hyaluronan structures synthesized by rat mesangial cells in response to hyperglycemia induce monocyte adhesion.* J Biol Chem, 2004. **279**(11): p. 10279-85.
283. Day, A.J. and G.D. Prestwich, *Hyaluronan-binding proteins: tying up the giant.* J Biol Chem, 2002. **277**(7): p. 4585-8.
284. Gallatin, W., *In cellular and molecular mechanisms of inflammation.* Academic Press, London, UK., 1991.
285. Tammi, R., et al., *Hyaluronan enters keratinocytes by a novel endocytic route for catabolism.* J Biol Chem, 2001. **276**(37): p. 35111-22.

286. Aruffo, A., et al., *CD44 is the principal cell surface receptor for hyaluronate.* Cell, 1990. **61**(7): p. 1303-13.

287. Stamenkovic, I., et al., *The hematopoietic and epithelial forms of CD44 are distinct polypeptides with different adhesion potentials for hyaluronate-bearing cells.* Embo J, 1991. **10**(2): p. 343-8.

288. Jalkanen, S. and M. Jalkanen, *Lymphocyte CD44 binds the COOH-terminal heparin-binding domain of fibronectin.* J Cell Biol, 1992. **116**(3): p. 817-25.

289. Belitsos, P.C., J.E. Hildreth, and J.T. August, *Homotypic cell aggregation induced by anti-CD44(Pgp-1) monoclonal antibodies and related to CD44(Pgp-1) expression.* J Immunol, 1990. **144**(5): p. 1661-70.

290. Singh, K., et al., *Differential processing of osteopontin transcripts in rat kidney- and osteoblast-derived cell lines.* J Biol Chem, 1992. **267**(33): p. 23847-51.

291. Weber, G.F., S. Ashkar, and H. Cantor, *Interaction between CD44 and osteopontin as a potential basis for metastasis formation.* Proc Assoc Am Physicians, 1997. **109**(1): p. 1-9.

292. Weber, G.F., et al., *Receptor-ligand interaction between CD44 and osteopontin (Eta-1).* Science, 1996. **271**(5248): p. 509-12.

293. Padanilam, B.J., D.R. Martin, and M.R. Hammerman, *Insulin-like growth factor I-enhanced renal expression of osteopontin after acute ischemic injury in rats.* Endocrinology, 1996. **137**(5): p. 2133-40.

294. Rodan, G.A., *Osteopontin overview.* Ann N Y Acad Sci, 1995. **760**: p. 1-5.

295. Lesley, J., et al., *Hyaluronan binding by cell surface CD44.* J Biol Chem, 2000. **275**(35): p. 26967-75.

296. Maiti, A., G. Maki, and P. Johnson, *TNF-alpha induction of CD44-mediated leukocyte adhesion by sulfation.* Science, 1998. **282**(5390): p. 941-3.

297. Katoh, S., et al., *Glycosylation of CD44 negatively regulates its recognition of hyaluronan.* J Exp Med, 1995. **182**(2): p. 419-29.

298. Knudson, W. and C.B. Knudson, *The hyaluronan receptor CD44.* Science of Hyaluronan Today [online], 1998. <**http://www.glycoforum.gr.jp/science/hyaluronan/HA10/HA10E.html**>.

299. Lesley, J., et al., *CD44 in inflammation and metastasis.* Glycoconj J, 1997. **14**(5): p. 611-22.

300. Stoop, R., et al., *Trafficking of CD44-deficient murine lymphocytes under normal and inflammatory conditions.* Eur J Immunol, 2002. **32**(9): p. 2532-42.

301. Jain, M., et al., *Role of CD44 in the reaction of vascular smooth muscle cells to arterial wall injury.* J Clin Invest, 1996. **98**(3): p. 877.

302. Pasonen-Seppanen, S., et al., *EGF upregulates, whereas TGF-beta downregulates, the hyaluronan synthases Has2 and Has3 in organotypic keratinocyte cultures: correlations with epidermal proliferation and differentiation.* J Invest Dermatol, 2003. **120**(6): p. 1038-44.

303. Denning, S.M., et al., *Antibodies against the CD44 p80, lymphocyte homing receptor molecule augment human peripheral blood T cell activation.* J Immunol, 1990. **144**(1): p. 7-15.

304. Shimizu, Y., et al., *Dual role of the CD44 molecule in T cell adhesion and activation.* J Immunol, 1989. **143**(8): p. 2457-63.

305. Webb, D.S., et al., *LFA-3, CD44, and CD45: physiologic triggers of human monocyte TNF and IL-1 release.* Science, 1990. **249**(4974): p. 1295-7.

306. Vivers, S., I. Dransfield, and S.P. Hart, *Role of macrophage CD44 in the disposal of inflammatory cell corpses.* Clin Sci (Lond), 2002. **103**(5): p. 441-9.

307. DeGrendele, H.C., et al., *CD44 activation and associated primary adhesion is inducible via T cell receptor stimulation.* J Immunol, 1997. **159**(6): p. 2549-53.

308. Brocke, S., et al., *Antibodies to CD44 and integrin alpha4, but not L-selectin, prevent central nervous system inflammation and experimental encephalomyelitis by blocking secondary leukocyte recruitment.* Proc Natl Acad Sci U S A, 1999. **96**(12): p. 6896-901.

309. Aziz, K., *CD44 mediates polymorphonuclear leukocyte motility on hyaluronan.* Saudi Medical Journal, 2003. **24**(8): p. 827-831.

310. Moffat, F.L., Jr., et al., *Involvement of CD44 and the cytoskeletal linker protein ankyrin in human neutrophil bacterial phagocytosis.* J Cell Physiol, 1996. **168**(3): p. 638-47.

311. Pericle, F., et al., *CD44 is a cytotoxic triggering molecule on human polymorphonuclear cells.* J Immunol, 1996. **157**(10): p. 4657-63.

312. Benz, P.S., X. Fan, and R.P. Wuthrich, *Enhanced tubular epithelial CD44 expression in MRL-lpr lupus nephritis.* Kidney Int, 1996. **50**(1): p. 156-63.

313. Lee, T.H., H.G. Wisniewski, and J. Vilcek, *A novel secretory tumor necrosis factor-inducible protein (TSG-6) is a member of the family of hyaluronate binding proteins, closely related to the adhesion receptor CD44.* J Cell Biol, 1992. **116**(2): p. 545-57.

314. Parkar, A.A. and A.J. Day, *Overlapping sites on the Link module of human TSG-6 mediate binding to hyaluronan and chrondroitin-4-sulphate.* FEBS Lett, 1997. **410**(2-3): p. 413-7.

315. Fulop, C., et al., *Impaired cumulus mucification and female sterility in tumor necrosis factor-induced protein-6 deficient mice.* Development, 2003. **130**(10): p. 2253-61.

316. Fujimoto, T., et al., *Induction of the hyaluronic acid-binding protein, tumor necrosis factor-stimulated gene-6, in cervical smooth muscle cells by tumor necrosis factor-alpha and prostaglandin E(2).* Am J Pathol, 2002. **160**(4): p. 1495-502.

317. Getting, S.J., et al., *The link module from human TSG-6 inhibits neutrophil migration in a hyaluronan- and inter-alpha -inhibitor-independent manner.* J Biol Chem, 2002. **277**(52): p. 51068-76.

318. Bayliss, M.T., et al., *Up-regulation and differential expression of the hyaluronan-binding protein TSG-6 in cartilage and synovium in rheumatoid arthritis and osteoarthritis.* Osteoarthritis Cartilage, 2001. **9**(1): p. 42-8.

319. Wisniewski, H.G., et al., *TSG-6, a glycoprotein associated with arthritis, and its ligand hyaluronan exert opposite effects in a murine model of inflammation.* Pflugers Arch, 1996. **431**(6 Suppl 2): p. R225-6.

320. Bardos, T., et al., *Anti-inflammatory and chondroprotective effect of TSG-6 (tumor necrosis factor-alpha-stimulated gene-6) in murine models of experimental arthritis.* Am J Pathol, 2001. **159**(5): p. 1711-21.

321. Mindrescu, C., et al., *Amelioration of collagen-induced arthritis in DBA/1J mice by recombinant TSG-6, a tumor necrosis factor/interleukin-1-inducible protein.* Arthritis Rheum, 2000. **43**(12): p. 2668-77.

322. Maier, R., et al., *TSG-6 expression in human articular chondrocytes. Possible implications in joint inflammation and cartilage degradation.* Arthritis Rheum, 1996. **39**(4): p. 552-9.

323. Stove, J., et al., *Interleukin-1beta induces different gene expression of stromelysin, aggrecan and tumor-necrosis-factor-stimulated gene 6 in human osteoarthritic chondrocytes in vitro.* Pathobiology, 2000. **68**(3): p. 144-9.

324. Wisniewski, H.G., et al., *TNF/IL-1-inducible protein TSG-6 potentiates plasmin inhibition by inter-alpha-inhibitor and exerts a strong anti-inflammatory effect in vivo.* J Immunol, 1996. **156**(4): p. 1609-15.

325. Wight, T.N., *Versican: a versatile extracellular matrix proteoglycan in cell biology.* Curr Opin Cell Biol, 2002. **14**(5): p. 617-23.

326. Zimmermann, D.R. and E. Ruoslahti, *Multiple domains of the large fibroblast proteoglycan, versican.* Embo J, 1989. **8**(10): p. 2975-81.

327. Chang, Y., et al., *Proteoglycans synthesized by smooth muscle cells derived from monkey (Macaca nemestrina) aorta.* J Biol Chem, 1983. **258**(9): p. 5679-88.

328. Aspberg, A., et al., *Fibulin-1 is a ligand for the C-type lectin domains of aggrecan and versican.* J Biol Chem, 1999. **274**(29): p. 20444-9.

329. Sakko, A.J., et al., *Versican accumulation in human prostatic fibroblast cultures is enhanced by prostate cancer cell-derived transforming growth factor beta1.* Cancer Res, 2001. **61**(3): p. 926-30.

330. Kawashima, H., et al., *Identification and characterization of ligands for L-selectin in the kidney. I. Versican, a large chondroitin sulfate proteoglycan, is a ligand for L-selectin.* Int Immunol, 1999. **11**(3): p. 393-405.

331. Lemire, J.M., et al., *Versican/PG-M isoforms in vascular smooth muscle cells.* Arterioscler Thromb Vasc Biol, 1999. **19**(7): p. 1630-9.

332. Shi, Y., et al., *Myofibroblast involvement in glycosaminoglycan synthesis and lipid retention during coronary repair.* J Vasc Res, 2000. **37**(5): p. 399-407.

333. Passi, A., et al., *The sensitivity of versican from rabbit lung to gelatinase A (MMP-2) and B (MMP-9) and its involvement in the development of hydraulic lung edema.* FEBS Lett, 1999. **456**(1): p. 93-6.

334. Huang, J., et al., *Enhanced proteoglycan deposition in the airway wall of atopic asthmatics.* Am J Respir Crit Care Med, 1999. **160**(2): p. 725-9.

335. Chana, R.S., et al., *Low-density lipoprotein stimulates mesangial cell proteoglycan and hyaluronan synthesis.* Nephrol Dial Transplant, 2000. **15**(2): p. 167-72.

336. Carrino, D.A., J.M. Sorrell, and A.I. Caplan, *Age-related changes in the proteoglycans of human skin.* Arch Biochem Biophys, 2000. **373**(1): p. 91-101.

337. Enghild, J.J., et al., *Chondroitin 4-sulfate covalently cross-links the chains of the human blood protein pre-alpha-inhibitor.* J Biol Chem, 1991. **266**(2): p. 747-51.

338. Diarra-Mehrpour, M., et al., *Human plasma inter-alpha-trypsin inhibitor is encoded by four genes on three chromosomes.* Eur J Biochem, 1989. **179**(1): p. 147-54.

339. Salier, J.P., et al., *The inter-alpha-inhibitor family: from structure to regulation.* Biochem J, 1996. **315 (Pt 1)**: p. 1-9.

340. Kobayashi, H., et al., *Inhibition of the soluble and the tumor cell receptor-bound plasmin by urinary trypsin inhibitor and subsequent effects on tumor cell invasion and metastasis.* Cancer Res, 1994. **54**(3): p. 844-9.

341. Chan, P., et al., *The three heavy-chain precursors for the inter-alpha-inhibitor family in mouse: new members of the multicopper oxidase protein group with differential transcription in liver and brain.* Biochem J, 1995. **306 (Pt 2)**: p. 505-12.

342. Iida, S., et al., *Temporal changes in mRNA expression for bikunin in the kidneys of rats during calcium oxalate nephrolithiasis.* J Am Soc Nephrol, 1999. **10**(5): p. 986-96.

343. Janssen, U., et al., *Expression of inter-alpha-trypsin inhibitor and tumor necrosis factor-stimulated gene 6 in renal proximal tubular epithelial cells.* Kidney Int, 2001. **60**(1): p. 126-36.

344. Blom, A., H. Pertoft, and E. Fries, *Inter-alpha-inhibitor is required for the formation of the hyaluronan-containing coat on fibroblasts and mesothelial cells.* J Biol Chem, 1995. **270**(17): p. 9698-701.

345. Thomas, G.J., S. Yung, and M. Davies, *Bikunin present in human peritoneal fluid is in part derived from the interaction of serum with peritoneal mesothelial cells.* Am J Pathol, 1998. **153**(4): p. 1267-76.

346. Mukhopadhyay, D., et al., *Two distinct populations of tumor necrosis factor-stimulated gene-6 protein in the extracellular matrix of expanded mouse cumulus cell-oocyte complexes.* Arch Biochem Biophys, 2001. **394**(2): p. 173-81.

347. Chen, L., et al., *Proteins of the inter-alpha-trypsin inhibitor family stabilize the cumulus extracellular matrix through their direct binding with hyaluronic acid.* J Biol Chem, 1994. **269**(45): p. 28282-7.

348. Zhuo, L. and K. Kimata, *Cumulus oophorus extracellular matrix: its construction and regulation.* Cell Struct Funct, 2001. **26**(4): p. 189-96.

349. Romisch, J., et al., *Quantification of hemostatic proteins and activation products in synovial fluids from arthritic joints prior to and after induction of chemical synoviorthesis.* Haemostasis, 1996. **26**(3): p. 170-7.

350. Dawson, C.J., et al., *Inter-alpha-inhibitor in calcium stones.* Clin Sci (Lond), 1998. **95**(2): p. 187-93.

351. Bourguignon, J., et al., *Immunohistochemical distribution of inter-alpha-trypsin inhibitor chains in normal and malignant human lung tissue.* J Histochem Cytochem, 1999. **47**(12): p. 1625-32.

352. Yoshida, E., et al., *Immunohistochemical demonstration of bikunin, a light chain of inter-alpha-trypsin inhibitor, in human brain tumors.* Inflammation, 1994. **18**(6): p. 589-96.

353. Mizon, C., et al., *The chondroitin sulfate chain of bikunin-containing proteins in the inter-alpha-inhibitor family increases in size in inflammatory diseases.* Eur J Biochem, 2001. **268**(9): p. 2717-24.

354. Tian, Y.C. and A.O. Phillips, *TGF-beta1-mediated inhibition of HK-2 cell migration.* J Am Soc Nephrol, 2003. **14**(3): p. 631-40.

355. Tian, Y.C., et al., *TGF-beta1-mediated alterations of renal proximal tubular epithelial cell phenotype.* Am J Physiol Renal Physiol, 2003. **285**(1): p. F130-42.

356. Sundstrom, C. and K. Nilsson, *Establishment and characterization of a human histiocytic lymphoma cell line (U-937).* Int J Cancer, 1976. **17**(5): p. 565-77.

357. Yam, L.T., C.Y. Li, and W.H. Crosby, *Cytochemical identification of monocytes and granulocytes.* Am J Clin Pathol, 1971. **55**(3): p. 283-90.

358. Ralph, P., M.A. Moore, and K. Nilsson, *Lysozyme synthesis by established human and murine histiocytic lymphoma cell lines.* J Exp Med, 1976. **143**(6): p. 1528-33.

359. Abita, J.P., et al., *Binding of 125I-insulin to the human histiocytic lymphoma cell line U-937: effect of differentiation with retinoic acid.* Leuk Res, 1984. **8**(2): p. 213-21.

360. Larrick, J.W., et al., *Characterization of a human macrophage-like cell line stimulated in vitro: a model of macrophage functions.* J Immunol, 1980. **125**(1): p. 6-12.

361. Ralph, P., et al., *Induction of antibody-dependent and nonspecific tumor killing in human monocytic leukemia cells by nonlymphocyte factors and phorbol ester.* Cell Immunol, 1982. **71**(2): p. 215-23.

362. DiCorleto, P.E. and C.A. de la Motte, *Characterization of the adhesion of the human monocytic cell line U937 to cultured endothelial cells.* J Clin Invest, 1985. **75**(4): p. 1153-61.

363. Zhang, X.L., et al., *Bone Morphogenic Protein-7 Inhibits Monocyte-Stimulated TGF-{beta}1 Generation in Renal Proximal Tubular Epithelial Cells.* J Am Soc Nephrol, 2005. **16**(1): p. 79-89.

364. Boyum, A., *Isolation of mononuclear cells and granulocytes from human blood. Isolation of monuclear cells by one centrifugation, and of granulocytes by combining centrifugation and sedimentation at 1 g.* Scand J Clin Lab Invest Suppl, 1968. **97**: p. 77-89.

365. Phillips, H.J. and J.E. Terryberry, *Counting actively metabolizing tissue cultured cells.* Exp Cell Res, 1957. **13**(2): p. 341-7.

366. Ahmed, S.A., R.M. Gogal, Jr., and J.E. Walsh, *A new rapid and simple non-radioactive assay to monitor and determine the proliferation of lymphocytes: an alternative to [3H]thymidine incorporation assay.* J Immunol Methods, 1994. **170**(2): p. 211-24.

367. Pagano, J.S. and A. Vaheri, *Enhancement of infectivity of poliovirus RNA with diethylaminoethyl-dextran (DEAE-D).* Arch Gesamte Virusforsch, 1965. **17**(3): p. 456-64.

368. Graham, F.L. and A.J. van der Eb, *A new technique for the assay of infectivity of human adenovirus 5 DNA.* Virology, 1973. **52**(2): p. 456-67.

369. Fraley, R., et al., *Introduction of liposome-encapsulated SV40 DNA into cells.* J Biol Chem, 1980. **255**(21): p. 10431-5.

370. Felgner, P.L., et al., *Lipofection: a highly efficient, lipid-mediated DNA-transfection procedure.* Proc Natl Acad Sci U S A, 1987. **84**(21): p. 7413-7.

371. San, H., et al., *Safety and short-term toxicity of a novel cationic lipid formulation for human gene therapy.* Hum Gene Ther, 1993. **4**(6): p. 781-8.

372. Felgner, P.L., et al., *Improved cationic lipid formulations for in vivo gene therapy.* Ann N Y Acad Sci, 1995. **772**: p. 126-39.

373. Yeh, L.C., et al., *Osteogenic protein-1-mediated insulin-like growth factor gene expression in primary cultures of rat osteoblastic cells.* Endocrinology, 1996. **137**(5): p. 1921-31.

374. Lamb, B.T. and J.D. Gearhart, *YAC transgenics and the study of genetics and human disease.* Curr Opin Genet Dev, 1995. **5**(3): p. 342-8.

375. Malone, R.W., P.L. Felgner, and I.M. Verma, *Cationic liposome-mediated RNA transfection.* Proc Natl Acad Sci U S A, 1989. **86**(16): p. 6077-81.

376. Debs, R.J., et al., *Regulation of gene expression in vivo by liposome-mediated delivery of a purified transcription factor.* J Biol Chem, 1990. **265**(18): p. 10189-92.

377. Felgner, P.L., R.H. Zaugg, and J.A. Norman, *Synthetic recombinant DNA delivery for cancer therapeutics.* Cancer Gene Ther, 1995. **2**(1): p. 61-5.

378. Farhood, H., N. Serbina, and L. Huang, *The role of dioleoyl phosphatidylethanolamine in cationic liposome mediated gene transfer.* Biochim Biophys Acta, 1995. **1235**(2): p. 289-95.

379. Mulsant, P., et al., *Phleomycin resistance as a dominant selectable marker in CHO cells.* Somat Cell Mol Genet, 1988. **14**(3): p. 243-52.

380. Yao, F., et al., *Tetracycline repressor, tetR, rather than the tetR-mammalian cell transcription factor fusion derivatives, regulates inducible gene expression in mammalian cells.* Hum Gene Ther, 1998. **9**(13): p. 1939-50.

381. Cheng, S., et al., *Effective amplification of long targets from cloned inserts and human genomic DNA.* Proc Natl Acad Sci U S A, 1994. **91**(12): p. 5695-9.

382. Thomas, G.J., et al., *Rat mesangial cells in vitro synthesize a spectrum of proteoglycan species including those of the basement membrane and interstitium.* Kidney Int, 1995. **48**(4): p. 1278-89.

383. Laemmli, U.K., *Cleavage of structural proteins during the assembly of the head of bacteriophage T4.* Nature, 1970. **227**(5259): p. 680-5.

384. Bacallao, R. and E.H. Stelzer, *Preservation of biological specimens for observation in a confocal fluorescence microscope and operational principles of confocal fluorescence microscopy.* Methods Cell Biol, 1989. **31**: p. 437-52.

385. Lesley, J., et al., *Hyaluronan binding properties of a CD44 chimera containing the link module of TSG-6.* J Biol Chem, 2002. **277**(29): p. 26600-8.

386. Yung, S. and M. Davies, *Response of the human peritoneal mesothelial cell to injury: an in vitro model of peritoneal wound healing.* Kidney Int, 1998. **54**(6): p. 2160-9.

387. Young, B.A., et al., *Cellular events in the evolution of experimental diabetic nephropathy.* Kidney International, 1995. **47**: p. 935-944.

388. Lavaud, S., et al., *Early influx of glomerular macrophages precedes glomerulosclerosis in the Obese Zucker Rat model.* Journal of the American Society of Nephrology, 1996. **7**(12): p. 2604-2615.

389. Sassy-Pringent, C., et al., *Early glomerular macrophage recruitment in streptozotocin induced diabetic rats.* Diabetes, 2000. **49**: p. 466-475.

390. Aridor, M. and W.E. Balch, *Integration of endoplasmic reticulum signaling in health and disease.* Nat Med, 1999. **5**(7): p. 745-51.

391. Kaufman, R.J., *Orchestrating the unfolded protein response in health and disease.* J Clin Invest, 2002. **110**(10): p. 1389-98.

392. Pahl, H.L., *Signal transduction from the endoplasmic reticulum to the cell nucleus.* Physiol Rev, 1999. **79**(3): p. 683-701.

393. Lee, A.S., *The glucose-regulated proteins: stress induction and clinical applications.* Trends Biochem Sci, 2001. **26**(8): p. 504-10.

394. Kharroubi, I., et al., *Free fatty acids and cytokines induce pancreatic beta-cell apoptosis by different mechanisms: role of nuclear factor-kappaB and endoplasmic reticulum stress.* Endocrinology, 2004. **145**(11): p. 5087-96.

395. Oyadomari, S., et al., *Nitric oxide-induced apoptosis in pancreatic beta cells is mediated by the endoplasmic reticulum stress pathway.* Proc Natl Acad Sci U S A, 2001. **98**(19): p. 10845-50.

396. Weber, S.M., et al., *PPARgamma ligands induce ER stress in pancreatic beta-cells: ER stress activation results in attenuation of cytokine signaling.* Am J Physiol Endocrinol Metab, 2004. **287**(6): p. E1171-7.

397. Levesque, M.C. and B.F. Haynes, *In vitro culture of human peripheral blood monocytes induces hyaluronan binding and up-regulates monocyte variant CD44 isoform expression.* The Journal of Immunology, 1996. **156**(4): p. 1557-1565.

398. Morisaki, N., et al., *Platelet-derived growth factor is a potent stimulator of expression of intercellular adhesion molecule-1 in human arterial smooth muscle cells.* Biochem Biophys Res Commun, 1994. **200**(1): p. 612-8.

399. van de Stolpe, A., et al., *12-O-tetradecanoylphorbol-13-acetate- and tumor necrosis factor alpha-mediated induction of intercellular adhesion molecule-1 is inhibited by dexamethasone. Functional analysis of the human intercellular adhesion molecular-1 promoter.* J Biol Chem, 1994. **269**(8): p. 6185-92.

400. Rothlein, R., et al., *Induction of intercellular adhesion molecule 1 on primary and continuous cell lines by pro-inflammatory cytokines. Regulation by pharmacologic agents and neutralizing antibodies.* J Immunol, 1988. **141**(5): p. 1665-9.

401. Chin, J.E., et al., *Role of cytokines in inflammatory synovitis. The coordinate regulation of intercellular adhesion molecule 1 and HLA class I and class II antigens in rheumatoid synovial fibroblasts.* Arthritis Rheum, 1990. **33**(12): p. 1776-86.

402. Tammi, R., et al., *Hyaluronan enters keratinocytes by a novel endocytic route for catabolism.* The Journal of Biological Chemistry, 2001. **276**(37): p. 35111-35122.

403. Munro, S. and H.R. Pelham, *An Hsp70-like protein in the ER: identity with the 78 kd glucose-regulated protein and immunoglobulin heavy chain binding protein.* Cell, 1986. **46**(2): p. 291-300.

404. Munro, S. and H.R. Pelham, *A C-terminal signal prevents secretion of luminal ER proteins.* Cell, 1987. **48**(5): p. 899-907.

405. Hua, Q., C.B. Knudson, and W. Knudson, *Internalisation of hyaluronan by chondrocytes occurs via receptor mediated endocytosis.* Journal of Cell Science, 1993. **106**: p. 365-375.

406. Nishida, Y., et al., *Osteogenic protein-1 promotes the synthesis and retention of extracellular matrix within bovine articular cartilage and chondrocyte cultures.* Osteoarthritis Cartilage, 2000. **8**(2): p. 127-36.

407. Fülop, C., A. Salustri, and V.C. Hascall, *Coding sequence of a hyaluronan synthase homologue expressed during expansion of the mouse cumulus-oocyte complex.* Archives of Biochemistry and Biophysics, 1997. **337**(2): p. 261-266.

408. Springer, T.A., *Adhesion receptors of the immune system.* Nature, 1990. **346**(6283): p. 425-34.

409. Daniel, L., et al., *Tubular lesions and tubular cell adhesion molecules for the prognosis of lupus nephritis.* Kidney International, 2001. **60**(6): p. 2215-2221.

410. Clayton, A., et al., *ICAM-1 dependent binding to renal fibroblasts initiates de novo adhesion molecule synthesis.* Journal of Cell Science, 1998. **111**: p. 443-453.

411. van Kooten, C., M.R. Daha, and L.A. van Es, *Tubular epithelial cells: A critical cell type in the regulation of renal inflammatory processes.* Experimental Nephrology, 1999. **7**(5-6): p. 429-37.

412. Oertli, B., et al., *Mechanisms of hyaluronan-induced up-regulation of ICAM-1 and VCAM-1 expression by murine kidney tubular epithelial cells: Hyaluronan triggers cell adhesion molecule expression through a mechanism involving activation of nuclear factor -kB activating protein-1.* The Journal of Immunology, 1998. **161**: p. 3431-3437.

413. Beck-Schimmer, B., et al., *Hyaluronan induces monocyte chemoattractant protein-1 expression in renal tubular epithelial cells.* Journal of the American Society of Nephrology, 1998. **9**: p. 2283-2290.

414. Sheehan, K.M., et al., *Hyaluronic acid of high molecular weight inhibits proliferation and induces cell death in U937 macrophage cells.* Life Sci, 2004. **75**(26): p. 3087-102.

415. Oertli, B., X. Fan, and R.P. Wüthrich, *Characterization of CD44-mediated hyaluronan binding by renal tubular epithelial cells.* Nephrology Dialysis Transplantation, 1998. **13**: p. 271-278.

416. Sun, L.K., et al., *Hyaluronan-induced cyclooxygenase-2 expression promotes thromboxane a2 production by renal cells.* Kidney International, 2001. **59**: p. 190-196.

417. Ito, T., et al., *Hyaluronan and proximal tubular epithelial cell migration.* Kidney International, 2004. **65**(3): p. 823-833.

418. Ito, T., et al., *Hyaluronan attenuates transforming growth factor-beta1-mediated signaling in renal proximal tubular epithelial cells.* Am J Pathol, 2004. **164**(6): p. 1979-88.

419. Ito, T., et al., *Hyaluronan regulates transforming growth factor-beta1 receptor compartmentalization.* J Biol Chem, 2004. **279**(24): p. 25326-32.

420. Di Guglielmo, G.M., et al., *Distinct endocytic pathways regulate TGF-beta receptor signalling and turnover.* Nature Cell Biology, 2003. **5**(5): p. 410-21.

421. Spicer, A.P. and J.A. McDonald, *Characterisation and molecular evolution of a vertebrate hyaluronan synthase gene family.* The Journal of Biological Chemistry, 1998. **272**(4): p. 1923-1932.

422. Cohen, M., et al., *Organization and adhesive properties of the hyaluronan pericellular coat of chondrocytes and epithelial cells.* Biophys J, 2003. **85**(3): p. 1996-2005.

423. Knudson, W., et al., *CD-44 anchored hyaluronan-rich pericellular matrices: An ultrastructural and biochemical analysis.* Experimental Cell Research, 1996. **228**: p. 216-228.

424. Chen, L., et al., *Covalent linkage between proteins of the inter-alpha-inhibitor family and hyaluronic acid is mediated by a factor produced by granulosa cells.* J Biol Chem, 1996. **271**(32): p. 19409-14.

425. Mahoney, D.J., C.D. Blundell, and A.J. Day, *Mapping the hyaluronan-binding site on the link module from human tumor necrosis factor-stimulated gene-6 by site-directed mutagenesis.* J Biol Chem, 2001. **276**(25): p. 22764-71.

426. Nentwich, H.A., et al., *A novel allelic variant of the human TSG-6 gene encoding an amino acid difference in the CUB module. Chromosomal localization, frequency analysis, modeling, and expression.* J Biol Chem, 2002. **277**(18): p. 15354-62.

427. Blundell, C.D., et al., *The link module from ovulation- and inflammation-associated protein TSG-6 changes conformation on hyaluronan binding.* J Biol Chem, 2003. **278**(49): p. 49261-70.

428. Lesley, J., et al., *TSG-6 modulates the interaction between hyaluronan and cell surface CD44.* J Biol Chem, 2004. **279**(24): p. 25745-54.

429. Rugg, M.S., et al., *Characterization of complexes formed between TSG-6 and inter-alpha -inhibitor that act as intermediates in the covalent transfer of heavy chains on to hyaluronan.* J Biol Chem, 2005.

430. Zoltan-Jones, A., et al., *Elevated hyaluronan production induces mesenchymal and transformed properties in epithelial cells.* J Biol Chem, 2003. **278**(46): p. 45801-10.

431. Culty, M., et al., *Binding and degradation of hyaluronan by human breast cancer cell lines expressing different forms of CD44: correlation with invasive potential.* J Cell Physiol, 1994. **160**(2): p. 275-86.

432. Hua, Q., C.B. Knudson, and W. Knudson, *Internalization of hyaluronan by chondrocytes occurs via receptor-mediated endocytosis.* J Cell Sci, 1993. **106 (Pt 1)**: p. 365-75.

433. Nedvetzki, S., et al., *RHAMM, a receptor for hyaluronan-mediated motility, compensates for CD44 in inflamed CD44-knockout mice: A different interpretation of redundancy.* Proc Natl Acad Sci U S A, 2004.

434. Zhuo, L., V.C. Hascall, and K. Kimata, *Inter-alpha-trypsin inhibitor, a covalent protein-glycosaminoglycan-protein complex.* J Biol Chem, 2004. **279**(37): p. 38079-82.

435. Kobayashi, H., et al., *Inter-alpha-trypsin inhibitor bound to tumor cells is cleaved into the heavy chains and the light chain on the cell surface.* J Biol Chem, 1996. **271**(19): p. 11362-7.

436. Lesley, J., et al., *Hyaluronan binding properties of a CD44 chimera containing the link module of TSG-6.* The Journal of Biological Chemistry, 2002. **277**(29): p. 26600-8.

437. Enghild, J.J., et al., *Analysis of inter-alpha-trypsin inhibitor and a novel trypsin inhibitor, pre-alpha-trypsin inhibitor, from human plasma. Polypeptide chain stoichiometry and assembly by glycan.* J Biol Chem, 1989. **264**(27): p. 15975-81.

438. Jessen, T.E. and L. Odum, *TSG-6 and calcium ions are essential for the coupling of inter-alpha-trypsin inhibitor to hyaluronan in human synovial fluid.* Osteoarthritis Cartilage, 2004. **12**(2): p. 142-8.

439. Sobue, M., et al., *Production and immunohistochemical characterization of a monoclonal antibody raised to proteoglycan purified from a human yolk sac tumour.* Histochem J, 1989. **21**(8): p. 455-60.

440. Zhang, Y., et al., *The G3 domain of versican enhances cell proliferation via epidermial growth factor-like motifs.* J Biol Chem, 1998. **273**(33): p. 21342-51.

441. Qwarnstrom, E.E., et al., *Interleukin-1 beta regulation of fibroblast proteoglycan synthesis involves a decrease in versican steady-state mRNA levels.* Biochem J, 1993. **294 (Pt 2)**: p. 613-20.

442. Wisniewski, H.G., et al., *TSG-6 protein binding to glycosaminoglycans: formation of stable complexes with hyaluronan and binding to chondroitin sulfates.* J Biol Chem, 2005. **280**(15): p. 14476-84.

443. Matsumoto, K., et al., *Distinct interaction of versican/PG-M with hyaluronan and link protein.* J Biol Chem, 2003. **278**(42): p. 41205-12.

444. Eriksen, G.V., et al., *Isolation and characterization of proteoglycans from human follicular fluid.* Biochem J, 1999. **340 (Pt 3)**: p. 613-20.

445. Hirose, J., et al., *Versican interacts with chemokines and modulates cellular responses.* J Biol Chem, 2001. **276**(7): p. 5228-34.

446. Tammi, R., et al., *Hyaluronan synthase induction and hyaluronan accumulation in mouse epidermis following skin injury.* J Invest Dermatol, 2005. **124**(5): p. 898-905.

447. Bullard, K.M., et al., *Hyaluronan synthase-3 is upregulated in metastatic colon carcinoma cells and manipulation of expression alters matrix retention and cellular growth.* Int J Cancer, 2003. **107**(5): p. 739-46.

448. Brinck, J. and P. Heldin, *Expression of recombinant hyaluronan synthase (HAS) isoforms in CHO cells reduces cell migration and cell surface CD44.* Exp Cell Res, 1999. **252**(2): p. 342-51.

449. Itano, N., et al., *Abnormal accumulation of hyaluronan matrix diminishes contact inhibition of cell growth and promotes cell migration.* Proc Natl Acad Sci U S A, 2002. **99**(6): p. 3609-14.

450. McKee, C.M., et al., *Hyaluronan (HA) fragments induce chemokine gene expression in alvoelar macropahges.* The Journal of Clinical Investigation, 1996. **98**: p. 2403-2413.

451. Rooney, P., et al., *Angiogenic oligosacharides of hyaluronan enhance the production of collagens by endothelial cells.* Journal of Cell Science, 1993. **105**: p. 213-218.

452. Yasui, T., et al., *Effects of hyaluronan on the production of stromolysin and tissue inhibitor of metalloproteinase-1 (TIMP-1) in bovine articular chondrocytes.* Biomedical Research, 1992. **13**(5): p. 343-348.

453. Locci, P., et al., *Transforming growth factor beta 1-hyaluronic acid interaction.* Cell Tissue Res, 1995. **281**(2): p. 317-24.

454. Nakamura, K., et al., *High, but not low, molecular weight hyaluronan prevents T-cell-mediated liver injury by reducing proinflammatory cytokines in mice.* J Gastroenterol, 2004. **39**(4): p. 346-54.

455. Brady, H.R., *Leukocyte adhesion molecules and kidney diseases.* Kidney Int, 1994. **45**(5): p. 1285-300.

456. Kelly, K.J., et al., *Antibody to intercellular adhesion molecule 1 protects the kidney against ischemic injury.* Proc Nat Acad Sci, 1994. **18**(2): p. 812-816.

457. Mullegger, J. and G. Lepperdinger, *Degradation of hyaluronan by a Hyal2-type hyaluronidase affects pattern formation of vitelline vessels during embryogenesis of Xenopus laevis.* Mech Dev, 2002. **111**(1-2): p. 25-35.

458. Bourguignon, L.Y., et al., *CD44 interaction with Na+-H+ exchanger (NHE1) creates acidic microenvironments leading to hyaluronidase-2 and cathepsin B activation and breast tumor cell invasion.* The Journal of Biological Chemistry, 2004. **279**(26): p. 26991-7007.

459. Mio, K. and R. Stern, *Inhibitors of the hyaluronidases.* Matrix Biol, 2002. **21**(1): p. 31-7.

460. Rilla, K., et al., *Plasma membrane residence of hyaluronan synthase is coupled to its enzymatic activity.* J Biol Chem, 2005. **280**(36): p. 31890-7.